Synthetic methodology towards ADP-ribosylation related molecular tools

Engelsma, S.B.

Synthetic Methodology Towards ADP-Ribosylation Related Molecular Tools

PROEFSCHRIFT

Ter verkrijging van

degraad van Doctor aan de Universiteit Leiden,

op gezag van Rector Magnificus prof. mr. C. J. J. M. Stolker,

volgens besluit van het College voor Promoties

te verdedigen op 5 september 2019

klokke 16:15

door

Sander B. Engelsma

Geboren te Amsterdam in 1986

Promotiecommissie

Promotor:	Prof. dr. G. A. van der Marel
Co-promotor:	Dr. D. V. Filippov
Overige Leden:	Prof. dr. J. Brouwer. Prof. dr. H. S. Overkleeft Prof. dr. A. J. Minnaard, Rijksuniversiteit Groningen. Dr. K. M. Bonger, Radbound Universiteit Nijmegen.

Cover-design by Ayşegül Ipek
Printed by Ridderprint B.V.
ISBN: 978-94-6375-521-4

“Absorb what is useful, discard what is not, and add what is uniquely your own.”

– Bruce Lee

Table of Contents

1 General Introduction

Introduction

During the first half of the twentieth century the significance of the phosphate esters in biochemistry was established. In 1910, Levene made the major discovery that deoxyribonucleic acids (DNA) consist of nucleosides linked together by phosphodiesters.[1] His research set a scientific foundation, that proved crucial in the elucidation of the three-dimensional structure and function of DNA in the 1950s. In the same era it was also discovered that the conversion of adenosine diphosphate to adenosine triphosphate, facilitated by pyrophosphate co-enzyme A, forms the cornerstone of cellular respiration, thereby further signifying the importance of phosphorylation in biological processes.[2] In the following decades, the number of known biochemical processes involving phosphorylation reactions rapidly expanded. For example: protein phosphorylation, a regulatory mechanism that activates or deactivates proteins, became known as the most widespread type of post-translational modification (PTM) and recognized as a key reaction in cellular signal transduction. It is now clear that phosphorylation affects all four major biomolecules – proteins, lipids, carbohydrates and nucleic acids – and plays a pivotal role in the most basic cellular functions, such as cellular energy transfer, signal transduction, protein regulation and the biosynthesis and maintenance of the genome. Considering both the relevance and vastness of these biological processes, it is not surprising that there is a growing demand for well-defined phosphorylated molecular tools that facilitate the studying of the corresponding molecular mechanisms. In addition to a fundamental understanding of normal cell function, such tools can also be effective at elucidating the molecular mechanisms behind various pathologies and help to define potential therapeutics. Synthetic organic chemistry has already proven to be invaluable for the preparation of phosphorylated molecular tools that were designed to this end. However, most natural phosphates are inherently susceptibility to hydrolysis, trans-esterification and enzymatic cleavage. This property limits their use through possible premature degradation or restricted synthetic accessibility; the latter especially when considering the chemical complexity which biomolecules tend to present.

The research described in this Thesis focuses on the development of new molecular tools intended to facilitate the study of the PTM, adenosine diphosphate ribosylation. In this context new reagents and methodologies have been developed for the synthesis of stabilized pyrophosphorylated bioisosteres.

ADP-Ribose Transferases

Adenosine diphosphate ribosylation (ADP-ribosylation) is a post-translational modification regulated by ADP-ribose transferases (ARTs), in which NAD^+ is used to transfer ADP-ribose onto a nucleophilic heteroatom of an acceptor biomolecule, with simultaneous release of nicotinamide. Mono-ADP-ribosylation (MARylation) is a highly conserved PTM that is thought to have evolved in primal prokaryotes as a cellular-defense mechanism against viruses and antimicrobial biomolecules. Most ARTs expressed by these organisms MARylate viral DNA, RNA and proteins in order to disrupt the replication cycle. Over time, however, these originally defensive ADP-ribosylating proteins mutated into bacterial toxins, giving rise to various species of pathogenic bacteria; including infamous examples such as *Bordetella pertussis* (pertussis toxin)[3], *Clostridium botulinum* (C2-toxin, C3-toxin)[4,5], *Corynebacterium diphtheria* (diphtheria toxin)[6] and *Vibrio cholera* (cholera toxin)[7]. Each ART-toxin MARylates specific key regulatory proteins of the eukaryotic host cell; a modification highly detrimental to their function. Interestingly, all ARTs expressed in eukaryotes share similar substrates, catalytic triads and a specific structural fold (known as the ART-folds) with prototypical bacterial toxins, indicating an evolutionary lineage. Based on the homology of the catalytic domain, all eukaryotic ARTs can be categorized as cholera toxin-like or diphtheria toxin-like. In humans, 21 ARTs are expressed that can be differentiated into two subfamilies: 17 poly(ADP-ribose) polymerases (PARPs) and 4 ecto-ADP-ribose transferases (ARCTs). PARPs 1 to 5 are diphtheria toxin-like, sharing the highly conserved ART-fold and the histidine-tyrosine-glutamate (HYE) motif, which facilitates the binding of NAD^+.[8] The ARCTs are cell surface enzymes that are excreted in the extracellular department.[9] They are related to cholera-toxin and make use of an alternative arginine-serine-glutamate (RSE) motif.[10] In this chapter, the discussion will be focused on the HYE-PARPs, as their role in DNA damage repair, telomere maintenance and regulation of apoptosis have highlighted these proteins of biomedical importance, most notably in relation to cancer therapy and inflammatory disorders.

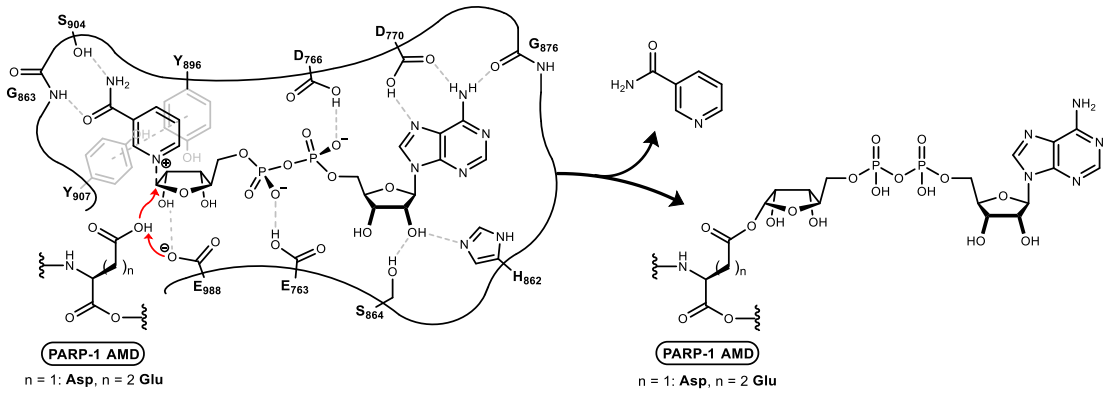

Figure 1: The catalytic mechanism of auto-ADP-ribosylation of chicken PARP-1, at the auto-modification domain (AMD). NAD^+ is shown bound in the ART-fold of PARP-1. The conserved HYE triad refers to H_{862}-Y_{896}-E_{988}. Bonding interactions are shown as grey dashed lines.[11]

PARP Mono- & Poly-ADP-Ribosylation

Both mono(ADP)ribosylation (MARylation) and the succeeding poly(ADP)ribosylation (PARylation) are modifications catalyzed by enzymes belonging to the PARP family. In contrast to their name, most PARPs are actually transferases and only capable of transferring a single mono-ADP-ribose onto a nucleophilic amino-acid at the auto-modification domain, or that of another target protein. However, at least PARP-1, PARP-2, and PARP-5a/b (tankyrases) are capable of catalyzing PARylation.[12,13] PARP-1 to 5 catalyzed ADP-ribosylation starts with the binding of NAD^+ in the ART-fold. The histidine imidazole side-chain, belonging to the conserved HYE motif (Figure 1; H_{862}-Y_{896}-E_{988}), forms a hydrogen bond with the C^2-*OH* of the NAD^+ adenosine moiety.[11] On the other end of the molecule, the electron-poor nicotinamide undergoes π-π stacking with two electron-rich tyrosine residues (Figure 1; Y_{896}-Y_{907}). These binding interactions, among various others, force a spatial orientation that instills strain on the pyridinium *N*-glycosidic bond, lowering the activation energy.[14] The exact function of HYE-glutamate during the initial ADP-ribosylation reaction is different from its role during the PARylating elongation reactions. The inherent nucleophilicity of proposed acceptor side chains, primarily those of glutamate and aspartate, is sufficient for the transfer to occur without the aid of the HYE-glutamate.[13,15,16] This theory is supported by PARP-1 mutant studies, where the absence of the Glu_{988} only gave a 3-fold decrease in auto-MARylation activity.[17] However, the HYE-glutamate is likely to facilitate the reaction through favorable hydrogen bonding and assisting in polarization of the acceptor side chain.

During PARylation, additional ADP-ribose residues are sequentially transferred onto a previously attached acceptor ADP-ribose, to form linear or branched chains of poly-ADP-ribose, consisting of up to 200 monomeric units. Most elongations proceed via α-ribosylation of NAD^+ onto the C^2-*OH* of the terminal adenosine moiety, resulting in a linear extension of the ADPR-polymer chain (Figure 2). In this instance, the HYE-glutamate residue forms a hydrogen bonding network between the acceptor C^2-*OH* of the terminal adenosine and the C^2-*OH* of the bound NAD^+ nicotinamide ribose.[18] Subsequent basic catalysis by the HYE-glutamate enables the S_N2-displacement of the nicotinamide. For PARP-1, branching of the chain irregularly occurs once every 20 to 50 ADP-ribose units, when a similar NAD^+ glycosylation reaction takes place at the C^2-*OH* of an internal ribose moiety.[19] The branching sites are ribosylated following the same linear-branching extension pattern, providing the polymer with a dendritic macrostructure.

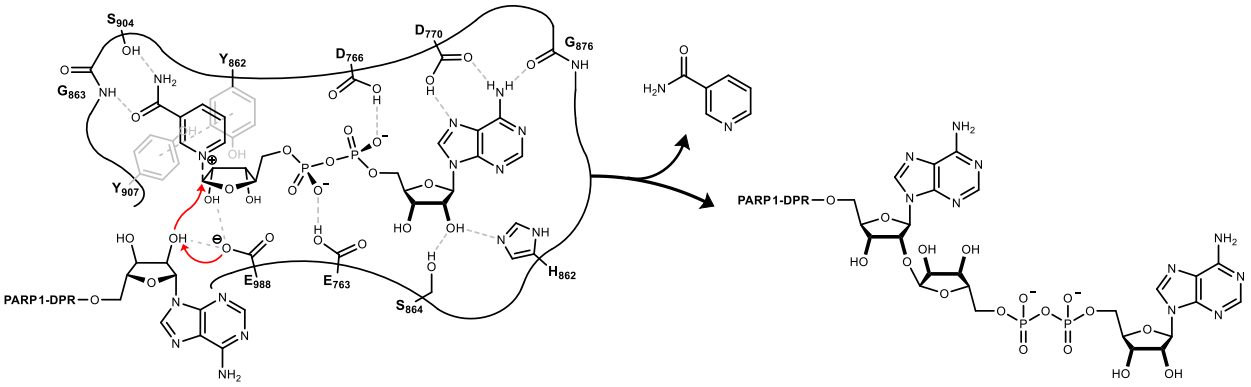

Figure 2: Catalytic mechanism of linear auto-poly-ADP-ribosylation of chicken PARP-1.

Poly-ADP-Ribosylation in DNA Repair

In eukaryotes, PARP-1, PARP-2 and PARP-3 are involved in the detection and initiation of single- and double-strand DNA break repair mechanisms, including base- and nucleotide excision repair.[20,21] Particularly PARP-1 has been subject of extensive studying, as it is the primary target for poly-ADP-ribosylation through auto-modification in response to DNA damage. The mechanism of PARP-1 activation starts by ligation of the zinc finger domains to the disconnected nucleobases at the DNA break.[22] The enforced proximity caused by this interaction allows PARP-1's Trp-Gly-Arg (WGR) domain to bind DNA, triggering a cascade of conformational changes that initiate its catalytic activity.[23] The auto-PARylation of PARP-1 promotes the recruitment of co-enzyme Histone PARylation factor 1 (HPF1), which is responsible for *trans*-ADP-ribosylation of the histones (H1, H2B and H3).[24] It is postulated that the negative charge carried by the phosphate rich poly(ADP-ribose) chains relaxes the histone and partially dissociates the DNA-bound PARP-1, creating a binding cavity for DNA repair proteins XRCC1, DNA ligase-3 and DNA polymerase-β.[25,26] After DNA repair, the PARylated proteins are regenerated through hydrolysis of the PAR-polymers by hydrolases PAR, MacroD1, MacroD2 and TARG1, completing the ADP-ribosylation cycle.

The glutamic acid and aspartate have shown to be primarily acceptor amino acids for ADP-ribosylation at the histone, and more recently lysine, arginine, cysteine and serine have also been reported.[27–30] However, data regarding the covalent poly-ADP-ribosylation of histone proteins at glutamate or aspartate residues is conflicting, and can be viewed as controversial when considering the chemical sensitivity of anomeric esters. Furthermore, non-covalent complexes between poly-ADP and the histone have also been reported.[31–33] Overall the relation between ADP-ribosylation and the target protein's acceptor amino acids and the corresponding biochemical function is poorly understood. Synthetic organic research towards well-defined mono- and poly-ADPr fragments and ADPr-functionalized oligopeptides have already proven to be incredible useful in advancing our understanding of this complex PTM.[16,34–36] The chemically diverse nature of these constructs makes them synthetically challenging. The main difficulty arises from necessity to combine several specialized subfields of organic chemistry, namely carbohydrate-, peptide- and nucleic chemistry, each associated with their own unique reactivity, tailor-made protecting groups and corresponding orthogonality. This, combined with the various labile bonds within these constructs (Figure 3), constrains the synthetic accessibility and biochemical applicability. An organic

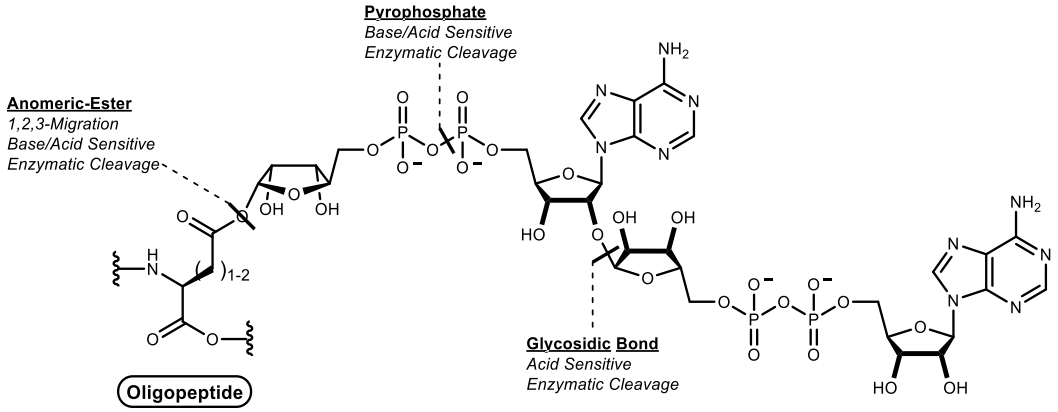

Figure 3: The general structure of an ADPr-functionalized oligopeptide, depicting the three most labile bonds; the pyrophosphate bridge, the stereospecific anomeric ester and the glycosidic bond.

chemical approach to address such limitations is to introduce chemical modifications that stabilize specific labile bonds, while, at the same time, retaining similar overall physical and chemical properties.

Stabilized NAD$^+$ Analogues

Carbanicotinamide Adenine Dinucleotide. In the 1980s scientific evidence signifying the importance of ADP-ribosylation as a regulatory PTM was rapidly being accumulated. As both the exact function and mechanism were still barely understood, there was a growing demand for molecular tools that could help to elucidate this class of PTMs.[37] In 1988, Slama and co-workers were the first to design and synthesize a stabilized analogue to this end, which came in the form of carbocyclic-nicotinamide adenine dinucleotide (*C*-NAD$^+$).[38] It was reasoned that substituting the ring oxygen of the nicotinamide riboside moiety with a methylene would stabilize the adjacent C-N bond, making it resistant to cleavage, while retaining a similar structure and polarity profile to that of natural NAD$^+$.

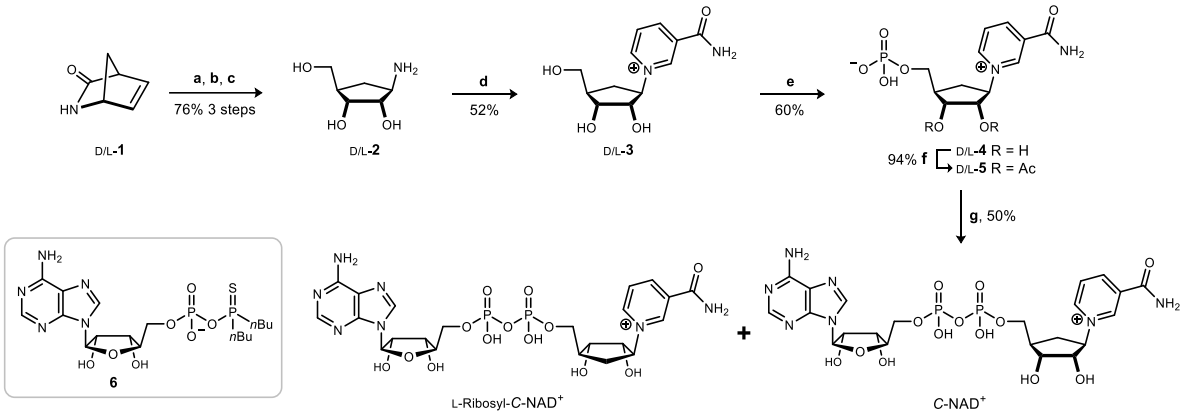

Scheme 1: Synthesis overview of *C*-NAD$^+$ as described by Slama and co-workers. Reagents and conditions: [**a**] OsO_4, MNO, *t*BuOH/H_2O, 50 °C. [**b**] HCl, MeOH. [**c**] $LiEt_3BH$, THF, 0 °C. [**d**] 1-(2,4-dinitrophenyl)-3-carbamoylpyridiniumchloride, H_2O. [**e**] $(CH_3O)_3PO$, $POCl_3$, 0 °C. [**f**] Ac_2O, pyr, 10 °C. [**g**] **6**, DMF/pyr.

Their synthesis started from D/L-ribofuranosylamine **2**, which was prepared on multigram-scale by adopting three literature procedures. The route commenced with a Diels-Alder reaction between achiral cyclopentadiene and tosylcyanide, followed by acidic hydrolysis, to produce **1**[39]. After the *cis*-dihydoxylation and lactam methanolysis of **1**, as described by Cermak *et al*.[40], the sequance is finalized by reduction of the methyl ester[41], providing racemic ribofuranosylamine **2** in 76% yield over three steps. From here, the nicotinamide moiety could be introduced via application of the Zincke reaction, reacting the secondary amine in **2** with 1-(2,4-dinitrophenyl)nicotinamide chloride.[42] Selective phosphorylation of the primary alcohol, by treatment with phosphoryl chloride, lead to produce D/L-**4** as a single product. The coupling of **4** to adenosine monophosphate (AMP) proved to be the most difficult step during the synthesis. Various unsatisfactory coupling conditions were attempted, including Bovine adenylyltransferase catalyzed phosphorylation and Michelson activation. The latter involves the formation of a reactive mixed anhydride between a donor phosphate monoester (e.g. **4**) and diphenyl phosphorochloridate. Controlled substitution of the diphenoxyphosphoryloxy-moiety with an acceptor phosphate leads to the formation of the desired pyrophosphate. Finally, the authors adopted a more

refined iteration of this activation-displacement method, as described by Furusawa *et al.*[43], to successfully couple di-*n*-butylphosphinothioic anhydride **6**, under the agency of silver nitrate, with D/L-*C*-NMN **4**, providing *C*-NAD$^+$ and its respective diastereoisomer. A simple but effective optimization was found in the acetyl protection of the 2,3-diol in **4**. The improved solubility of **5** allowed for the use of more favorable solvent mixtures during the subsequent coupling reaction, significantly improving yield and reproducibility. After ammonia mediated deacylation during work-up, the two diastereoisomeric *C*-NAD analogues could be separated chromatographically. The structures were assigned by exposing both diastereoisomers to yeast and equine liver alcohol dehydrogenases, that naturally use NAD$^+$ as a co-substrate in the oxidation of alcohols. Both enzymes showed activity with the compound that was accordingly assigned as *C*-NAD$^+$, while no enzymatic activity was observed with L-ribosyl-C-NAD$^+$. Although the authors did not evaluate *C*-NAD$^+$ in context of PARPs, it was demonstrated that the analogue was capable of non-covalently inhibiting NAD glycohydrolase from *Bungarus Fasciatus* venom at micromolar concentrations. In 1998, *C*-NAD$^+$ was used by Ruf and co-workers to obtain the first crystal structure of PARP-1 with a NAD$^+$ mimetic bound in the active site.[14]

Benzamide Adenine Dinucleotide. At the beginning of the 1990s the importance of poly-ADP-ribosylation in DNA-repair mechanism was well-established, and PARPs were considered as interesting therapeutic targets in relation to cancer research. However, at this time, no suitable PARP inhibitors were known. In response Krohn *et al.* proposed benzamide riboside (**10**) and benzamide mononucleotide (**11**, Scheme 2), which were predicted to be anabolized intracellularly to the actual envisioned PARP inhibitor and NAD$^+$ analogue; benzamide adenine dinucleotide (BAD, Scheme 3).[44] In this design the riboside ring-oxygen is retained, instead the labile anomeric C^1-N$^+$ bond is removed by substituting the nicotinamide moiety with benzamide.

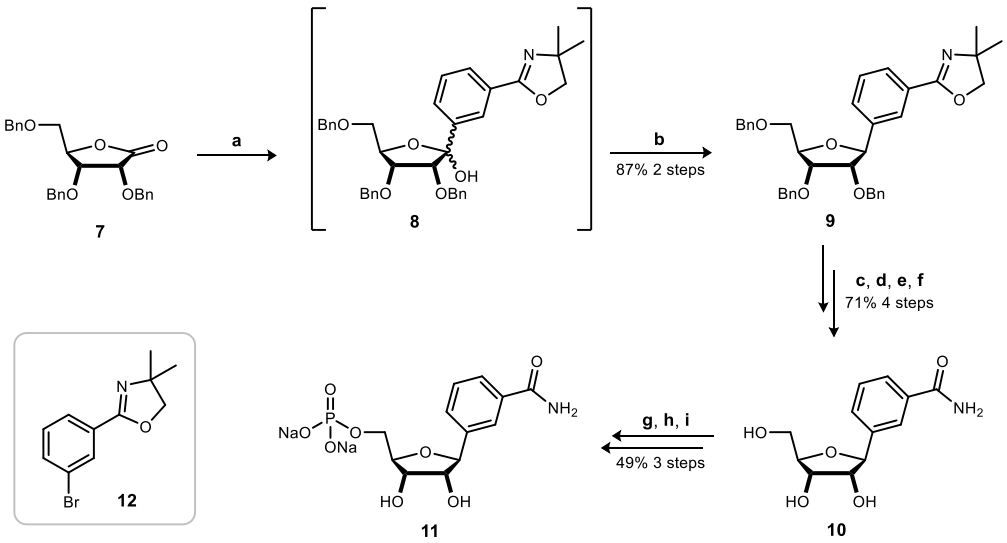

Scheme 2: Synthesis of benzamide mononucleotide as described by Krohn and co-workers. Reagents and conditions: [**a**] *n*BuLi, **12**, THF, -85 °C. [**b**] $BF_3{\cdot}Et_2O$, Et_3SiH, DCM, -78 °C. [**c**] MeI, $MeNO_3$, 100 °C. [**d**] NaOH, MeOH, reflux. [**e**] i: $SOCl_2$, DMF, reflux. ii: NH_4OH. [**f**] Pt/C, H_2, THF. [**g**] Acetone, H_2SO_4, 0 °C. [**h**] $POCl_3$, $PO(OMe)_3$, 0 °C [**i**] HCl, H_2O, 70 °C.

After various investigative reactions and refinements, the final synthesis commenced with the nucleophilic addition of lithiated 3-bromophenyl oxazoline **12** onto benzylated D-ribonolactone **7**. Subsequent silane deoxygenation of the anomeric hydroxyl, in intermediate **8**, afforded protected riboside **9** in stereoselective fashion. Recovery of the amide from the oxazoline moiety and ensuing debenzylation provided benzamide riboside (**10**). To facilitate the installation of the phosphate the 2,3-diol was protected as an isopropylidene acetal. Phosphorylation of the primary alcohol and acidic cleavage of the isopropylidene were carried out in a single operation, yielding target benzamide mononucleotide **11**. As part of their study, Krohn *et al.* evaluated **11** for its biological activity. Although no poly(ADP)ribosylation inhibition was found, **11** showed up to nanomolar level toxicity towards various human tumor cell lines.[45] This potent anti-proliferate activity could indeed be contributed to the anabolic conversion of **11** to BAD, which acted through the inhibition of inosine-5-monophosphate dehydrogenase (IMPDH).

Zatorski and co-workers expanded on the synthesis of BAD (Scheme 3) to determine if the analogue showed selective inhibition between the two IMPDH isoforms (type I and II).[46] Experiencing disappointing yields with the P^V-phosphorylation method reported by Krohn *et al*, the authors turned to a phosphoramidite approach for the preparation of **15**. The reaction of benzamide riboside **13** with 2-cyanoethyl *N*,*N*-diisopropylchlorophosphoramidite, followed by tetrazole mediated installment of the second 2-cyanoethanol and oxidation with *tert*-butyl peroxide, gave the desired dicyanoethyl phosphate. The crude intermediate was treated with methanolic ammonia during work-up, providing phosphate diester **14**. After elimination of the second cyanoethyl, protected benzamide riboside **15** was converted to activated imidazolium species **16** followed by reaction with 2,3-*O*-isopropylidene AMP in a one-pot procedure. Final, acidic deprotection of the isopropylidene groups provided the desired NAD^+ analogue BAD in excellent yield. Unfortunately, BAD did not show selective inhibition between the two isoforms of IMPDH. In 2018, however, Langelier and co-workers established that BAD inhibits the DNA-dependent PARP-1 automodification activity, starting at 50 micromolar concentration.[35] In contrast, *C*-NAD^+ only showed similar levels of inhibition at concentrations twelve times higher. Additionally, the authors were able to obtain the crystal structure of the PARP-1 catalytic domain bound to BAD.

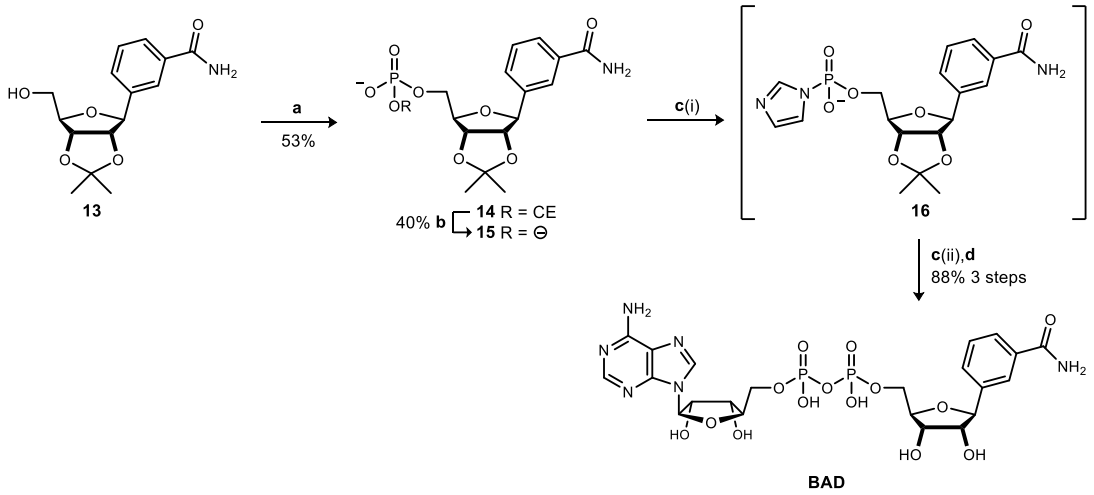

Scheme 3: Synthesis of BAD as described by Zatorski and co-workers. Reagents and conditions: [**a**] i: 2-cyanoethyl *N*,*N*-diisopropylchlorophosphoramidite, DIPEA, DCM. ii: β-cyanoethanol, tetrazole, MeCN. iii: *t*BuOOH. iv: NH_3, MeOH. [**b**] NH_3, MeOH, 55 °C. [**c**] i: CDI, DMF. ii: 2,3-*O*-isopropylidene AMP. [**d**] Dowex-50·H^+, H_2O.

Fluoro-Nicotinamide Adenine Dinucleotide. In the continuous search for NAD^+ analogues Sleath *et al* explored substituting the C^2-*OH* at the nicotinamide riboside.[47] Previous research had shown that the native NAD^+ hydroxyl at the C^2-position participates in base-catalyzed nicotinamide-glycosyl bond cleavage performed by enzymes such as ADP-ribosyltransferases and NAD^+-glycohydrolases. As part of their investigation three arabino-NAD^+ derivatives were synthesized, including fluoro-nicotinamide mononucleotide **25β** and fluoro-NAD^+ analogue ***F*-NAD$^+$** (Scheme 4).

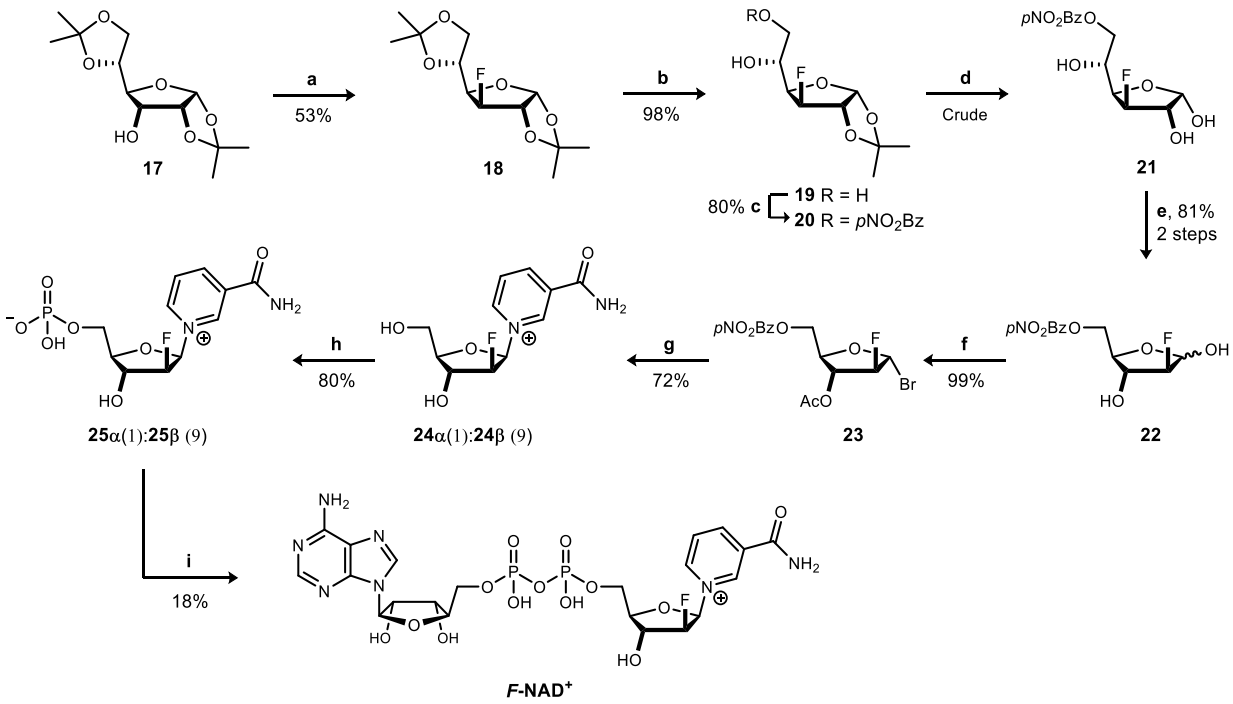

Scheme 4: Synthesis of *F*-NAD^+ as described by Sleath and co-workers. Reagents and conditions: [**a**] DAST, DCM/pyr, 0 °C. [**b**] H_2SO_4, dioxane/ethanol. [**c**] *p*-nitrobenzoyl chloride, DCM/pyr, -30 °C. [**d**] Dowex-50·H^+, dioxane:water, 80 °C. [**e**] $NaHCO_3$, $NaIO_4$, H_2O/MeCN. [**f**] i: Ac_2O, pyr. ii: HBr, AcOH, DCM. [**g**] i: Nicotinamide, MeCN. ii: NH_3, MeOH, 0 °C. [**h**] $POCl_3$, *m*-cresol, 5 °C. [**i**] i: Ac_2O, pyr. ii: $(PhO)_2POCl$, Bu_3N, DMF. iii: AMP, DMF. iv: NH_3, MeOH, 0 °C.

Sleath's synthesis started with DAST mediated fluorination of protected allofuranose **17**, showing typical S_N2-inversion of the stereochemistry. Selective deprotection of the terminal isopropylidene with dilute acid, followed by reprotection of primary hydroxyl with *p*-nitrobenzoyl chloride, provided alloside **20**. Transformation to the arabino-conformation was carried out via an oxidative cleavage method. After removal of the 1,2-*O*-isopropylidene, the produced diol was cleaved with sodium periodate, effectively converting the C^2-*OH* into the (open-chain) anomeric aldehyde, which, upon ring-closure with the original C^5-*OH*, generates the desired fluoro-arabinofuranose **22**. A one-pot acetylation-bromination procedure gave α-bromide **23** in over 95% diastereoisomeric excess. Anomeric displacement of the bromine with nicotinamide and consecutive ammonolysis of the ester-based protecting groups produced primarily beta-anomer **24β**. Separation of the α/β-mixture was postponed until after formation of *F*-NAD^+. To facilitate the solubility of the α/β-nicotinamide nucleotide derivative, the phosphorylation reaction was carried out in *m*-cresol with phosphoryl chloride[48], yielding fluorinated NMN analogue **25α** and **25β** as a diastereoisomeric mixture. The coupling reaction was accomplished via a modified version of the earlier discussed Michelson method, in which the secondary hydroxyl in **25** is acetylated *in situ* to accommodate

for the otherwise poor solubility of the NAD^+ derivative under the succeeding coupling conditions. Activation with diphenyl chlorophosphate and reaction of the activated intermediate with AMP successfully gave a mixture of *F*-NAD^+ and the α-nicotinamide diastereoisomer. *F*-NAD^+ was then isolated by chromatographic separation.

Fluoro-nicotinamides have been applied extensively to study ARTs, including a subclass of enzymes known as ADP-ribose cyclases (ARCs). The best-known ARCs are CD38 and CD157.[49] These transmembrane enzymes are employed by mammalian cells to metabolize NAD^+, generating ADPR and to a lesser extent cyclic ADP-ribose (cADPR).[50,51] The latter is a second messenger that regulates intercellular Ca^{2+} concentrations as part of cell signal transductions. CD38 has become known as a powerful marker for several human hematological tumor cell lines, and is directly involved in various cellular immune response mechanisms.[52] The involvement of CD38 in these type of physiological processes has led to a persistent scientific interest in its catalytic mechanism. In 2000, Sauve and co-workers established the active site's catalytic residue as the side chain carboxylate of glutamic acid 226.[53] This was demonstrated by exposing the enzyme to the above described fluorinated NMN analogue **25β** (Scheme 4), which reacted with Glu_{226} to provide a stable covalent enzyme-inhibitor intermediate, as was determined by mass spectrometry. The electronegative fluorine atom at the C^2-position significantly increases the dissociation energy of the anomeric ester bond towards the oxocarbenium-ion transition state, thereby drastically slowing down the succeeding hydrolysis or cyclization step. In 2010, Zhang *et al* complemented these results by publishing the first X-ray crystal structure of CD38, with irreversible covalent inhibitor *F*-NAD^+ bound to Glu_{226}.[54] By crystalizing *F*-NAD^+ with a Glu_{146}-mutant CD38, it was also discovered that the point removal of this second key residue abolishes CD38s hydrolytic activity, while greatly enhancing its cyclization activity.

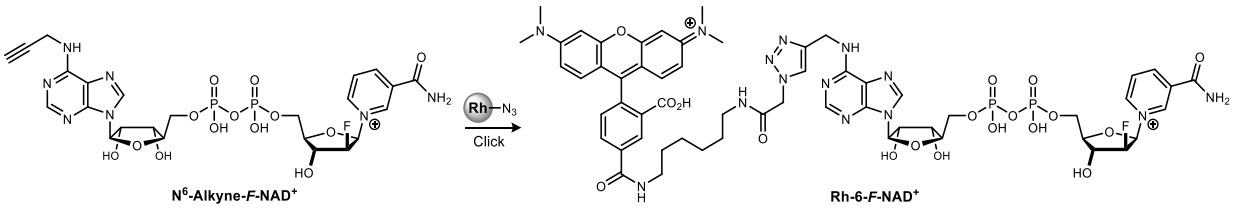

Figure 4: The structure of fluorescent activity-based probe Rh-6-F-NAD^+.

To study the CD38-mediated signal processes, Jiang and co-workers sought to develop a labeling method for the real-time monitoring of the enzyme. To this end they designed and synthesized a fluorescent activity-based probe based on *F*-NAD^+, aiming to take advantage of the covalent nature of the inhibitor.[55] Installation of a propargyl group onto the N^6-position of the adenine moiety enables click-conjugation with an azido bearing fluorophore (Figure 4). In their study Rhodamine was selected at the reporter group of choice. The resulting probe, Rh-6-*F*-NAD^+, successfully labeled CD38 in life cells.

Stabilized ADP-ribosylated Oligopeptides

Ever since poly-ADP-ribosylation of chromatin proteins was discovered to be involved in processes such as DNA-repair, cell division, inflammatory response and aging, there has been a growing interest in understanding these processes at a molecular level. However, the complexity of PARylation has led to scientific controversy regarding the target proteins and, most notably, the nature of the acceptor amino-acid(s). Structurally well-defined ADP-ribosylated oligopeptides were conceived as tools to help elucidate the biochemistry of PARylation. The first chemical synthesis of such constructs was described by van der Heden van Noort *et al* in 2011.[56] They recognized that the main difficulty in constructing the native mono- and poly-ADP-ribosylated peptides would be the chemical compatibility between the anomeric linkage (at the ribosylated amino acid), the pyrophosphate bridge and solid-phase peptide chemistry. The MARylation sites of a mammalian RhoA protein and a heptapeptide, based on the natural occurring *N*-terminus of the human histone, were selected as target molecules for their chemical endeavor. Although the latter is naturally PARylated at the glutamic acid residue, the presence of an anomeric ester bond was considered to be not feasible in the synthesis of the construct. Instead glutamine was incorporated as a bioisostere, having the more stable anomeric amide.

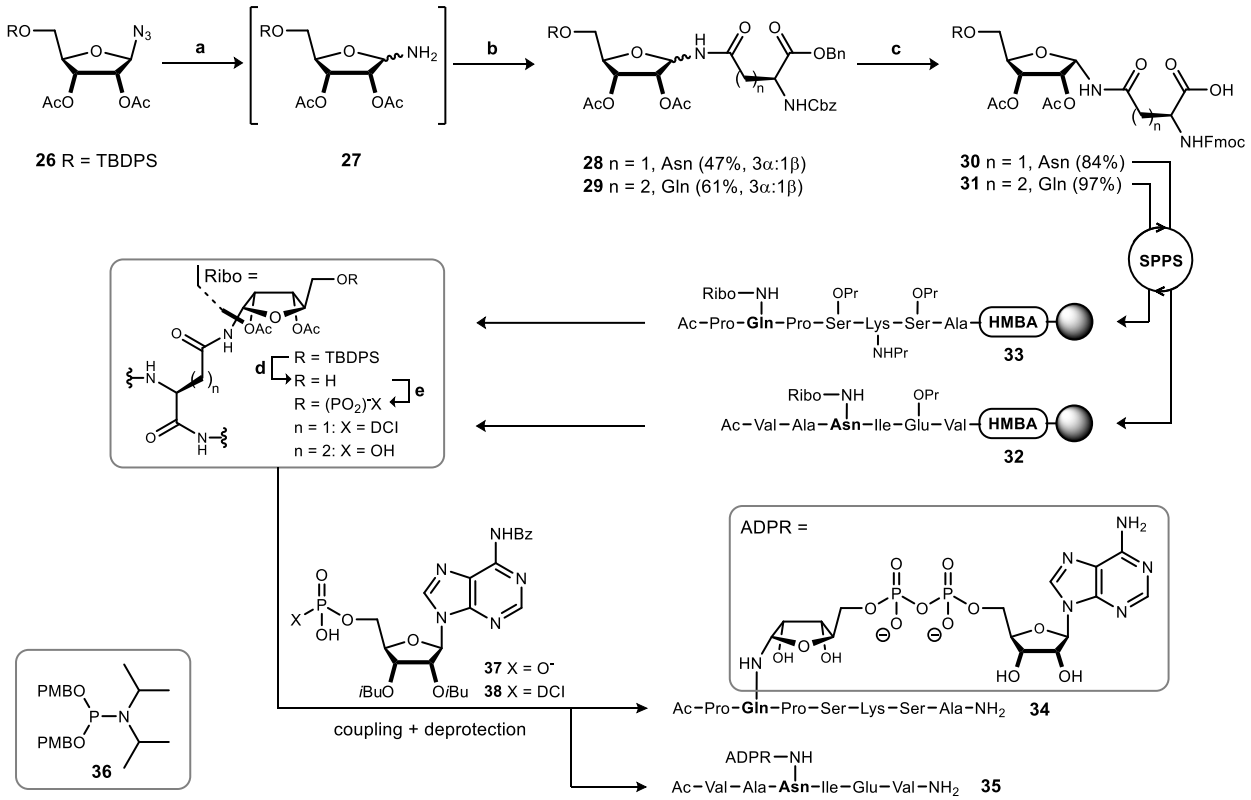

Scheme 5: Synthesis of ADP-ribosylated oligopeptides as described by van der Heden van Noort *et al*. Reagents and conditions: [**a**] PtO_2, H_2, EtOAc, 10 °C. [**b**] Z-Asp-OBn or Z-Glu-OBn, EDC·HCl, DCM. [**c**] i: 10% Pd/C, H_2, MeOH. ii: FmocOSu, $NaHCO_3$, H_2O /acetone. [**d**] HF in pyridine, 0 °C. [**e**] i: **38**, DCI, MeCN, 0 °C. ii: I_2, pyridine, 0 °C for **32** *or* *t*BuOOH ›› TFA for **33**.

A key step in the synthesis entailed the careful hydrogenation of β-azido-riboside **26**, to provide the unstable intermediate hemiaminal ether **27** (Scheme 5). Immediate *in situ* condensation with the corresponding Asn and Gln building blocks gave ribosylated amino acids **28** and **29**, respectively, as α/β-anomeric mixtures. After chromatographically separation, followed by protecting group manipulations, the acquired α-derivatives **30** and **31** were applied as building blocks in a standard solid-phase peptide synthesis. Phosphorylation of the immobilized ribosylated peptides was carried out with di(*p*-methoxybenzyl)-*N*,*N*-diisopropyl phosphoramidite (**36**), using dicyanoimidazole (DCI) as an activator. Constructing the ADPR pyrophosphate bridge for both peptides comprised the same methodology, using a different sequence of event. For ribosylated peptide **32**, iodine mediated oxidation of the installed di-*p*-methoxybenzyl phosphite led to the formation of an phosphorimidazolidate. This immobilized activated phosphate species was then coupled to adenosine monophosphate **37**. Alternatively, for peptide **33**, the introduced phosphite moiety was oxidized with *tert*-butyl hydroperoxide. Cleavage of the *p*-methoxybenzyl groups yielded the terminal phosphate, that was subsequently condensed with adenosine phosphorimidazolidate **38**. The latter approach turned out advantageous as an excess of the activated species could be applied. Global deprotection and release from solid support provided the desired ADP-ribosylated peptides **34** and **35**.

This line of research was continued by Kistemaker *et al*, who refined the strategy by preparing pre-phosphorylated amino acid-riboside building blocks (Scheme 6, **39**-**41**) and applying these in an improved methodology for the on-resin installment of the pyrophosphate.[34] The ribosylated amino-acid building blocks were incorporated into peptide fragments via a standard SPPS protocol to give immobilized ribosylated oligopeptide **42**. Using finely-tuned conditions, the *tert*-butyl groups could be eliminated, leaving the anomeric configuration intact. Next, the pyrophosphate was assembled by adapting the phosphoramidite–phosphonate methodology, as described by Gold and van Delft *et al*,[57] to the synthesis on solid-phase. The immobilized phosphate species **43** was condensed with adenosine phosphoramidite **45** in presence of 5-ethylthiotetrazole as an activator. Oxidation of the phosphite–phosphate intermediate by CSO, followed by global deprotection and concomitant release from solid support, yielded the respective ADP-ribosylated peptide **44**. In this way a multitude of biologically relevant MARylated peptides

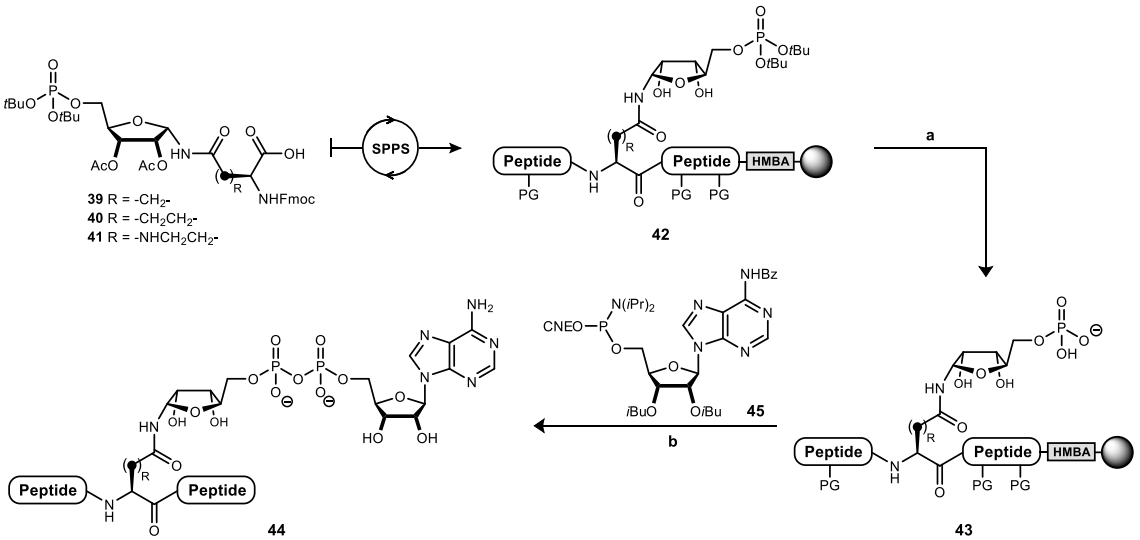

Scheme 6: Synthesis of ADP-ribosylated oligopeptides as described by Kistemaker *et al*. Reagents and conditions: [**a**] i: HCl:HFIP ii: Pyridine [**b**] i: ETT, MeCN ii: CSO, iii: DBU, iv: NH_3, TFE v: NH_4OH.

were synthesized and successfully used to study the substrate specificity of human MacroD2 and TARG1 macro-domains. **Chapter 4** of this thesis describes the synthesis of a mono-ADP-ribosylated H2B conjugate bioisostere wherein a *carba*-riboside is synthetically incorporated to stabilized the peptide-ribose glycosidic bond.

Although the synthesis strategies discussed above were successful in providing several MARylated peptides, each required distinct chemical modifications and highly tailored reaction conditions, and thus are not generally applicable. A practical approach which addressed this limitation was presented by Liu *et al* (Scheme 7).[58] By implementing click-chemistry, they enabled the post-synthetic introduction of the ADPr-moiety onto oligopeptides. First an azide functionalized amino acid is incorporated into the target peptide (**47**) through standard solid phase peptide synthesis. After release from solid support, an α-propargyl configured ADP-ribose building block is installed via the copper catalyzed azide-alkyne cycloaddition (CuAAC), resulting in a triazole-based linkage (**48**). Several derivatives of biologically relevant ADP-ribosylated proteins were prepared this way, including an ADPr-ubiquitin analogue that was phosphorylated naturally during biological evaluation, even though it contained an artificial triazole linkage.

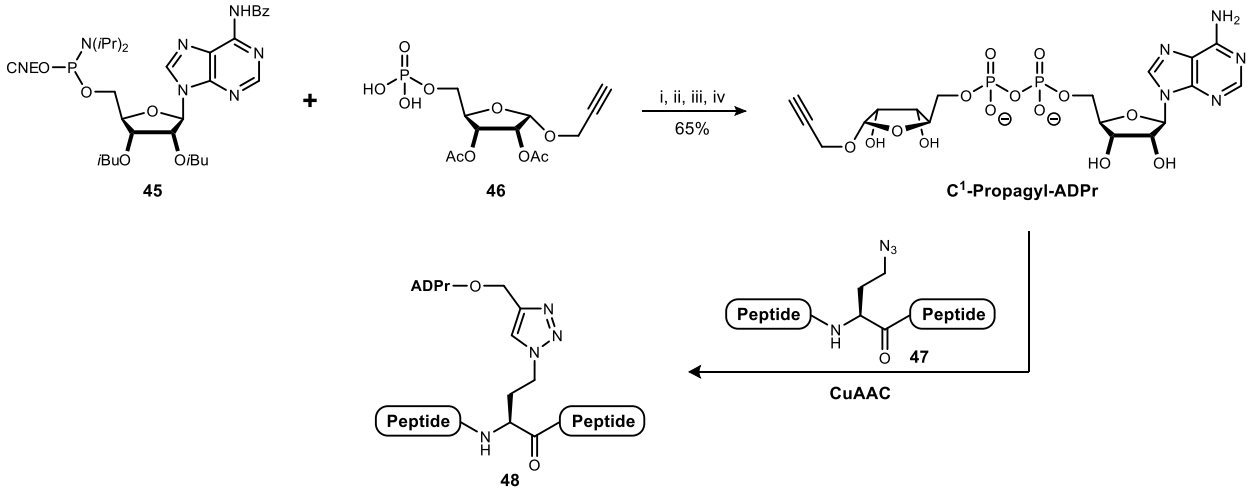

Scheme 7: Click based synthesis of artificial ADP-ribosylated peptides. Reagents and conditions: i: DCI, MeCN ii: *t*BuOOH, iii: DBU, iv: NH_4OH.

Methylene Bisphosphonates

Molecular tools are commonly designed on the basis of functionally relevant natural substrates, intermediates or metabolites. However, care should be taken when reactive or (enzymatically) degradable functionalities are involved in biological process of interest. This also holds true for pyrophosphates. A pyrophosphate moiety within a molecular tool can be considered a labile functionality for both synthesis and biological application, as it is susceptible to hydrolytic or enzymatic degradation. Methylene bisphosphonate are considered stable analogues of pyrophosphates and several common methods for installing these are discussed in the following section.

Terminal Methylene Bisphosphonates. Between 1963 and 1965, Meyers and co-workers published a series of articles on the preparation and implementation of methylene bisphosphates as stabilized

bioisosteres for pyrophosphates (Scheme 8).[59–61] In methylene bisphosphates the oxygen atom conjoining the two phosphates in the original pyrophosphate is replaced by a methylene, providing resistance to cleavage. The synthesis of adenosine methylene diphosphate (me-ADP, **42**) was accomplished by activation of methylenediphosphonic acid with *N*,*N*-dicyclohexylcarbodiimide (DCC), followed by coupling onto adenosine. A similar approach was applied in the synthesis of 2-me-ATP **43**. Here AMP was preactivated with DCC and subsequent condensation with methylenediphosphonic acid gave 2-me-ATP **43**. An alternative method entailing the reaction of adenosine 5-monophosphoramidate with methylenediphosphonic acid also led to the isolation of methylene triphosphate **43**.

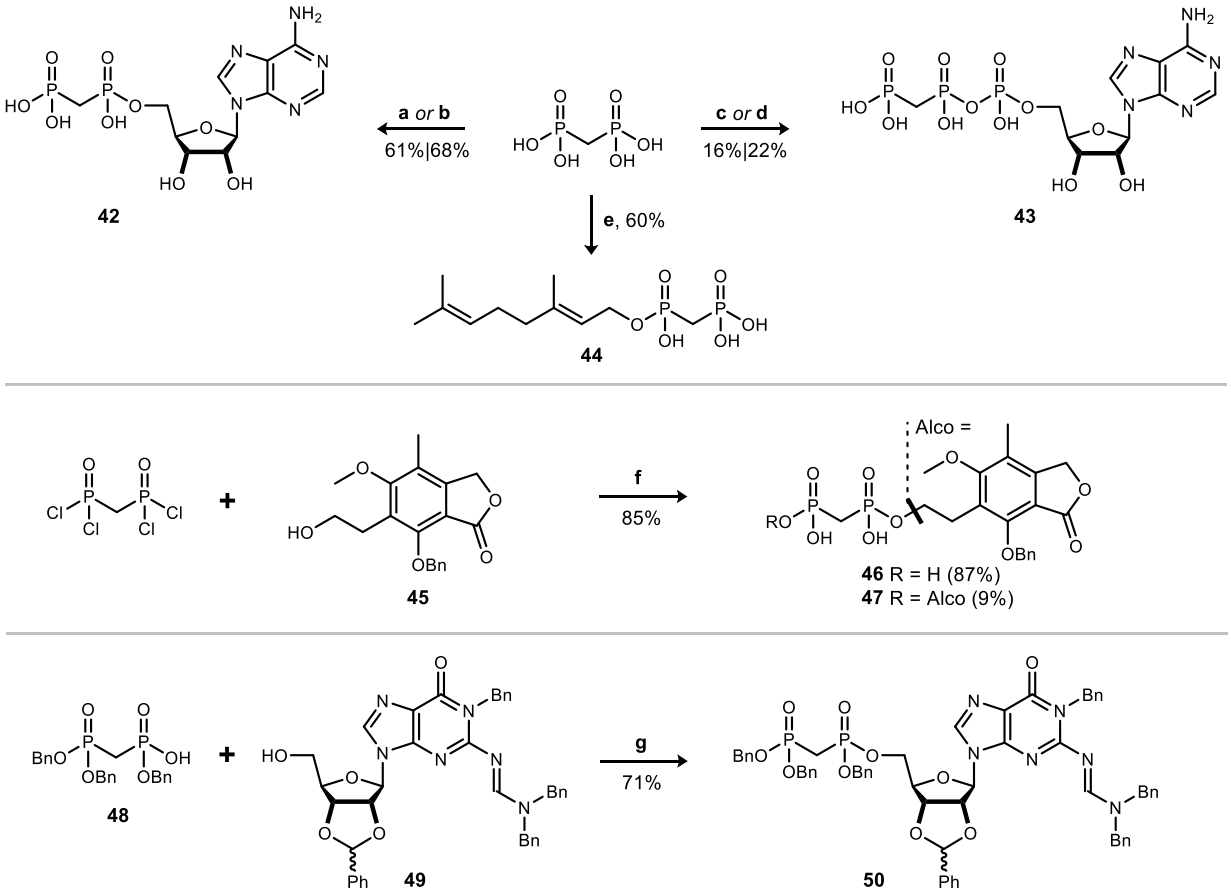

Scheme 8: Exemplified common methods for installing methylene bisphosphates. Reagents and conditions: [**a**] i: 2,3-isopropyl adenosine, DCC, pyr, 60 °C. ii: AcOH/H_2O, 100 °C. [**b**] i: Bu_4NOH, H_2O. ii: 5-tosyl-adenosine, MeCN. [**c**] AMP, DCC, pyr/H_2O. [**d**] Adenosine 5-monophosphoramidate, *o*-chlorophenol, pyr. [**e**] i: Bu_4NOH, H_2O. ii: 1-geranyl chloride, MeCN. [**f**] i: Alco-OH, $(EtO)_3PO$. ii TEAB, H_2O. [**g**] PPh_3, DEAD, THF, 60 °C.

Carbodiimide activation of methylenediphosphonic acid became a well-known strategy for the installation of methylene bisphosphonates. Another procedure to methylenediphosphates include the conversion of a specific alcohol into a leaving group through alkylsulfonation or halogenation and subsequent nucleophilic substitution by anionic methylene diphosphonate (Scheme 8, conditions b and e).[62,63] Alternatively, Lesiak *et al* make use of methylene bisphosphonic(dichloride) to directly phosphorylate alcohol **45** under basic conditions.[64] Upon quenching with water, the trichloromethylene diphosphonate ester intermediate is converted into respective methylenediphosphonic acid **46**. The small discrepancy in

reactivity between formed trichloromethylene diphosphonate ester and unreacted methylene bisphophonic(dichloride) results in the formation of minor amounts of symmetric diester **47**.[65] Hence, symmetric methylene bisphosphonates diesters can be accessed conveniently and in high yields by applying two equivalents of the alcohol instead.[66,67] Each of the discussed strategies install the bisphosphonate moiety in an unprotected fashion, which can be disadvantageous in terms of the solubility degree in common reaction solvents and the ease of purification. In 1998, Vincent and co-workers adopted a reported method for preparing phosphonate mono-esters, using modified Mitsunobu conditions, to the synthesis of guanosine methylene diphosphonate (me-GDP).[68,69] The tribenzylester of methylenediphosphonic acid (**48**) was coupled to the C^5-*OH* of protected guanosine **49** to give fully protected **50** that after silica column purification, reductive global debenzylation provided me-GDP in near quantitative yield.

Unsymmetric Methylene Bisphosphonates. Numerous biologically relevant pyrophosphates are unsymmetric diesters with two different alcohols incorporated; for example NAD^+ and ADPr. In 1986, Meyer and co-workers were the first to synthesize an unsymmetric methylene bisphosphonate bioisostere, based on NAD^+, with the objective to raise antibodies for the detection of ADP-ribose conjugates.[70] me-NAD^+ (Figure 5) was prepared by coupling me-ADP **51** with 2,3-*O*-isopropylidene nicotinamide riboside using the earlier described DCC coupling conditions, followed by acidic deprotection. At the same time, Marquez *et al* implemented the methylene bisphosphonate moiety in an effort to further enhance the effectiveness of known antitumor agent thiazole-4-carboximade adenine dinucleotide (TAD), using identical coupling conditions.[71] In both cases the yields were relatively low; 20% and 36% respectively. Mechanistic study of the DCC-coupling reaction by Pankiewicz and co-workers

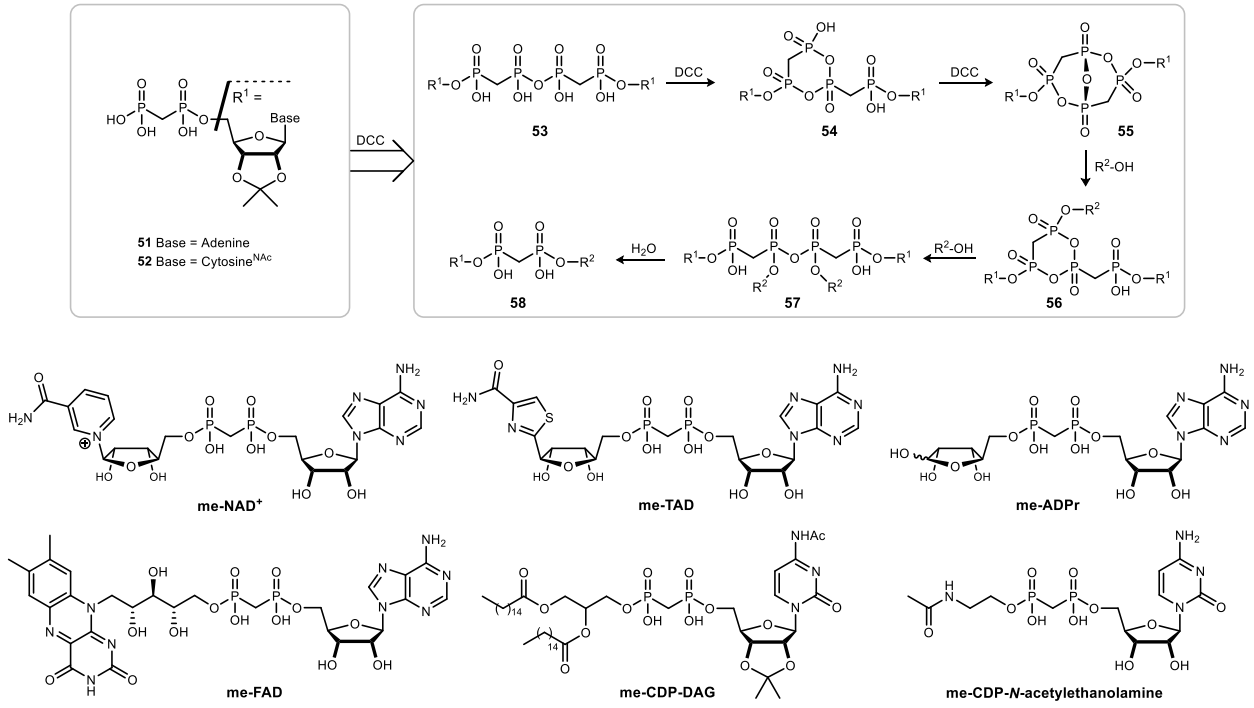

Figure 5: Outlined in grey: The mechanism behind the formation of unsymmetric methylene bisphosphonate nucleotides via carbodiimide activation. Below: An overview of unsymmetric methylene bisphosphonate bioisosteres prepared via DCC coupling. With the exception of me-NAD^+, each of these were prepared by Pankiewicz *et al* using the appropriate acceptor building blocks, in order: 2,3-*O*-isopropyl thiazofurin, 2,3-*O*-isopropyl D-ribose, riboflavin, 1,3-dipalmitoyl glycol, *N*-acetylethanolamine.

revealed that me-ADP dimerizes rapidly upon activation with stoichiometric DCC, forming the corresponding tetraphosphonate analogue (i.e. **53**). The dimer was isolated and proved to be unreactive towards alcohols. This guided them to investigate alternative reaction pathways towards the formation of unsymmetric diesters. ^{31}P NMR spectroscopy revealed that tetraphosphonate **53** could undergo a second and third DCC-activation, followed by two respective intramolecular condensation reactions, giving rise to bicyclic intermediate **55**. Addition of an acceptor alcohol to **55** at 60 °C allows for nucleophilic attack on either bispyrophosphonic position (**56**). Iteration of this reaction on the remaining bispyrophosphonate leads to tetraester **57**, which is effectively the pyrophosphoric dimer of the desired (un)symmetric methylene bisphosphonate. Hence, final hydrolysis of **57** by the addition of water produces two equivalents of methylene bisphosphonate **58**. By implementing these findings into an improved procedure, five unsymmetric methylene bisphosphonates were prepared; me-TAD, me-ADPr, me-FAD, me-CDP-DAG and me-CDP-*N*-acetylethanolamine. In 1999, Ikeda reported an adaptation of Vincent's Mitsunobu methodology for the synthesis of phosphor-protected unsymmetric methylene bisphosphonates.[72] After coupling tribenzyl methylene phosphonate ester **48**, the acquired thiazofurin tetraester could selectively be mono-debenzylated at the terminal phosphonate using stoichiometric amounts of DABCO in refluxing toluene. This set the stage for the installment of an adenosine building block, using the same Mitsunobu conditions, yielding fully protected me-TAD in 72% yield. The carbodiimide and Mitsunobu activations have become established coupling methods for the synthesis of both terminal and unsymmetric methylene bisphosphonates. However, the conditions these methods impose were considered too constraining when it came to the synthesis of methylene bisphosphonate analogues of complex biomolecules such as poly-ADP-ribose fragments. Therefore, an improved methodology for the synthesis of terminal-, symmetric- and unsymmetric methylene bisphosphonates could facilitate PARylation related research. New reagents and complimentary methodology to this end are described in detail in **Chapter 2** and **Chapter 3** of this thesis.

NAD$^+$ Analogues in PARylation Target Labeling

NAD$^+$ analogues functionalized with a ligation handle have been developed and employed in the mapping of ADP-ribosylation activity. The analogues that are accepted as cofactors by a PARP will be metabolically incorporated, carrying over the ligation handles to the produced ADPr-polymer, thereby enabling the visualization of the ADP-ribosylated protein via bioorthogonal labeling. This was first demonstrated by the group of Lin, who used 6- or 8-*N*-propargyl-NAD$^+$ to study PARP-1 activity *in vitro* (Figure 6).[73] Thirty minute incubation of ssDNA with either *N*-propargyl-NAD$^+$ was followed by click-chemistry conjugation of an azido-bearing Rhodamine label. After SDS-PAGE, this allowed for Western blot analysis of tagged auto-ADP-ribosylated PARP-1. In a similar manner, the more efficient 6-*N*-propargyl-NAD$^+$ was employed to label over 70 PARP-1 PARylation substrate proteins. Complimentary results were found by the group of Marx using a 2-alkyne-NAD$^+$ analogue to visualize the PARylation of PARP-1 and Histone H1.2.[74] Complete removal of the modified adenosine C^2-*OH* resulted, as expected, in total loss of poly-ADP-ribose assembly, while deletion of the C^3-*OH* only leads to diminished PAR formation. Small handle modifications were tolerated at the 6-position of adenine, but most optimal were modifications at the 2-position, at which even bulky substituents are accepted.[75] Two accordingly fitted NAD$^+$ analogues, using a cyclooctyne for strain-promoted azide-alkyne cycloaddition ligation and a cyclopropene for the inverse-electron-demand Diels–Alder ligation, were successfully applied in the intracellular visualization of DNA damage induced PARylation.

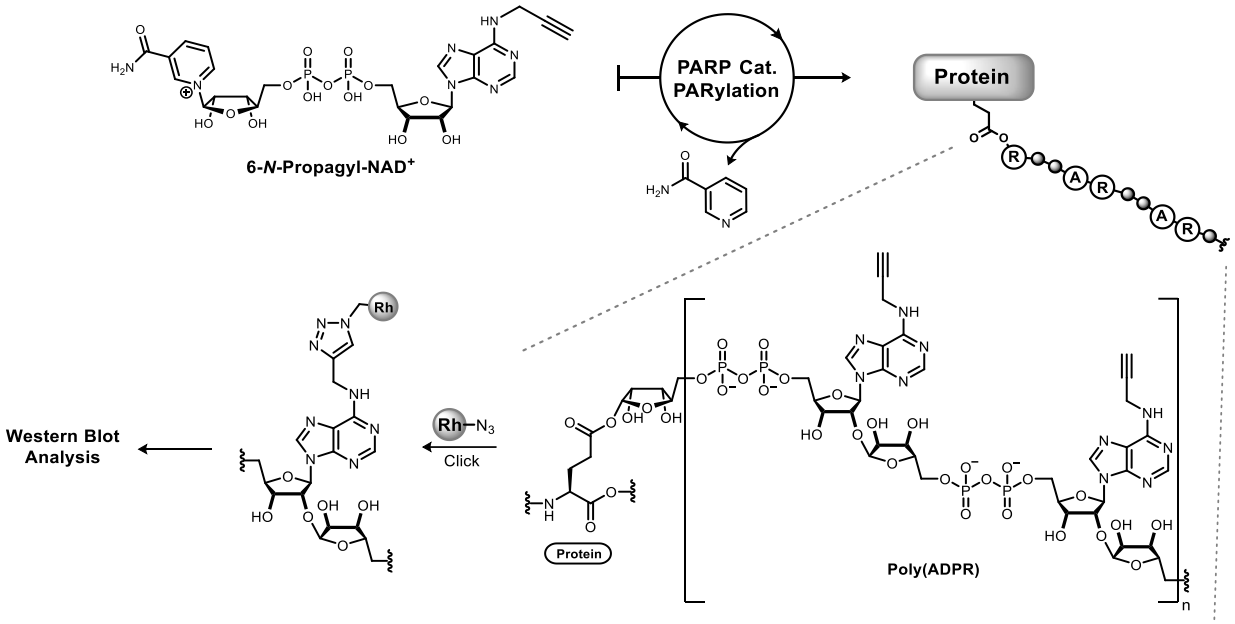

Figure 6: The labeling of PARylated proteins exemplified with 6-*N*-propagyl-NAD$^+$ as reported by the team of Lin. The propargyl bearing NAD$^+$ analogue is metabolically incorporated into the ADPr-polymer. A rhodamine reporter-group is then linked using click chemistry, allowing for Western Blot analysis.

Although global identification of PARylation targets had been achieved through use of handle fitted NAD$^+$ analogues, identifying specific PARylation targets for each of the 17 PARP members remained complicated due to their unanimous use of NAD$^+$ as a cofactor. Cohen and co-workers presented an elegant solution by engineering individual PARP binding pockets to match an orthogonally attuned NAD$^+$ analogue.[76] Based on the crystal structure of substrate-bound PARP-1, it was established that mutating Lys_{903} to an alanine would create a unique hydrophobic pocket. A complementary ethyl substituent at the C^5-position on the nicotinamide moiety was installed to achieve specific pairing with the engineered PARP. Using this analogue-sensitive strategy, 42 PARylation targets were identified for PARP-1 and 301 for PARP-2, with a 52% and 7% respective target overlap. The group of Kraus reported a similar analogue-sensitive approach.[77] The 8-position of the adenine moiety was instead selected as the modification site, as substituents at this position are poorly tolerated by wild-type PARPs. A library of 11 NAD$^+$ analogues were synthesized bearing various R-groups at the 8-position and screened against 20 PARP-1 mutants. From the data it was deduced that mutating Leu_{877} to alanine would result in the desired analogue-sensitivity. Modifying the 8-position of the adenine had the additional advantage that the introduced R-group could simultaneously bear function as a ligation handle. With this in mind, clickable 8-Bu(3-yne)T-NAD$^+$ was designed as the complementary analogue for asPARP-1. Moreover, this particular analogue also demonstrated activity with similarly engineered asPARP-2 and asPARP-3 mutants. Interestingly, 167 protein targets were found for PARP-1, 87 for PARP-2 and 401 for PARP-3, which differs significantly from the findings of Cohen. A reason for this discrepancy was not discussed in the article, but a possible explanation is that the mutations affect protein targeting.

Bioorthogonal Ligation

The field of bioorthogonal chemistry aims to develop chemical reactions that are applicable *in vivo* without affecting natural occurring biochemical processes. In order to do so effectively, the artificially introduced reactive moieties have to be inert to the diverse spectrum of functional groups that reside in a biological system, while still demonstrating specific reactivity towards each other. In addition, a bioorthogonal reaction must be tolerable to aqueous conditions and physiological pH, while displaying sufficiently fast kinetics for the reaction to proceeds rapidly at sub-micromolar concentrations, as this is desired for most biological labeling experiments. Bioorthogonal reactions have made a significant impact to the field of molecular biology, granting tools to study glycosylation chemistry in living cells and animals[78], enable the conjugation of functional moieties to therapeutically relevant proteins[79], and facilitate the *in vivo* assembly of imaging agents.

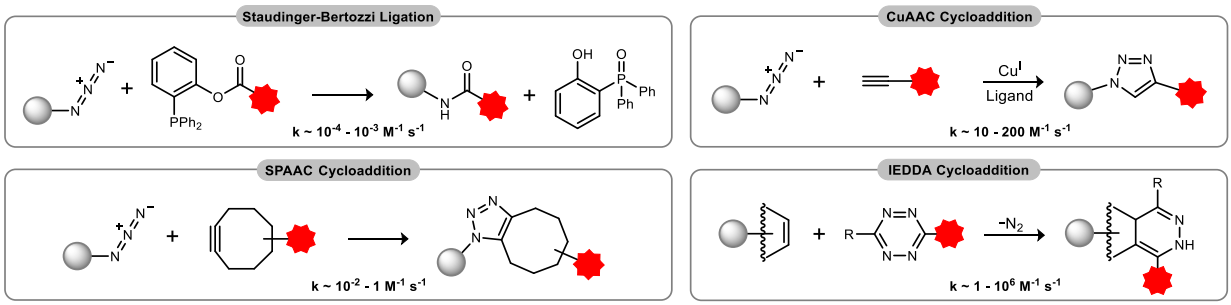

Figure 7: Examples of bioorthogonal reactions used as labeling and conjugation strategies and their relative approximate rates.

Several (pseudo) bioorthogonal two-step labeling techniques have been developed, the most established methods of which are (Figure 7); Staudinger–Bertozzi ligation[80], Cu^{I}-catalyzed alkyne–azide cycloaddition (CuAAC)[81,82], Huisgen strain-promoted alkyne–azide cycloadditions (SPAAC)[83,84] and inverse-electron-demand Diels–Alder reaction (IEDDA).[85] Except for the last, each of these methods utilizes the azide functionality. Azides have virtually no precedence among biomolecules and show exceptional biocompatibility. The groups isoelectric nature allows it to act as both an electrophile and a nucleophile, which enables participation in a wide variety of reactions, often thermodynamically driven by the expulsion of nitrogen. Staudinger–Bertozzi ligation applies an *o*-triarylphosphine benzoate handle to react with an azide functionalized (bio)molecule. After nucleophilic attack of the phosphine onto the azide, the intermediate aza-ylide cyclizes onto the adjacent ester to covalently link the azide substituent in the form of an amide bond. The reaction has been used to label biomolecules in cells and living animals.[86,87] The primary disadvantage of the Staudinger–Bertozzi ligation are the relative slow reaction kinetics, with a second order rate constant of approximately 10^{-3} M^{-1} s^{-1}.[88] Secondly, the *o*-triarylphosphine benzoate moiety is susceptibility to oxidation and enzymatic cleavage.

Ligation strategies based on alkyne-azide [3 + 2] cycloadditions comes in two variation; CuAAC and SPAAC. The reactions are similar in that they conjoin the two reaction partners by producing a triazole linkage. The first entails the reaction of an azide with a terminal alkyne, catalyzed by Cu^{I} salts. The reaction displays considerably faster kinetics than the Staudinger–Bertozzi ligation (± 10 – 200 M^{-1} s^{-1})[89], but cannot be considered fully bioorthogonal because of the reliance on a cytotoxic copper catalyst. The SPAAC variant utilizes ring strained cyclooctynes to accelerate the alkyne-azide reaction into a bioorthogonally acceptable range without depending on a copper catalyst, demonstrating rate constants of 10^{-2} to 1 M^{-1}

s^{-1}.[90] The hydrophobic nature of the cyclooctyne moiety can, however, negatively affect water solubility of the often already lipophilic reporter groups. Both CuAAC and SPAAC have been used to label biomolecules within complex biological systems, including living mammalian cells and animals.[91–93]

The IEDDA reaction is the most recent addition to bioorthogonal reactions. It involves a Diels–Alder reaction between an electron deficient tetrazine (diene) and strained alkene or alkyne. The initial [4+2]-cycloaddition results in a highly strained bicyclic intermediate, consisting of two fused six-membered rings. Driven by the elevation of ring strain, the adduct undergoes a retro-Diels–Alder reaction to expulse nitrogen. Alkene dienophiles afford the corresponding 4,5-dihydropyridazine, while alkynes yield the respective pyridazines.

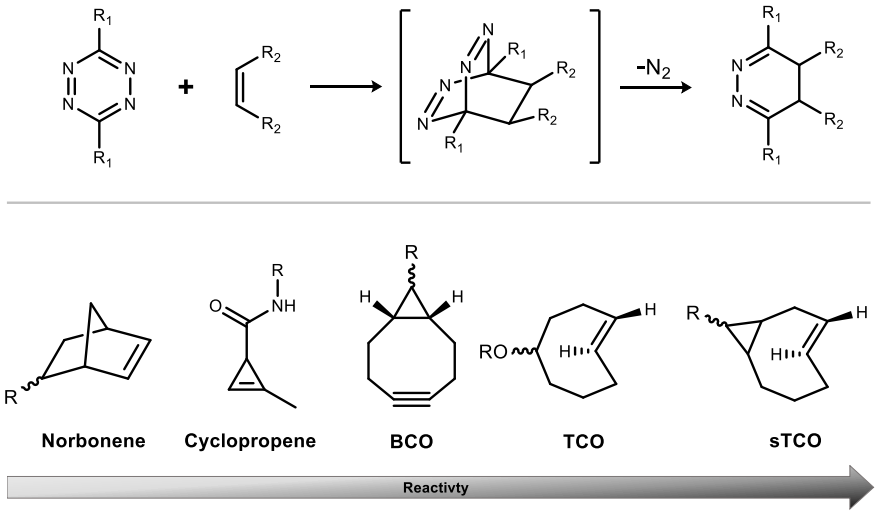

Figure 8: Top: The mechanism of the IEDDA reaction. Bottom: In order of increasing reactivity, five strained alkenes that have been applied as tetrazine reaction partners for the IEDDA-based ligation strategy.

The IEDDA reaction rates are affected by electronic effects of the substituents in the reaction partners, dienophile ring strain and steric effects. For the tetrazine reactant, electron withdrawing substituents lower the LUMO energy and thereby accelerate the reaction rate, whereas electron donating substituents adjacent to the dienophile act conversely by raising the respective HOMO energy.[94–96] Ring strain plays an even more profound role in determining the reaction rate constants. The increase in reactivity caused by this phenomena is two-sided. Firstly, strain heightens the dienophiles HOMO energy and as a result the reaction rate constant. This was empirically substantiated by Saur *et al* who demonstrated that the rate constant correlated with ring strain in the following order: cyclopropene › cyclobutene › cyclopentene › cyclohexene › cyclooctene.[97] The most highly reactive dienophiles were found to be *trans*-cyclooctenes (TCO), however, which have a lower degree of ring strain than for example the less reactive cyclopropenes. A computational study by Houk *et al* endorsed these findings, and additionally exposed that the structural distortion, caused by the adopted TCO crown conformation, mimics the transition state geometry.[98] Consequently, significantly less distortion energy is required for the dienophile to enter a productive transition state, increasing the rate constant. Installing an opposing cyclopropane in TCO forces the ring from a crown conformation to a half-chair conformation, further lowering the distortion energy required, thereby enhancing the reaction rate 160-fold.[99]

Steric effects induced by substituents on either tetrazine or dienophile side have similar dampening effect on reactivity, which can be contributed to both steric repulsion and raised distortion energies. Overall, the IEDDA reaction exhibiting the fastest reaction kinetics among bioorthogonal reactions, with reported rate constants of up to 10^6 M^{-1} s^{-1}. The main drawback of the IEDDA ligation strategy is that both the tetrazine and most reactive dienephiles are relative lipophilic and sterically encumbered. These properties may influence the water solubility and biological response of the functionalized molecules. **Chapter 5** describes the synthesis, reaction kinetics and biochemical implementation of *N*-acylazetines as compact hydrophilic ligation handles for the IEDDA-based bioorthogonal strategy. While **Chapter 6** delves further into the reaction kinetics, isolating the effects of electron induction and ring strain on the dienophilicity of acylenamines.

References

1. P. A. Levene, *J. Biol. Chem.* **1919**, *40*, 415–424.
2. F. Lipmann, *Bacteriol. Rev.* **1953**, *17*, 1–16.
3. P. E. Stein, A. Boodhoo, G. D. Armstrong, S. A. Cockle, M. H. Klein, R. J. Read, *Structure* **1994**, *2*, 45–57.
4. C. Schleberger, H. Hochmann, H. Barth, K. Aktories, G. E. Schulz, *J. Mol. Biol.* **2006**, *364*, 705–715.
5. S. Han, A. S. Arvai, S. B. Clancy, J. A. Tainer, *J. Mol. Biol.* **2001**, *305*, 95–107.
6. C. E. Bell, D. Eisenberg, *Biochemistry* **1996**, *35*, 1137–1149.
7. R.-G. Zhang, D. L. Scott, M. L. Westbrook, S. Nance, B. D. Spangler, G. G. Shipley, E. M. Westbrook, *J. Mol. Biol* **1995**, *115*, 563–573.
8. M. O. Hottiger, P. O. Hassa, B. Lüscher, H. Schüler, F. Koch-Nolte, *Trends Biochem. Sci.* **2010**, *35*, 208–219.
9. G. Glowacki, R. Braren, K. Firner, M. Nissen, M. Kühl, P. Reche, F. Bazan, M. Cetkovic-Cvrlje, E. Leiter, F. Haag, et al., *Protein Sci.* **2009**, *11*, 1657–1670.
10. S. Laing, M. Unger, F. Koch-Nolte, F. Haag, *Amino Acids* **2011**, *41*, 257–269.
11. J. D. Steffen, J. R. Brody, R. S. Armen, J. M. Pascal, *Front. Oncol.* **2013**, *3*.
12. B. A. Gibson, W. L. Kraus, *Nat. Rev. Mol. Cell Biol.* **2012**, *13*, 411–424.
13. S. Vyas, I. Matic, L. Uchima, J. Rood, R. Zaja, R. T. Hay, I. Ahel, P. Chang, *Nat. Commun.* **2014**, *5*, 4426.
14. A. Ruf, V. Rolli, G. De Murcia, G. E. Schulz, *J. Mol. Biol.* **1998**, *278*, 57–65.
15. Y. Zhang, J. Wang, M. Ding, Y. Yu, *Nat. Methods* **2013**, *10*, 981–984.
16. R. K. Morgan, M. S. Cohen, *ACS Chem. Biol.* **2015**, *10*, 1778–1784.
17. G. T. Marsischky, B. A. Wilson, R. J. Collier, *J. Biol. Chem.* **1995**, *270*, 3247–3254.
18. E. Barkauskaite, G. Jankevicius, I. Ahel, *Mol. Cell* **2015**, *58*, 935–946.
19. R. Martello, A. Mangerich, S. Sass, P. C. Dedon, A. Bürkle, *ACS Chem. Biol.* **2013**, *8*, 1567–1575.
20. A. Pines, M. G. Vrouwe, J. A. Marteijn, D. Typas, M. S. Luijsterburg, M. Cansoy, P. Hensbergen, A. Deelder, A. de Groot, S. Matsumoto, et al., *J. Cell Biol.* **2012**, *199*, 235–249.
21. P. Reynolds, S. Cooper, M. Lomax, P. O'Neill, *Nucleic Acids Res.* **2015**, *43*, 4028–4038.
22. S. Petrucco, *Nucleic Acids Res.* **2003**, *31*, 6689–6699.
23. M. Langelier, P. Adp-ribosyl, J. L. Planck, S. Roy, J. M. Pascal, *Structure* **2012**, *728*, 728–733.
24. I. Gibbs-Seymour, P. Fontana, J. G. M. Rack, I. Ahel, *Mol. Cell* **2016**, *62*, 432–442.
25. G. G. Poirier, G. de Murcia, J. Jongstra-Bilen, C. Niedergang, P. Mandel, *Proc. Natl. Acad. Sci. U. S. A.* **1982**, *79*, 3423–3427.
26. K. W. Caldecott, S. Aoufouchi, P. Johnson, S. Shall, *Nucleic Acids Res.* **1996**, *24*, 4387–4394.
27. S. Messner, M. Altmeyer, H. Zhao, A. Pozivil, B. Roschitzki, P. Gehrig, D. Rutishauser, D. Huang, A. Caflisch, M. O. Hottiger, *Nucleic Acids Res.* **2010**, *38*, 6350–6362.
28. Y. Zhang, J. Wang, M. Ding, Y. Yu, *Nat. Methods* **2013**, *10*, 981–984.
29. F. Rosenthal, P. Nanni, S. Barkow-Oesterreicher, M. O. Hottiger, *J. Proteome Res.* **2015**, *14*, 4072–4079.
30. O. Leidecker, J. J. Bonfiglio, T. Colby, Q. Zhang, I. Atanassov, R. Zaja, L. Palazzo, A. Stockum, I. Ahel, I. Matic,

Nat. Chem. Biol. **2016**, *12*, 998–1000.
31. J. M. Pleschke, H. E. Kleczkowska, M. Strohm, F. R. Althaus, *J. Biol. Chem.* **2000**, *275*, 40974–40980.
32. P. L. Panzeter, C. A. Realini, F. R. Althaus, *Biochemistry* **1992**, *31*, 1379–85.
33. P. O. Hassa, S. S. Haenni, M. Elser, M. O. Hottiger, *Microbiol. Mol. Biol. Rev.* **2006**, *70*, 789–829.
34. H. A. V. Kistemaker, A. P. Nardozza, H. S. Overkleeft, G. A. van der Marel, A. G. Ladurner, D. V. Filippov, *Angew. Chemie - Int. Ed.* **2016**, *55*, 10634–10638.
35. M. F. Langelier, L. Zandarashvili, P. M. Aguiar, B. E. Black, J. M. Pascal, *Nat. Commun.* **2018**, *9*, DOI 10.1038/s41467-018-03234-8.
36. A. C. Nottbohm, R. S. Dothager, K. S. Putt, M. T. Hoyt, P. J. Hergenrother, **2007**, *1*, 2066–2069.
37. K. Ueda, O. Hayaishi, *Annu. Rev. Biochem.* **1985**, *54*, 73–100.
38. J. T. Slama, A. M. Simmons, *Biochemistry* **1988**, *27*, 183–193.
39. J. C. Jagt, A. M. van Leusen, *J. Org. Chem.* **1974**, *39*, 564–566.
40. R. C. Cermak, R. Vince, *Tetrahedron Lett.* **1981**, *22*, 2331–2332.
41. B. L. Kam, N. J. Oppenheimer, *J. Org. Chem.* **1981**, *46*, 3268–3272.
42. J. T. Slama, C. Radziejewski, S. R. Oruganti, E. T. Kaiser, *J. Am. Chem. Soc.* **1984**, *106*, 6778–6785.
43. K. Furusawa, M. Sekine, T. Hata, *J. Chem. Soc. Perkin Trans. 1* **1976**, 1711–1716.
44. K. Krohn, H. Heins, K. Wielckens, *J. Med. Chem.* **1992**, *35*, 511–517.
45. G. Kamran, P. K. D., K. J. A., B. J. J., M. V. E., C. D. A., M. Anne, S. Dominic, K. Karsten, J. H. N., *Int. J. Cancer* **1994**, *56*, 892–899.
46. A. Zatorski, K. A. Watanabe, S. F. Carr, B. M. Goldstein, K. W. Pankiewicz, *J. Med. Chem.* **1996**, *39*, 2422–2426.
47. A. L. Handlon, N. J. Oppenheimer, P. R. Sleath, *J. Org. Chem.* **1991**, *56*, 3608–3613.
48. K. ichi Imai, S. Fujii, K. Takanohashi, Y. Furukawa, T. Masuda, M. Honjo, *J. Org. Chem.* **1969**, *34*, 1547–1550.
49. A. Czura, C. Czura, *Mol. Med.* **2006**, *12*, 1.
50. H. Kim, E. L. Jacobson, M. K. Jacobson, *Science (80-.).* **1993**, *261*, 1330 LP – 1333.
51. M. Howard, J. C. Grimaldi, J. F. Bazan, F. E. Lund, L. Santos-Argumedo, R. M. Parkhouse, T. F. Walseth, H. C. Lee, *Science (80-.).* **1993**, *262*, 1056 LP – 1059.
52. S. Partida-Sánchez, D. A. Cockayne, S. Monard, E. L. Jacobson, N. Oppenheimer, B. Garvy, K. Kusser, S. Goodrich, M. Howard, A. Harmsen, et al., *Nat. Med.* **2001**, *7*, 1209.
53. A. A. Sauve, H. Deng, R. H. Angeletti, V. L. Schramm, *J. Am. Chem. Soc.* **2000**, *122*, 7855–7859.
54. H. Zhang, R. Graeff, Z. Chen, L. Zhang, L. Zhang, H. Lee, Q. Hao, *J. Mol. Biol.* **2011**, *405*, 1070–1078.
55. H. Jiang, J. Congleton, Q. Liu, P. Merchant, F. Malavasi, H. C. Lee, Q. Hao, A. Yen, H. Lin, **2009**, 1658–1659.
56. G. J. Van Der Heden Van Noort, M. G. Van Der Horst, H. S. Overkleeft, G. A. Van Der Marel, D. V. Filippov, *J. Am. Chem. Soc.* **2010**, *132*, 5236–5240.
57. H. Gold, P. Van Delft, N. Meeuwenoord, J. D. C. Codée, D. V. Filippov, G. Eggink, H. S. Overkleeft, G. A. Van Der Marel, *J. Org. Chem.* **2008**, *73*, 9458–9460.
58. Q. Liu, H. A. V Kistemaker, S. Bhogaraju, I. Dikic, H. S. Overkleeft, G. A. van der Marel, H. Ovaa, G. J. van der Heden van Noort, D. V Filippov, *Angew. Chemie Int. Ed.* **2017**, *57*, 1659–1662.
59. T. C. Myers, K. Nakamura, J. W. Flesher, *J. Am. Chem. Soc.* **1963**, *85*, 3292–3295.
60. T. C. Myers, L. N. Simon, *J. Org. Chem.* **1965**, *30*, 443–446.
61. T. C. Myers, K. Nakamura, A. B. Danielzadeh, *J. Org. Chem.* **1965**, *30*, 1517–1520.
62. V. M. Dixit, C. D. Poulter, *Tetrahedron Lett.* **1984**, *25*, 4055–4058.
63. V. J. Davisson, A. B. Woodside, T. R. Neal, K. E. Stremler, M. Muehlbacher, C. D. Poulter, *J. Org. Chem.* **1986**, *51*, 4768–4779.
64. K. Lesiak, K. A. Watanabe, J. George, K. W. Pankiewicz, *J. Org. Chem.* **1998**, *63*, 1906–1909.
65. K. W. Pankiewicz, K. B. Lesiak-Watanabe, K. A. Watanabe, S. E. Patterson, H. N. Jayaram, J. A. Yalowitz, M. D. Miller, M. Seidman, A. Majumdar, G. Prehna, et al., *J. Med. Chem.* **2002**, *45*, 703–712.
66. D. C. Stepinski, D. W. Nelson, P. R. Zalupski, A. W. Herlinger, *Tetrahedron* **2001**, *57*, 8637–8645.
67. D. C. Stepinski, A. W. Herlinger, *Synth. Commun.* **2002**, *32*, 2683–2690.
68. D. A. Campbell, *J. Org. Chem.* **1992**, *57*, 6331–6335.
69. S. Vincent, S. Grenier, A. Valleix, C. Salesse, L. Lebeau, C. Mioskowski, *J. Org. Chem.* **1998**, *63*, 7244–7257.
70. T. Meyer, H. Hilz, *Eur. J. Biochem.* **1986**, *155*, 157–165.
71. V. E. Marquez, C. K. H. Tseng, G. Gebevehu, D. A. Cooney, G. S. Ahluwalia, J. A. Kelley, M. Dalai, R. W. Fuller,

Y. A. Wilson, D. G. Johns, *J. Med. Chem.* **1986**, *29*, 1726–1731.
72. H. Ikeda, E. Abushanab, V. E. Marquez, *Bioorganic Med. Chem. Lett.* **1999**, *9*, 3069–3074.
73. H. Jiang, J. H. Kim, K. M. Frizzell, W. L. Kraus, H. Lin, *J. Am. Chem. Soc.* **2010**, *132*, 9363–9372.
74. Y. Wang, D. Rösner, M. Grzywa, A. Marx, *Angew. Chemie - Int. Ed.* **2014**, *53*, 8159–8162.
75. S. Wallrodt, A. Buntz, Y. Wang, A. Zumbusch, A. Marx, *Angew. Chemie - Int. Ed.* **2016**, *55*, 7660–7664.
76. I. Carter-O'Connell, H. Jin, R. K. Morgan, L. L. David, M. S. Cohen, *J. Am. Chem. Soc.* **2014**, *136*, 5201–5204.
77. B. A. Gibson, Y. Zhang, H. Jiang, K. M. Hussey, J. H. Shrimp, H. Lin, F. Schwede, Y. Yu, W. L. Kraus, *Science (80-.).* **2016**, *353*, 45–50.
78. A. A. Neves, H. Stöckmann, Y. A. Wainman, J. C.-H. Kuo, S. Fawcett, F. J. Leeper, K. M. Brindle, *Bioconjug. Chem.* **2013**, *24*, 934–941.
79. B. Oller-Salvia, G. Kym, J. W. Chin, *Angew. Chemie Int. Ed.* **2018**, *57*, 2831–2834.
80. E. Saxon, C. R. Bertozzi, *Science (80-.).* **2000**, *287*, 2007–2010.
81. V. V Rostovtsev, L. G. Green, V. V Fokin, K. B. Sharpless, **2002**, 2596–2599.
82. C. W. Tornøe, C. Christensen, M. Meldal, *J. Org. Chem.* **2002**, *67*, 3057–3064.
83. R. Huisgen, *Proc. Chem. Soc.* **1964**, 349.
84. N. J. Agard, J. A. Prescher, C. R. Bertozzi, *J. Am. Chem. Soc.* **2004**, *126*, 15046–15047.
85. M. L. Blackman, M. Royzen, J. M. Fox, *J. Am. Chem. Soc.* **2008**, *130*, 13518–13519.
86. H. Ovaa, P. F. van Swieten, B. M. Kessler, M. A. Leeuwenburgh, E. Fiebiger, A. M. C. H. van den Nieuwendijk, P. J. Galardy, G. A. van der Marel, H. L. Ploegh, H. S. Overkleeft, *Angew. Chemie Int. Ed.* **2003**, *42*, 3626–3629.
87. J. A. Prescher, D. H. Dube, C. R. Bertozzi, *Nature* **2004**, *430*, 873.
88. F. L. Lin, H. M. Hoyt, H. van Halbeek, R. G. Bergman, C. R. Bertozzi, *J. Am. Chem. Soc.* **2005**, *127*, 2686–2695.
89. N. J. Agard, J. M. Baskin, J. A. Prescher, A. Lo, C. R. Bertozzi, *ACS Chem. Biol.* **2006**, *1*, 644–648.
90. J. A. Codelli, J. M. Baskin, N. J. Agard, C. R. Bertozzi, *J. Am. Chem. Soc.* **2008**, *130*, 11486–11493.
91. S. I. Presolski, V. Hong, S.-H. Cho, M. G. Finn, *J. Am. Chem. Soc.* **2010**, *132*, 14570–14576.
92. N. J. Agard, J. A. Prescher, C. R. Bertozzi, *J. Am. Chem. Soc.* **2004**, *126*, 15046–15047.
93. J. M. Baskin, J. A. Prescher, S. T. Laughlin, N. J. Agard, P. V Chang, I. A. Miller, A. Lo, J. A. Codelli, C. R. Bertozzi, *Proc. Natl. Acad. Sci.* **2007**, *104*, 16793 LP – 16797.
94. D. L. Boger, R. P. Schaum, R. M. Garbaccio, *J. Org. Chem.* **1998**, *63*, 6329–6337.
95. A. Hamasaki, R. Ducray, D. L. Boger, *J. Org. Chem.* **2006**, *71*, 185–193.
96. J. Sauer, D. K. Heldmann, J. Hetzenegger, J. Krauthan, H. Sichert, J. Schuster, *European J. Org. Chem.* **1998**, *1998*, 2885–2896.
97. F. Thalhammer, U. Wallfahrer, J. Sauer, *Tetrahedron Lett.* **1990**, *31*, 6851–6854.
98. F. Liu, Y. Liang, K. N. Houk, *J. Am. Chem. Soc.* **2014**, *136*, 11483–11493.
99. M. T. Taylor, M. L. Blackman, O. Dmitrenko, J. M. Fox, *J. Am. Chem. Soc.* **2011**, *133*, 9646–9649.

2 Phosphanylmethylphosphonates as Reagents for the Synthesis of Terminal Methylene Bisphosphates

Introduction

Pyrophosphates are present in numerous natural products that are involved in a wide variety of fundamental physiological processes, including cell metabolism, immunity and genome maintenance.[1–5] Consequently, pyrophosphates are important components of molecular tools or probes that aim to study and influence these processes.[6–8] Pyrophosphates are inherently susceptible to hydrolysis, trans-esterification and enzymatic cleavage.[9,10] If a higher stability is desired, methylene bisphosphonates are attractive pyrophosphate bioisosteres that are less prone to undergo hydrolysis both during synthesis and in physiological surroundings.[11] Methylene bisphosphonate isosteres of sugar nucleotides and nucleoside di- and triphoshates have been applied in studies that aim to elucidate the function of various enzymes.[8,12,13] Terminal methylene bisphosphonates monoesters have been synthesized in the past using either methylene bisphosphonic dichloride or partially protected monochloridite derivatives as the phosphonylating agent[14,15]. (Un)symmetric methylene bisphosphonates diesters can be accessed using Mitsunobu chemistry or by condensing a hydroxyl of a target (bio)molecule with an independently prepared terminal methylene bisphosphonate.[16,17] The published methods use unselective reagents and limit the regioselectivity of substitution reactions at the bisphosphonate core. Moreover, no generic strategy exists that readily allows for the introduction of methylene bisphosphonate moieties in structurally diverse pyrophosphate-containing (bio)molecules. This chapter describes the development of such a strategy and its application in the synthesis of terminal methylene bisphosphates.

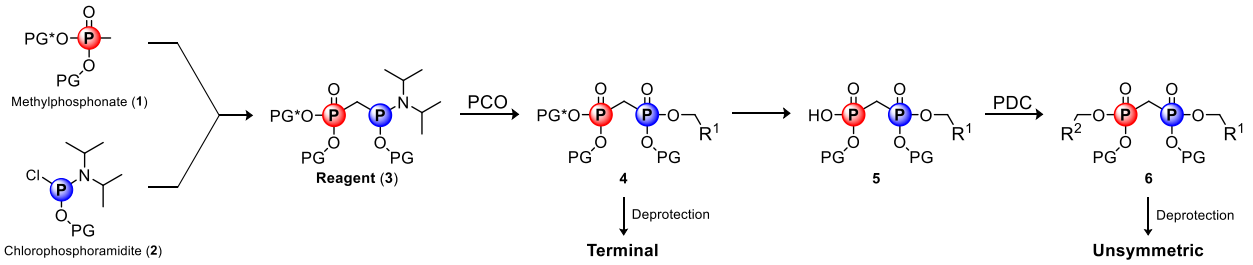

Figure 1: Methodology for the synthesis of terminal or unsymmetric methylene bisphosphates. Reagent **3** features orthogonal removable protecting groups PG and PG* and can be prepared from methylphosphonate **1** and chlorophosphoramidite **2**. The reagent is coupled to an alcohol containing substrate (R^1OH) via a (P^{III}) phosphoramidite coupling-oxidation sequence (PCO), to give protected intermediate **4**, a precursor for terminal methylene bisphosphonates. Alternatively, after selective PG*-deprotection (**5**), a second alcohol (R^2OH) can be introduced through phosphordiester condensation (PDC), leading to protected intermediate **6**, precursor of unsymmetric methylene bisphosphates.

Results and Discussion

It was envisioned that universal reagents capable of providing access to both terminal and unsymmetric methylene bisphosphonates had to be orthogonally protected to allow two sequential condensations under conditions compatible with common biomolecules. These requirements could be met through the application of phosphanylmethylphosphonate reagents (**3**, Figure 1). Azole-mediated condensation between an alcohol and **3**, followed by *in situ* oxidation, would give fully protected methylene bisphosphonate tetraester **4**. Global deprotection of **4** would provide terminal methylene bisphosphonate functionalized molecules. Alternatively, selective deprotection of **4** to bisphosphonotriester **5**, consecutive P^V-condensation with a second alcohol would give bisphosphonotetraester **6** and removal of the protecting groups in **6** would provide unsymmetric methylene bisphosphonates. This chapter describes the development and optimization of the syntheses of several phosphanylmethylphosphonate reagents and their application in the preparation of terminal methylene bisphosphonates, both in solution and on solid-support.

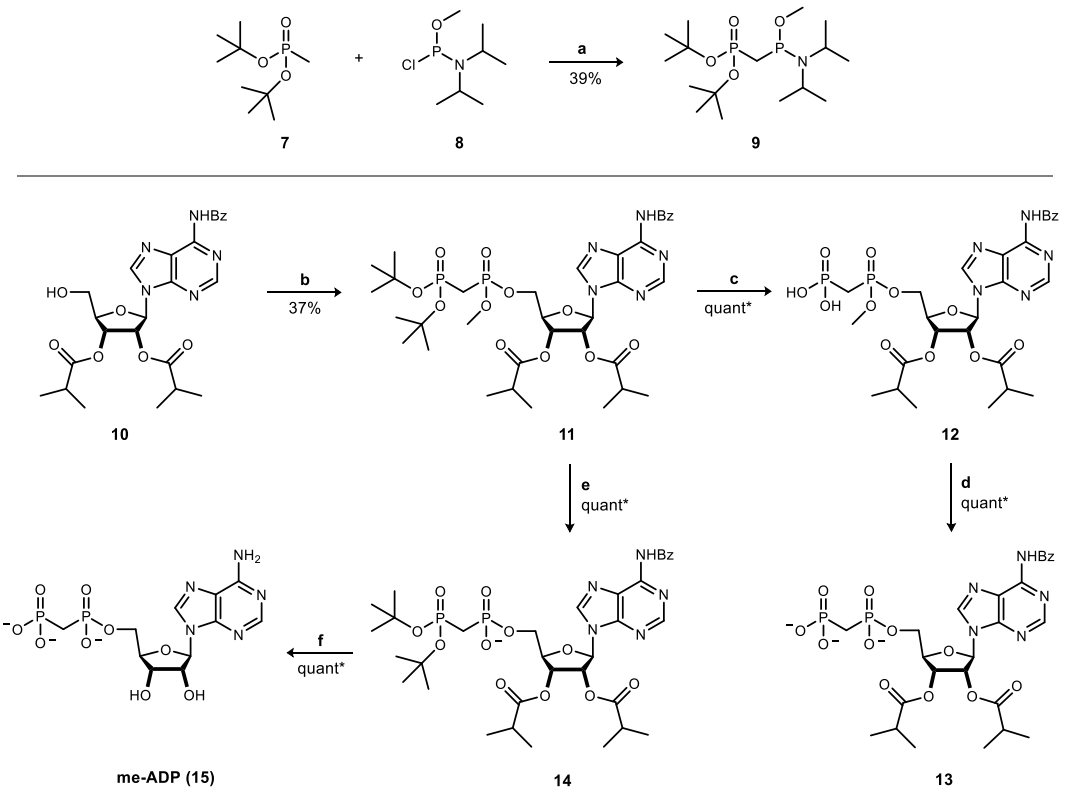

Scheme 1: Exploratory study towards the synthetic accessibility and application of phosphanylmethylphosphonates. Reagents and conditions: [**a**] *n*-BuLi, THF, -78 ˚C, 0.5h » add **16**, 15 min. [**b**] i: N^6-Benzoyl-2,3-*O*-di-*iso*-butyryladenosine (**9**), tetrazole, MeCN, 10 min. ii: ^{t}BuOOH, 15 min. [**c**] 10% TFA in DCM, 0.5h. [**d**] PhSH/Et_3N/dioxane (1:2:2), 48h. [**e**] PhSH/Et_3N/dioxane (1:2:2), 16h. [**f**] i: 10% TFA in DCM, 0.5h. ii: NH_4OH, 16h. [*] Yields based on ^{31}P NMR and LCMS analysis.

To evaluate the proposed methodology, phosphanylmethylphosphonate **9** was chosen as a reagent suitable for the introduction of terminal methylene bisphosphonate monoesters (Scheme 1). Lithiation of di-*tert*-butyl methylphosphonate (**7**) with 1 equivalent of *n*-BuLi, followed by the addition of

phosphoramidite **8**, provided the desired phosphanylmethylphosphonate **9** in 39% yield.[18] The phosphorylating properties of reagent **9** were investigated by exploring the synthesis of known adenosine-5'-methylene bisphosphonates (**13**, Scheme 1).[19] Condensation of phosphoramidite **9** with partially protected adenosine **10**[20] was accomplished using 1*H*-tetrazole as activator. Subsequent *in situ* *t*BuOOH-mediated oxidation of the phosphonite-phosphonate intermediate afforded methylene bisphosphonates of adenosine **11** in 37% yield. Next, the deprotection of the *tert*-butyl groups was investigated. ^{31}P-NMR spectroscopy was used to screen the reaction progression at varying concentrations of trifluoroacetic acid (TFA) in DCM. Optimal conditions were found at 10% TFA; providing clean conversion within 30 minutes. Successive demethylation of **12** with thiophenol in the presence of TEA proceeded sluggishly, taking 48

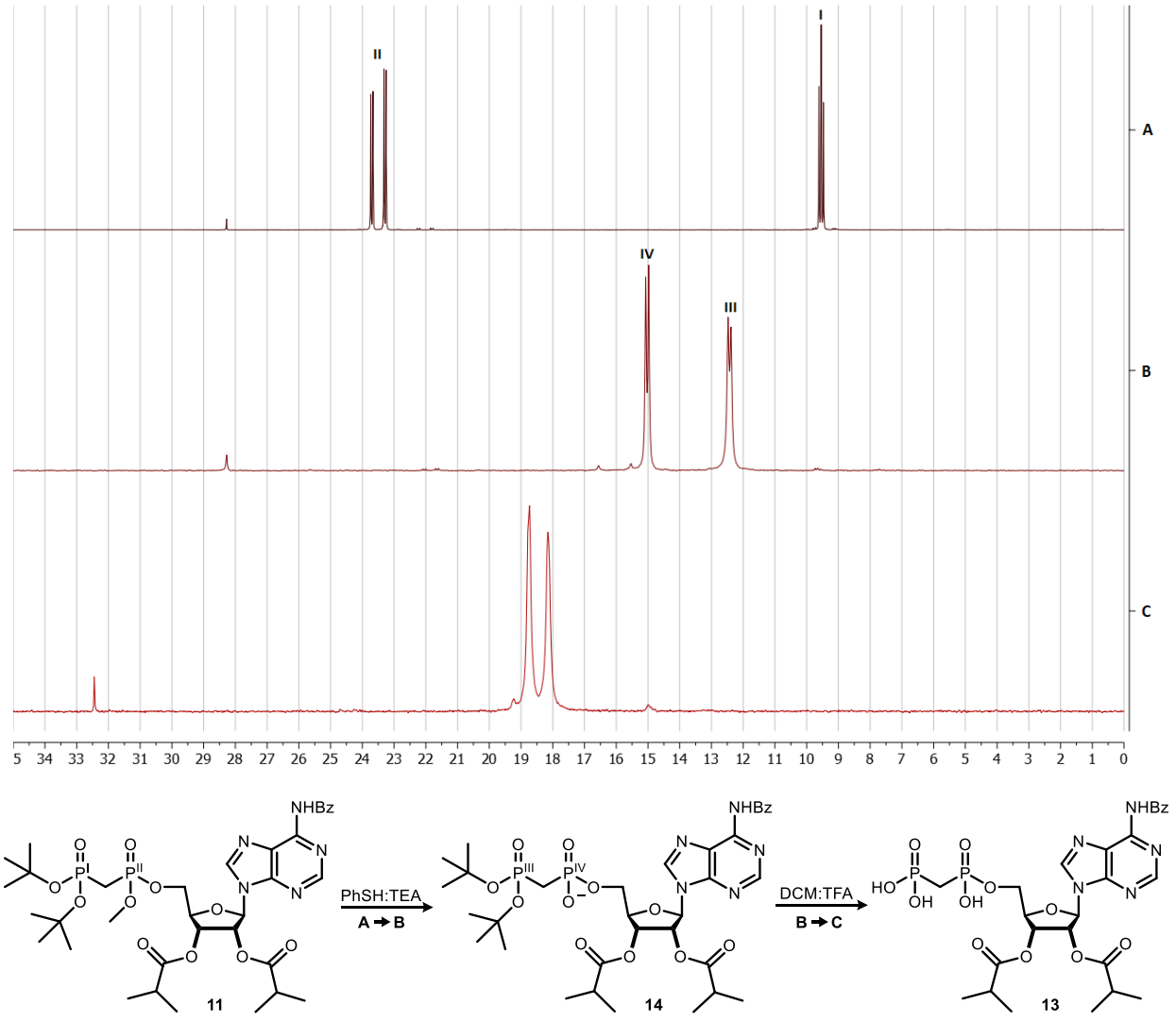

Figure 2: Exploratory sequential deprotection of compound **11**, monitored by ^{31}P NMR spectrometry (162 MHz). A NMR tube was charged with an aliquot of the reaction mixture and fitted with an acetone-d_6 capillary (required for locking). **A:** Fully protected **11**, before addition of PhSH:TEA. **B:** The reaction mixture after 16h treatment with PhSH:TEA:dioxane (1:2:2); showing complete conversion into demethylated intermediate **14**. **C:** After extractive work-up (removal of PhSH and TEA) and concentration, the residue was treated with 10% TFA in DCM for 30 minutes, resulting in cleavage of the *tert*-butyl groups (intermediate **13**).

hours to complete. It was reasoned that the terminal phosphate becomes deprotonated under basic demethylation conditions. The resulting increased electron density surrounding the phosphor lowers the leaving group capacity of the methyl phosphate. Indeed, demethylation proceeded significantly smoother after reversing the order of deprotection (Figure 2, **11** » **14**).). ^{31}P-NMR spectrometry and LCMS analysis showed clean peak-to-peak conversion of **11** (Figure 2, A) to **14** (Figure 2, B) within 16 hours. After extractive work-up, crude methylene diphosphate **14** was deprotected using the previously determined TFA conditions, providing protonated bisphosphonate monoester **13** (Figure 2). Finally, ammonia mediated deacylation provided me-ADP (Scheme 1, **15**) in quantitative yield (based on ^{31}P-NMR spectrometry and LCMS).

With the proposed methodology validated, efforts were directed towards the preparation of protected phosphanyl methylphosphonates **17** and **20**. Reagent **17** is orthogonally protected with a *tert*-butyl group at the terminal phosphate. After the coupling-oxidation sequence of reagent **17** with a specific alcohol, selective deprotection of the *tert*-butyl group in the acquired intermediate would allow for a P^V-condensation with second relevant alcohol, leading to unsymmetric methylene bisphosphonate diesters. The application of reagent **17** will be discussed in Chapter 3. Reagent **20** contains the base labile 2-cyanoethanol protecting group to accommodate the synthesis of terminal methylene bisphosphonates monoesters both in solution and on solid-support.

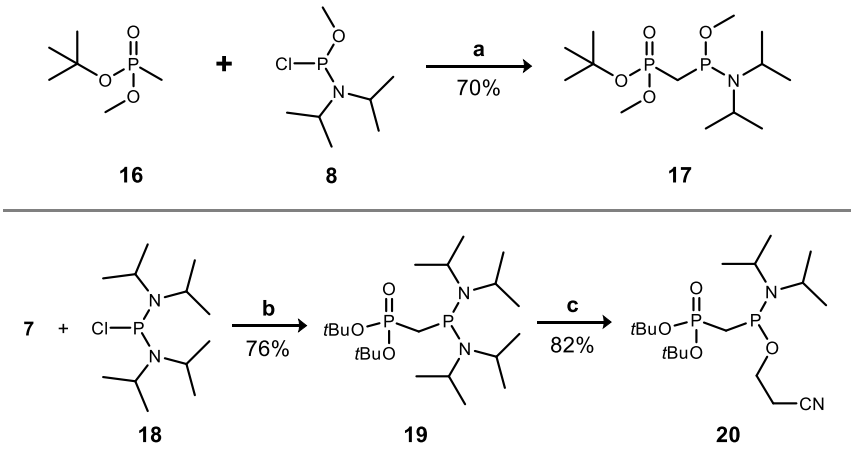

Scheme 2: Synthesis of phosphanyl methylphosphonate **17** and **20**. Reagents and conditions: [**a**] i: *n*-BuLi, THF, -78 °C, 0.5 h. ii: **8**, -78 °C, 15 min [**b**] i: LDA, THF, -78 ˚C, 0.5h. ii: **18**, -78 ˚C » RT, 16h. [**c**] DCI, 2-cyanoethanol, DCM, 3.5h.

Phosphanylmethylphosphonate reagent **17** is prepared according to a similar procedure as described for the synthesis of otherwise protected reagent **9** (Scheme 2). Lithiation of methylphosphonate **16** with 1 equivalent of *n*-BuLi was followed by the addition of chlorophosphine **8**, providing target phosphoramidite **17** in 32% yield. During refinement of this reaction, it was found that the relatively low yield could be attributed to two unwanted modes of quenching and partial P^{III}-oxidation during column purification. First of all, the diminished yield was partially caused by proton-exchange between emerging bisphosphonate **17** and lithiated methylphosphonate **16**, neutralizing the reactant. This problem was circumvented by switching to 2.1 equivalents LDA, increasing the yield to 45%. In addition, it was found that commercially

available **8** was contaminated with diisopropylamine hydrochloride (DIPA·HCl), another species capable of quenching the lithiated methylphosphonate **16**. Removal of DIPA·HCl, by precipitation in *n*-hexane prior to addition and applying the solution through a filter, further increased the yield of the reaction. During the purification of **17**, partial oxidation of the P^{III} (up to 30%) would sporadically occur during column purification. It was empirically determined that this could be attributed to silica gel impurities (potentially trace metals). The oxidation was prevented when high-purity grade silica was used to purify **17**. After these refinements were implemented the synthesis of **17** proceeded cleanly, as determined by ^{31}P NMR spectroscopy (Figure 3), increasing product yield to 70%. The monitoring of the synthesis of **17** is shown in Figure 3. Addition of lithiated **16** onto chlorophosphoramidite **8** gave rise to wide variety of phosphor species. The lithiation of formed **17** by excess LDA introduces an additional stereocenter, providing four additional (distinguishable) diastereoisomers (Figure 3, A). Subsequent quenching with aqueous sodium

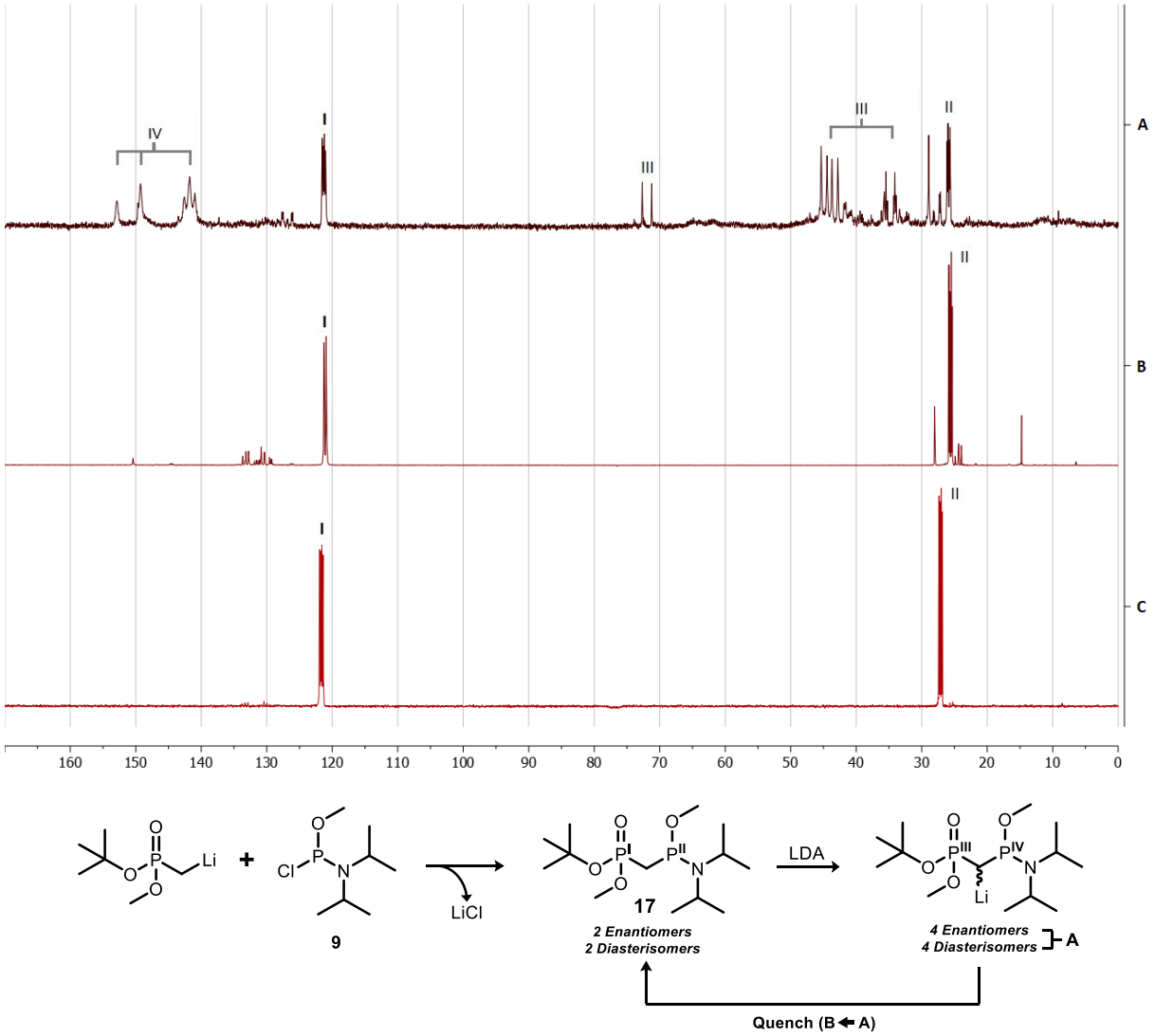

Figure 3: Synthesis of phosphanyl methylphosphonate reagent **17**, monitored by ^{31}P NMR spectrometry (162 MHz). A NMR tube was charged with an aliquot of the reaction mixture and fitted with an acetone-d6 capillary (required for locking). **A:** The reaction mixture after complete addition of the chlorophosphoramidite. **B:** The crude reaction mixture after quenching with aqueous sodium bicarbonate. **C:** The product after column purification using high purity grade silica.

bicarbonate protonates the lithium species, converting it into the desired bisphosphonate (Figure 3, B) which was isolated cleanly using high-purity grade silica (Figure 3, C).

Reagent **20**, fitted with the more labile cyanoethyl protecting group, was prepared via adjustment of the above described protocol (Scheme 2). *tert*-Butyl methylphosphonate **7** was deprotonated by LDA and subsequent reaction with bis(diisopropylamino)chlorophosphoramidite **18** afforded bis-amidite **19** in 76% yield. Selective substitution of one of the diisopropylamine groups with 2-cyanoethanol, under the agency of 0.6 eq. 4,5-dicyanoimidazole (DCI), provided reagent **20** in 82% yield.

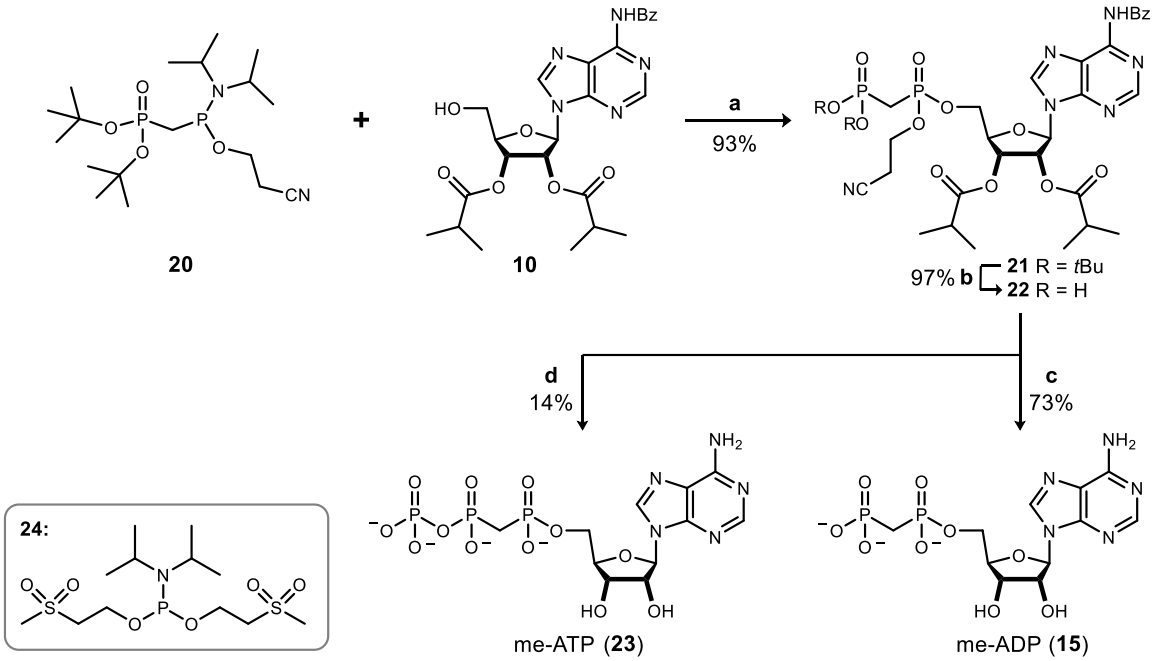

Scheme 3: Solution-phase synthesis of me-ADP **15** and methylene analogue of ATP **23** Reagents and conditions: [**a**] i: **20**, DCI, MeCN, 15 min. ii: *t*BuOOH, 15 min. [**b**] HCl (1.2 eq, 0.5M), HFIP, 4h. [**c**] Ammonia, 16h. [**d**] i: **23**, ETT, MeCN, 15 min. ii: *t*BuOOH, 15 min. iii: DBU, 0.5h. iv: ammonia, 16h.

Having the reagents in hand, the synthesis of the methylene bisphosphonate analogues of adenosine di- and triphosphate[21] (me-ADP **15** and me-ATP **23**, Scheme 3) with reagent **20** was undertaken. Coupling of **20** with adenosine derivative **10** under the influence of DCI and subsequent oxidation of the P^{III}-P^{V} intermediate gave protected me-ADP **21** in 93% isolated yield. Removal of the terminal *tert*-butyl protecting groups was carried out with HCl in hexafluoroisopropanol (HFIP), to obtain partially protected ADP analogue **22** in 97% yield. Global deprotection of **22** by treatment with aqueous ammonia provided adenosine methylene bisphosphonate (**15**) in 73% yield. The syntheses of adenosine methylene triphosphate **23** was effectuated in a one-pot procedure. Methylene diphosphate **22** was first phosphorylated with bis(methylsulfonyl)ethyl diisopropylphosphoramidite (**24**)[22] in the presence of 5-ethylthiotetrazole (ETT). Ensuing *in situ* oxidation of the phosphite-phosphate anhydride intermediate by *t*BuOOH gave the desired methylene triphosphate intermediate, as was determined by ^{31}P-NMR spectroscopy. The cyanoethyl and methylsulfonyl)ethyl protective groups were simultaneously cleaved

by DBU, followed by global deacylation with ammonia. Crude me-ATP **23** was purified by size-exclusion and anion-exchange chromatography.

Next, the applicability of newly developed methodology for automated solid-phase synthesis was investigated. For this purpose, the methylene bisphosphonates analogues of all nucleosides (me-ADP **15**, me-CDP **28**, me-GDP **29** and me-UDP **30**, Scheme 4) were selected as target molecules. Commercially available controlled pore glass (CPG), pre-loaded with the respective suitably protected nucleoside through a succinyl linker (**25**)[23], was loaded into an automated solid-phase oligonucleotide synthesizer. The four-step cycle procedure started with coupling of the immobilized nucleoside with phosphanyl methylphosphonate reagent **20**, using ETT as the activating agent. Subsequent oxidation with (1S)-(+)-(10-camphorsulfonyl)-oxaziridine (CSO) yielded protected resin-bound methylene bisphosphonate nucleotide **26**. The terminal *tert*-butyl groups in intermediate **26** were cleaved with HCl in HFIP (**27**), followed by DBU mediated removal of the 2-cyanoethyl group. Final ammonolysis of the acyl protecting groups with concomitant release from the solid support was effected by treatment with aqueous ammonia. The crude products were purified by gel filtration, providing methylene bisphosphonate nucleotides **15** (39%), **28** (46%), **29** (44%) and **30** (52%).

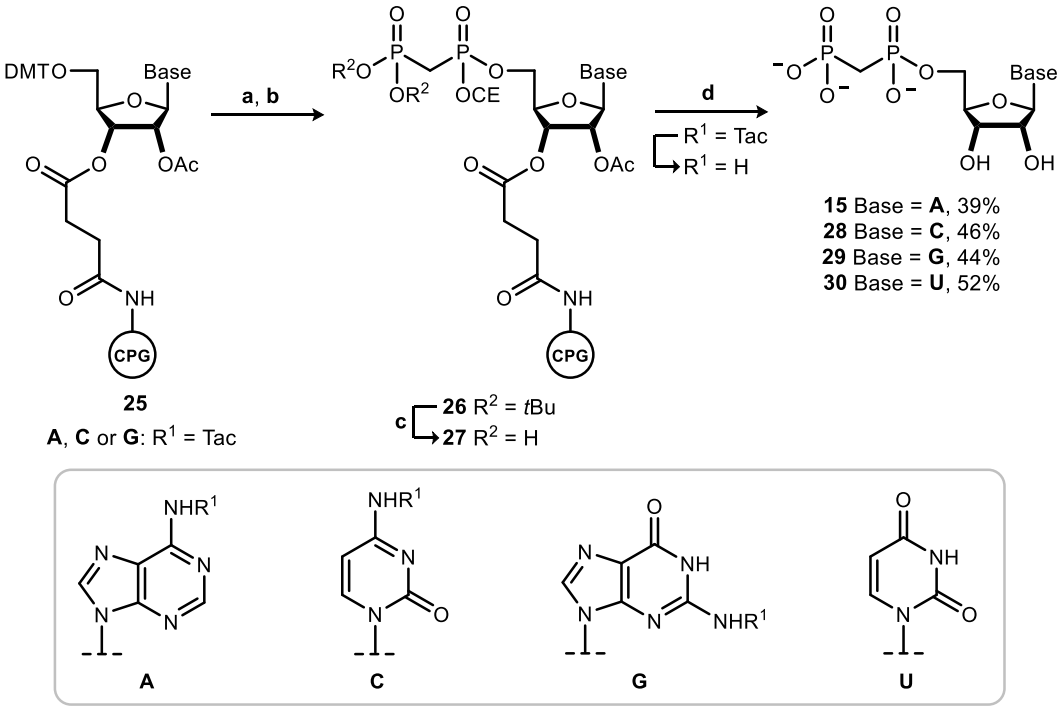

Scheme 4: Automated solid-phase synthesis of methylene bisphosphonate nucleotides. Reagents and conditions: [**a**] 4 x HCl (50 mM), HFIP, 1 min. [**b**] i: 2 x ETT and **20**, MeCN, 5 min. ii: 2 x CSO, MeCN, 5 min. [**c**] i: 4 x HCl (50 mM), HFIP, 1 min. [**d**] i: 2 x DBU, DMF, 2 min. ii: NH_4OH (35%), 1h. CE = 2-cyanoethanol

The necessity of strong basic conditions during the preparation of the phosphanylmethylphosphonate reagents impedes the use of base-labile protecting groups at the P^{V}-position. The use of bis(diisopropylamino)-chlorophosphoramidite circumvents this issue at the P^{III}-position, as was demonstrated for compound **20**. The reliance on base-stable protecting groups, such as the *tert*-butyl, limits the scope to acid stable substrates. This restriction became evident while attempting to synthesize the acid labile mono-substituted methylene bisphosphonate analogue of farnesyl pyrophosphate[24] and isopentenyl pyrophosphate[25]. Although the key phosphoramidite coupling proceeded efficiently (**32a** in 71%, **32b** in 65%), the acid sensitive aliphatic tails decomposed during *tert*-butyl removal. It can be concluded that the method, in its present form, is limited to substrates stable to at least diluted TFA. In Chapter 7 (Future Prospects) strategies are discussed that enable the installation of base-labile protecting groups.

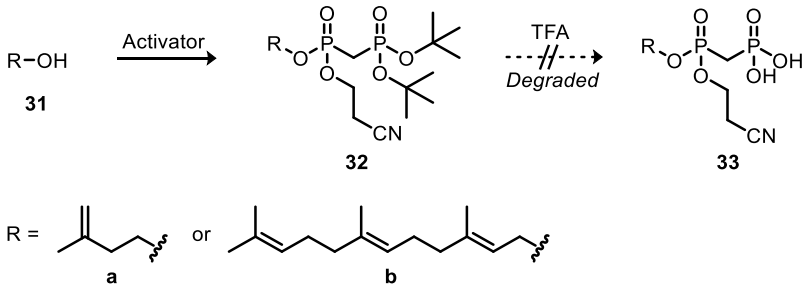

Scheme 6: Attempted **s**ynthesis of isopentenyl- (**a**) and farnesyl (**b**) methylene bisphosphonate phosphonate analogues.

Conclusion

A new class of orthogonally protected phosphanylmethylphosphonate reagents has been developed for the synthesis of methylene bisphosphonate esters. Relevant examples are **17**, **19** and **20**, which are provided with selectively removable *tert*-butyl groups. These reagents are readily accessible through a one-pot procedure by reacting a lithiated methylphosphonate diester with the corresponding chlorophosphoramidite. Terminal methylene bisphosphonates could be prepared by phosphitylation of an alcohol with phosphanyl-methylphosphonate **20**, followed by *in situ* oxidation using *t*BuOOH, as has been demonstrated in the solution-phase synthesis of analogues of adenosine di- and triphosphate (me-ADP **15** and me-ATP **23**). In addition, the method has proven to be suitable for solid-phase synthesis, as shown for nucleotides methylene bisphosphonates (**15**, **28**-**30**). Phosphanylmethyl bis(amidite) **19** enables potential installation of other relevant protecting groups. Reagent **17** was designed and prepared while its application for the synthesis of unsymmetric methylene bisphosphates is described in the next Chapter.

Experimental Section

General: All solvents used under anhydrous conditions were stored over 4Å molecular sieves except for methanol which was stored over 3Å molecular sieves. Solvents used for workup and column chromatography were of technical grade from Sigma Aldrich and used directly. Unless stated otherwise, solvents were removed by rotary evaporation under reduced pressure at 40 °C. Reactions were monitored by TLC-analysis using Merck aluminum DC Silicagel 60 F_{254} with detection by spraying with 20% H_2SO_4 in EtOH, $(NH_4)_6Mo_7O_{24}{\cdot}4(H_2O)$ (25 g/L) and $(NH_4)_4Ce(SO_4)_4{\cdot}2(H_2O)$ (10 g/L) in 10% sulfuric acid or by spraying with a solution of ninhydrin (3 g/L) in EtOH / AcOH (20/1 v/v), followed by charring at approx. 250°C. Column chromatography was performed on Fluka silicagel (0.04 – 0.063 mm) or for methylene bis(phosphorus) compounds on high-purity grade silica (Sigma-Aldrich, Davisil Grade, 633).

NMR: ^{1}H-, ^{13}C- and ^{31}P-NMR Experiments were carried out on a Brüker AV-400 (400 MHz) or a Brüker AV-500 (500 MHz) and AVIII-Brüker DMX-600 (600 MHz). Chemical shifts are given in ppm (δ) and directly referenced to TMS (0.00 ppm) in $CDCl_3$ or D_2O via the solvent residual signal. $CDCl_3$ used in the characterization of phosphoramidite containing compounds was neutralized before use by filtering over aluminum oxide (Type WB-5: Basic). ^{31}P Chemical shifts are indirectly referenced to H_3PO_4 (0.00 ppm) according to the IUPAC method. ^{31}P NMR spectra measured to monitor reactions were made by charging a NMR tube with an aliquot of the reaction mixture and fitting the tube with an acetone-d_6 capillary.

LC-MS: Analysis were carried out on a JASCO HPLC system (detection simultaneously at 214 and 254 nm) coupled to a PE/SCIEX API 165 single quadruple mass spectrometer (Perkin-Elmer) using an analytical Gemini C18 column (Phenomex, 50 x 4.60 mm, 3 micron) in combination eluents A: H_2O; B: MeCN and C: 0.1 M aq. NH_4OAc or a Thermo Finnigan LCQ Advantage MAX ion-trap mass spectrometer with an electrospray ion source coupled to Surveyor HPLC system (Thermo Finnegan) using an analytical Gemini C18 column (Phenomex, 50 x 4.60 mm, 3 micron) in combination with eluents A: H_2O; B: MeCN and C: 1% aq. TFA as the solvent system. High resolution mass spectra were recorded by direct injection (2 µL of a 2 µM solution in water/acetonitrile; 50/50; v/v and 0.1% formic acid) on a mass spectrometer (Thermo Finnigan LTQ Orbitrap) equipped with an electrospray ion source in positive mode (source voltage 3.5 kV, sheath gas flow 10, capillary temperature 250 °C) with resolution R = 60000 at m/z 400 (mass range m/z = 150-2000) and dioctylpthalate (m/z = 391.2842) as a “lock mass”.

Trace Metal Chelation: High purity grade silica should be used when purifying methylene mono-phosphonic acids by silica gel column chromatography. Methylene mono-phosphonic acids (**8**) could be purified using silica gel column chromatography. However, it was found that after column purification the characteristic ^{31}P NMR peaks showed extreme signal broadening, to such an extent that the signals became difficult to detect. This broadening effect could be reversed by passing the purified methylene mono-phosphonic acid over an EDTA functionalized resin (a resin used to capture metal ions). This indicates that signal broadening resulted from metal ions bound to the phosphate, which could only have occurred during column purification.

Preparation of Phosphoramidite Reagents:

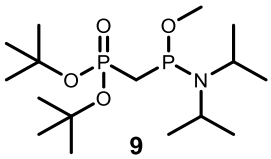

9

Phosphanylmethylphosphonate 9: Reagent was prepared according to the procedure described for **17**, using the following amounts: 2.5M solution of *n*-BuLi in *n*-hexane (4.2 ml, 10.5 mmol, 2.1 eq), diisopropylamine (1.6 ml, 11.2 mmol, 2.2 eq), di-*tert*-butyl methylphosphonate[26] (1.0 g, 5.0 mmol, 1.0 eq) in THF (5 mL) and chloro(diisopropylamino) methoxyphosphine (1.17 ml, 6.0 mmol, 1.2 eq) in *n*-hexane (5 mL). Purification by silica gel column chromatography (12.5% » 15% EtOAc in PE + 1% TEA) provided the product as a colorless oil (1.0 g, 2.7 mmol, 54%). **^{1}H NMR:** (400 MHz, $CDCl_3$) δ 3.53 – 3.36 (m, 2H), 3.45 (d, *J* = 14.0, 3H), 2.23 (ddd, *J* = 18.8, 14.4, 1.5 Hz, 1H), 1.86 (ddd, *J* = 20.2, 14.5, 1.0 Hz, 1H), 1.51 (s, 18H), 1.20 (d, *J* = 6.7 Hz, 6H), 1.13 (d, *J* = 6.8 Hz, 6H). **^{13}C NMR:** (101 MHz, $CDCl_3$) δ 81.62, 81.54, 81.47, 54.18, 53.97, 44.63, 44.52, 36.55, 36.23, 35.17, 34.85, 30.41, 30.37, 30.30, 24.36, 24.25, 24.17. **^{31}P NMR:** (122 MHz, $CDCl_3$) δ 122.04 (d, *J* = 57.1 Hz), 19.41 (d, *J* = 57.1 Hz). **HRMS:** Calculated for $C_{16}H_{38}NO_4P_2$ 370.22761 $[M+H]^+$; found 370.22703

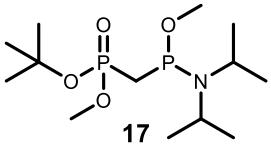

17

Phosphanylmethylphosphonate 17: A 2.5 M solution of *n*-BuLi in *n*-hexane (3.4 ml, 8.4 mmol, 2.1 eq) was carefully added to a cooled solution of (-78 ˚C) diisopropylamine (1.2 ml, 8.4 mmol, 2.1 eq) in dry THF (4 mL), under argon atmosphere. The reaction mixture was stirred for 30 minutes. Next, a solution of *tert*-butyl methyl methylphosphonate[27] (0.63ml, 4.0 mmol, 1 eq) in THF (4 mL) was added dropwise over 5 minutes, and the reaction was stirred for an additional 30 minutes. Lastly, commercially acquired chloro(diisopropylamino)methoxyphosphine (0.93 ml, 4.8 mmol, 1.2 eq) was purified by dissolving in *n*-hexane (4 mL), to precipitating DIPA·HCl contaminates. The resulting solution was added dropwise (±5 minutes) through a syringe fitted with silica filter and small layer of molecular sieves (±1 cm, 4Å). The cold reaction mixture was stirred for 30 minutes, before it was quenched with ethanol (2 mL) and poured into a two-layer system of DCM and saturated aqueous sodium bicarbonate. After extraction, the organic layer was dried over sodium sulfate, filtered and concentrated *in vacuo*. The concentrate was purified by silica gel column chromatography (30% EtOAc in PE + 1% TEA), providing **17** as a colorless oil (0.91 g, 2.8 mmol, 70%). **^{1}H NMR:** (400 MHz, $CDCl_3$) δ 3.72 (d, *J* = 11.2 Hz, 3H), 3.44 (dd, *J* = 14.2, 1.2 Hz, 3H), 2.32 (dddd, *J* = 19.8, 14.8, 11.8, 2.9 Hz, 1H), 1.89 (dddd, *J* = 20.9, 17.5, 14.5, 2.9 Hz, 1H), 1.52 (d, *J* = 2.2 Hz, 9H), 1.21 (d, *J* = 6.7 Hz, 6H), 1.13 (d, *J* = 6.8 Hz, 6H). **^{13}C NMR:** (101 MHz, $CDCl_3$) δ 82.26, 82.18, 82.13, 82.05, 54.18, 53.97, 51.73, 44.52, 44.41, 33.32, 33.20, 33.01, 32.89, 31.96, 31.84, 31.65, 31.53, 30.27, 30.23, 30.22, 30.21, 30.17, 24.32, 24.27, 24.10, 24.02. **^{31}P NMR:** (162 MHz, $CDCl_3$) δ = 121.03 (d, *J* = 56.7 Hz), 120.85 (d, *J* = 55.1

Hz), 26.20 (d, *J* = 56.7 Hz), 26.03 (d, *J* = 55.1 Hz). **HRMS:** Calculated for $C_{13}H_{31}NO_4P_2$ 328.18011 $[M+H]^+$; found 328.17960.

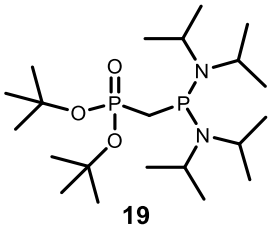

19

Phosphanylmethylphosphonate 19: A 2.5M solution of *n*-BuLi in *n*-hexane (8.4 ml, 21 mmol, 2.1 eq) was carefully added to a cooled solution (-78 ˚C) of diisopropylamine (3.14 ml, 21 mmol, 2.1 eq) in dry THF (10 mL), under argon atmosphere. The reaction mixture was stirred for 30 minutes. Next, a solution of di-*tert*-butyl methylphosphonate (2.08 g, 10 mmol) in THF (10 mL) was added dropwise over 5 minutes, and the reaction mixture was stirred for an additional 30 minutes. Lastly, a solution of bis(diisopropylamino)chlorophosphoamidite (3.2 g, 12 mmol) in *n*-hexane:THF (2:1 v:v, 15 mL) was prepared and added dropwise (±5 minutes) through a syringe fitted with a silica filter. After addition, the cooling bath was removed and the solution was stirred overnight at room temperature. The reaction mixture was poured into saturated aqueous sodium bicarbonate and was extracted with EtOAc. The organic layer was dried over sodium sulfate, filtered and concentrated *in vacuo*. Purification by silica gel column chromatography (5% » 10% EtOAc in PE + 2% TEA) yielded the product as a colorless oil (3.33 g, 7.6 mmol, 76%), that crystalized to a white solid. **^{1}H NMR:** (400 MHz, $CDCl_3$) δ 3.38 (dq, *J* = 18.0, 6.6 Hz, 4H), 2.12 (dd, *J* = 20.7, 1.6 Hz, 2H), 1.52 (s, 18H), 1.19 (t, *J* = 7.5 Hz, 24H). **^{13}C NMR:** (101 MHz, $CDCl_3$) δ 81.15, 81.06, 46.98, 46.86, 32.31, 32.00, 30.93, 30.63, 30.46, 30.43, 24.16, 24.10, 23.89, 23.81. **^{31}P NMR:** (162 MHz, $CDCl_3$) δ 39.63 (d, *J* = 89.1 Hz), 21.78 (d, *J* = 89.1 Hz). **HRMS:** Calculated for $C_{21}H_{51}NO_4P_2$ 457.33186 $[M+H+H_2O]^+$; found 457.33178.

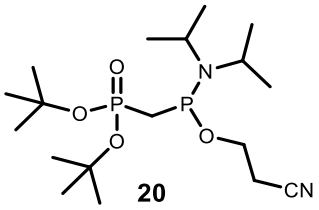

20

Phosphanylmethylphosphonate 20: DCI (0.538 g, 4.56 mmol, 0.6 eq) was added to a dry solution of di-*tert*-butyl ((bis(diisopropylamino)phosphaneyl)methyl)phosphonate (3.33 g, 7.59 mmol) and 2-cyanoethanol (0.519 ml, 7.59 mmol) in DCM (50 mL). The reaction progression was followed by ^{31}P NMR, which indicated completion after 3.5 hours. The solution was concentrated *in vacuo* and purified by silica gel column chromatography (30% » 40% EtOAc + 1% TEA), providing phosphanyl methylphosphonate **20** (2.54 g, 6.22 mmol, 82%) as a colorless oil. **^{1}H NMR:** (500 MHz, $CDCl_3$) δ 3.92 – 3.74 (m, 2H), 3.58 – 3.40 (m, 2H), 2.65 (q, *J* = 6.3, 5.9 Hz, 2H), 2.30 (ddd, *J* = 19.0, 14.4, 1.1 Hz, 1H), 1.89 (ddd, *J* = 20.3, 14.5, 1.5 Hz, 1H), 1.58 – 1.45 (m, 18H), 1.21 (d, *J* = 6.7 Hz, 6H), 1.14 (d, *J* = 6.8 Hz, 6H). **^{13}C NMR:** (126 MHz, $CDCl_3$) δ = 117.57, 81.62, 81.58, 81.55, 81.51, 61.58, 61.38, 44.80, 35.99, 35.74, 34.89, 34.64, 30.22, 30.19, 23.95,

20.08, 20.02. **^{31}P NMR:** (202 MHz, $CDCl_3$) δ = 117.95 (d, *J* = 60.6 Hz), 15.25 (d, J = 60.6 Hz). Calculated for $C_{18}H_{39}N_2O_4P_2$ 409.23796 $[M+H]^+$; found 409.23792.

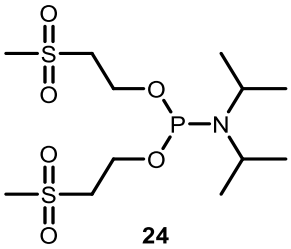

24

Bis(methylsulfonylethanol) Phosphoramidite 24: Diisopropylamine (1.63 ml, 11.46 mmol, 2 eq) was added to a cooled (0 °C) solution of DIPEA (2,0 ml, 11,46 mmol) and trichlorophosphane (0.50 ml, 5.73 mmol, 1 eq) in THF (20 mL). After 10 minutes, a solution of methylsulfonylethanol (1.42 g, 11.46 mmol, 2 eq) in THF (10 mL) was carefully added. The cooling bath was removed and the reaction mixture was stirred for 3 hours, after which ^{31}P NMR: indicated completion of the reaction. The mixture was filtered, rinsed and diluted with EtOAc. The filtrate was washed with saturated aqueous sodium bicarbonate and brine. The organic layer was isolated, dried over magnesium sulfate and concentrated *in vacuo*. The solid residue was recrystallized by cooling a supersaturated solution of the impure product in acetone : *n*-hexane (1:2 v:v, 5 mL), affording phosphoramidite **24** (1.15 g, 3.05 mmol, 53%) as a white crystalline substance.[22] Alternatively, the residue can be purified using silica gel column chromatography (20% » 30% acetone in PE + 1% TEA). **^{1}H NMR:** (400 MHz, $CDCl_3$) δ = 4.19 – 3.98 (m, 2H), 3.58 (dh, *J*=10.4, 6.8, 1H), 3.38 – 3.20 (m, 2H), 3.01 (d, *J*=0.9, 3H), 1.20 (d, *J*=6.9, 6H). **^{13}C NMR:** (101 MHz, $CDCl_3$) δ = 57.51, 57.31, 56.00, 55.92, 43.17, 43.04, 42.67, 24.49, 24.42. **^{31}P NMR:** (162 MHz, $CDCl_3$) δ = 148.27.

Coupling Reactions in Solution:

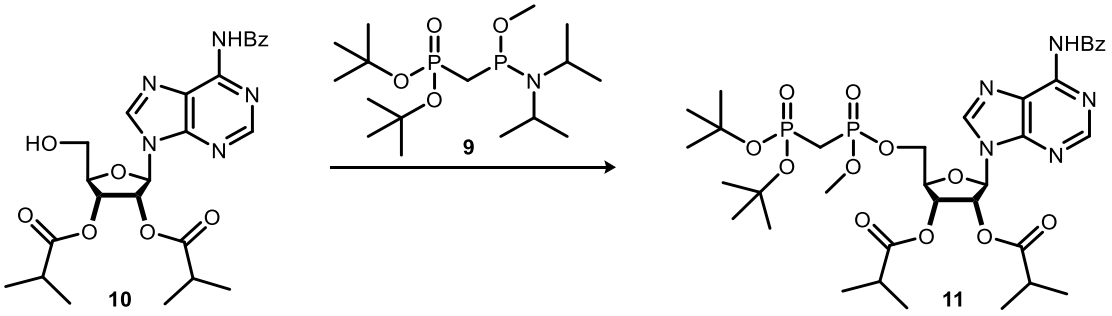

10 **9** **11**

Protected me-ADP 11: N^6-Benzoyl-2,3-*O*-di-*iso*-butyryladenosine (0.213 g, 0.416 mmol) was co-evaporated with pyridine (10 mL) and MeCN (10 mL) and put under argon atmosphere. Phosphanyl methylphosphonate **9** (122 mg, 0.330 mmol) was added as a solution (1 mL; 15% pyridine in MeCN) and the mixture was reduced in volume. The concentrated mixture was co-evaporated once more with MeCN, redissolved in MeCN (4 mL) and put under argon atmosphere. Tetrazole (1.1 mL, 0.495 mmol) in MeCN (0.45M) was added. ^{31}P NMR indicated full conversion within 10 minutes. *tert*-butyl hydroperoxide (180 µl, 0.991 mmol) was added, and the reaction mixture was stirred for an additional 15 minutes. The reaction was concentrated *in vacuo* and redissolved in EtOAc. The solution was washed with aqueous

sodium bicarbonate and brine. The organic layer was dried over magnesium sulfate and concentrated *in vacuo*. Purification by silica gel column chromatography (100% EtOAc » 1% MeOH in EtOAc » 3% MeOH) yielded methylene bisphosphonate **11** as a colorless oil (86 mg, 0.108 mmol, 33%). **^{1}H NMR:** (400 MHz, $CDCl_3$) δ 9.48 (d, J = 10.0 Hz, 1H), 8.82 (s, 1H), 8.53 (d, J = 20.4 Hz, 1H), 8.10 – 7.99 (m, 2H), 7.63 – 7.55 (m, 1H), 7.51 (dd, J = 8.2, 6.7 Hz, 2H), 6.34 (t, J = 6.3 Hz, 1H), 5.89 (dt, J = 18.0, 5.9 Hz, 1H), 5.70 (ddd, J = 15.6, 5.7, 3.3 Hz, 1H), 4.46 (d, J = 6.4 Hz, 2H), 3.85 – 3.64 (m, 4H), 2.65 (dt, J = 14.0, 6.9 Hz, 1H), 2.58 – 2.31 (m, 3H), 1.52 (dd, J = 3.7, 1.4 Hz, 18H), 1.23 (d, J = 7.0 Hz, 6H), 1.11 (dd, J = 14.6, 7.0 Hz, 6H). **^{13}C NMR:** (101 MHz, $CDCl_3$) δ 175.61, 175.55, 175.21, 164.72, 152.82, 151.70, 151.66, 149.70, 141.59, 133.55, 132.63, 128.67, 127.88, 122.96, 85.58, 83.88, 83.82, 83.80, 83.74, 83.71, 81.93, 81.86, 81.79, 81.72, 73.21, 73.11, 70.54, 70.45, 65.06, 64.99, 64.93, 53.27, 53.21, 53.11, 33.68, 33.49, 30.20, 30.16, 30.13, 18.82, 18.80, 18.71, 18.64, 18.54. **^{31}P NMR:** (162 MHz, CDCl3) δ 23.73, 23.66, 23.32, 23.25, 9.61, 9.54, 9.47. **LCMS:** Calculated for $C_{35}H_{52}N_5O_{12}P_2$ 796.31 $[M+H]^+$; found 796.00

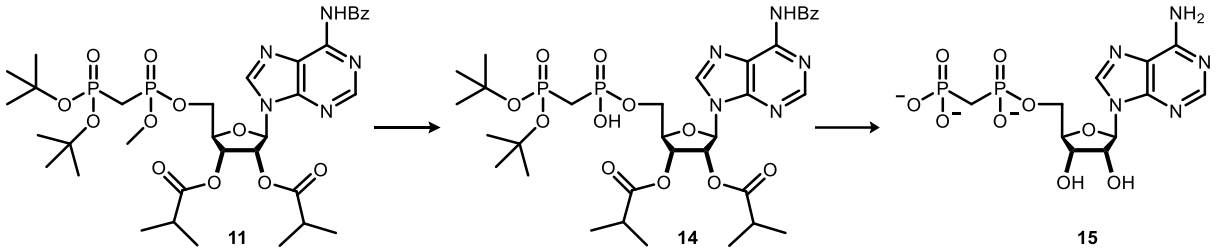

me-ADP 15: Methylene bisphosphonate **11** (37 mg, 46 µmol, 1 eq) was dissolved in a mixture of thiophenol:dioxane: TEA 1:2:2 (1.94 M, 0.5 mL) and the reaction was stirred overnight. ^{31}P NMR and LCMS analysis indicated complete conversion into intermediate **14** (see page S16). The reaction mixture was poured into a separation funnel containing water, acidified with acetic acid and washed with Et_2O (3x, to remove thiophenol). The water layer was isolated and concentrated *in vacuo*. The residue was dissolved in 10% TFA in DCM (0.5 mL). After 30 minutes, the reaction mixture was analyzed by ^{31}P NMR spectrometry, showing complete conversion. The reaction mixture co-evaporated with dioxane and chloroform. Ammonia (30%, 1 mL) was added and solution was stirred overnight. The final reaction mixture was analyzed by LCMS analysis. This was an exploratory experiment to determine the effectiveness of the deprotection conditions, therefore the product was not isolated.

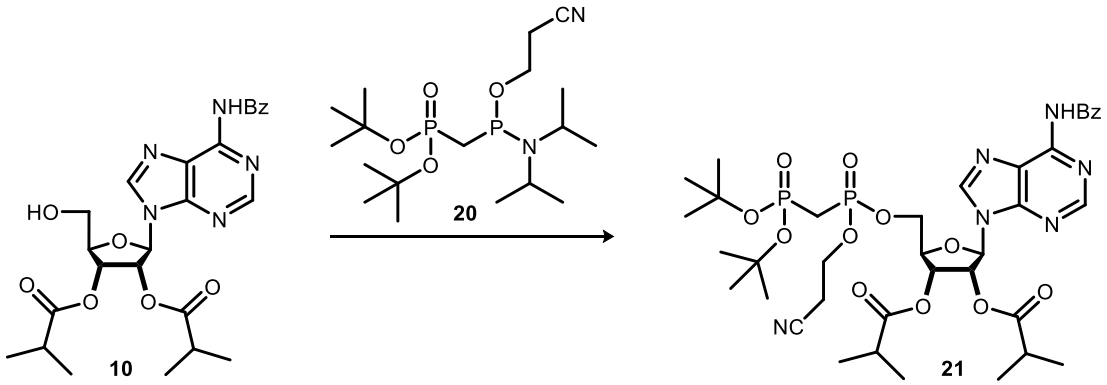

Protected me-ADP 21: Adenosine **10** (0.465 g, 0.909 mmol, 1.1 eq) and phosphanyl methylphosphonate **20** (0.408 g, 1.00 mmol, 1 eq) were co-evaporated with MeCN (8 mL), redissolved in MeCN (4 mL) and put under argon atmosphere. The reaction was stirred until all solids were dissolved and DCI (0.161 g, 1.36 mmol, 1.5 eq) was added. ^{31}P-NMR indicated full conversion within 15 minutes. Oxidation was initiated the addition of *tert*-butyl hydroperoxide (0.331 ml, 1.82 mmol, 2 eq) in decane (5.5 M). The reaction mixture was stirred for an additional 15 minutes. The solution was poured into a separation funnel containing water and EtOAc, washed with aqueous sodium bicarbonate (to remove DCI) and brine. The organic layer was dried over Na_2SO_4 and concentrated *in vacuo*. Purification by silica gel column chromatography (25% » 50% acetone in DCM) yielded compound **21** (705 mg, 0.845 mmol, 93%) as white foam. **^{1}H NMR:** (500 MHz, $CDCl_3$) δ 9.31 (s, 1H), 8.76 (d, J = 2.9 Hz, 1H), 8.40 (d, J = 44.2 Hz, 1H), 8.06 – 7.93 (m, 2H), 7.60 – 7.52 (m, 1H), 7.47 (dd, J = 8.4, 7.0 Hz, 2H), 6.27 (dd, J = 21.0, 5.9 Hz, 1H), 5.88 (dt, J = 38.9, 5.8 Hz, 1H), 5.68 (ddd, J = 23.2, 5.6, 3.7 Hz, 1H), 4.51 – 4.38 (m, 3H), 4.35 – 4.23 (m, 2H), 2.74 (dp, J = 7.6, 6.2 Hz, 2H), 2.60 (h, J = 7.0 Hz, 1H), 2.55 – 2.39 (m, 3H), 1.53 – 1.42 (m, 18H), 1.19 (d, J = 7.0 Hz, 6H), 1.12 – 1.03 (m, 7H). **^{13}C NMR:** (126 MHz, $CDCl_3$) δ 175.77, 175.66, 175.43, 175.40, 164.86, 152.94, 151.87, 151.82, 149.85, 133.63, 132.83, 128.86, 128.01, 123.60, 123.48, 116.95, 116.86, 86.24, 85.77, 84.25, 84.23, 84.18, 84.17, 84.16, 84.09, 84.07, 84.01, 81.88, 81.82, 81.61, 81.55, 73.19, 73.08, 70.48, 70.39, 65.33, 64.98, 61.28, 61.24, 33.82, 33.63, 30.73, 30.55, 30.37, 30.34, 30.31, 30.28, 29.65, 29.61, 29.48, 29.43, 28.53, 28.36, 19.90, 19.85, 18.98, 18.96, 18.86, 18.82, 18.81, 18.70. **^{31}P NMR:** (202 MHz, $CDCl_3$) δ 22.86 (d, *J* = 6.1 Hz), 22.53 (d, *J* = 6.1 Hz), 8.73, 8.64. **HRMS:** Calculated for $C_{37}H_{53}N_6O_{12}P_2$ 835.31912 $[M+H]^+$; found 835.31958

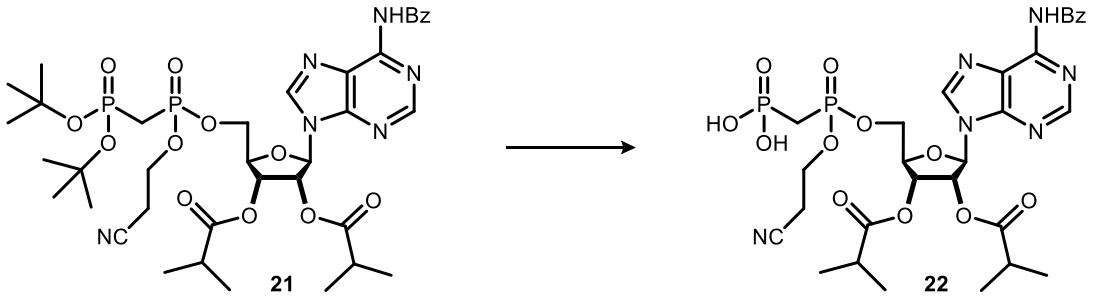

Protected me-ADP 22: A 6M HCl in dioxane : water (1:1 v:v, 84 µl, 0.505 mmol, 1.2 eq) was added to a solution of adenosine methylene bisphosphonate **21** (351 mg, 0.420 mmol, 1 eq) in HFIP (1 mL). The reaction was shortly sonicated until the HCl solution was dissolved in the HFIP. The reaction was monitored by ^{31}P NMR, which indicated full conversion after 4 hours. The reaction was diluted with dioxane : toluene (1:1 v:v, 20 mL) and co-evaporated, this was repeated thrice to remove all traces of HFIP, providing adenosine methylenephosphonic acid **22** as a colorless oil (295 mg, 0.408 mmol, 97%). The product was used without further purification. **^{31}P NMR:** (162 MHz, Acetone-D_6) δ = 22.08 (d, *J* = 8.1 Hz), 21.68 (d, *J* = 8.1 Hz), 16.55 (d, *J* = 8.1 Hz), 16.46 (d, *J* = 8.1 Hz).

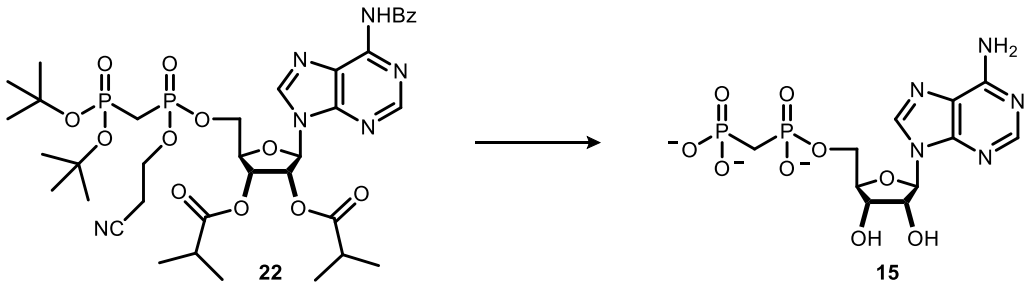

me-ADP 15: A 6M HCl in dioxane : water (1:1 v:v, 39 µL, 0.236 mmol, 1.2 eq) was added to a solution of adenosine methylene bisphosphonate **22** (164 mg, 0.196 mmol) in HFIP (1 mL). The reaction was monitored by ^{31}P NMR spectrometry, which indicated full conversion after 4 hours. The reaction was quenched with ammonium hydroxide (0.1 mL) and concentrated *in vacuo*. The concentrate was redissolved in ammonium hydroxide (1 mL, 17.5 mmol) and the reaction was stirred overnight. The excess ammonia was purged by stirring under vacuum. The crude material was purified using size-exclusion (HW40-column, 0.15 M aqueous NH_4OAc) chromatography. Lyophilization provided me-ADP **15** (61 mg, 0.143 mmol, 73%) as a white powder. **^{1}H NMR:** (600 MHz, D_2O) δ 8.25 (s, 1H), 7.87 (s, 1H), 5.87 (d, J = 5.3 Hz, 1H), 4.57 (t, J = 5.2 Hz, 1H), 4.37 (t, J = 4.7 Hz, 1H), 4.22 (d, J = 3.8 Hz, 1H), 4.03 (m, J = 4.9, 4.3 Hz, 2H), 2.05 (t, J = 19.9, 2.0 Hz, 2H). **^{13}C NMR:** (151 MHz, D_2O) δ 155.95, 153.36, 149.39, 140.58, 119.08, 88.00, 84.58, 75.15, 71.10, 64.47, 29.33, 28.51, 27.68. **^{31}P NMR:** (202 MHz, D_2O) δ = 18.20 (d, *J* = 8.1 Hz), 21.68 (d, *J* = 8.1 Hz), 16.55 (d, *J* = 8.1 Hz), 16.46 (d, *J* = 8.1 Hz).

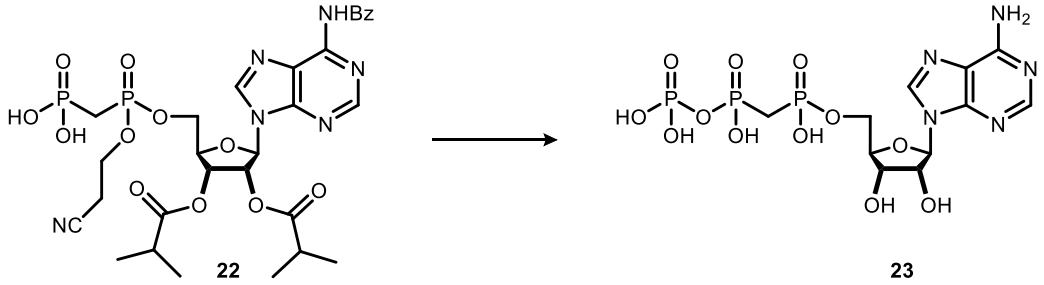

me-ATP 23: Crude adenosine methylene bisphosphonate **22** (295 mg, 0.408 mmol, 1 eq) and bis(2-(methylsulfonyl)ethyl) diisopropylphosphoramidite **24** (185 mg, 0.490 mmol, 1.2 eq) were co-evaporated with MeCN (8 mL), redissolved in dry MeCN (4 mL) and put under argon atmosphere. The reaction was stirred until all solids were dissolved, after which ETT (80 mg, 0.612 mmol, 1.5 eq) was added. 31P-NMR indicated full conversion within 15 minutes. Oxidation was initiated by the addition of *tert*-butyl hydroperoxide (111 µl, 0.612 mmol, 1.5 eq) in decane (5.5 M). After 15 minutes, DBU (431 µl, 2.86 mmol, 7 eq) was added and the reaction mixture was stirred for an additional 30 minutes. Ammonia (30%, 5 mL) was added and the reaction mixture was stirred overnight. The excess ammonia was purged by stirring under vacuum. The crude material was purified using size-exclusion (HW40-column, 0.15 M aqueous NH_4OAc) and anion-exchange chromatography (Source 15Q, 10 mM » 1 M, aqueous NH_4OAc). Lyophilization provided me-ATP **23** (14.4 mg, 0.029 mmol, 14%) as a white powder. **^{1}H NMR:** (500 MHz, D_2O) δ 8.55 (s, 1H), 8.20 (s, 1H), 6.06 (d, *J* = 5.4 Hz, 1H), 4.96 – 4.92 (m, 1H), 4.72 (t, *J* = 5.2 Hz, 1H), 4.53 (t, *J* = 4.5 Hz, 1H), 4.36 (t, *J* = 3.4 Hz, 1H), 4.18 (q, *J* = 4.2 Hz, 2H), 2.37 (t, *J* = 20.3 Hz, 2H). **^{13}C NMR:** (126 MHz,

D_2O) δ 153.86, 150.58, 148.66, 118.37, 87.16, 84.03, 83.97, 74.36, 70.16, 63.61, 63.57, 28.63, 27.62, 26.58. **^{31}P NMR** (202 MHz, D_2O) δ 18.25 (d, *J* = 9.9 Hz), 7.72 (dd, *J* = 25.3, 9.2 Hz), -9.65 (d, *J* = 24.6 Hz). **HRMS:** Calculated for $C_{11}H_{19}N_5O_{12}P_3$ 506.02431 $[M+H]^+$; found 506.02347.

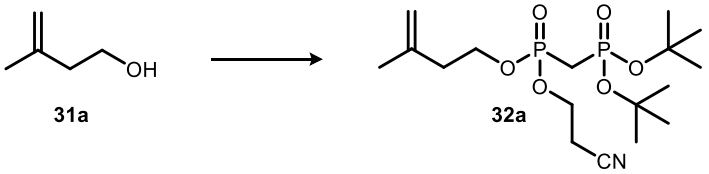

Protected me-Isopentenyl Diphosphate 32a: Isoprenol (41.8 µL, 0.414 mmol) and di-*tert*-butyl (((2-cyanoethoxy) (diisopropylamino) phosphanyl)methyl)phosphonate (203 mg, 0,497 mmol, 1.2 eq) were co-evaporated with MeCN (4 mL), redissolved in MeCN (2 mL) and put under argon atmosphere. The reaction was stirred until all solids were dissolved and DCI (73.4 mg, 0.621 mmol, 1.5 eq) was added. 31P-NMR indicated full conversion within 15 minutes. Oxidation was initiated the addition of *tert*-butyl hydroperoxide (151 µl, 0.828 mmol, 2 eq) in decane (5.5 M). The reaction mixture was stirred for an additional 15 minutes. The solution was poured into a separation funnel containing water and EtOAc, washed with sodium bicarbonate. The organic layer was dried over Na_2SO_4 and concentrated *in vacuo*. Purification by silica gel column chromatography (25% » 50% acetone in DCM) yielded the title compound (121 mg, 0.296 mmol, 71%) as colorless oil. **^{1}H NMR:** (400 MHz, $CDCl_3$) δ 4.81 (d, *J* = 23.3 Hz, 2H), 4.39 – 4.28 (m, 2H), 4.24 (q, *J* = 7.2 Hz, 2H), 2.86 – 2.70 (m, 2H), 2.50 – 2.34 (m, 4H), 1.77 (s, 3H), 1.56 – 1.51 (m, 18H). **^{13}C NMR:** (101 MHz, $CDCl_3$) δ 140.96, 116.69, 112.71, 64.45, 60.75, 38.40, 30.90, 30.28, 29.54, 28.14, 22.41, 19.90. **^{31}P NMR:** (162 MHz, $CDCl_3$) δ 21.00, 8.80.

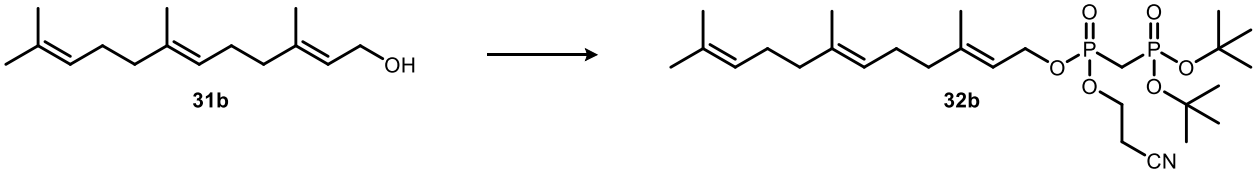

Protected Farnesol me-Diphosphate (32b): Farnesol (125 µL, 0.5 mmol) and (((2-cyanoethoxy) (diisopropylamino)phosphanyl)methyl)phosphonate (245 mg, 0.600 mmol, 1.2 eq) were co-evaporated with MeCN (4 mL), redissolved in MeCN (2 mL), put under argon atmosphere and charged with 2,6-lutidine (116 µL, 1.00 mmol, 2 eq). 2,6-lutidine·HCl (108 mg, 0.750 mmol, 1.5 eq) was added. ^{31}P-NMR indicated full conversion within 15 minutes. Oxidation was initiated the addition of *tert*-butyl hydroperoxide (182 µL, 1.00 mmol, 2 eq) in decane (5.5 M). The reaction mixture was stirred for an additional 15 minutes. The solution was poured into a separation funnel containing water and EtOAc, washed with sodium bicarbonate (to remove DCI). The organic layer was dried over sodium carbonate and concentrated *in vacuo*. Purification by silica gel column chromatography (10% » 25% acetone in DCM) yielded the title compound (176 mg, 0.323 mmol, 65%) as colorless oil. **^{1}H NMR:** (400 MHz, $CDCl_3$) δ 5.47 – 5.35 (t, 1H), 5.16 – 5.03 (m, 2H), 4.65 (t, *J* = 8.0 Hz, 2H), 4.33 (dtd, *J* = 7.8, 6.4, 4.3 Hz, 2H), 2.79 (q, *J* = 6.3 Hz, 2H), 2.53 – 2.30 (m, 2H), 2.07 (ddd, *J* = 18.6, 10.6, 4.7 Hz, 7H), 1.97 (dd, *J* = 9.2, 6.2 Hz, 1H), 1.75 – 1.65

(m, 7H), 1.61 (d, *J* = 4.7 Hz, 5H), 1.54 (d, *J* = 2.4 Hz, 18H). **^{31}P NMR:** (162 MHz, $CDCl_3$) δ 21.20 (d, *J* = 10.7 Hz), 8.86 (d, *J* = 10.5 Hz). **HRMS:** Calculated for $C_{27}H_{49}NO_6P_2Na$ 568.29273 $[M+Na]^+$; found 568.29244.

Nucleotide Synthesis on Solid Phase

Methylene bisphosphonate functionalized nucleotides me-ADP, me-CDP, me-GDP and me-UDP were prepared from CPG resin pre-loaded with the respective nucleoside. The nucleosides were attached to the resin through a succinyl linker connected at the O^3-position. The O^5-positions were capped with a DMT and the exocyclic amine in **A**, **C** and **G** were protected with the 4-*tert*-butylphenoxyacetyl (Tac) moiety:

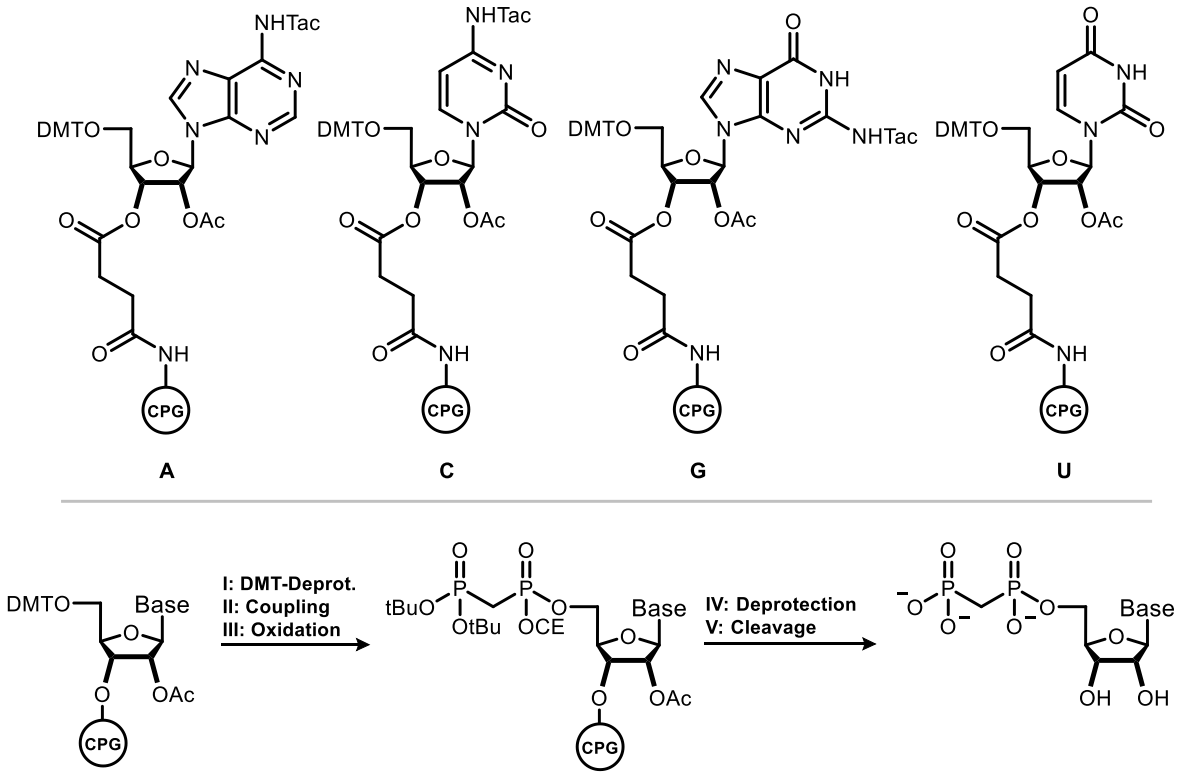

Figure S1: Overview of the solid-phase synthesis of the methylene bisphosphonate nucleotides me-ADP, me-CDP, me-GDP and me-UDP.

For each experiment 300 mg of pre-loaded GPC resin (±10 µmol loaded nucleoside) was loaded in a Mermade 6 oligonucleotide synthesizer. The synthesis was fully carried out under argon atmosphere. The nucleotides were purified using size-exclusion (HW40-column, 0.15 M aqueous NH_4OAc) chromatography.

I. DMT-Deprotection: The DMT was removed by treatment with HCl in hexafluoroisopropanol (50 mM, 1 mL) four times for 1 minute. The resin was washed with MeCN (3 x 2 mL).

II. **Coupling:** The reaction vessel was charged with phosphanyl methylphosphonate **20** (0.1 M in MeCN, 300 µL) and ETT (0.5 M in MeCN, 600 µL) and left to stand for 5 minutes. This cycle was repeated once, before the resin was rinsed with MeCN (3 x 2 mL).

III. **Oxidation:** The phosphinite-phosphonate intermediate was oxidized by treatment with (1S)-(+)-(10-camphorsulfonyl)oxaziridine (0.5 M in MeCN, 2 mL) twice for 5 minutes, and washed with MeCN (3 x 2 mL).

IV. **Deprotection:** The *tert*-butyl groups were removed by treating the resin with HCl in hexafluoroisopropanol (50 mM, 1 mL) four times for 1 minute. The resin was washed with MeCN (3 x 2 mL), before being treated with DBU (1 M in DMF, 1 mL) twice for 2 minutes, to eliminate the 2-cyanoethanol (CE). The resin was washed with MeCN (3 x 2 mL).

V. **Cleavage:** The resin was treated with NH_4OH (35%) for 1 hour, removing the remaining acyl-based protecting groups (Ac, TAC) and releasing the nucleotide from resin.

Yields and Data[28]**:**

me-ADP (15): 1.66 mg, 3.9 µmol, ±39%. For NMR data see solution phase synthesis for compound **15**.

me-CDP (28): 1.86 mg, 4.64 µmol, ±46%. **^{1}H NMR:** (500 MHz, D_2O) δ 8.17 (d, *J* = 7.8 Hz, 1H), 6.20 (d, J = 7.8 Hz, 1H), 5.91 (d, *J* = 2.9 Hz, 1H), 4.35 – 4.30 (m, 2H), 4.27 – 4.23 (m, 1H), 4.16 (m, *J* = 43.9, 11.9, 5.1, 2.4 Hz, 2H), 2.15 (td, *J* = 19.8, 1.5 Hz, 2H). **^{31}P NMR** (202 MHz, D_2O) δ 18.92 (d, *J* = 10.3 Hz), 15.29 (d, *J* = 10.1 Hz).

me-GDP (29): 1.92 mg, 4.35 µmol, ±44%. **^{1}H NMR**: (500 MHz, D_2O) δ 8.32 (s, 1H), 5.91 (d, *J* = 5.5 Hz, 1H), 4.73 (t, *J* = 5.4 Hz, 1H), 4.48 (t, *J* = 4.6 Hz, 1H), 4.30 (d, *J* = 3.8 Hz, 1H), 4.17 – 4.08 (m, 2H), 2.20 – 2.09 (t, *J* = 19.9, 2H). **^{31}P NMR:** (202 MHz, D_2O) δ 18.80, 15.78.

me-UDP (30): 2.07 mg, 5.25 µmol, ±52%. **^{1}H NMR** (500 MHz, D_2O) δ 7.87 (dt, *J* = 8.6, 1.3 Hz, 1H), 5.87 – 5.78 (m, 2H), 4.29 – 4.21 (m, 2H), 4.13 (d, *J* = 3.9 Hz, 1H), 4.10 – 3.93 (m, 2H), 2.05 (t, *J* = 19.7 Hz, 2H). **^{31}P NMR** (202 MHz, D_2O) δ 18.84 (d, *J* = 10.2 Hz), 15.50 (d, *J* = 9.7 Hz).

References

1. D. D'Amours, S. Desnoyers, I. D'Silva, G. G. Poirier, *Biochem. J.* **1999**, *342*, 249–268.
2. M. Daugherty, B. Polanuyer, M. Farrell, M. Scholle, A. Lykidis, V. De Crécy-Lagard, *J. Biol. Chem.* **2002**, *277*, 21431–21439.
3. J. R. Knowles, *Annu. Rev. Biochem.* **1980**, *49*, 877–919.
4. A. M. Marmelstein, L. M. Yates, J. H. Conway, D. Fiedler, *J. Am. Chem. Soc.* **2014**, *136*, 108–111.
5. W. Winkler, A. Nahvi, R. R. Breaker, *Nature* **2002**, *419*, 952–6.
6. M. Wu, L. S. Chong, S. Capolicchio, H. J. Jessen, A. C. Resnick, D. Fiedler, *Angew. Chemie Int. Ed.* **2014**, *53*, 7192–7197.
7. R. G. Yount, D. Babcock, W. Ballantyne, D. Ojala, *Biochemistry* **1971**, *10*, 2484–2489.
8. L. M. Yates, D. Fiedler, *ACS Chem. Biol.* **2016**, *11*, 1066–1073.
9. D. Mistry, N. Powles, *Org. Biomol. Chem.* **2013**, *11*, 5727–33.
10. F. H. Westheimer, *Science* **1987**, *235*, 1173–1178.
11. T. C. Myers, K. Nakamura, J. W. Flesher, *J. Am. Chem. Soc.* **1963**, *85*, 3292–3295.
12. C. Grison, H. Chibli, N. Barthe, P. Coutrot, *J. Org. Chem.* **2006**, 7978–7988.
13. H. J. Korhonen, L. P. Conway, D. R. W. Hodgson, *Curr. Opin. Chem. Biol.* **2014**, *21*, 63–72.
14. M. Kalek, J. Jemielity, J. Stepinski, R. Stolarski, E. Darzynkiewicz, *Tetrahedron Lett.* **2005**, *46*, 2417–2421.
15. J. K. Bitok, C. F. Meyers, *Medchemcomm* **2013**, *4*, 130–134.
16. H. Ikeda, E. Abushanab, V. E. Marquez, *Bioorg. Med. Chem. Lett.* **1999**, *9*, 3069–3074.
17. V. E. Marquez, C. K. Tseng, G. Gebeyehu, D. A. Cooney, G. S. Ahluwalia, J. A. Kelley, M. Dalal, R. W. Fuller, Y. A. Wilson, D. G. Johns, *J. Med. Chem.* **1986**, *29*, 1726–1731.
18. D. A. Stephanie Ortial, Thompson, J. Montchamp, **2010**, 8166–8179.
19. V. M. Dixit, C. D. Poulter, *Tetrahedron Lett.* **1984**, *25*, 4055–4058.
20. G. J. Van Der Heden Van Noort, C. P. Verhagen, M. G. Van Der Horst, H. S. Overkleeft, G. A. Van Der Marel, D. V. Filippov, *Org. Lett.* **2008**, *10*, 4461–4464.
21. M. Strenkowska, P. Wanat, M. Ziemniak, J. Jemielity, J. Kowalska, *Org. Lett.* **2012**, *14*, 4782–4785.
22. A. Beld, C. A. A. Claesen, E. S. Roersma, W. J. M. Schippers, L. M. Keizer, G. I. Tesser, *Recl. Trav. Chim. Pays-Bas* **1984**, *103*, 196–202.
23. J. Winkler, E. Urban, D. Losert, V. Wacheck, H. Pehamberger, C. R. Noe, *Nucleic Acids Res.* **2004**, *32*, 710–718.
24. B. A. Kellogg, C. D. Poulter, *Curr. Opin. Chem. Biol.* **1997**, *1*, 570–578.
25. A. Banerjee, T. D. Sharkey, *Nat. Prod. Rep.* **2014**, *31*, 1043–1055.
26. K. Clinch, D. R. Crump, G. B. Evans, K. Z. Hazleton, J. M. Mason, V. L. Schramm, P. C. Tyler, *Bioorg. Med. Chem.* **2013**, *21*, 5629–5646.
27. R. M. Kissling, M. R. Gagné, *J. Org. Chem.* **1999**, *64*, 1585–1590.
28. M. Kalek, J. Jemielity, J. Stepinski, R. Stolarski, E. Darzynkiewicz, *Tetrahedron Lett.* **2005**, *46*, 2417–2421.

3 *Combined Phosphoramidite-Phosphodiester Reagents for the Synthesis of Unsymmetric Methylene Bisphosphonates*

Introduction

Pyrophosphate monoesters and unsymmetric pyrophosphate diesters are ubiquitous structural elements in biomolecules that fulfill essential roles in processes such as: biosynthesis, DNA repair, cellular metabolism and cell signaling. For instance, in cellular respiration four unsymmetric pyrophosphates, adenosine diphosphate (ADP)[1], coenzyme A[2], flavin adenine dinucleotide (FAD)[3] and nicotinamide adenine dinucleotide (NAD^+) work in unison to provide the required energy to sustain life.[4] Redox cofactor FAD not only functions in the electron transport chain, but also acts as a strong oxidizing agent that participates in a broad spectrum of oxidative metabolic pathways.[5] Another prevalent group of unsymmetric pyrophosphates are nucleotide diphosphate sugars. These are utilized by glycosyltransferases to transfer monosaccharides onto acceptor molecules, such as saccharides, lipids or proteins.[6] Both glycosylation and phosphorylation of amino acid side chains within proteins are well-known post-translational modifications (PTM), that regulate protein intracellular transport and activity.[7] A lesser studied PTM concerns the indirect transfer of pyrophosphates onto peptides. Adenosine diphosphate ribosylation (ADP-ribosylation) is a prominent example of indirect (pyro)phosphorylation, where a monomer or polymer of ADPr is linked to an amino acid side chain in an acceptor protein.[8,9] ADP-ribosylation plays an important role in DNA repair and the recent synthesis of molecules (or analogues thereof) involved in ADP-ribosylation has attracted a lot of scientific interest.[10,11] However, existing methodologies are considered unsuited for the synthesis of unsymmetric methylene bisphosphonate analogues of complex biomolecules, such as poly-ADP-ribose fragments. Therefore, an improved methodology to this end could facilitate PARylation related research. Chapter 2 introduces phosphanyl-methylphosphonate reagents for the synthesis of terminal methylene bisphosphonates as stabilized

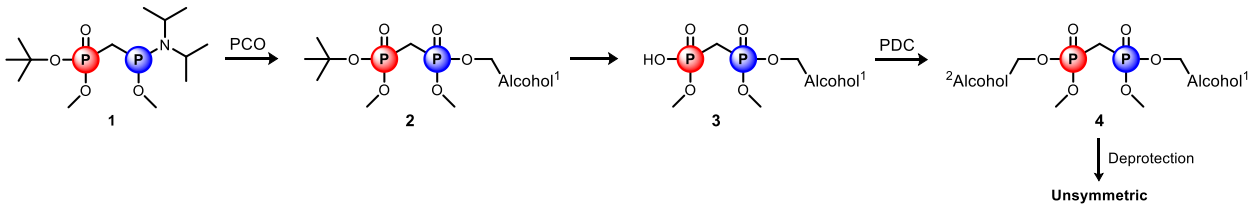

Figure 1: An overview of the methodology for the synthesis of unsymmetric methylene bisphosphonates. PCO: Phosphoramidite coupling-oxidation sequence. PDC: Phosphodiester condensation.

analogues of pyrophosphates monoesters. In this chapter the scope of the methodology based on such reagents is broadened by the preparation of the more complex unsymmetric methylene bisphosphonates, as showcased by the synthesis of adenosine bisphosphate ribose (ADPR) analogue **14** and flavin adenine dinucleotide (FAD) analogue **17** (Scheme 3). As depicted in Figure 1, orthogonal protected phosphanylmethylphosphonate **1** reacts with an alcohol of choice using the phosphoramidite coupling-oxidation sequence to give fully protected methylene bisphosphonate diester **2**. Selective removal of the *tert*-butyl group results in the formation of **3** that is amenable for condensation with another alcohol of choice using an suitable condensation agent.

Results and Discussion

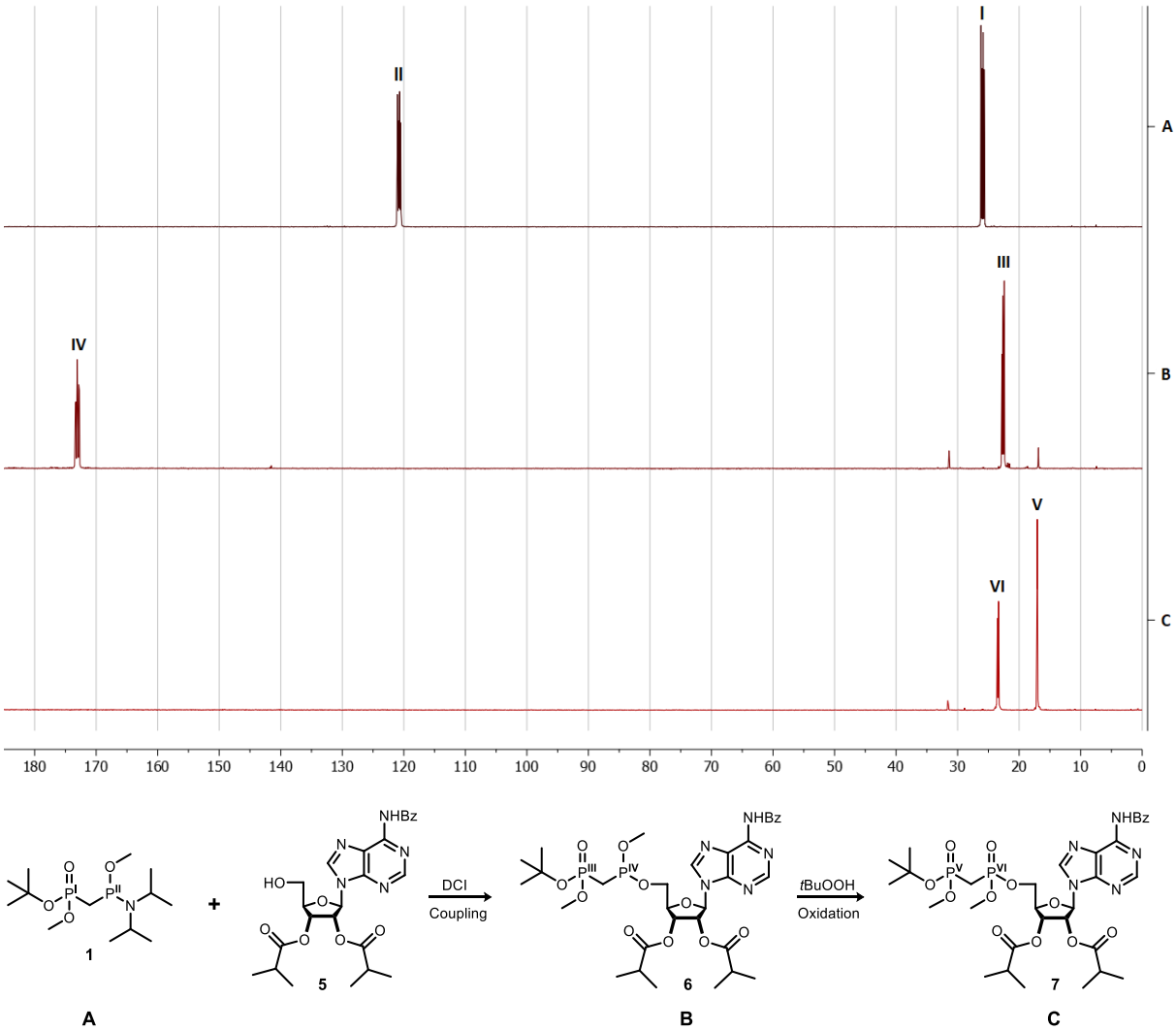

Figure 2: Phosphorylation of adenosine building block **5** using phosphanyl methylphosphonate reagent **1**, monitored by ^{31}P NMR spectroscopy (162 MHz). A NMR tube was charged with an aliquot of the reaction mixture and fitted with an acetone-d6 capillary (required for locking). **A:** The reagent before addition of the activator (DCI). **B:** The reaction mixture 10 minutes after addition of DCI; shows clean conversion into the phosphonite-phosphonate intermediate (peak II » IV). **C:** The reaction mixture 15 minutes after addition of *t*BuOOH; oxidation of the phosphonite (peak IV » VI).

First, the condensation efficiency of reagent **1** (Figure 2) with partially protected adenosine derivative **5** was evaluated using various activators. Based on ^{31}P-NMR spectroscopic analysis and the obtained yields, 5-(ethylthio)-1H-tetrazole (ETT) and 1H-tetrazole performed equally well, while (dicyanoimidazole) DCI gave cleaner conversions and more reproducible results (Figure 2). As determined by ^{31}P-NMR spectroscopy, subsequent oxidation of **6** by *tert*-butyl hydroperoxide provided me-ADP **7** (Figure 2, B » C). Although NMR analysis showed clean conversion of the DCI mediated coupling, the isolated yield of me-ADP **7** was unsatisfactory, never exceeding 55%. Exclusion of product loss during column purification and washing steps led to the tentative conclusion that the methylene bisphosphonate moiety in **7** binds Mg^{2+} from magnesium sulfate (used during work-up). Indeed, switching to the use of sodium sulfate as a drying agent resulted in the isolation of **7** in significantly higher yields (76-85%). Subsequent removal of the *tert*-butyl group in **7**, to give **8**, would permit the next condensation with the C^5-*OH* from methyl 2,3-diacetyl-ß-D-ribofuranoside (**13**, Scheme 3). Cleavage of the *tert*-butyl group using 10% TFA in DCM quantitatively provided phosphonic acid **8** as determined by ^{31}P-NMR and ^{1}H-NMR spectroscopy. Surprisingly, the following condensation of 2,3-di-*O*-acetyl-D-ribofuranoside and **8** under influence of the reagent combination, 2-mesitylenesulfonyl chloride (TMBSC) and 4-methoxypyridine-*N*-oxide (MNO) was unsuccesful.[12]

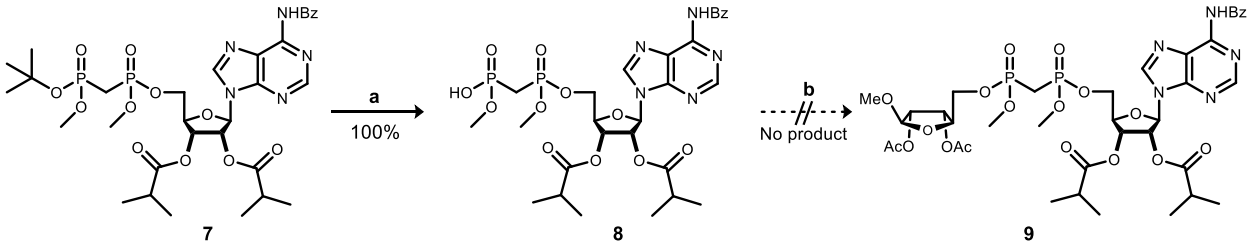

Scheme 1: First attempted synthesis of Me-ADPR (**36**), while using TFA during *t*Bu-deprotection. Reagents and conditions: [**a**] 10% TFA in DCM, 0.5h. [**b**] TMBSC, MNO, pyridine/MeCN » methyl 2,3-diacetyl-ß-D-ribofuranoside, 3h.

In order to investigate this unexpected outcome, various conditions were screened using methylene bisphosphonate tetraester **10** as a model compound. By monitoring the coupling reactions with ^{31}P-NMR spectrometry, it became evident that the activator was quenched by the presence of one equivalent of TFA in each batch of methylphosphonic acid **11a** (Scheme 2). It was found that the TFA used during *tert*-

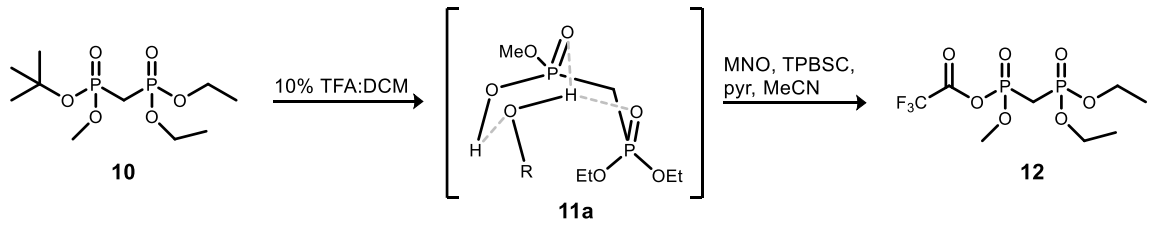

Scheme 2: *tert*-Butyl deprotection of model substrate **10** using TFA (R = ·$COCF_3$), showing the postulated caged structure **11a** for binding the acid. Applying activation conditions resulted in the formation of mixed anhydride **12**. TPBSC: 2,4,6-Triisopropylbenzenesulfonyl chloride.

butyl deprotection formed an inseparable (by co-evaporation) complex with the formed methylphosphonic acid. This was substantiated by ^{1}H-NMR spectrometric analysis of the deprotected compounds, where in each instance the phosphonic acid proton formed a singlet that integrating for two protons. It was postulated that the formation of a putative acid-acid complex **11a** could be attributed to favorable "caged" hydrogen bonding, as depicted in scheme 2 (**11a**). Applying activation conditions to the TFA-phosphonic complex showed the formation of a single new phosphonate species on ^{31}P-NMR spectrometry, which was identified as an unproductive mixed anhydride of TFA and the bisphosphonate. Switching to 1.5 equivalents of HCl in hexafluoroisopropanol (HFIP) effectively cleaved the *tert*-butyl group, providing **8** in quantitative yield. Indeed, the subsequent key P^{V}-coupling reaction of **8** with **13**, under the agency of TMBSC and MNO, afforded a mixture of the fully protected target me-ADPR **9** and its

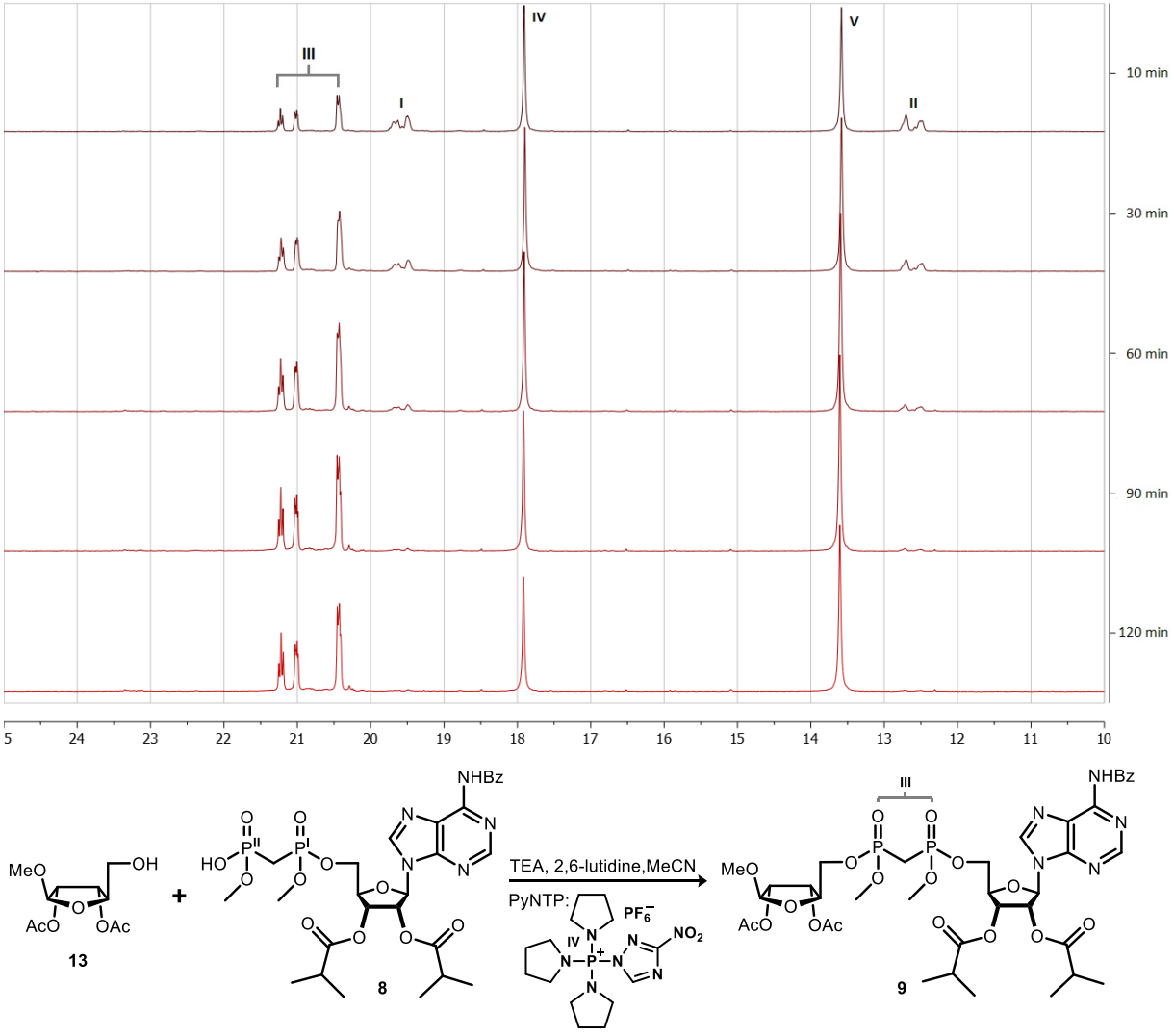

Figure 3: Condensation of ribose **13** with me-ADP **8**, monitored over 120 minutes by ^{31}P NMR spectrometry (162 MHz). A NMR tube was charged with an aliquot of the reaction mixture and fitted with an acetone-d_6 capillary (required for locking). The experiment shows the conversion of the phosphonic acid (**II**) into methylene bisphosphonate tetraester (**III**). During the condensation PyNTP (**IV**) is converted into tripyrrolidine-*N*-phosphine oxide (**V**).

mono-demethylated derivative, in a combined yield of 60% (Scheme 3). Previously Wada and co-workers have shown that phosphonium reagents are selective and effective agents to facilitate condensation of methylphosphonates with alcohols.[13] Implementing 3-nitro-1,2,4-triazol-1-yl-tris(pyrrolidin-1-yl) phosphonium hexafluorophosphate (PyNTP) as the condensing agent further improved the yield of protected me-ADPR **9** to 84% yield. The monitoring of this condensation by ^{31}P-NMR spectroscopy is shown in Figure 3. Two-step removal of all protecting groups in **9** was accomplished through demethylation by thiophenol in MeCN/TEA, followed by deacylation using aqueous ammonia. Purification of the crude product by gel filtration, provided the desired me-ADPR in 52% yield (**14**, Scheme 3).

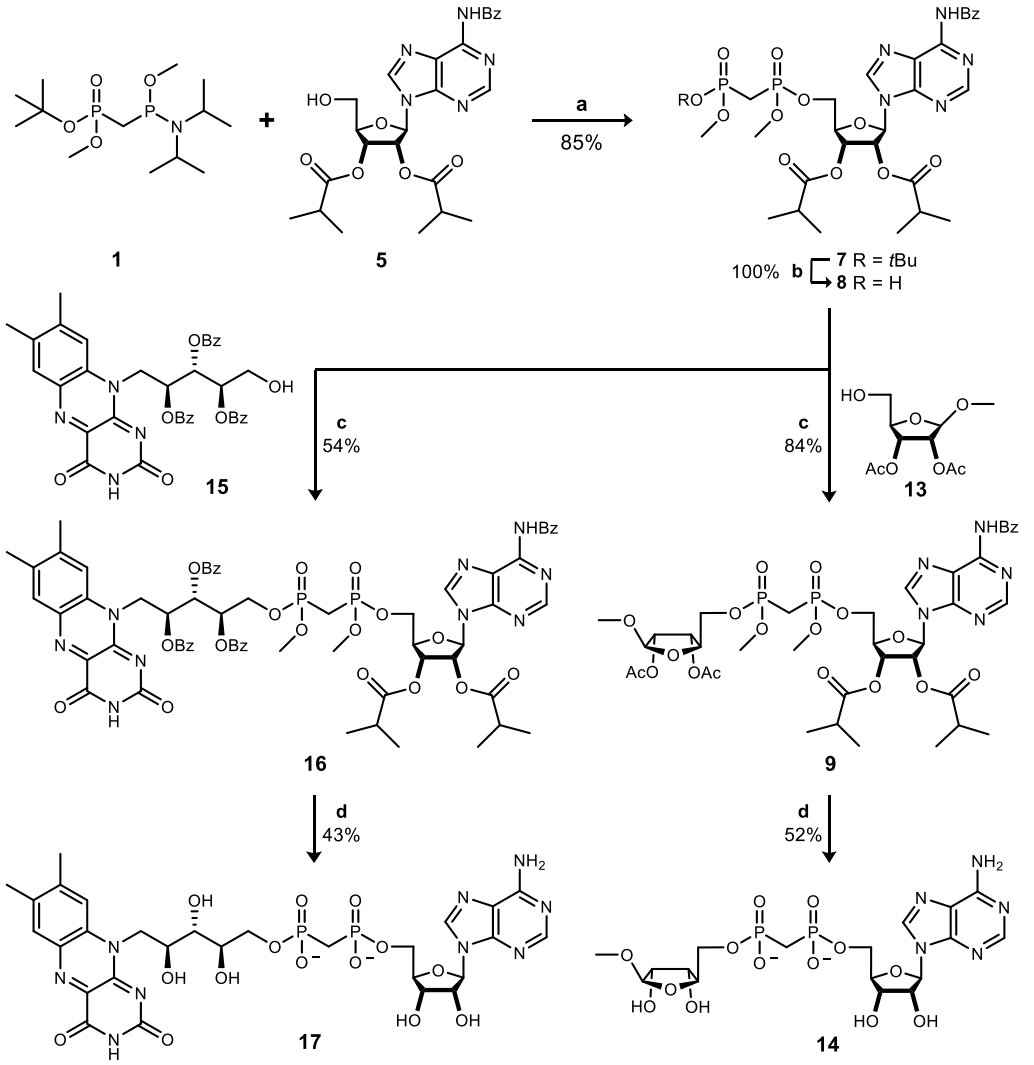

Scheme 3: Synthesis of Me-ADPR (**14**) and Me-FAD (**17**). Reagents and conditions: [**a**] i: DCI, MeCN, 15 min. ii: *t*BuOOH, 15 min. [**b**]. HCl (1.5 eq, 0.2 M), HFIP [**c**] PyNTP, **13**, 2,6-lutidine, MeCN, 1h **or** PyNTP, **15**, 2,6-lutidine, MeCN, 1h. [**d**] i: PhSH/Et_3N/MeCN (3:2:3), 35 ˚C, 4.5h. ii: 30% NH_4OH, 16h.

The thus obtained optimal protocol for the installation of unsymmetric methylene bisphosphonates was implemented in the synthesis of **17**, a known bioisostere for FAD.[14] Riboflavin building block **15** was condensed with **8** under the agency of PyNTP to furnish protected me-FAD derivative **16** in 54% yield. Ensuing two-step deprotection, followed by purification with size-exclusion chromatography, gave me-FAD **17** in 43% isolated yield. The synthesis towards me-FAD proved to be challenging as the poor solubility of the flavin moiety slowed the conversion rate and complicated the purification processes. Regardless, the yield significantly exceeded the 12% reported for protected me-FAD using the DCC-dimir coupling methodology.

Conclusion

The phosphanylmethylphosphonate reagent **1**, described in Chapter 2 was successfully adopted in the synthesis of unsymmetric methylene bisphosphonates me-ADPR **14** and me-FAD **17**. Reagent **1** is fitted with a *tert*-butyl protective group that is orthogonal relative to the methyl esters. Reagent **1** reacts with an alcohol of choice using the phosphoramidite coupling-oxidation sequence to give the respective, fully protected, methylene bisphosphonate tetraester. These reactions could conveniently be monitored with ^{31}P NMR spectroscopy, which indicated fast and clean conversions. An investigation of the cleavage of the *tert*-butyl by TFA revealed that the produced phosphonic acid formed a complex with TFA, the presence of which was detrimental for the subsequent P^V-condensation. An efficient alternative cleavage procedure for the *tert*-butyl group was found in HFIP·HCl. From here, the second alcohol could be introduced through condensation using PyNTP as an activator, yielding the protected unsymmetric methylene bisphosphonates. Global deprotection via a two-step-one-pot procedure, provided me-ADPR **14** and me-FAD **17**. The successful synthesis of me-ADPR **14** and me-FAD **17** indicates that a general procedure is developed for the synthesis of unsymmetrical methylene bisphosphonates.

Experimental

General: All solvents used under anhydrous conditions were stored over 4Å molecular sieves except for methanol which was stored over 3Å molecular sieves. Solvents used for workup and column chromatography were of technical grade from Sigma Aldrich and used directly. Unless stated otherwise, solvents were removed by rotary evaporation under reduced pressure at 40 °C. Reactions were monitored by TLC-analysis using Merck aluminum DC Silicagel 60 F_{254} with detection by spraying with 20% H_2SO_4 in EtOH, $(NH_4)_6Mo_7O_{24}{\cdot}4(H_2O)$ (25 g/L) and $(NH_4)_4Ce(SO_4)_4{\cdot}2(H_2O)$ (10 g/L) in 10% sulfuric acid or by spraying with a solution of ninhydrin (3 g/L) in EtOH / AcOH (20/1 v/v), followed by charring at approx. 250°C. Column chromatography was performed on Fluka silicagel (0.04 – 0.063 mm) or for methylene bis(phosphorus) compounds on high-purity grade silica (Sigma-Aldrich, Davisil Grade, 633).

NMR: ^{1}H-, ^{13}C- and ^{31}P-NMR Experiments were carried out on a Brüker AV-400 (400 MHz) or a Brüker AV-500 (500 MHz) and AVIII-Brüker DMX-600 (600 MHz). Chemical shifts are given in ppm (δ) and directly referenced to TMS (0.00 ppm) in $CDCl_3$ or D_2O via the solvent residual signal. $CDCl_3$ used in the characterization of phosphoramidite containing compounds was neutralized before use by filtering over aluminum oxide (Type WB-5: Basic). ^{31}P Chemical shifts are indirectly referenced to H_3PO_4 (0.00 ppm) according to the IUPAC method. ^{31}P NMR spectra measured to monitor reactions were made by charging a NMR tube with an aliquot of the reaction mixture and fitting the tube with an acetone-d_6 capillary.

LC-MS: Analysis were carried out on a JASCO HPLC system (detection simultaneously at 214 and 254 nm) coupled to a PE/SCIEX API 165 single quadruple mass spectrometer (Perkin-Elmer) using an analytical Gemini C18 column (Phenomex, 50 x 4.60 mm, 3 micron) in combination eluents A: H_2O; B: MeCN and C: 0.1 M aq. NH_4OAc or a Thermo Finnigan LCQ Advantage MAX ion-trap mass spectrometer with an electrospray ion source coupled to Surveyor HPLC system (Thermo Finnegan) using an analytical Gemini C18 column (Phenomex, 50 x 4.60 mm, 3 micron) in combination with eluents A: H_2O; B: MeCN and C: 1% aq. TFA as the solvent system. High resolution mass spectra were recorded by direct injection (2 µL of a 2 µM solution in water/acetonitrile; 50/50; v/v and 0.1% formic acid) on a mass spectrometer (Thermo Finnigan LTQ Orbitrap) equipped with an electrospray ion source in positive mode (source voltage 3.5 kV, sheath gas flow 10, capillary temperature 250 °C) with resolution R = 60000 at m/z 400 (mass range m/z = 150-2000) and dioctylpthalate (m/z = 391.2842) as a “lock mass”.

Trace Metal Chelation: High purity grade silica should be used when purifying methylene mono-phosphonic acids by silica gel column chromatography. Methylene mono-phosphonic acids (**8**) could be purified using silica gel column chromatography. However, it was found that after column purification the characteristic ^{31}P NMR peaks showed extreme signal broadening, to such an extent that the signals became difficult to detect. This broadening effect could be reversed by passing the purified methylene mono-phosphonic acid over an EDTA functionalized resin (a resin used to capture metal ions). This indicates that signal broadening resulted from metal ions bound to the phosphate, which could only have occurred during column purification.

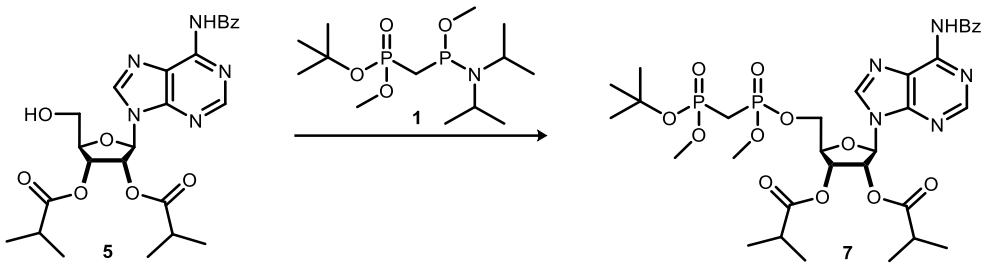

Fully Protected me-ADP 7: N^6-Benzoyl-2,3-*O*-di-*iso*-butyryladenosine (1.60 g, 3.12 mmol, 1 eq) and phosphanyl methylphosphonate **1** (1.12 g, 3.43 mmol, 1.1 eq) were co-evaporated with MeCN (15 mL), redissolved in MeCN (13 mL) and put under argon atmosphere. The reaction mixture was stirred until all solids were dissolved, then DCI (0.737 g, 6.24 mmol, 2 eq) was added. ^{31}P-NMR indicated full conversion within 15 minutes. Oxidation was initiated by the addition of *tert*-butyl hydroperoxide (1.134 ml, 6.24 mmol, 2 eq) in decane (5.5M). The reaction mixture was stirred for an additional 15 minutes. The solution was poured into a separation funnel containing water and washed with aqueous sodium bicarbonate (to wash away DCI). The organic layer was dried over sodium sulfate and concentrated *in vacuo*. Purification by silica gel column chromatography (20% acetone in DCM » 30% acetone in DCM + 2% MeOH) yielded **7** as a colorless oil (2.00 g, 2.65 mmol, 85%). **^{1}H NMR:** (500 MHz, $CDCl_3$) δ 9.30 – 9.20 (m, 1H), 8.81 (s, 1H), 8.59 – 8.47 (m, 1H), 8.07 – 7.98 (m, 2H), 7.63 – 7.57 (m, 1H), 7.52 (dd, *J* = 8.4, 7.0 Hz, 2H), 6.38 – 6.30 (m, 1H), 5.95 – 5.84 (m, 1H), 5.72 (ddt, *J* = 31.8, 5.7, 3.5 Hz, 1H), 4.57 – 4.37 (m, 3H), 3.87 – 3.72 (m, 6H), 2.72 – 2.39 (m, 4H), 1.58 – 1.44 (m, 9H), 1.23 (dd, *J* = 7.0, 1.2 Hz, 6H), 1.11 (ddt, *J* = 18.6, 7.0, 1.3 Hz, 6H). **^{13}C NMR:** (126 MHz, $CDCl_3$) δ 175.59, 175.52, 175.48, 175.19, 175.16, 164.58, 152.78, 151.81, 151.76, 151.73, 149.60, 133.54, 133.51, 132.65, 128.72, 127.79, 123.18, 123.15, 123.13, 99.89, 85.56, 85.49, 85.41, 84.53, 84.52, 84.49, 84.46, 84.45, 84.42, 81.90, 81.88, 81.84, 81.83, 81.80, 81.77, 81.74, 81.71, 73.20, 73.17, 73.13, 73.12, 70.55, 70.53, 70.39, 70.35, 65.25, 65.23, 65.21, 65.19, 65.05, 65.02, 64.97, 53.50, 53.45, 53.30, 53.25, 53.20, 53.15, 53.06, 53.01, 52.97, 52.96, 52.92, 52.87, 33.67, 33.48, 30.18, 30.16, 30.13, 27.28, 27.25, 27.21, 27.13, 26.19, 26.16, 26.14, 26.12, 26.09, 26.05, 26.02, 25.07, 25.05, 25.01, 24.93, 18.81, 18.78, 18.71, 18.69, 18.64, 18.62, 18.54. **^{31}P NMR:** (202 MHz, $CDCl_3$) δ 23.44 (d, *J* = 5.3 Hz), 23.37 (d, *J* = 6.1 Hz), 22.93, 22.91, 22.89, 16.19, 16.18, 16.15, 16.12. **HRMS:** Calculated for $C_{32}H_{45}N_5O_{12}P_2$ 754.26127 $[M+H]^+$; found 754.26141.

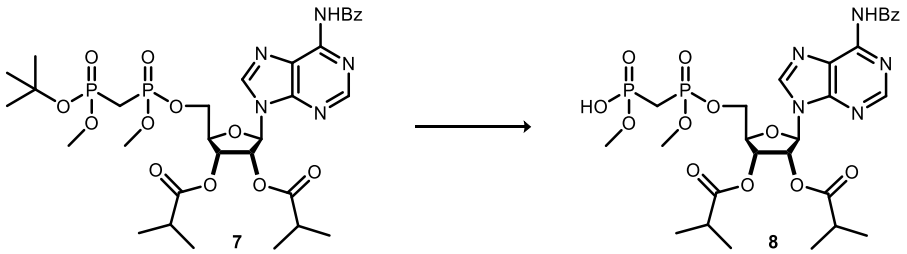

Protected me-ADP Triester 8: HCl (0.223 mL, 1.34 mmol, 1.5 eq) in dioxane : water (1:1 v:v, 6M) was added to a solution of me-Phos-62-2 (0.672 g, 0.892 mmol, 1 eq) in HFIP (6.6 mL). Reaction progress was monitored by 31P NMR; which showed complete conversion within 1h. The solution was co-evaporated with toluene, dioxane (2x) and chloroform (2x) to thoroughly remove all HFIP. This yielded the target compound as a white brittle foam (620 mg, 0.889, 100%). **^{1}H NMR:** (500 MHz, $CDCl_3$) δ 9.38 (d, J = 65.2

Hz, 1H), 8.85 (d, J = 6.7 Hz, 1H), 8.17 – 8.08 (m, 2H), 7.60 (td, J = 7.4, 2.1 Hz, 1H), 7.51 (td, J = 7.8, 2.1 Hz, 2H), 6.42 (d, J = 5.9 Hz, 1H), 5.90 (dt, J = 27.2, 5.8 Hz, 1H), 5.67 (ddd, J = 42.0, 5.7, 3.4 Hz, 1H), 4.53 – 4.36 (m, 3H), 3.77 – 3.61 (m, 6H), 2.67 – 2.47 (m, 4H), 1.24 – 1.18 (m, 6H), 1.11 (ddd, J = 15.0, 7.0, 1.6 Hz, 6H). **^{31}P NMR:** (202 MHz, $CDCl_3$) δ 25.19, 25.15, 25.13, 17.22 (d, *J* = 6.1 Hz), 16.94 (d, *J* = 6.1 Hz). **HRMS:** Calculated for $C_{28}H_{38}N_5O_{12}P_2$ 698.19867 $[M+H]^+$; found 698.19873

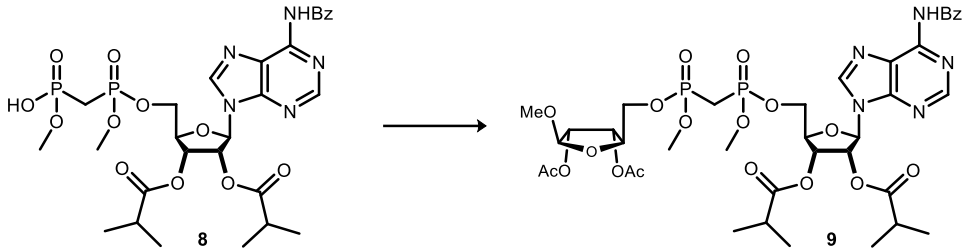

Fully Protected me-ADPR 9: Protected me-ADP **8** (0.225 g, 0.323 mmol, 1 eq), TEA (0.045 ml, 0.323 mmol, 1 eq), 2,6-lutidine (0.346 g, 3.23 mmol, 10 eq) and 1-methoxy-2,3-acetyl-D-Ribose (0.120 g, 0.484 mmol, 1.5 eq) were put under argon atmosphere and dissolved in dry MeCN (1.6 mL). PyNTP (0.483 g, 0.968 mmol, 3 eq) was added and the reaction progression was monitored using ^{31}P NMR, which indicated full conversion after 2 hours. The reaction mixture was quenched with NaOAc in MeOH (1 mL, 1 M). After an additional 10 minutes of stirring, the reaction mixture was poured into DCM and washed with 0.5M aqueous HCl. The organic layer was dried over sodium sulfate, filtered and concentrated *in vacuo*. Purification by silica gel column chromatography (3% MeOH in DCM) afforded me-ADPR as a mixture of diastereoisomers (251 mg, 271 mmol, 84%). The product mixture was isolated as a white foam. No efforts were made to separate the diastereoisomers, as both phosphonates lose chirality during the next step of demethylation. **NMR Data:** The NMR spectra were obtained from the mixture of four diastereoisomers. As a result the NMR spectra contained numerous partially overlapping product peaks. **^{31}P NMR:** (162 MHz, $CDCl_3$) δ 21.66, 21.62, 21.21, 21.19, 20.63, 20.60, 20.54, 20.51, 20.48, 20.45, 20.27, 20.23. **HRMS:** Calculated for $C_{38}H_{52}N_5O_{18}P_2$ 928.27771 $[M+H]^+$; found 928.27875.

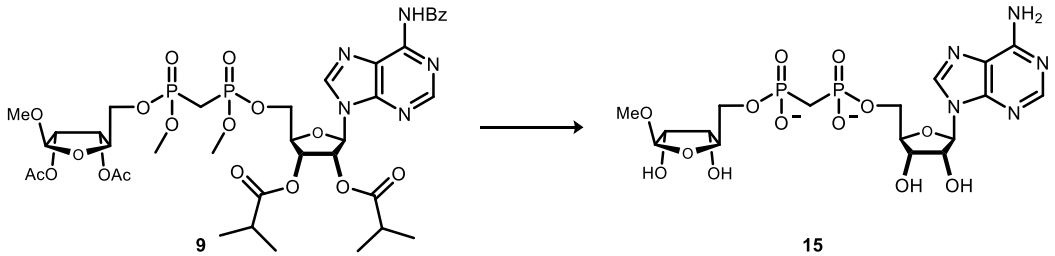

me-ADPR (15): Protected me-ADPR **9** (150 mg, 0.162 mmol) was dissolved in MeCN:TEA:PhSH (3:3:2, 1.6 mL) and stirred for 4 hours at 35 °C. Reaction progression was monitored by ^{31}P NMR, which indicated complete demethylation after 4.5 hours. The solution was partially reduced *in vacuo* to remove MeCN and pyridine. The residue was dissolved in ammonia (30%, 5 mL) and stirred overnight. The excess ammonia was purged by stirring under vacuum. The resulting solution was diluted with water, acidified to pH 4 using acetic acid and poured into a separation funnel. The water layer was washed with DCM (3x)

to remove excess thiophenol. The water layer was lyophilized to acquire the crude product. Purification by size-exclusion chromatography (HW40-column, 0.15 M aqueous NH_4OAc) followed by lyophilisation, yielded me-ADPR (48 mg, 0.084 mmol, 52%) as a colorless powder. **^{1}H NMR:** (600 MHz, Deuterium Oxide) δ 8.48 (s, 1H), 8.16 (s, 1H), 6.07 (d, *J* = 5.4 Hz, 1H), 4.82 (d, *J* = 1.3 Hz, 1H), 4.74 (t, *J* = 5.3 Hz, 1H), 4.51 (dd, *J* = 5.2, 4.1 Hz, 1H), 4.36 – 4.33 (m, 1H), 4.18 (dd, *J* = 6.6, 4.8 Hz, 1H), 4.17 – 4.13 (m, 2H), 4.06 (td, *J* = 6.2, 4.2 Hz, 1H), 4.00 – 3.94 (m, 2H), 3.89 (dt, *J* = 11.0, 6.1 Hz, 1H), 3.31 (s, 3H), 2.18 (td, *J* = 20.0, 2.1 Hz, 2H). **^{13}C NMR:** (151 MHz, D_2O) δ 156.01, 153.15, 149.72, 140.90, 119.43, 108.79, 88.01, 84.85, 84.79, 82.45, 82.40, 75.11, 74.97, 71.91, 71.10, 65.88, 65.84, 64.46, 64.43, 56.10, 27.93, 27.08, 26.24. 31P NMR: (162 MHz, D2O) δ 17.65, 17.59, 17.38, 17.32. **HRMS:** Calculated for $C_{17}H_{28}N_5O_{13}P_2$ for 571.11534 $[M+H]^+$; found 571.11530.

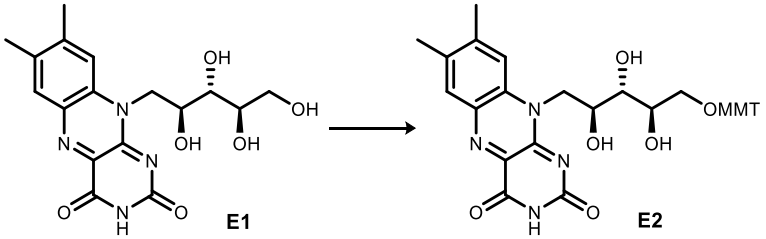

5-*O*-MMT-riboflavin (E2): MMT-Cl (2.71 g, 8.77 mmol, 1.1 eq) was added to a solution of riboflavin (3.00 g, 7.97 mmol, 1 eq) in pyridine (100 mL), under argon atmosphere. Reaction was heated to 100 °C and stirred overnight. After cooling to room temperature, the reaction was quenched by the addition of MeOH (1 mL) and concentrated. The residue was redissolved in chloroform (160 mL) and filtered. The filtrate was washed with aqueous sodium bicarbonate. The organic layer was dried over magnesium sulfate and concentrated *in vacuo*. The residue was purified by silica gel column chromatography (2% TEA in DCM preflush, eluent: 1% » 3% » 5% MeOH in DCM) yielded 5-*O*-MMT-riboflavin (2.15 g, 3.48 mmol, 44%) as bright yellow flakes. NMR spectrometry showed strong rotameric effects – **^{1}H NMR:** (600 MHz, $CDCl_3$) δ 10.03 (s, 1H), 7.85 (s, 2H), 7.41 (d, J = 8.2 Hz, 4H), 7.28 (d, J = 14.4 Hz, 4H), 7.18 (t, J = 7.8 Hz, 4H), 7.09 (t, J = 7.6 Hz, 2H), 6.71 (d, J = 8.4 Hz, 2H), 5.20 (s, 1H), 4.83 (d, J = 33.7 Hz, 3H), 4.41 (s, 1H), 4.08 (d, J = 79.3 Hz, 3H), 3.65 (s, 3H), 3.43 (d, J = 34.0 Hz, 2H), 2.33 (d, J = 28.5 Hz, 6H). **^{13}C NMR:** (151 MHz, $CDCl_3$) δ 159.77, 158.32, 156.15, 150.54, 148.49, 144.09, 137.34, 135.29, 135.15, 135.07, 131.90, 131.69, 130.27, 128.23, 127.70, 126.74, 117.10, 113.41, 113.20, 112.97, 86.63, 74.22, 71.93, 71.48, 65.39, 55.03, 48.34, 21.33, 19.35. **HRMS:** Calculated for $C_{37}H_{37}N_4O_7$ 649.26568 $[M+H]^+$; found 649.26636.

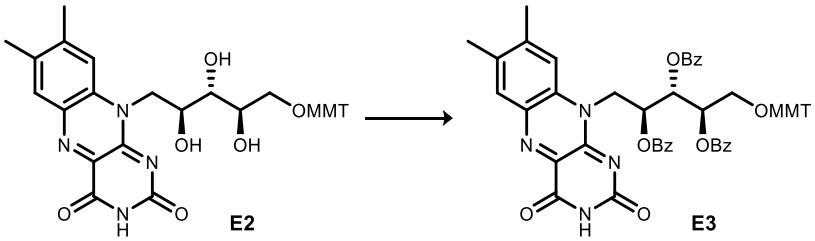

5-*O*-MMT-2,3,4-tri-*O*-Benzoylriboflavin (E3): Benzoyl chloride (1.19 ml, 10.3 mmol, 3.1 eq) was added dropwise to a solution of 5-*O*-MMT-riboflavin (2.15 g, 3.31 mmol, 1 eq) in pyridine (70 mL) at 0 °C. The

reaction mixture was stirred for 1h, before being quenched with water (5 mL) and concentrated *in vacuo*. The residue was redissolved on DCM and washed saturated aqueous sodium bicarbonate. The organic layer was dried over magnesium sulfate, filtered and concentrated *in vacuo*. Purification by silica gel column chromatography (0% » 10% acetone in DCM + 1% TEA) yielded hydroxyl protected 5-*O*-MMT-2,3,4-tri-*O*-Benzoylriboflavin (1.5 g, 2.4 mmol, 73%) as a bright yellow powder. **HRMS:** Calculated for $C_{58}H_{48}N_4O_{10}Na$ 983.32626 $[M+Na]^+$; found mass 983.32638.

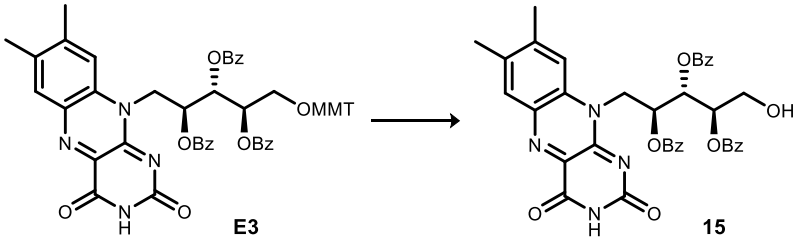

2,3,4-tri-*O*-Benzoylriboflavin (15): 5-*O*-MMT-2,3,4-tri-*O*-Benzoylriboflavin (1.5 g, 1,561 mmol) was added to a cooled (0 °C) solution of and triisopropylsilane (0.96 ml, 4.7 mmol, 3 eq) in DCM:DCA (9:1 v:v, 15 mL). The reaction was stirred for 1 hour. Methanol was added and the reaction mixture was washed with aqueous sodium bicarbonate. The organic layer was dried over magnesium sulfate, filtered and concentrated *in vacuo*. The concentrate was purified by silica gel column chromatography, providing riboflavin **15** (0.923 g, 1.34 g, 86%) as a bright yellow powder. **^{1}H NMR:** (500 MHz, $CDCl_3$) δ 9.46 (s, 1H), 8.20 – 8.05 (m, 4H), 7.84 (s, 1H), 7.79 – 7.71 (m, 2H), 7.67 (s, 1H), 7.59 (t, *J* = 7.5 Hz, 1H), 7.54 – 7.42 (m, 6H), 7.37 (t, *J* = 7.8 Hz, 2H), 7.30 (t, *J* = 7.7 Hz, 2H), 6.26 (dt, *J* = 8.3, 3.9 Hz, 1H), 6.10 (dd, *J* = 5.7, 3.1 Hz, 1H), 5.81 (q, *J* = 4.4, 4.0 Hz, 1H), 4.23 (d, *J* = 11.5 Hz, 1H), 4.18 – 4.01 (m, 2H), 2.21 (d, *J* = 17.1 Hz, 6H). **^{13}C NMR:** (126 MHz, $CDCl_3$) δ 165.65, 165.30, 159.49, 155.56, 150.51, 148.10, 136.72, 135.89, 134.56, 133.71, 133.49, 133.31, 132.38, 131.16, 129.95, 129.58, 129.17, 128.88, 128.68, 128.42, 128.30, 115.84, 73.28, 71.79, 70.62, 61.03, 20.96, 19.18. **HRMS:** Calculated for $C_{37}H_{37}N_4O_7$ 689.22421 $[M+H]^+$; found 689.22375.

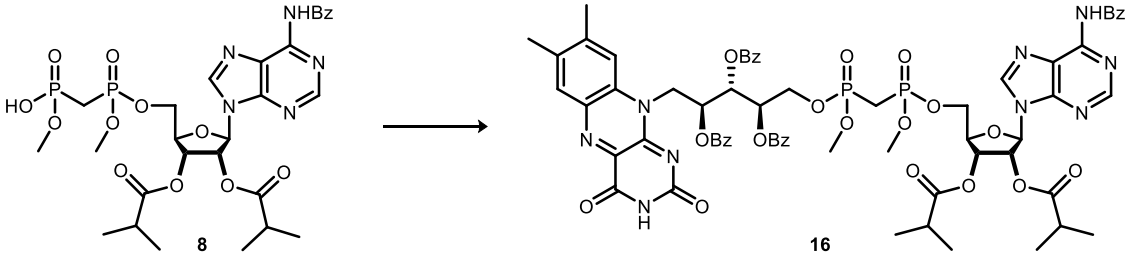

Protected me-FAD 16: me-ADP **8** (0.180 g, 0.258 mmol), TEA (36 µl, 0.258 mmol), 2,6-lutidine (301 µl, 2.58 mmol, 10 eq) and 2,3,4-*O*-Bz-Riboflavin (267 mg, 0.387 mmol, 1.5 eq) were put under argon atmosphere and dissolved in dry MeCN (0.5 mL). PyNTP (387 mg, 0.774 mmol, 3 eq) was added. Reaction proceeded within one hour, ^{31}P-NMR and LCMS showed conversion of the starting material into protected me-FAD **16**. The reaction mixture was quenched with NaOAc in MeOH (1 mL, 1M). After an additional 10 minutes of stirring, the reaction mixture was poured into DCM and washed with 0.5M aqueous HCl. The organic layer was dried over sodium sulfate, filtered and concentrated *in vacuo*. Purification by silica gel column chromatography (30% » 100% acetone in DCM) yielded the product (191 mg, 0.140 mmol, 54%) as a bright

yellow solid. **NMR Data:** The NMR spectra were obtained from the mixture of four diastereoisomers and showed significant peak broadening as a result of rotameric effects. **HRMS:** Calculated for $C_{66}H_{68}N_9O_{20}P_2$ 1368.40504 $[M+H]^+$; found 1368.40515.

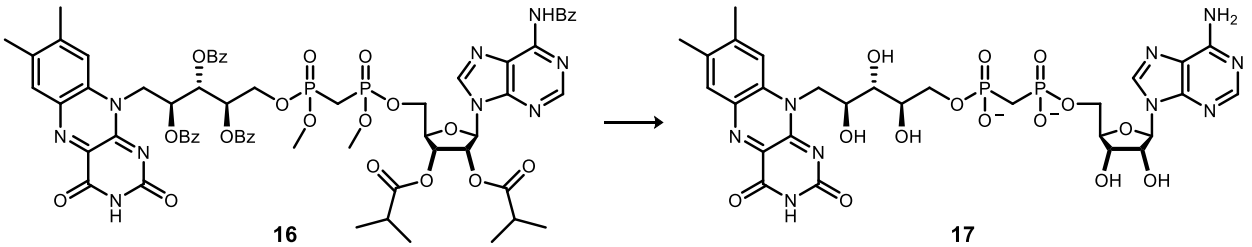

me-FAD (17): Protected me-FAD **16** (153 mg, 0.112 mmol) was dissolved in MeCN:TEA:PhSH (3:3:2, 1.6 mL) and stirred for 16 hours at 35 °C, after which ^{31}P NMR spectroscopy indicated complete demethylation. The solution was partially reduced *in vacuo* to remove MeCN and pyridine. The residue was dissolved in ammonia (30%, 5 mL) and stirred overnight. The excess ammonia was purged by stirring under vacuum. The resulting solution was diluted with water, acidified to pH 4 using acetic acid and poured into a separation funnel. The water layer was washed with DCM (3x) to remove excess thiophenol. The water layer was concentrated *in vacuo*. Purification by size-exclusion chromatography (HW40-column, 0.15 M aqueous NH_4OAc) followed by lyophilisation, yielded me-FAD (38 mg, 0.048 mmol, 43% yield). **^{1}H NMR:** (600 MHz, D_2O) δ 8.40 (s, 1H), 7.94 (s, 1H), 7.52 (s, 1H), 7.43 (s, 1H), 5.86 (d, *J* = 5.1 Hz, 1H), 4.55 (t, *J* = 5.1 Hz, 1H), 4.48 (t, *J* = 4.7 Hz, 1H), 4.40 (d, *J* = 13.7 Hz, 1H), 4.33 (d, *J* = 3.9 Hz, 2H), 4.21 (d, *J* = 15.6 Hz, 2H), 4.05 (dt, *J* = 11.4, 5.8 Hz, 1H), 4.01 – 3.95 (m, 1H), 3.93 (dd, *J* = 7.9, 4.4 Hz, 1H), 2.39 – 2.14 (m, 9H). **^{13}C NMR:** (151 MHz, D_2O) δ = 161.74, 158.45, 153.66, 151.42, 150.70, 150.60, 148.82, 141.23, 140.03, 135.15, 134.61, 132.24, 131.09, 118.58, 117.55. **^{31}P NMR:** (162 MHz, D_2O) δ 18.60, 18.11. **HRMS:** Calculated for $C_{28}H_{36}N_9O_{14}P_2$ 784.18569 $[M+H]^+$; found 784.18555.

References

1. A. I. Jonckheere, J. A. M. Smeitink, R. J. T. Rodenburg, *J. Inherit. Metab. Dis.* **2012**, *35*, 211–225.
2. J. Baddiley, E. M. Thain, G. D. Novelli, F. Lipmann, *Nature* **1953**, *171*, 76.
3. L. V Eggleston, D. H. Williamson, *Biochem. J.* **1954**, *56*, 250–256.
4. P. R. Rich, *Biochem. Soc. Trans.* **2003**, *31*, 1095–1105.
5. R. Teufel, A. Miyanaga, Q. Michaudel, F. Stull, G. Louie, J. P. Noel, P. S. Baran, B. Palfey, B. S. Moore, *Nature* **2013**, *503*, 552–556.
6. S. Singh, G. N. Phillips Jr., J. S. Thorson, *Nat. Prod. Rep.* **2012**, *29*, 1201.
7. G. A. Khoury, R. C. Baliban, C. A. Floudas, *Sci. Rep.* **2011**, *1*, 90.
8. P. O. Hassa, S. S. Haenni, M. Elser, M. O. Hottiger, *Microbiol. Mol. Biol. Rev.* **2006**, *70*, 789–829.
9. B. A. Gibson, W. L. Kraus, *Nat. Rev. Mol. Cell Biol.* **2012**, *13*, 411–424.
10. A. Pines, M. G. Vrouwe, J. A. Marteijn, D. Typas, M. S. Luijsterburg, M. Cansoy, P. Hensbergen, A. Deelder, A. de Groot, S. Matsumoto, et al., *J. Cell Biol.* **2012**, *199*, 235–249.
11. H. A. V. Kistemaker, A. P. Nardozza, H. S. Overkleeft, G. A. van der Marel, A. G. Ladurner, D. V. Filippov, *Angew. Chemie - Int. Ed.* **2016**, *55*, 10634–10638.
12. V. A. Efimov, O. G. Chakhmakhcheva, *Nucleosides and Nucleotides* **1985**, *4*, 265.
13. N. Oka, M. Shimizu, K. Saigo, T. Wada, *Tetrahedron* **2006**, *62*, 3667–3673.
14. K. W. Pankiewicz, K. Lesiak, K. A. Watanabe, *J. Am. Chem. Soc.* **1997**, *119*, 3691–3695.

4 Synthesis of *Carba*-Ribose Incorporated Mono-ADP-Ribosylated H2B Histone Peptide

Introduction

Adenosine diphosphate ribosylation (ADP-ribosylation) is a post-translational modification in which, for a long period of time, glutamate and aspartate were considered to be the main acceptor amino-acids. Recently, the number of target amino acids in proteins for ADP-ribosylation is broadened with lysine, arginine and serine.[1–4] Besides, the reported data on the covalent poly-ADP-ribosylation of histone proteins at glutamate or aspartate residues seem to be conflicting. Furthermore, non-covalent complexes between poly-ADP and the histone have also been reported.[5–7] To acquire more insight in the function of ADP-ribosylation of specific proteins and to indentify the involved amino acids, synthetically prepared, well-defined mono-ADP-ribosylated oligopeptides are important tools. In this respect the synthetic preparation and biochemical application of Asp and Glu ADP-ribosylated oligopeptides is restricted by the inherent susceptibility of anomeric esters to hydrolyze and/or migrate. For this reason attention was directed to the design and synthesis of analogues of mono-ADP-ribosylated oligopeptides, in which the glycosidic bond with Asp and Glu is stabilized.

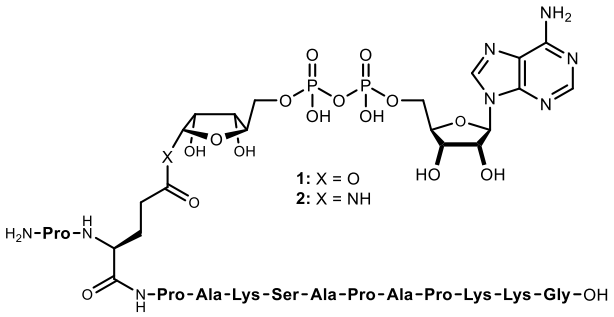

Figure 1: The structures of a native mono-ADP-ribosylated *N*-terminal H2B conjugate **1** and its glutamine incorporated bioisostere **2**.

A relevant target is the human histone H2B peptide in which the Glu-2, corresponding to the *N*-terminal sequence, is one of the earliest discovered sites for ADP-ribosylation.[8] Kistemaker *et al.* argued that the synthesis of the native mono-ADP-ribosylated H2B oligopeptide (Figure 1, **1**) was deemed to be

unsuccessful due to the propensity of the anomeric glutamyl ester to migrate.[9] To circumvent this side-reaction attention was directed to the synthesis and evaluation glutamate bioisostere (**2**) having a more stable anomeric amide bond. Although interesting results were obtained with oligopeptide **2**, the glycosidic bond in **2** is prone to acidic hydrolysis and anomerisation was also observed.[10] The intrinsic lability of O- and N-glycosidic bonds can be circumvened by the use of *carba*-ribose, an analogue where the ring-oxygen is substituted for a methylene. The resulting enhanced stability towards acidic conditions has the added benefit of significantly improving the compatibility with solid-phase peptide synthesis. This chapter describes the synthesis of stabilized conjugate **3** (Figure 2).

Results and Discussion

Retrosynthetic Analysis. The general strategy towards conjugate **3** was analogous to that reported for glutamate bioisostere **2**.[9] Retrosynthetically phosphorylated building block **4**, containing the pre-constructed glutamyl functionalized *carba*-riboside, would be installed into the peptide as a whole via solid-phase synthesis (Figure 2). Subsequent selective deprotection of the di-*tert*-butyl phosphate, followed by on-resin phosphorylation with an adenosine phosphoramidite derivative, would construct the pyrophosphate bridge. Disconnecting building block **4** at the C^1-glutamylamide and O^5-phosphodiester residues, after suitable deprotection steps, reveals the core *carba*-riboside **5**. The timely removal of the chemically robust isopropylidene acetal in **5** is required, as later stage constructs are incompatible with the deprotection conditions. Furthermore, it was anticipated that the unprotected C^2- and C^3-*OH*'s would not impair the later stage solid-phase synthesis. In 1996, Parry *et al.* had reported the synthesis for a similar *carba*-riboside as **5**, containing an α-hydroxyl at the C^1-position.[11] They were able to install the C^5-*CH_2OH* through the photochemical addition of methanol onto the β-position of cyclopentenone **6**. Subsequent reduction of the ketone provided the desired α-hydroxyl. In both cases the reactions proceeded stereoselectively, owing to the envelope conformation induced by the isopropylidene. It was envisioned that a reductive amination would provide the α-C^1-amine in a similar fashion. The route described by Perry *et al.* for the conversion of D-ribonolactone to cyclopentenone **6**, however, entailed several low yielding steps with an overall yield of 10% after four steps. Therefore an alternative route, described by Borcherdinger and co-workers, for the synthesis of a cyclohexylidene protected analogue of **6** was considered more efficient.[12] Unfortunately, attempts to reproduce or improve upon their results were unsuccessful. Additional perusing of literature revealed that the exact same complications were experienced by Mariën *et al.*, and their thorough reinvestigation yielded results conflicting with those

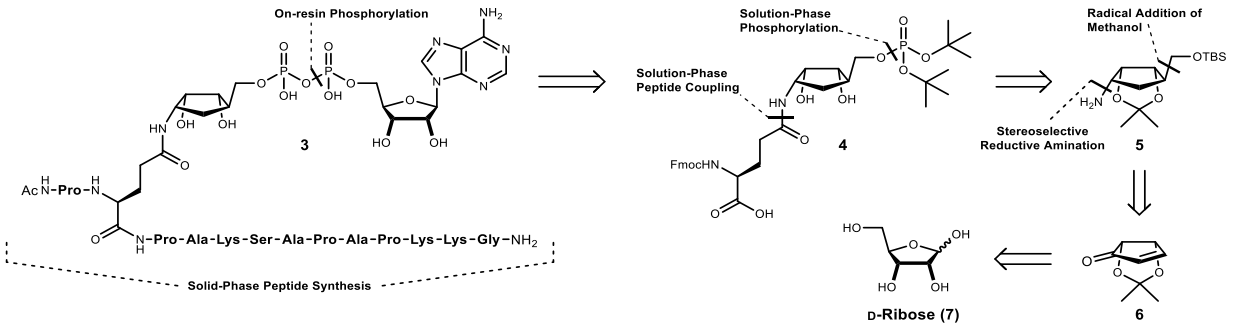

Figure 2: Retrosynthetic analysis of the proposed stabilized mono-ADP-ribosylated H2B conjugate **3**.

reported by Borcherdinger.[13] At this point it was concluded that no satisfactory route for the synthesis of cyclopentenone **6** was available in literature, and thus a new route was designed.

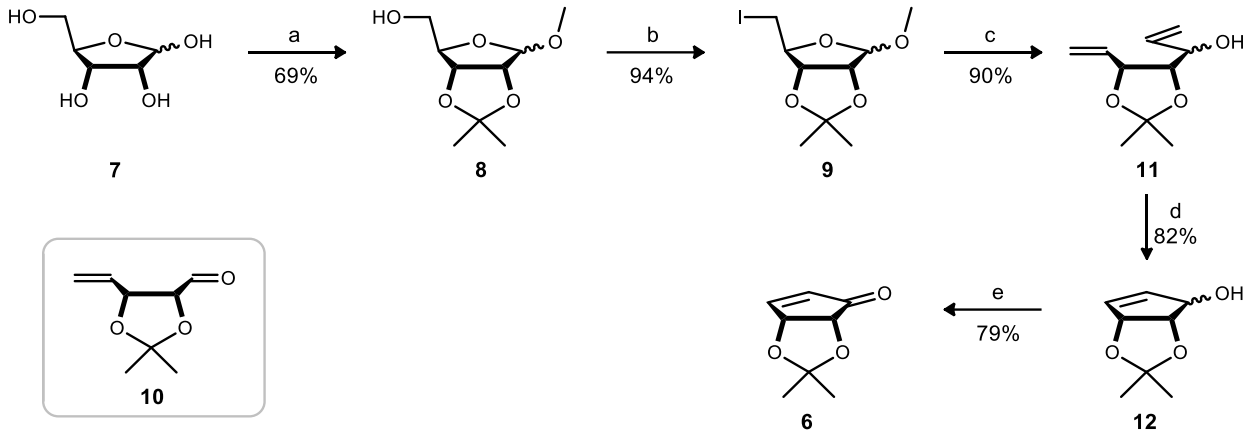

Scheme 1: The newly developed route towards enone **6**. Reagents and conditions: [**a**] i: AcCl, MeOH, 1.5h. ii: 2,2-dimethoxypropane, CSA, acetone 0.5h. [**b**] I_2, PPh_3, 1*H*-imidazole, toluene/MeCN, 100 ˚C, 45 min. [**c**] i: *n*-BuLi, THF, -78 ˚C, 2h. ii: vinylmagnesium bromide, THF, -78 ˚C, 30 min. [**d**] Grubbs-I, DCM, 16h. [**e**] MnO_2, DCM, 16h.

Synthesis of cyclopentenone 6. The new route towards cyclopentenone **6** commenced with the methanolic Fischer glycosylation of D-ribose. After neutralization and concentration, the crude α/β-methoxy-D-ribose was directly subjected to isopropylidene protection of the C^2-C^3-diol. Treatment with 2,2-dimethoxypropane and a catalytic amount of camphorsulfonic acid provided riboside **8** in 69% yield over 2 steps. Subsequent iodination of the primary alcohol with iodine and triphenylphosphine, under the agency of 1*H*-imidazole at 100 °C in toluene/MeCN, produced iodo-riboside **9** in 94%. It was envisioned that a lithium-halogen exchange induced fragmentation under controlled temperatures would cleanly convert **9** into aldehyde **10**. This would allow for a combined one-pot procedure with the subsequent vinyl Grignard. Hence, fragmentation of **9** into intermediate **10** with *n*-butyllithium in THF at -78 °C, was directly followed by addition of vinylmagnesium bromide, to produce *R*/*S*-diallyl **11** in 90% yield over two steps. No efforts were undertaken to separate the diastereoisomers of **11**, as the chiral center is lost during later stage oxidation. Ring-closing metathesis of diallyl **11** using 1st generation Grubbs catalyst in DCM provided *R*/*S*-cyclopentenoid **12** in 82% yield. During reaction refinement it was found that after thoroughly purging the solvent (DCM) of oxygen, the 1st generation Grubbs catalyst performed as well as the more expensive 2nd generation variant. In addition, the catalyst loading could be reduced to 0.6 mol% on a 100 mmol scale. Final oxidation of *R*/*S*-cyclopentenoid **12** with excess manganese dioxide afforded target cyclopentenone **6** in 79% yield. The new route for the conversion of D-ribose into enone **6** entailed seven steps, carried out in five reaction vessels, with an overall yield of 38%.

Synthesis of glutamine *carba*-riboside 4. Next, efforts were directed to the synthesis of glutamine *carba*-riboside **4** (Scheme 2). The photochemical addition of methanol onto the β-position of cyclopentenone **6** provided *carba*-riboside **13** in 61% yield.[11] On larger scale, the dilute photochemical conditions made it increasingly difficult to adequately remove solvated oxygen from the copious amounts of methanol, and resulted in lower isolated yields. At this stage, it was envisioned that the photochemistry protocol could potentially be adapted to directly add trimethyl phosphate onto the β-position of cyclopentenone **6**, which would reduce the overall length of the synthesis. Unfortunately, the envisioned phosphorylated product could no be prepared in this manner. Protection of the alcohol in **13** with TBSCl gave silylated product **14** in 86% yield. The quantitative condensation of ketone **14** with methoxylamine delivered imine **15** as a mixture of *cis*/*trans*-isomers. Stereoselective reduction of the imine proved difficult and various conditions (BH_3, $LiAlH_4$, $NaBH_3CN$, Zn/H^+) were explored, of which $LiAlH_4$ in refluxing THF proved to be the most effective, providing *carba*-ribosamine **16** in 30% yield. It was later found that the low yields were due to either inertness of the starting material to the reagents, or degradation of the TBS group. During preliminary optimization experiments it was found that a significant higher yield (81%) was obtained when the C^5OH was protected with a trityl instead of the TBS. PyBOB-mediated condensation of amine **16** with commercial Fmoc-Glu(OBn)-OH gave *carba*-ribosylated glutamine **17** in quantitative yield. Simultaneous deprotection of the TBS and isopropylidene using aqueous acetic acid at 60 °C gave **18** in 42% yield. Phosphorylation of primary alcohol with di-*tert*-butyl-*N*,*N*-diisopropyl-phosphoramidite and 1*H*-tetrazole, followed by *in situ* oxidation, afforded phosphate **19** in 50% yield. Hydrogenolysis of the benzyl ester provided SPS-building block **4** in 72% yield.

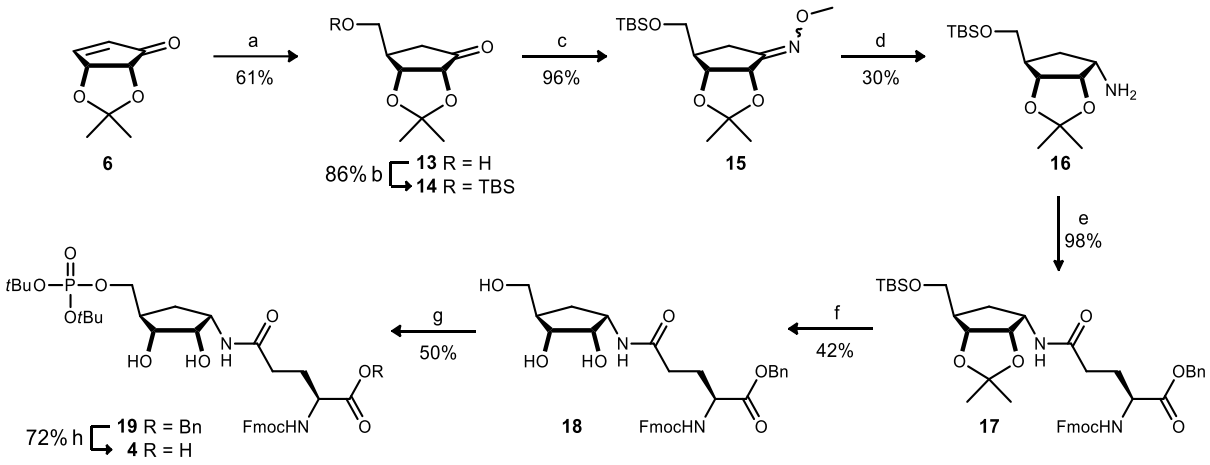

Scheme 2: Synthesis of glutamine *carba*-riboside **4**. Reagents and conditions: [**a**] Benzophenone, MeOH, hv, 16h. [**b**] TBSCl, 1*H*-imidazole, DCM, 16 h. [**c**] Methoxylamine, DCM, 3h. [**d**] $LiAlH_4$, THF, 75 °C, 2h. [**e**] PyBOB, Fmoc-Glu(OBn)-OH, DMF, 16h. [**f**] AcOH, H_2O, 60 °C, 16h. [**g**] i: 1-methylimidazole, 1-methylimidazole·HCl, di-*tert*-butyl-*N*,*N*-diisopropylphosphoramidite, DMF, 30 min. ii: *t*BuOOH, 10 min. [**h**] Pd/C, H_2, MeOH, 16h.

With *carba*-riboside building block **4** in hand, the solid-phase peptide synthesis (SPPS) of stabilized mono-ADP-ribosylated H2B conjugate **3** was undertaken (Scheme 3). The core peptide was constructed from a Tentagel resin functionalized with Fmoc-glycine through a 4-hydroxymethylbenzoic acid (HMBA) linker, using standard Fmoc-based SPPS methodology. Base-labile protecting groups were selected for the adenosine moiety and the nucleophilic amino acid side-chains, to later enable simultaneous global

deprotection and release from solid support. Instalment of artificial amino acid **4** into resin-bound conjugate **20** proceeded uneventfully, as was determined by LC-MS analysis of a resin-released and deprotected aliquot of the peptide. Deprotection of the *tert*-butyl groups in **20** with 10% TFA in DCM proceeded cleanly, as monitored by on-resin ^{31}P NMR spectroscopy. From here the stage was set for construction of the ADP-pyrophosphate bridge. On-resin phosphorylation of **21** with adenosine phosphoramidite **22**, under the agency of 5-ethylthiotetrazole (ETT), followed by CSO-mediated oxidation of the phosphate-phosphite intermediate, produced the protected resin-bound *carba*-ribosylated peptide. Final deprotection consisted of DBU-assisted elimination of the 2-cyanoethanol group, and subsequent global deacylation and concomitant release from solid-support through ammonolysis. The crude *carba*-ribosylated peptide was precipitated and HPLC purified, to provided mono-ADP-*carba*-ribosylated H2B conjugate **3** in 9% (8.2 mg, 0.6 µmol) overall yield.

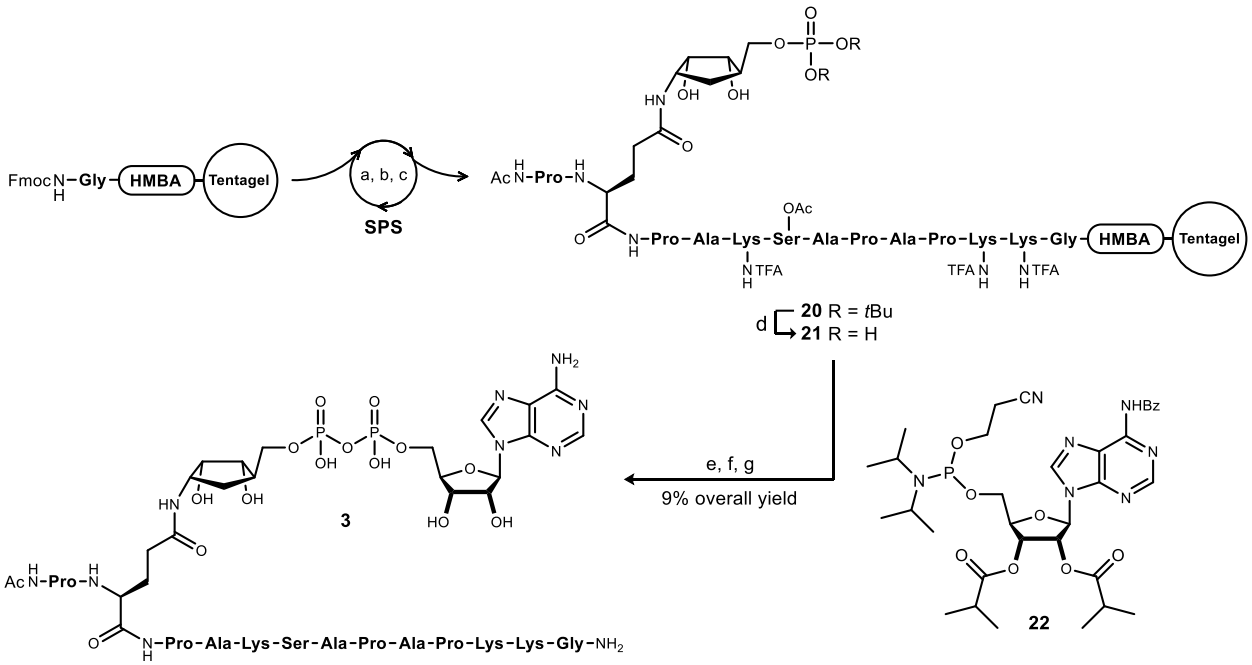

Scheme 3: The solid-phase peptide synthesis of *Carba*-ribose incorporated mono-ADP-ribosylated H2B conjugate **3**. Assembly of core peptide **20**: [**a**] Piperidine, DMF, 20 min. [**b**] Corresponding amino acid building block*, DIPEA, PyBOP, NMP, 1h. [**c**] Ac_2O, DIPEA, DMAP, NMP, 20 min. [*] After installment of the 8-Ser-Trt, the Trt was exchanged for Ac | Construction of the pyrophosphate: [**d**] 10% TFA, DCM, 1h. [**e**] i: Adenosine **22**, ETT, MeCN, 30 min. ii (1*S*)-(+)-(10-camphorsulfonyl) oxaziridine (CSO), MeCN, 10 min. [**f**] DBU, THF, 10 min. | Global acyl deprotection and release from solid-support: [**g**] Ammonia, TFE, 16h.

Conclusion

This chapter describes the synthesis of a mono-ADP-ribosylated *N*-terminal H2B conjugate bioisostere, wherein a c*arba*-riboside was incorporated as a stabilized replacement of the naturally occurring riboside. A new synthesis for the key intermediate cyclopentenone was developed. D-Ribose was converted into a protected 5-iodo-riboside and subjected to a tandem fragmentation-vinylation reaction. The diallylic product was ring-closed and oxidized, providing cyclopentenone **6** in 38% overall yield. Subsequent instalment of the C^5-*CH_2OH* through the photochemical addition of methanol, efficiently produced the *Carba*-ribose core structure (**13**). The ketone was converted into a methoxyimine and stereoselectively

reduced to obtain the pseudo-anomeric α-amine. Coupling of the amine with a glutamic acid derivative, followed by deprotection and phosphorylation of the primary alcohol afforded final *carba*-ribosylated glutamine building block **4**. The building block was successfully installed into the H2B sequence through solid-phase peptide synthesis. On-resin phosphorylation of the *carba*-ribosyl phosphate was used to construct the ADP-pyrophosphate. Successive global deprotection and release from resin provided the target mono-ADP-*carba*-ribosylated H2B conjugate **3** in multi milligram amounts.

Experimental Section

General: Reactions were executed at ambient temperatures unless stated otherwise. All solvents used under anhydrous conditions were stored over 4Å molecular sieves, except for methanol which was stored over 3Å molecular sieves. Reactions were monitored by TLC-analysis using Merck aluminum DC Silicagel 60 F_{254} with detection by spraying with 20% H_2SO_4 in EtOH, $(NH_4)_6Mo_7O_{24}{\cdot}4(H_2O)$ (25 g/L) and $(NH_4)_4Ce(SO_4)_4{\cdot}2(H_2O)$ (10 g/L) in 10% sulfuric acid or by spraying with a solution of ninhydrin (3 g/L) in EtOH / AcOH (20/1 v/v), followed by charring at approximately 250°C. Column chromatography was performed on Fluka silicagel (0.04 – 0.063 mm). Unless otherwise stated, solvents were evaporated under reduced pressure at 40 °C. Analysis by NMR and HRMS were performed as described in the experimental section of chapter 2. The reported peptide was synthesized using an automated peptide synthesizer (ABI-433A, Applied Biosystems, Perkin-Elmer).

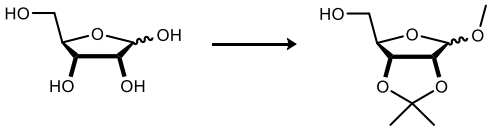

7 **8**

D-ribose (15.31 g, 101.98 mmol, 1 eq) was dissolved in MeOH (100 ml) and acetic chloride (2 ml, 30 mmol, 0.3 eq.) was added. After 1.5h, the reaction mixture was quenched by the addition of Et_3N (10 ml) and concentrated *in vacuo*. The resulting clear oil was dissolved in 2,2-dimethoxypropane (100 ml) and camphorsulfonic acid (4.7 g, 20.2 mmol, 0.2 eq.) was added. The reaction mixture was stirred for 30 minutes, before it was neutralized with saturated aqueous sodium bicarbonate and extracted EtOAc. The organic layers were combined, dried with magnesium sulfate filtered and the filtrate was evaporated under reduced pressure. The resulting oil was purified using silica gel column chromatography (5% » 10% » 20% EtOAc in PE) to yield the title compound as a colorless oil (14.41 g, 70.56 mmol, 69%). **^{1}H NMR:** (300 MHz, $CDCl_3$) δ 4.88 (d, *J* = 3.4 Hz, 1H), 4.72 (d, *J* = 5.7 Hz, 1H), 4.49 (d, *J* = 5.7 Hz, 1H), 4.32 (s, 1H), 3.56 (s, 2H), 3.33 (s, 3H), 3.23 (s, 1H), 1.39 (s, 3H), 1.23 (s, 3H). **^{13}C NMR:** (75 MHz, $CDCl_3$) δ 112.03, 109.81, 88.16, 85.67, 81.45, 63.86, 55.33, 26.30, 24.66.

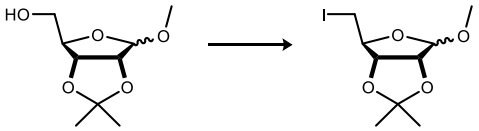

8 **9**

Riboside **8** (13.0 g, 63.8 mmol, 1 eq) was co-evaporated with dioxane and dissolved in dry toluene : acetonitrile (3:1 v:v, 400 mL). Imidazole (6.52 g, 95.8 mmol, 1.5 eq.), triphenylphosphine (20.1 g, 76.7 mmol, 1.2 eq.) and iodine (19.4 g, 76.4 mmol, 1.2 eq.) were added in succession and the reaction was left to stir overnight. The solvents were carefully evaporated under reduced pressure and the resulting was re-dissolved in Et_2O (200 ml). The organic layer was washed with a saturated aqueous sodium bicarbonate (2 x 100 mL), dried with magnesium sulfate, filtered and concentrated *in vacuo*. The resulting yellow oil was purified using silica gel column chromatography (5% Et_2O in PE) to yield the title compound as a colorless oil (18.9 g, 60.2 mmol, 94%). **^{1}H NMR:** (300 MHz, $CDCl_3$) δ 4.98 (s, 1H), 4.69 (dd, J = 5.9, 1.0 Hz, 1H), 4.56 (d, J = 5.9 Hz, 1H), 4.37 (dd, J = 10.0, 6.1 Hz, 1H), 3.30 (s, 3H), 3.22 (dd, J = 9.9, 6.1 Hz, 1H), 3.09

(t, J = 10.0 Hz, 1H), 1.40 (s, 3H), 1.25 (s, 3H). **^{13}C NMR:** (75 MHz, $CDCl_3$) δ 112.51, 109.59, 87.35, 85.29, 82.97, 55.18, 26.43, 25.02, 6.80.

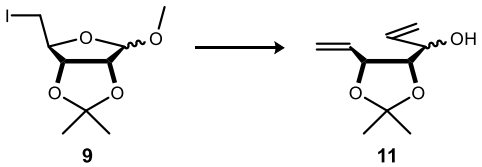

9 **11**

Iodo-riboside **9** (28.6 g, 91.2 mmol, 1 eq) was co-evaporated with dioxane, dissolved in dry THF (500 ml) and put under argon atmosphere. The solution was cooled to -78 ˚C and a 2.5 M solution of *n*-BuLi in THF (40 ml, 100 mmol, 1.1 eq.) was added drop-wise. After 4 hours, TLC analysis indicated full conversion of the starting material into the lower running aldehyde intermediate **10**. A 1 M solution of vinylmagnesium bromide in THF (110 ml, 110 mmol, 1.2 eq.) was slowly added and the reaction was left to stir overnight at -78 ˚C. The reaction mixture was allowed to warm to RT, after which the solvent was evaporated *in vacuo*. The resulting oil was dissolved in EtOAc (200 ml) and washed with water (100 ml). The aqueous layer was acidified using 1 M aqueous HCl to dissolve the white precipitate and was extracted with EtOAc (3 x 100 ml). The organic layers were combined, dried with magnesium sulfate, filtered and concentrated *in vacuo*. The residual yellow oil was purified using silica gel column chromatography (10% EtOAc in PE) to yield *R*/*S*-diallyl **11** as a pale-yellow oil (15.2 g, 82.2 mmol, 90%).

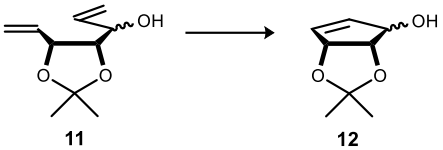

11 **12**

A solution of *R*/*S*-diallyl **11** (11.7 g, 63.4 mmol. 1 eq) in dry MeOH (250 ml) was purged of oxygen by ultra sonification while bubbling through argon (±10 min). Grubbs 1st generation catalyst (306 mg, 0.37 mmol, 0.6 mol%) was added and the reaction mixture was left to stir overnight. TLC analysis indicated full conversion of the starting materials into *R/S*-cyclopentenoid products. The reaction mixture was concentrated *in vacuo*, and the residue was purified using silica gel column chromatography (15% EtOAc in PE) to yield *R*/*S*-cyclopentenoid **12** as a colorless oil (8.09 g, 51.78 mmol, 82%). **^{1}H NMR:** (400 MHz, $CDCl_3$) δ 5.95 (d, J = 5.8 Hz, 1H), 5.83 (d, J = 6.7 Hz, 1H), 5.22 (d, J = 5.7 Hz, 1H), 4.68 (s, 1H), 4.43 (d, J = 5.7 Hz, 1H), 3.47 (s, 1H), 1.34 (s, 3H), 1.28 (s, 3H). **^{13}C NMR:** (101 MHz, $CDCl_3$) δ 135.19, 134.80, 111.73, 85.92, 84.31, 80.70, 27.30, 25.72.

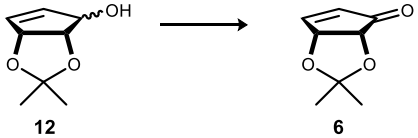

12 **6**

MnO_2 (107.3 g, 1.23 mol, 15 eq) was added to a solution of *R*/*S*-cyclopentenoid **12** (12.8 g, 82.2 mmol) in DCM (450 mL). After 16h, the reaction mixture was filtered through celite and concentrated *in vacuo*. The resulting oil was purified using silica gel column chromatography (20% EtOAc in PE), providing cyclopentenone **6** as a colorless crystalline material (10.1 g, 65.2 mmol, 79%). **^{1}H NMR:** (400 MHz, $CDCl_3$) δ 7.51 (dd, J = 5.9, 2.3 Hz, 1H), 6.08 (d, J = 5.9 Hz, 1H), 5.17 (dd, J = 5.5, 2.3 Hz, 1H), 4.34 (d, J = 5.5 Hz, 1H),

1.28 (s, 3H), 1.27 (s, 3H). **^{13}C NMR:** (101 MHz, $CDCl_3$) δ 202.88, 159.68, 134.04, 115.20, 78.45, 76.32, 27.23, 25.96.

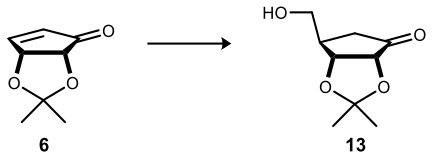

A solution of cyclopentenone **6** (4.97 g, 32.2 mmol, 1 eq) and benzophenone (891 mg, 4.89 mmol, 0.15 eq) in MeOH (2 L) was purged of oxygen by ultra sonification while bubbling through argon (± 1h). The solution was irradiated with a 360 nm UVA lamp for 16 hours. The residual yellow oil was purified using silica gel column chromatography (20% » 40% EtOAc) to yield the *carba*-riboside **13** as a colorless oil (3.635 g, 19.52 mmol, 61%). **^{1}H NMR:** (400 MHz, $CDCl_3$) δ 7.51 (dd, J = 5.9, 2.3 Hz, 1H), 6.08 (d, J = 5.9 Hz, 1H), 5.17 (dd, J = 5.5, 2.3 Hz, 1H), 4.34 (d, J = 5.5 Hz, 1H), 1.28 (s, 3H), 1.27 (s, 3H). **^{13}C NMR:** (101 MHz, $CDCl_3$) δ 202.88, 159.68, 134.04, 115.20, 78.45, 76.32, 27.23, 25.96. **HRMS:** Calculated for $C_9H_{15}O_4$ $[M+H]^+$; 187.0965, found 187.0966.

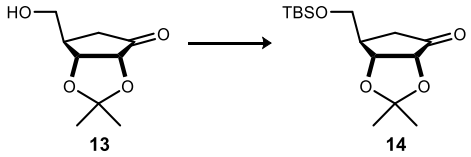

carba-riboside **13** and imidazole (1.31 g, 19.2 mmol, 1.5 eq) were co-evaporated with dioxane, put under argon atmosphere and dissolved in dry DCM (100 mL). TBSCl (2.31 g, 15.3 mmol, 1.2 eq) was added to the solution and the reaction mixture was stirred for 16 h. The reaction was quenched by the addition of MeOH (5 mL) and washed twice with water (100 mL). The organic layer was dried over magnesium sulfate, filtered and concentrated *in vacuo*. The residual yellow oil was purified using silica gel column chromatography (20% EtOAc in PE) to yield the title compound as a yellow oil (3.28 g, 10.9 mmol, 86%). **^{1}H NMR:** (400 MHz, Chloroform-d) δ 4.61 (d, J = 5.4 Hz, 1H), 4.19 (d, J = 5.4 Hz, 1H), 3.79 (dd, J = 9.8, 2.3 Hz, 1H), 3.60 (dd, J = 9.8, 2.7 Hz, 1H), 2.69 (dd, J = 18.1, 9.0 Hz, 1H), 2.48 (d, J = 8.9 Hz, 1H), 2.05 (d, J = 18.1 Hz, 1H), 1.39 (s, 3H), 1.31 (s, 3H), 0.81 (s, 9H), -0.00 (s, 3H), -0.02 (s, 3H). **^{13}C NMR:** (101 MHz, CDCl3) δ 212.88, 111.03, 82.01, 79.08, 65.32, 39.07, 37.27, 26.84, 25.87, 24.65, 18.26, -5.67, -5.75. **HRMS:** Calculated for $C_{15}H_{29}O_4Si$ 301.1830 $[M+H]^+$; found 301.1833.

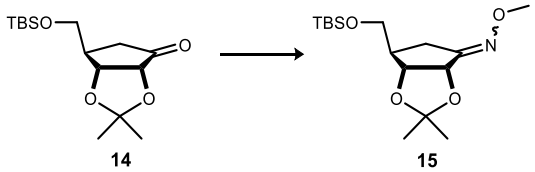

Sodium acetate (3.58 g, 43.6 mmol, 4.0 eq) and methoxylamine · HCl (1.83 g, 21.91 mmol, 2.0 eq) were added to a solution of compound **14** (3.28 g, 10.9 mmol, 1 eq) in dry MeOH (100 ml). After 3 hours, TLC analysis indicated full conversion of the starting material into the *cis*/*trans*-imine. The reaction mixture was concentrated *in vacuo* and taken-up into EtOAc (100 ml). The solution was washed with water (100 ml), dried with magnesium sulfate, filtered and concentrated *in vacuo*. The resulting yellow oil was

purified using silica gel column chromatography (10% Et_2O in pentane) to provide the *cis*/*trans*-imine **15** mixture as a yellow oil (3.45 g, 10.5 mmol, 96%). ***Trans*-isomer ^{1}H NMR:** (300 MHz, $CDCl_3$) δ 4.81 (d, J = 5.4 Hz, 1H), 4.54 (d, J = 5.5 Hz, 1H), 3.86 (s, 3H), 3.61 (dd, J = 10.0, 3.8 Hz, 1H), 3.47 (dd, J = 10.0, 4.1 Hz, 1H), 2.63 (dd, J = 18.1, 8.6 Hz, 1H), 2.49 (d, J = 16.4 Hz, 1H), 2.40 (s, 1H), 1.42 (s, 3H), 1.32 (s, 3H), 0.84 (s, 9H), 0.00 (s, 3H), -0.01 (s, 3H). **^{13}C NMR:** (75 MHz, $CDCl_3$) δ 162.18, 110.96, 82.67, 79.75, 65.08, 61.89, 43.09, 27.86, 27.13, 25.88, 24.90, 18.29, -3.71, -5.60. ***Cis*-isomer ^{1}H NMR:** (300 MHz, $CDCl_3$) δ 5.04 (d, J = 5.5 Hz, 1H), 4.55 (d, J = 5.5 Hz, 1H), 3.85 (s, 3H), 3.65 (dd, J = 10.0, 3.7 Hz, 1H), 3.53 (dd, J = 10.0, 3.8 Hz, 1H), 2.87 (ddd, J = 16.7, 8.4, 1.3 Hz, 1H), 2.37 (dt, J = 7.6, 3.5 Hz, 1H), 2.25 (dd, J = 16.7, 1.0 Hz, 1H), 1.44 (s, 3H), 1.34 (s, 3H), 0.85 (s, 9H), 0.01 (s, 3H), 0.00 (s, 3H). **^{13}C NMR:** (75 MHz, CDCl3) δ 162.19, 110.84, 83.37, 74.96, 65.11, 62.02, 42.08, 30.93, 26.93, 25.86, 24.61, 18.23, -5.63, -5.65. **HRMS:** Calculated for $C_{16}H_{32}NO_4Si$ 330.2095 $[M+H]^+$; found 330.2093.

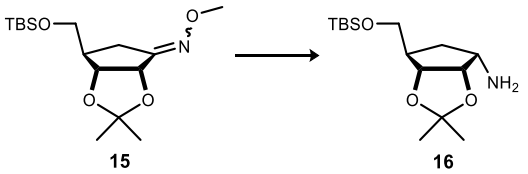

cis/*trans*-imine **15** (0.968 g, 2.94 mmol, 1 eq) was co-evaporated with dioxane and dissolved in dry THF (30 ml). A 2.4 M solutions of $LiAlH_4$ (11.76 mmol 4.9 ml, 4 eq) was added and the reaction mixture was refluxed for 2 hours. After cooling to RT, the reaction was quenched with water (1 mL). The reaction mixture was poured into a separation funnel containing water (30 ml) and extracted with Et_2O (3 x 50 ml). The organic layers were combined, dried with magnesium sulfate, filtered and concentrated *in vacuo*. The resulting yellow oil was purified using silica gel column chromatography (2% MeOH in DCM) to yield *carba*-ribosamine **16** as a yellow oil (0.681 g, 2.26 mmol, 30%). **^{1}H NMR:** (400 MHz, Chloroform-d) δ 4.45 (d, J = 5.6 Hz, 1H), 4.33 (t, J = 5.4 Hz, 1H), 3.53 (dd, J = 10.1, 5.7 Hz, 1H), 3.46 (dd, J = 10.1, 5.9 Hz, 1H), 3.34 (ddd, J = 12.5, 7.0, 5.4 Hz, 1H), 2.08 (q, J = 6.2 Hz, 1H), 1.73 (s, 1H), 1.71 (s, 1H), 1.67 (s, 2H), 1.45 (s, 3H), 1.31 (s, 3H), 0.86 (s, 9H), 0.02 (s, 6H). **^{13}C NMR:** (101 MHz, $CDCl_3$) δ 109.98, 83.37, 81.25, 64.79, 54.48, 45.21, 35.31, 26.40, 26.03, 24.26, 18.35, -5.36. **HRMS:** Calculated for $C_{15}H_{32}NO_3Si$ 302.2146 $[M+H]^+$; found 302.2140.

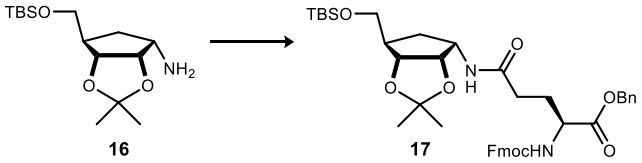

carba-ribosamine **16** (0.143 g, 0.48 mmol, 1 eq) and Fmoc-Glu(OBn)-OH (0.252 g, 0.55 mmol, 1.15 eq) were co-evaporated with dioxane and dissolved in dry THF (5 ml). DIPEA (0.12 ml, 0.72 mmol, 1.5 eq), PyBOP (0.273 g, 0.525 mmol, 1.1 eq) and 1-methylimidazole (4 µl, 0.05 mmol, 0.1 eq) were added and the reaction mixture was stirred overnight. The reaction mixture was poured into a separation funnel containing water (15 mL) and extracted with Et_2O (2 x 15 mL). The organic layers were combined, dried with magnesium sulfate, filtered and concentrated *in vacuo*. The resulting oil was purified using silica gel column chromatography (20% » 40% EtOAc in PE + 1% TEA) to provide *carba*-ribosylated glutamine **17** as a yellow oil (0.351 g, 0.47, 98%). **^{1}H NMR:** (400 MHz, $CDCl_3$) δ 7.76 (d, J = 7.5 Hz, 2H), 7.60 (d, J = 6.6 Hz, 2H), 7.40 (t, J = 7.5 Hz, 2H), 7.37 – 7.28 (m, 7H), 5.98 (d, J = 7.5 Hz, 1H), 5.78 (d, J = 8.0 Hz, 1H), 5.18 (d, J = 2.7 Hz, 2H), 4.49 (d, J = 4.7 Hz, 1H), 4.47 – 4.37 (m, 4H), 4.34 (dd, J = 10.5, 7.4 Hz, 1H), 4.21 (t, J = 7.0 Hz,

1H), 3.57 (dd, J = 10.2, 5.4 Hz, 1H), 3.47 (dd, J = 10.2, 6.3 Hz, 1H), 2.22 (d, J = 9.0 Hz, 2H), 2.15 (q, J = 6.1 Hz, 1H), 2.04 – 1.98 (m, 1H), 1.88 (dd, J = 12.6, 6.8 Hz, 1H), 1.78 – 1.69 (m, 1H), 1.66 (s, 2H), 1.47 (s, 3H), 1.29 (s, 3H), 0.88 (s, 9H), 0.06 (s, 3H), 0.04 (s, 3H). **^{13}C NMR:** (101 MHz, $CDCl_3$) δ 189.19, 172.03, 171.26, 156.31, 144.09, 141.43, 128.77, 128.64, 128.49, 127.85, 127.21, 125.32, 125.27, 120.10, 110.24, 100.10, 82.88, 79.53, 67.46, 67.18, 64.46, 53.80, 51.21, 47.29, 45.16, 32.51, 28.27, 26.37, 26.05, 24.07, 18.37, -5.32. **HRMS:** Calculated for $C_{42}H_{55}N_2O_8Si$ 743.3722 $[M+H]^+$; found 743.3728.

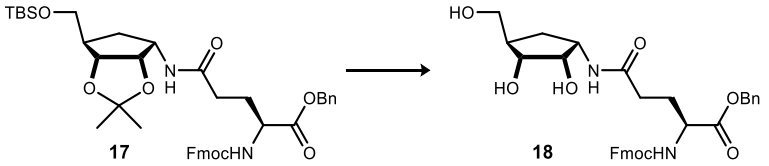

A suspension of compound **17** (0.409 g; 0.55 mmol) in water : AcOH (15 mL, 2:1 v.v) was heated 60 °C and stirred overnight. The solvents were evaporated *in vacuo*. The white residue was purified using silica gel column chromatography (5% » 10% » 20% EtOH in EtOAc) to yield the title compound as white crystals (0.138 g, 0.23 mmol, 42%). **^{1}H NMR:** (300 MHz, D_2O) δ 7.74 (t, J = 8.3 Hz, 2H), 7.64 – 7.55 (m, 2H), 7.36 – 7.21 (m, 9H), 5.15 – 5.06 (m, 2H), 4.40 – 4.22 (m, 2H), 4.21 – 4.15 (m, 1H), 4.10 (dd, J = 13.1, 5.3 Hz, 1H), 4.04 (dd, J = 8.1, 4.5 Hz, 1H), 3.87 (t, J = 3.9 Hz, 1H), 3.76 (dd, J = 7.7, 3.9 Hz, 1H), 3.59 (dd, J = 10.7, 4.8 Hz, 1H), 3.53 – 3.42 (m, 1H), 3.27 (dt, J = 3.3, 1.6 Hz, 1H), 2.26 (d, J = 6.6 Hz, 2H), 2.21 – 2.06 (m, 3H), 1.97 – 1.84 (m, 1H), 1.83 – 1.73 (m, 2H). **^{13}C NMR:** (75 MHz, D_2O) δ 129.54, 129.27, 129.20, 128.79, 128.18, 128.15, 126.30, 126.21, 120.91, 103.11, 77.12, 75.57, 74.68, 68.05, 67.95, 64.57, 55.16, 51.73, 51.16, 48.35, 45.88, 44.65, 33.18, 31.79(CH2), 28.43(CH2), 25.17(CH2). **HRMS:** Calculated for $C_{33}H_{37}N2O_8$ 589.2544 $[M+H]^+$; found 589.2544.

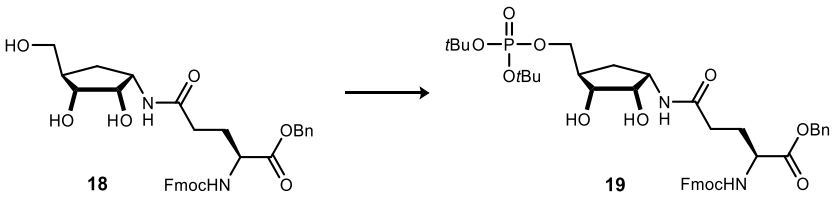

Compound **18** (0.206 g, 0.343 mmol, 1 eq), 1-methylimidazolium chloride (0.122 g, 1.03 mmol, 3 eq), 1-methylimidazole (54 µl, 0.69 mmol, 2 eq) and several molecular sieves were co-evaporated together with dioxane, dissolved in dry DMF (3.33 ml) and put under argon atmosphere. di-*tert*-butyl-*N*,*N*-diisopropylphosphoramidite (0.12 ml, 0.38 mmol, 1.1 eq.) was added. ^{31}P-NMR indicated full conversion within 30 minutes. Oxidation was initiated by the addition of *tert*-butyl hydroperoxide (0.3 ml, 1.65 mmol, 5 eq) in decane (5.5 M). The reaction mixture was stirred for an additional 15 minutes, before being filtered and concentrated *in vacuo*. The resulting yellow oil was purified using silica gel column chromatography (2% » 5% MeOH in EtOAc) to produce phosphate **19** as a colorless oil (0.134 g, 0.168 mmol, 50%). **^{1}H NMR:** (300 MHz, $CDCl_3$) δ 7.76 (d, J = 7.5 Hz, 2H), 7.60 (d, J = 6.8 Hz, 2H), 7.45 – 7.27 (m, 9H), 6.34 (d, J = 7.4 Hz, 1H), 5.86 (d, J = 8.1 Hz, 1H), 5.17 (s, 2H), 4.54 – 4.30 (m, 3H), 4.30 – 4.09 (m, 3H), 4.09 – 3.79 (m, 4H), 2.51 – 2.36 (m, 1H), 2.35 – 2.09 (m, 3H), 2.08 – 1.98 (m, 1H), 1.90 – 1.76 (m, 3H), 1.48 (s, 18H). **^{13}C NMR:** (101 MHz, $CDCl_3$) δ 172.11, 171.83, 156.35, 144.02, 143.79, 141.36, 141.34, 135.30, 128.72, 128.58, 128.41, 127.80, 127.18, 125.31, 125.26, 120.05, 75.02, 73.76, 68.65, 67.40, 67.19, 53.81,

53.56, 50.02, 47.22, 43.45, 32.37, 31.52, 29.94, 28.01. **^{31}P NMR:** (121 MHz, $CDCl_3$) δ -10.16. **HRMS:** Calculated for $C_{41}H_{53}N_2NaO_{11}P$ 803.3279 $[M+Na]^+$; found 803.3277.

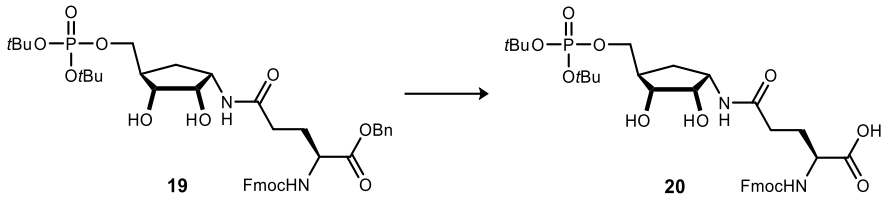

A solution of phosphate **19** (0.10 g, 0.128 mmol, 1 eq) in MeOH (2 ml), Pd/C (2 mg, 0.019 mmol, 0.15 eq) was degassed by ultra sonification. Hydrogen gas (±5 L) was bubbled through and the solution was stirred overnight under hydrogen atmosphere. The reaction mixture was filtered through celite and concentrated *in vacuo*. The resulting yellow oil was purified using silica gel column chromatography (5% » 10% MeOH in DCM + 1% AcOH) to yield compound **20** as a white foam (64 mg, 93 µmol, 72%). **^{1}H NMR:** (400 MHz, Methanol-d4) δ 7.79 (d, J = 7.3 Hz, 2H), 7.67 (t, J = 7.3 Hz, 2H), 7.38 (t, J = 7.3 Hz, 2H), 7.31 (t, J = 7.2 Hz, 2H), 4.35 (dq, J = 17.4, 10.3, 9.9 Hz, 2H), 4.25 – 4.15 (m, 2H), 4.13 (dt, J = 8.5, 4.3 Hz, 1H), 4.05 (dt, J = 9.1, 4.4 Hz, 1H), 4.00 – 3.95 (m, 1H), 3.94 (d, J = 3.8 Hz, 1H), 3.83 (dd, J = 8.1, 3.7 Hz, 1H), 2.34 (t, J = 7.2 Hz, 3H), 2.19 (dd, J = 12.6, 5.1 Hz, 1H), 2.03 – 1.91 (m, 1H), 1.88 (t, J = 8.6 Hz, 2H), 1.48 (s, 18H). **^{13}C NMR:** (101 MHz, MeOD) δ 175.41, 174.51, 158.61, 145.31, 145.15, 142.54, 128.77, 128.16, 126.30, 126.25, 120.90, 84.32, 84.24, 74.93, 74.51, 69.48, 67.99, 54.86, 51.39, 44.14, 33.31, 31.61, 30.20, 30.16, 28.75. **HRMS:** Calculated for $C_{34}H_{48}N_2O_{11}P$ 691.2990 $[M+H]^+$; found 691.2994.

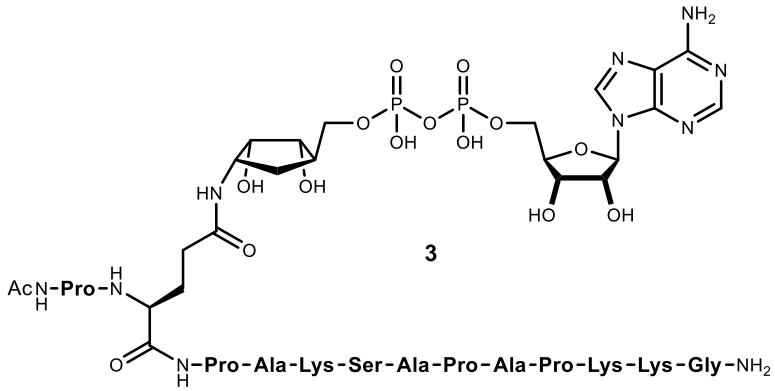

The intermediate peptide Fmoc-Pro-Ala-Lys-Ser-Ala-Pro-Ala-Pro-Lys-Lys-Gly-HMBA was synthesized on an automated peptide synthesizer using standard SPPS sequences: Starting from pre-loaded Fmoc-Gly-HMBA Tentagel S resin (0.238, 52 µmol), 5 equivalents of Fmoc-Lys(TFA)-OH, Fmoc-Pro-OH, Fmoc-Ala-OH and Fmoc-Ser(Trt)-OH were applied respectively. Activation was effectuated by treatment with 5 equivalents of HCTU in NMP (0.5 M) and 12.5 equivalents of DIPEA in NMP (1.25 M) for 1 hour. After each coupling, the Fmoc groups were cleaved using 20% piperidine in DMF. Next, the side-chain trityl group attached to Serine was cleaved by sequential treatment with 5% TFA in DCM, until no yellow discoloration of the solution occurred. The resin was washed with DCM and NMP, followed by the addition of Ac_2O (0.24 mL, 50 eq), DIPEA (0.44 mL, 50 eq), DMAP (cat.) and NMP (2 mL). The reaction vessel was shaken for 15 minutes, before being rinsed with NMP and DCM. From here the *carba*-ribosylated glutamine **20** was

introduced manually. After elimination of the terminal Fmoc-protective group, compound **20** (31 mg, 75 µmol, 1.5 eq), HCTU (31 mg, 1.5 eq), DIPEA (26 µL, 3 eq) in NMP (2 mL) were added and the resin was shaken for 16 h. The final Fmoc-Pro-OH was installed using the standard SPPS sequence. An aliquot of resin was treated with saturated aqueous ammonia (30%) and analyzed with LCMS, which revealed formation of the target peptide.

Next, the instalment of the pyrophosphate bridge was initiated by cleavage of the *tert*-butyl groups. The deprotection cycle of treatment with 10% TFA in DCM (2 ml) and shaking for 30 minutes was repeated twice. The resin was washed with dry MeCN and flushed with argon, before being taken-up in a 0.25 M solution of ETT in MeCN (1 ml, 0.25 mmol, 5.0 eq). A dry solution of adenosine-amidite **22** (80 mg, 2.5 eq) in MeCN (1 mL) was added. The was shaken for 30 minutes, filtered and rinsed with MeCN. A 0.5 M solution of CSO in MeCN (0.25 mmol, 5.0 eq) was added and the mixture was shaken for an additional 10 minutes. The resin was filtered, washed with MeCN and treated with a 0.5 M solution of DBU in DMF (1 mL) for 10 minutes. The resin was filtered and rinsed with DMF and DCM. ^{31}P-NMR of the resin indicated full conversion of the di-*tert*-butylphosphate into a pyrophosphate. The peptide was released from resin by treatment with 30% saturated aqueous ammonia in trifluorethanol (3 mL) for 16 h. The solvents were evaporated under reduced pressure and the resulting yellow foam was re-dissolved in MeOH : AcOH (1.5 mL, 15:1 v.v). The peptide was precipitated by injection of the solution in ice-cooled Et_2O. The resulting suspension was centrifuged and decanted to provide crude target peptide. Further purification by RP-HPLC, followed by lyophilization, gave mono-ADP-*carba*-ribosylated H2B conjugate **3** as a white powder (8.2 mg, 4.4 µmol, 9% based on initial loading). **^{1}H NMR:** (400 MHz, D_2O) δ 8.52 (s, 1H), 8.24 (s, 1H), 6.13 (d, J = 6.0 Hz, 1H), 4.59 (dt, J = 12.9, 6.9 Hz, 4H), 4.53 – 4.49 (m, 1H), 4.45 – 4.35 (m, 7H), 4.34 – 4.24 (m, 5H), 4.24 – 4.19 (m, 2H), 4.01 – 3.88 (m, 7H), 3.86 – 3.80 (m, 3H), 3.76 (dd, J = 13.4, 6.7 Hz, 3H), 3.69 – 3.57 (m, 5H), 3.57 – 3.44 (m, 1H), 3.02 – 2.92 (m, 6H), 2.37 (t, J = 7.5 Hz, 3H), 2.26 (dd, J = 11.8, 8.0 Hz, 5H), 2.10 (s, 3H), 2.06 – 1.93 (m, 11H), 1.85 (dd, J = 13.4, 7.2 Hz, 5H), 1.82 – 1.73 (m, 7H), 1.73 – 1.59 (m, 8H), 1.56 – 1.41 (m, 6H), 1.39 (d, J = 7.2 Hz, 4H), 1.35 (d, J = 7.0 Hz, 7H). **^{31}P NMR:** (162 MHz, D_2O) δ -10.29 (d, J = 21.0 Hz), -10.83 (d, J = 21.1 Hz). **HRMS:** Calculated for $C_{75}H_{126}N_{23}O_{28}P_2$ 1858.8601 $[M+3H]^{3+}$, compensated for triple charge 619.6200; found 619.6208.

References

1. S. Messner, M. Altmeyer, H. Zhao, A. Pozivil, B. Roschitzki, P. Gehrig, D. Rutishauser, D. Huang, A. Caflisch, M. O. Hottiger, *Nucleic Acids Res.* **2010**, *38*, 6350–6362.
2. Y. Zhang, J. Wang, M. Ding, Y. Yu, *Nat. Methods* **2013**, *10*, 981–984.
3. F. Rosenthal, P. Nanni, S. Barkow-Oesterreicher, M. O. Hottiger, *J. Proteome Res.* **2015**, *14*, 4072–4079.
4. O. Leidecker, J. J. Bonfiglio, T. Colby, Q. Zhang, I. Atanassov, R. Zaja, L. Palazzo, A. Stockum, I. Ahel, I. Matic, *Nat. Chem. Biol.* **2016**, *12*, 998–1000.
5. J. M. Pleschke, H. E. Kleczkowska, M. Strohm, F. R. Althaus, *J. Biol. Chem.* **2000**, *275*, 40974–40980.
6. P. L. Panzeter, C. A. Realini, F. R. Althaus, *Biochemistry* **1992**, *31*, 1379–85.
7. P. O. Hassa, S. S. Haenni, M. Elser, M. O. Hottiger, *Microbiol. Mol. Biol. Rev.* **2006**, *70*, 789–829.
8. N. Ogata, K. Ueda, O. Hayaishi, *J. Biol. Chem.* **1980**, *255*, 7610–7615.
9. H. A. V. Kistemaker, A. P. Nardozza, H. S. Overkleeft, G. A. van der Marel, A. G. Ladurner, D. V. Filippov, *Angew. Chemie - Int. Ed.* **2016**, *55*, 10634–10638.
10. H. A. V Kistemaker, G. J. V. D. H. Van Noort, H. S. Overkleeft, G. A. Van Der Marel, D. V Filippov, *Org. Lett.* **2013**, 9–12.
11. R. J. Parry, M. R. Burns, P. N. Skae, J. C. Hoyt, B. Pal, *Bioorganic Med. Chem.* **1996**, *4*, 1077–1088.
12. D. R. Borcherding, S. A. Scholtz, R. T. Borchardt, *J. Org. Chem.* **1987**, *52*, 5457–5461.
13. C. L. Mariën, E. L. Esmans, F. Lemière, R. A. Dommisse, **2006**, *7911*.

5 | *N*-Acylazetine as a Dienophile in Bioorthogonal Inverse-Electron-Demand Diels–Alder Ligation

Introduction

Bioorthogonal chemistry strives to chemoselectively modify biomolecules, such as proteins, carbohydrates and lipids, within the complex environments of cell-lysates, living cells and, ultimately, in living animals. Bioorthogonal chemistry has pushed forward various fields of research, such as activity-based protein profiling, *in vitro* and *in vivo* imaging and modified metabolite labeling.[1] Ideally, in a bioorthogonal process a reactive group incorporated into the biomolecule of interest reacts selectively with a complementary reactive group modified with a reporter moiety, such as a fluorescent label to enable visualization of the target or an affinity probe for post-labeling purification.[2] To enable this, a bioorthogonal tag should be inert to the broad spectrum of functional groups that reside in a biological system, while exerting fast enough reaction kinetics for conjugation to occur at nanomolar concentrations. Additives to facilitate the reaction between the tag and the reactive functionality of the reporter group are best avoided. Finally, the tag should be sterically compact to minimize unfavorable steric interactions with the biological system being studied and be synthetically accessible.

In the last decade, several bioorthogonal ligation strategies have been developed. Among these, prominent transformations are the Staudinger-Bertozzi ligation[3], the copper-catalysed[4] and the strain-promoted azide-alkyne [2+3] cycloaddition.[5] An important recent development is the inverse-electron-demand Diels-Alder reaction (IEDDA), which exhibits the fastest reaction kinetics among all commonly used bioorthogonal transformations, while being chemo-selective, efficient and additive-free.[6–8] In the most typical setup, IEDDA uses a strained alkene tag, while its reaction partner is a reporter-group functionalized tetrazine derivative. Well-established strained alkene handles are norbornene (Figure 1, A) and *trans*-cyclooctene (Figure 1, B). Although these alkenes react exceptionally fast, their steric bulk and

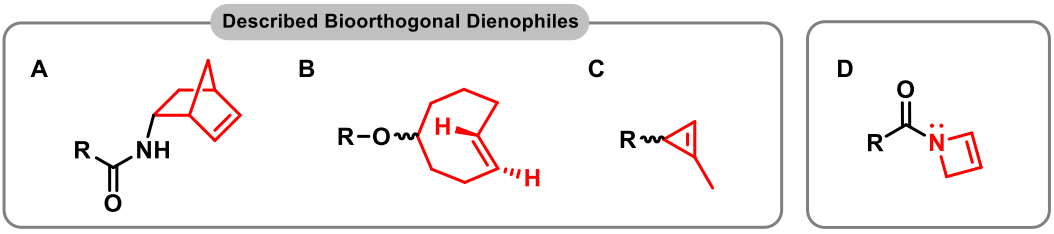

Figure 1: Known bioorthogonal dienophilic moieties (A-C) and the *N*-acylazetine tag (D) described in this chapter.

lipophilicity may induce a biological response, bringing a paradoxical problem, known as the observer effect, into chemical biology. Hence, there is room for the development of more compact dienophiles for tetrazine mediated bioorthogonal cycloadditions. Recently, Devaraj and co-workers introduced the methylcyclopropene core (Figure 1, C), as dienophile for IEDDA that combines small size with fast reaction kinetics.[9]

Currently, all contemporary dienophiles – norbornene, *trans*-cylcooctene and cyclopropene – used in IEDDA-based bioorthogonal chemistry rely on ring strain to attain the desired reactivity towards tetrazines. These were first described in the seminal 1990 report by Sauer and co-workers on the reactivity of cyclic dienophiles in IEDDA processes.[10] In the same paper, it was shown that alkenes activated by a single electron-donating heteroatom adjacent to the double bond, would exhibit a higher reactivity towards tetrazine relative to their non-conjugated analogues. Introduction of a heteroatom into the cyclobutene scaffold should therefore lead to a viable dienophile for IEDDA-based bioorthogonal chemistry. Following this reasoning, a 2-azetine would be the smallest viable core that could utilize this effect in addition to ring-strain, with the ring-nitrogen amenable for functionalization to yield a new and compact bioorthogonal tag. Although *N*-alkylazetines are theoretically the more electron-rich species, *N*-acylazetines (Figure 1, D) were considered more suitable candidates because of their reported stability.[11] This chapter describes the development and optimization of a synthetic route towards a bioorthogonal tag based on *N*-acylazetine moiety and a study towards its applicability in IEDDA-based bioorthogonal chemistry.

Synthesis Results and Discussion

The synthesis of linkable *N*-alkyl-azetines **6** and **7**, equipped with an activated ester for further modification, (Scheme 1) commenced with the preparation of the azetidine core.[12,13] Epichlorohydrin was reacted with benzhydrylamine in a two-step one-pot procedure to afford protected azetidine **2**. The hydroxy group of **2** was mesylated, affording methanesulfonate **3**. Deprotection of the benzhydryl with chloroethyl chloroformate provided the acyl-intermediate, which was degraded by refluxing in methanol to give 3-mesylazetidine hydrochloride **4**. The route from **1** to **4** was optimized in such a way that each intermediate could be purified through crystallization and washing steps (in 48% yield over three steps). With free amine **4** in hand, the ring-opening of glutaric anhydride could commence. Initially this was carried out under the agency of triethylamine. However, during the reaction, the methane sulfonate was substituted by chloride originating from 3-mesylazetidine hydrochloride. Furthermore, the use of triethylamine complicated the column purification of the formed carboxylic acid. These problems were addressed by switching to potassium carbonate as the base, and premixing **4** with silver methanesulfonate, to precipitate the chloride as AgCl. After successful conversion, the free acid was regenerated from the potassium salt by treating with Amberlite-H^+, providing **5** in 79% yield. The following elimination-esterification sequence was carried out in a one-pot procedure. First, methanesulfonic acid was eliminated with KO*t*Bu to afford the *N*-acylazetine moiety. Next, the carboxylate was converted to either pentafluorophenol (PFP, **6**) or *p*-nitrophenol (PNP, **7**) esters via EDC mediated condensation with the appropriate alcohol. Both esters were readily obtained, however PFP-ester **6** proved to be unstable and could not be stored for extended periods of time. Another disadvantage was its gel-like consistency

at room temperature, making it difficult to handle. On the other hand, PNP-ester **7** was isolated as a crystalline solid that is stable at room temperature for at least three months.

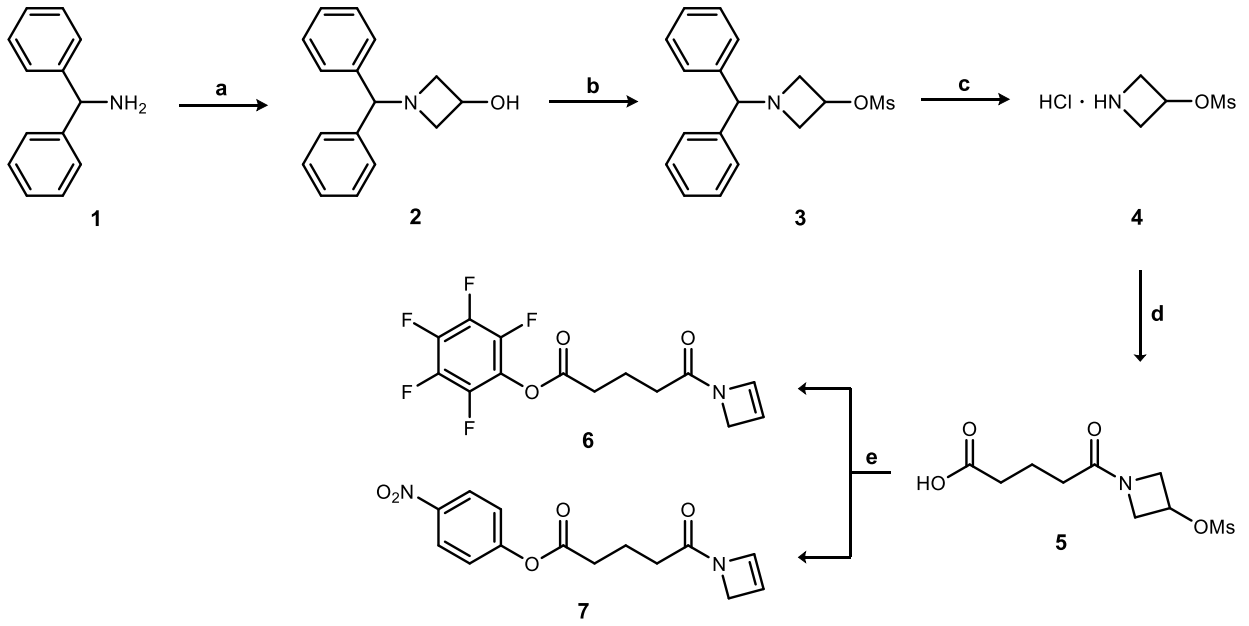

Scheme 1: Synthesis of active ester functionalized *N*-acylazetine **6** and **7**. Reagents and conditions: [**a**] i: Epichlorohydrin, *i*PrOH, 30 ˚C, 16h. ii: $NaHCO_3$, MeCN, reflux, 30h, 83%. [**b**] MsCl, TEA, DCM, -40 ˚C, 0.5h, 80%. [**c**] i: Chloroethyl chloroformate, DCE, reflux, 1.5h. ii: MeOH, reflux, 2h, 66%. [**d**] i: MsOAg, MeCN, 15 min. ii: K_2CO_3, glutaric anhydride, reflux, 2h, 79%. [**e**] i: KO*t*Bu, DMF, 50 ˚C, 2h. ii: EDC·HCl, PFP/PNP, 1.5h, **6:** 63% **7**: 85%.

Besides the required physical properties, the applicability of a ligation handle is also dependent on its synthetic accessibility. The above described synthesis to acylazetine **7** consists of six reactions of which the ring-opening of glutaric anhydride by 3-mesylazetidine and the sequential one-pot elimination–esterification sequence are the key steps. Despite various attempts of optimization, these steps constrain the overall efficiency and scalability. Therefore another synthetic route towards **7** was explored (Scheme 2). Commercially available 3-hydroxyazetidine **8** was used as starting compound and the mesyl group was replaced by the tosyl group that is UV-detectable and a slightly better leaving group. The synthesis started with the sequential Boc-protection and tosylation of 3-hydroxyazetidine (**8**), providing protected azetidine **9** in 72% over two steps. To prevent potential tosyl displacement the Boc-group was cleaved using *p*-toluenesulfonic acid. Purification by crystallization from MeOH yielded **10** in 80%. Ring-opening of succinic and glutaric anhydride with **10** was carried out under the agency of potassium carbonate in refluxing acetonitrile, yielding the four- (**11**) and five-carbon spacer (**12**), respectively. Next, the key elimination was initiated by the addition of a KO*t*Bu solution in THF. The use of the tosyl improved solubility while the reaction now proceeded readily at room temperature. The respective *N*-acylazetine intermediates were treated *in situ* with bis(*p*-nitrophenyl)carbonate, to provide linkable handles **7** (80%) and **13** (69%) in good yields over two steps. Initially, the *p*-nitrophenol was introduced using DIC or EDC as coupling reagents. However, the use of bis(*p*-nitrophenol)carbonate resulted in cleaner and more consistent conversions.

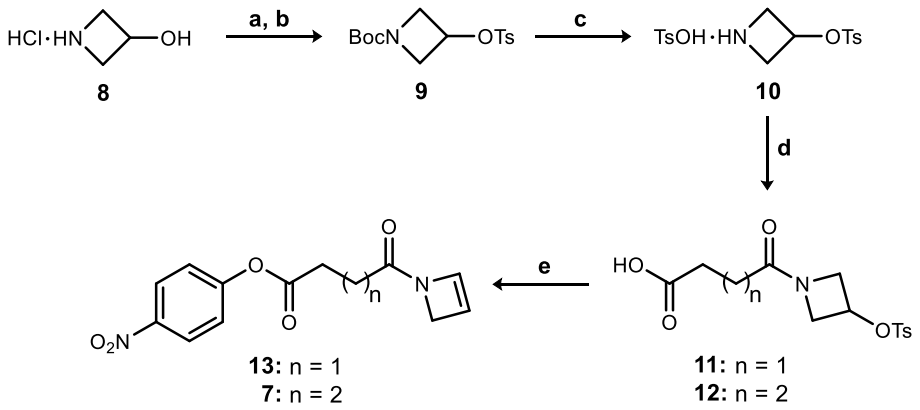

Scheme 2: Improved synthesis of activated *N*-acylazetine handle **7** and the four-carbon variant **13**. Reagents and conditions: [**a**] i: Boc_2O, TEA, MeOH, 0 ˚C, 2h, used crude. [**b**] TsCl, TEA, DCM, 2h, 86% over 2 steps. [**c**] *p*TsOH, DCE, reflux, 16h, 79% [**d**] Succinic- (**11**) or glutaric (**12**) anhydride, K_2CO_3, MeCN, reflux, 6h, 50% **11**, 70% **12**. [**e**] KO*t*Bu, DMF, 2h. ii: bis(*p*-nitrophenol)carbonate, 16h, **13**: 80% **7**: 69%.

Reaction Kinetics

To investigate the rate of the IEDDA reaction of *N*-acylazetine with tetrazine, **7** was coupled with morpholine to make water soluble *N*-acylazetine **14** (Figure 2). A ten-fold excess of model compound **14** was reacted with tetrazine **15**.[14] The rate was determined by monitoring the absorbance of the tetrazine at 517 nm (Figure 2). The pseudo-first order rate constant k_1 was established to be $4.5 \cdot 10^{-3} \pm 1.6 \cdot 10^{-3}$ s^{-1} at 20 °C in a solution of 12% DMSO in water. In a separate experiment, the second-order rate constant k_2 was approximated to be 0.39 ± 0.1 s^{-1} M^{-1}.

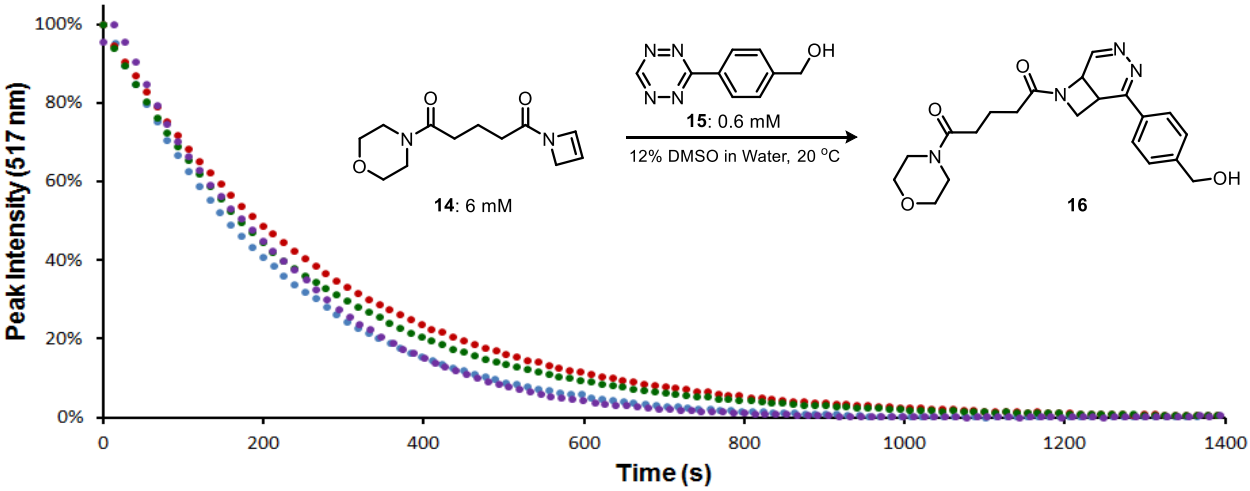

Figure 2: The graph consists of a data plot following the tetrazine absorption band over time in a reaction between *N*-acylazetine **14** (6 mM) and tetrazine **15** (0.6 mM) in 12% DMSO/water. The kinetics experiment was performed four times. Compound **16** is formed as a mixture of regioisomers and potentially as tautomers.

The mass-spectroscopic data of the reaction product, formed as a mixture of isomers, were fully consistent with putative structure **16**. However, characterization of **16** by NMR was complicated by the two tertiary amide bonds, which appeared to exist as rotamers on the NMR time scale. In order to obtain more conclusive spectroscopic data of the product, while simultaneously studying the course of the *N*-acylazetine cycloaddition in more detail, compound **17** was reacted with symmetrical tetrazine **18** (Scheme 2). During this experiment it was found that immediate IEDDA adduct **19** rapidly ring-opens to form compound **20** as the sole product. This process is likely thermodynamically driven by the restoration of aromaticity and relief of ring-strain, of which former is more favorable in higher conjugated systems. Trace amounts of product resulting from the same rearrangement were observed after the reaction of **14** with **15**, as evidenced by the resonance of the tertiary carbon of pyridazine at 123 ppm in the ^{13}C NMR spectrum of **16**.

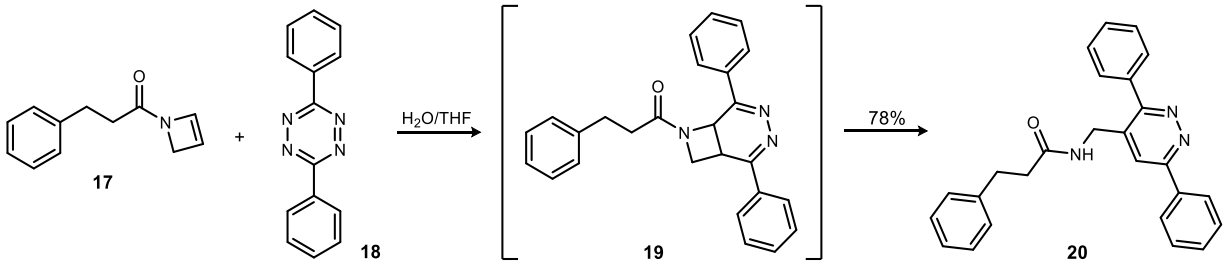

Scheme 2: Model cycloaddition between *N*-acylazetine **17** and tetrazine **18**, shows that direct adduct **19** completely rearranges to open-ring isomer **20**.

Labeling Evaluation

In order to evaluate the applicability of the novel *N*-acylazetine ligation handle for biological labeling strategies, the tag was incorporated into an activity-based proteasome probe to enable two-step activity-based protein profiling through ligation with a fluorescently labeled tetrazine (**23**, Figure 3). As a model target enzyme the constitutive proteasome was selected. The proteasome is a multi-subunit protein complex containing three different catalytically active subunits (β1, β2 and β5). These β-subunits each have a different substrate preference and can be targeted by various subunit-selective[15] or broad-spectrum[16] activity based probes (ABPs). The designed ABP **21** is based on the broad-spectrum irreversible proteasome inhibitor epoxomicin, functionalized at the *N*-terminus with the acylazetine moiety.[17–19] Compound **21** (Figure 3) was readily prepared from protected peptide epoxyketone.

The ability of the *N*-acylazetine-functionalized ABP **21** to target the catalytically active proteasome β-subunits was confirmed by performing competition experiments against the fluorescent broad-spectrum proteasome ABP MV151 in human embryonic kidney (HEK) cell extracts. These experiments revealed that 3 μM of ABP **21** was required to completely block the fluorescent labeling by MV151. Therefore, for all ensuing two-step labeling experiments a probe concentration of 5 μM was used. The utility of the *N*-acylazetine tag for two-step labeling of proteasome activity in cell extracts was established by exposure of HEK cell extracts to ABP **21**, followed by ligation with varying concentrations of tetrazine **23**. As a control, the same procedure was performed using the previously reported norbornene-functionalized

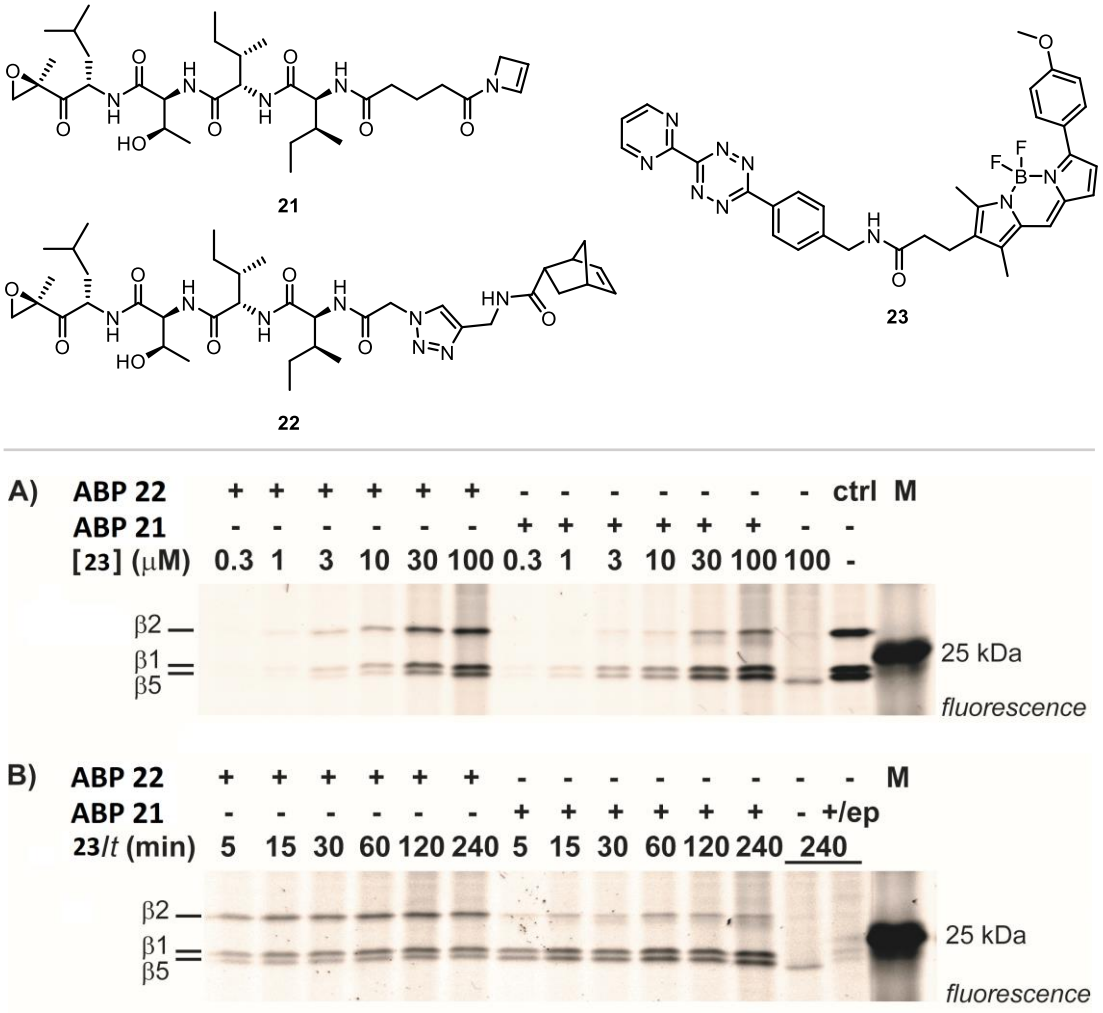

Figure 3: Structures of *N*-acylazetine- (**20**) and norbornene (**21**)-functionalized proteasome ABPs and tetrazine-BODIPY reporter reagent (**17**). [**A**] Labeling of proteasome activity in HEK cell extracts by exposure to 5 μM of ABP **21** or ABP **22** for 1 h followed by reaction with 0.3−100 μM of Bodipy-tetrazine **23** for 1 h. [**B**]: Labeling of proteasome activity in HEK cell extracts by exposure to 5 μM of ABP **21** or ABP **22** for 1 h followed by reaction with 10 μM of Bodipy-tetrazine **23** for 5−240 min. "ep": 100 μM epoxomicin added to incubation with ABP **21**.

ABP **22**.[20] Analysis of the labeled proteins on gel with fluorescent readout (Figure 3, A) revealed that tetrazine ligation of cell extracts treated with *N*-acylazetine-functionalized ABP **21** resulted in the specific fluorescent labeling of three bands, which correspond to the proteasome β-subunits labeled by fluorescent ABP MV151. The labeling is dependent on the concentration of tetrazine in a similar manner as for norbornene-functionalized ABP **22**. With both ABPs a comparable increase in fluorescent labeling was observed when the ligation step was performed at prolonged reaction times (Figure 3, B).

These results demonstrate that, in this experimental setup, the *N*-acylazetine moiety reacts with equal efficiency as the norbornene ligation handle in IEDDA reaction with tetrazine **23**. The absence of labeling in samples in which the proteasome activity was inhibited by an excess of epoxomicin, confirms that ABP **21** labels the catalytically active proteasome β-subunits. In order to determine whether *N*-acylazetine may cross-react with other commonly used ligation reagents, two-step proteasome labeling procedures were

performed in HEK cell extracts using alkyne-, azide- and phosphine-functionalized reagents instead of tetrazine for the ligation step. No proteasome labeling was detected when using Bodipy-alkyne[20], Bodipy-azide[21], biotin-phosphine[22] and biotinylated dibenzocyclooctene[23] reagents, demonstrating that these do not react with the *N*-acylazetine-tagged probe. Together these results demonstrate the utility of the new compact *N*-acylazetine ligation handle for bioorthogonal labeling of proteins or other biomolecules via tetrazine ligation.

Conclusion

In conclusion, two *N*-acylazetine handles (**7** and **13**) for the tetrazine ligation strategy were designed and synthesized. After optimization, these handles have become accessible through an efficient four-step synthesis. Determination of the reaction kinetics between the *N*-acylazetine and tetrazine showed a reaction rate constant in line with that of the methylcyclopropene mini-tag. The applicability of the *N*-acylazetine was demonstrated in an ABPP experiment, where epoxomicin – a broad-spectrum proteasome inhibitor – was functionalized with **7** and successfully used to label the proteasome through tetrazine ligation.

Experimental Section

General: Reactions were executed at ambient temperatures unless stated otherwise. All solvents used under anhydrous conditions were stored over 4Å molecular sieves, except for methanol which was stored over 3Å molecular sieves. Reactions were monitored by TLC-analysis using Merck aluminum DC Silicagel 60 F_{254}, using varying stains for visualization; an aqueous solution of cerium molybdate ($(NH_4)_6Mo_7O_{24}\cdot 4H_2O$ 25 g/L), an aqueous solution of potassium permanganate (5 g $KMnO_4$, 25 g K_2CO_3 per L) or an ethanolic solution bromocresol (0.4 g in 1 L, addition of 0.1M $NaOH_{(aq)}$ until the solution turns blue). Column chromatography was performed on silica gel (40-63 µm). Analysis by NMR and HRMS were performed as described in the experimental section of chapter 2.

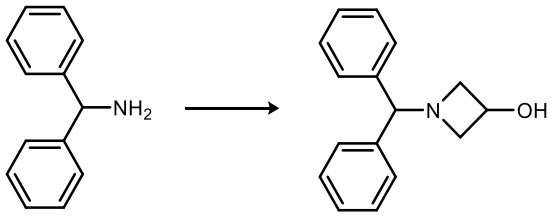

1 2

1-Benzhydrylazetidin-3-ol: Epichlorohydrin (10.75 ml, 138 mmol, 1.1 eq) was added to a solution of benzhydrylamine (21.55 ml, 125 mmol) in isopropanol (125 mL) and the reaction mixture was stirred overnight at 30 °C. LC/MS analysis showed full conversion into the open-chain intermediate. The reaction mixture was concentrated *in vacuo* and redissolved in MeCN (200 mL). Sodium bicarbonate (11.44 g, 188 mmol, 1.5 eq) was added and the reaction mixture was refluxed for 30 h. The reaction mixture was filtered and reduced *in vacuo*, providing a pale-yellow solid. The solid cake was thoroughly pulverized, suspended in an Et_2O/Pentane/EtOAc mixture (9:9:2, 50 mL) and sonicated for 15 minutes. The white residue was collected by filtration and dried under reduced pressure, yielding 1-benzhydrylazetidin-3-ol as a white solid (24.85 g, 104 mmol, 83%), which was used in the next step without further purification. R_f = 0.49 (1:1 ; EtOAc:PE). **^{1}H NMR** (400 MHz, $CDCl_3$) δ 7.40 – 7.12 (m, 10H), 4.42 (p, *J* = 5.8 Hz, 1H), 4.34 (s, 1H), 3.55 – 3.47 (m, 2H), 3.17 (s, 1H), 2.96 – 2.83 (m, 2H). **^{13}C NMR:** (101 MHz, $CDCl_3$) δ 141.80, 128.42, 127.38, 127.14, 78.43, 63.30, 61.89.

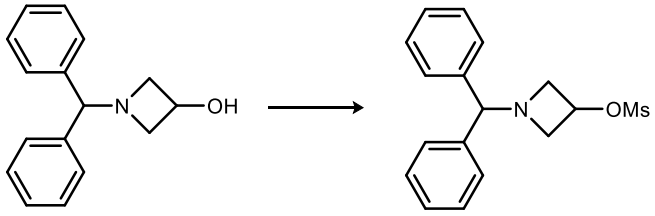

2 3

1-Benzhydrylazetidin-3-*O*-Mesyl: 1-benzhydrylazetidin-3-ol (24.65 g, 103 mmol) and triethylamine (21.53 ml, 155 mmol, 1.5 eq) were dissolved in DCM (80 mL) under argon atmosphere and cooled to -40 °C. Methanesulfonyl chloride (9.63 ml, 124 mmol, 1.2 eq) in DCM (20 mL) was slowly added dropwise, while

maintaining the temperature at -40 °C. The reaction mixture was stirred for 30 minutes, after which it was diluted with DCM (50 mL) and washed with water (2 x 100 mL). The organic phase was dried over magnesium sulfate, filtered and concentrated *in vacuo* (if the concentrate did not solidify, the oil was diluted with EtOAc and re-concentrated). The residual yellow solid was pulverized and thoroughly rinsed with cold Et_2O. The solid was suspended in a mixture of acetone/water (1:1, 50 mL) and sonicated for 15 minutes, filtered and vacuum dried, yielding product **3** as an off-white solid (26.3 g, 83 mmol, 80%). TLC R_f = 0.33 (1:3 ; EtOAc:PE). **^{1}H NMR:** (400 MHz, $CDCl_3$) δ = 7.53 – 7.25 (m, 10H), 5.16 (p, *J*=5.8, 1H), 4.50 (s, 1H), 3.73 – 3.66 (m, 2H), 3.31 – 3.23 (m, 2H), 2.93 (s, 3H). **^{13}C NMR:** (101 MHz, $CDCl_3$) δ 141.29, 128.46, 127.29, 127.19, 77.99, 67.86, 60.04, 37.91.

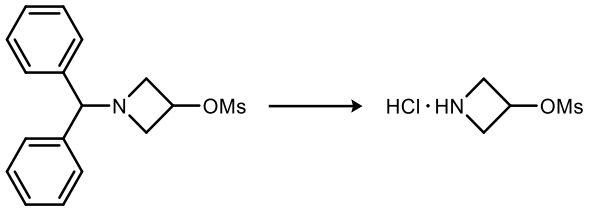

3 **4**

Azetidin-3-*O*-mesyl hydrochloride (4): A solution of 1-benzhydrylazetidin-3-yl methanesulfonate (26.3 g, 83 mmol) in DCE (150 mL) was charged with 1-Chloroethyl chloroformate (9.96 ml, 91 mmol, 1.1 eq) and heated to reflux. After 1.5 hour, TLC (Rf = 0.38 - 2:3 ; EtOAc:PE) indicated conversion of the starting material in a lower running product. The solution was concentrated *in vacuo*, redissolved in MeOH (150 mL) and refluxed for an additional 2 h. The reaction mixture was concentrated *in vacuo*. The residual yellow cake was suspended in a mixture of Et_2O:EtOH (2:1, 50 mL) and sonicated for 15 minutes. The remaining white solid was isolated by filtration, washed with Et_2O and dried *in vacuo*, yielding mesyl azetidine **4** (10.2 g, 54.4 mmol, 65.5 % yield) as a white solid. **^{1}H NMR:** (400 MHz, Methanol-d_4) δ 5.44 (ddd, *J* = 6.8, 4.8, 1.9 Hz, 1H), 4.52 (dt, *J* = 12.5, 4.4 Hz, 2H), 4.30 (dd, *J* = 12.6, 4.8 Hz, 2H), 3.23 (s, 3H). **^{13}C NMR:** (101 MHz, Methanol-d_4) δ 70.08, 54.51, 37.92.

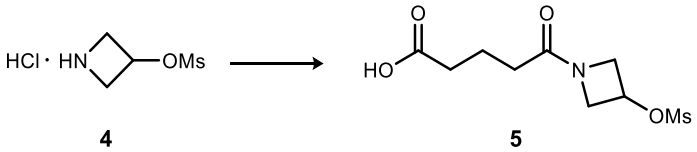

4 **5**

Glutaric Acylazetidine 5: A suspension of mesyl azetidine **4** (3.52 g, 18.8 mmol, 1.05 eq) and silver methanesulfonate (3.88 g, 19.1 mmol, 1.07 eq) in dry MeCN (25 mL) was prepared under argon atmosphere, and stirred vigorously at 40 °C for 15 minutes. Dry potassium carbonate (2.14, 35.7 mmol, 2 eq) and glutaric anhydride (2.04 g, 17.9 mmol, 1 eq) were added and the reaction was refluxed for 2 h. TLC indicated completion (10% EtOH in DCM), using bromocresol as a visualization agent. The reaction mixture was filtered over celite and carefully rinsed with water three times to remove product from the cake. The filtrate was diluted with 25% water in MeCN and acidified with Amberlite (IR120, H-form) to a pH below 3. After filtration, the solution was concentrated and purified by column chromatography (7% » 10% EtOH in DCM), yielding the title compound as a thick white solid (3.75 g, 14.1 mmol, 79%). **^{1}H NMR**

(400 MHz, $CDCl_3$) δ = 5.28 (tt, *J*=6.7, 4.1, 1H), 4.52 (ddd, *J*=10.1, 6.6, 1.5, 1H), 4.41 (ddd, *J*=11.5, 6.6, 1.4, 1H), 4.36 – 4.29 (m, 1H), 4.20 – 4.14 (m, 1H), 3.12 (s, 3H), 2.45 (t, *J*=7.0, 2H), 2.23 (t, *J*=7.3, 2H), 1.97 (p, *J*=7.1, 2H). **^{13}C NMR** (101 MHz, $CDCl_3$) δ 177.36, 172.75, 66.53, 57.47, 55.14, 38.37, 32.87, 30.29, 19.60. **HRMS:** Calculated for $C_{14}H_{10}F_5NO_3$ 266.06928 $[M+H]^+$; found 266.06919

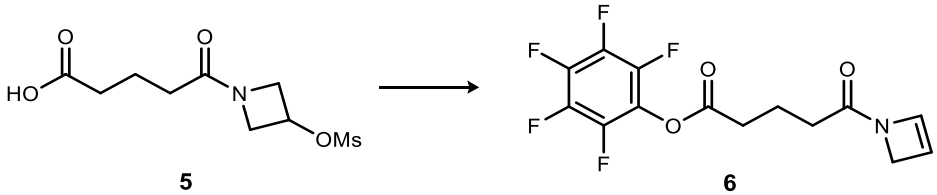

5 **6**

Pentafluorphenol Acylazetine 6: Potassium *tert*-butoxide in THF (20.5 mL, 1.6 M, 32.9 mmol, 2.3 eq) was added to a solution of mesylazetidine pentanoic acid spacer **5** in DMF (150 mL), under argon atmosphere. The reaction mixture was stirred at 50 °C for 2 h. After cooling to room temperature, EDC·HCl (8.23 g, 42.9 mmol, 3 eq.) and pentafluorophenol (4.58 mL, 42.9 mmol, 3 eq.) were added, and the reaction mixture was stirred for an additional 1.5 h. The mixture was poured into H_2O (150 mL) and extracted with DCM (150 mL). The organic layer was washed with brine (30 mL), dried over magnesium sulfate, filtrated and concentrated in *vacuo*. The crude product was purified by column chromatography (10% » 30% EtOAc in PE) to yield **6** as a colorless oil which solidified upon standing at -20°C (3 g, 9 mmol, 63%). **^{1}H NMR** (400 MHz, $CDCl_3$) δ = 6.93 – 6.69 (d, *J*=95.6, 1H), 5.75 (d, *J*=9.6, 1H), 4.52 (d, *J*=37.4, 2H), 2.90 – 2.76 (m, 2H), 2.42 (dt, *J*=36.0, 7.2, 2H), 2.15 (p, *J*=7.1, 2H). **^{13}C NMR** (101 MHz, $CDCl_3$) δ 177.36, 172.75, 66.53, 57.47, 55.14, 38.37, 32.87, 30.29, 19.60. **HRMS:** Calculated for $C_{14}H_{10}F_5NO_3$ 336.06536 $[M+H]^+$; found 336.06512.

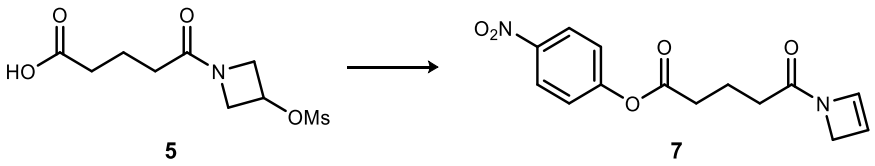

5 **7**

***p*-Nitrophenol Gluctaric Acylazetine 7:** A solution of mesylazetidine pentanoic acid spacer **5** (0.58 g, 2.186 mmol) in DMF (25 mL) was prepared and put under argon atmosphere. Next, potassium *tert*-butoxide (3.01 ml, 4.81 mmol) was slowly added and the reaction mixture was warmed to 50 °C and stirred vigorously for 2 hours. The reaction was allowed to cool to room temperature, after which *p*-nitrophenol (0.912 g, 6.56 mmol) was added. The reaction mixture was stirred until a clear yellow solution had formed. Then EDC·HCl (1.257 g, 6.56 mmol) was added and the reaction was stirred for additional 2 hours. The reaction mixture was poured into ether/EtOAc (2:1) and washed with water and brine. The organic layer was dried over magnesium sulfate, filtrated and concentrated in *vacuo*. The crude product was purified by column chromatography (30% » 80% EtOAc in PE) to yield **7** as a white crystalline substance (0.54 g, 1.86 mmol, 85%). **^{1}H NMR** (400 MHz, $CDCl_3$) δ = 8.27 (d, *J*=9.1, 2H), 7.29 (d, *J*=9.1, 2H), 6.80 (dd, *J*=100.2, 1.7, 1H), 5.73 (d, *J*=6.9, 1H), 4.51 (d, *J*=35.3, 2H), 2.74 (t, *J*=7.2, 2H), 2.46 (t, *J*=7.1, 1H), 2.37 (t, *J*=7.1, 1H), 2.13 (p, *J*=7.2, 2H). **^{13}C NMR** (101 MHz, $CDCl_3$) δ = 170.72, 155.28, 145.20, 137.40, 136.68, 125.13, 122.37, 113.71, 113.41, 58.53, 56.56, 33.23, 30.60, 29.56, 19.96, 19.78.

Improved Synthesis

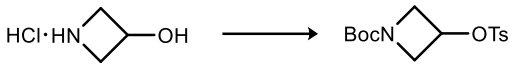

8 **9**

***N*-Boc-azetidin-3-*O*-mesyl (9):** A solution of commercially available 3-hydroxyazetidine hydrochloride (115 mmol, 10.55 g, 1 eq) and Et_3N (161 mmol, 22.5 mL, 1.4 eq) in MeOH (115 mL) was prepared at 0 ˚C. Boc_2O (126.5 mmol, 27.6 g, 1.1 eq) was added and the ice-bath was removed. After 5 hours of stirring, the reaction mixture was concentrated *in vacuo*, redissolved in DCM and washed twice with water. The water layers were combined and extracted twice with DCM. The organic layers were combined, dried with magnesium sulfate, filtered and concentrated *in vacuo*. The intermediate Boc-hydroxyazetidine was used without further purification. An ice-cooled solution of the crude **8** and Et_3N (172.5 mmol, 24 mL, 1.5 eq) in dry DCM (100 mL) was prepared under argon atmosphere. *p*-Toluenesulfonyl chloride (138 mmol, 26.3 g, 1.2 eq) was added in eight portions over 2 hours and the reaction mixture was stirred overnight. The reaction mixture was washed with water twice and the combined aqueous layers were extracted thrice with DCM. The organic layers were combined, dried over magnesium sulfate, filtered and concentrated *in vacuo*. The crude product was purified by column chromatography (5% » 10% EtOAc in pentane), yielding tosylate **9** as a yellow oil. (82.6 mmol, 27.7 g, 72% over two steps). **^{1}H NMR:** (300 MHz, $CDCl_3$) δ 7.75 (d, *J* = 8.1 Hz, 2H), 7.34 (d, *J* = 8.1 Hz, 2H), 4.97 (ddd, *J* = 10.8, 6.6, 4.3 Hz, 1H), 4.14 – 4.01 (m, 2H), 3.97 – 3.82 (m, 2H), 2.43 (s, 3H), 1.38 (s, 9H). **^{13}C NMR:** (75 MHz, $CDCl_3$) δ 155.86, 145.61, 132.91, 130.17, 127.92, 80.23, 67.84, 56.28, 28.30, 21.74. **HRMS:** Calculated for 327.11404 $[M+H]^+$; found 328.12132.

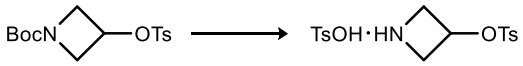

9 **10**

Azetidin-3-*O*-tosyl tosylate (10): A solution of compound **9** (82.6 mmol, 27.1g, 1 eq) in DCE (165 mL) was charged with *p*-toluenesulfonic acid (90.9 mmol, 17.3g, 1.1 eq) and refluxed for 20 hours. The reaction mixture was concentrated *in vacuo*. The crude product was crystalized from MeOH, yielding compound **20** as a white crystalline substance (65 mmol, 25.9 g, 79%). **^{1}H NMR** (400 MHz, $CDCl_3$) δ 9.00 (d, 2H), 7.70 (d, *J* = 8.2 Hz, 4H), 7.29 (d, *J* = 8.1 Hz, 2H), 7.19 (d, *J* = 7.8 Hz. **^{13}C NMR** (101 MHz, $CDCl_3$) δ 146.07, 141.26, 132.03, 130.38, 129.39, 128.17, 125.92, 67.85, 53.37, 21.86, 21.55.

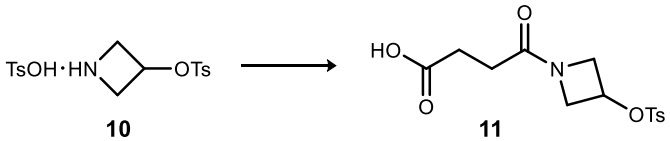

10 **11**

Succinic Acylazetidine 11: Compound **10** (20.0 mmol, 5.58 g, 1.1 eq) was co-evaporated with dioxane, redissolved in MeCN (200 mL), and put under argon atmosphere. Succinic anhydride (18.2 mmol, 1.82 g, 1 eq) was added to the reaction mixture, followed by potassium carbonate (45.5 mmol, 6.3 g, 2.5 eq) and the reaction mixture was refluxed for 6 hours. Reaction progress was monitored by TLC, using a bromocresol stain to visualize the produced carboxylic acid. The reaction mixture was diluted with water

(200 mL) and Amberlite-H^+ (IR120, ±70 g) was added until the pH fell below 3. The solution was filtered and the residual MeCN was removed *in vacuo*. The water layer was extracted twice with EtOAc. The organic layers were combined, dried over magnesium sulfate, filtered and concentrated *in vacuo*. The crude product was purified by column chromatography (5% » 10% EtOH in DCM), yielding compound **11** as a white crystalline substance (9.1 mmol, 3.09 g, 50%). **^{1}H NMR:** (400 MHz, $CDCl_3$) δ 7.80 (d, *J* = 8.3 Hz, 2H), 7.39 (d, *J* = 8.2 Hz, 2H), 5.08 (ddd, *J* = 11.1, 6.9, 4.3 Hz, 1H), 4.42 (dd, *J* = 9.4, 7.5 Hz, 1H), 4.30 – 4.08 (m, 2H), 3.94 (dd, *J* = 11.5, 4.0 Hz, 1H), 2.71 – 2.61 (m, 2H), 2.48 (s, 3H), 2.35 (t, *J* = 6.8 Hz, 2H). **^{13}C NMR:** (101 MHz, $CDCl_3$) δ 171.99, 145.99, 130.37, 128.07, 76.84, 67.22, 57.38, 55.23, 28.81, 26.20.

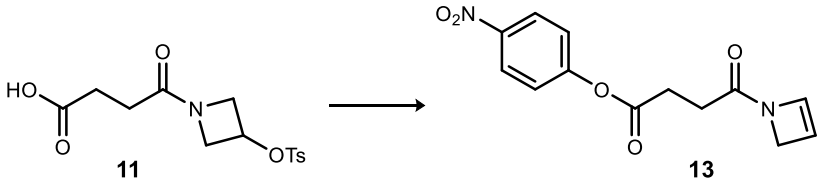

11 **13**

***p*-Nitrophenol Succinic Acylazetidine 13:** Compound **11** (9.1 mmol, 3.09 g, 1 eq) was co-evaporated with dioxane, redissolved in dry DMF (45.5 mL) and put under argon atmosphere. Next, a 1 M solution of potassium *tert*-butoxide in THF (20 mL, 2.1 eq) was added to the reaction mixture and the reaction was stirred for 1 hour. Subsequently the reaction mixture was charged with bis(para-nitrophenyl)carbonate (10 mmol, 3.01 g, 1.1 eq) and left stirring for an additional 3 hours. The reaction mixture was diluted with EtOAc and washed twice with 10% aqueous sodium bicarbonate, twice with water and once with brine. The combined organic layers were dried with $MgSO_4$, filtered and concentrated in *vacuo*. The crude product was purified with column chromatography (50% » 100% EtOAc in pentane), yielding compound **13** as a yellow crystalline substance (7.3 mmol, 2.0 g, 80%). **^{1}H NMR:** (400 MHz, $CDCl_3$) δ 8.26 (d, *J* = 9.2 Hz, 2H), 7.31 (d, *J* = 9.1 Hz, 2H), 6.91 (s, 0.5H), 6.71 (s, 0.5H), 5.75 (d, *J* = 5.3 Hz, 1H), 4.61 (s, 1H), 4.48 (s, 1H), 2.97 (t, *J* = 6.6 Hz, 2H), 2.75 (t, *J* = 6.5 Hz, 1H), 2.66 (t, *J* = 6.5 Hz, 1H). **^{13}C NMR:** (101 MHz, $CDCl_3$) δ 170.76, 165.26, 164.88, 155.48, 145.32, 137.43, 136.64, 125.22, 122.55, 114.19, 113.93, 77.16, 58.67, 56.91, 29.13, 29.03, 26.74, 25.76.

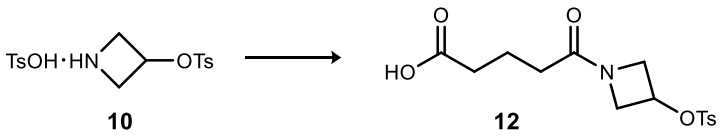

10 **12**

Succinic Acylazetidine 12: Compound **10** (14.0 mmol, 5.58g, 1.1 eq) was co-evaporated with dioxane, redissolved in MeCN (140 mL) and put under argon atmosphere. Glutaric anhydride (12.7 mmol, 1.45 g, 1 eq) was added to the reaction mixture, followed by potassium carbonate (31.8 mmol, 4.48 g, 2.5 eq) and the reaction mixture was refluxed for 6 hours. Reaction progression was monitored by TLC, using a bromocresol stain to visualize the produced carboxylic acid. The reaction mixture was diluted with water (200 mL) and Amberlite-H^+ (IR120, ±50 g) was added until the pH fell below 3. The solution was filtered and the residual MeCN was removed *in vacuo*. The water layer was extracted twice with EtOAc. The organic layers were combined, dried over magnesium sulfate, filtered and concentrated *in vacuo*. The crude product was purified by column chromatography (3% » 5% EtOH in DCM), yielding compound **12** as

a white crystalline substance (8.9 mmol, 3.06 g, 70%). **^{1}H NMR:** (400 MHz, $CDCl_3$) δ 7.81 (d, *J* = 8.3 Hz, 2H), 7.40 (d, *J* = 8.1 Hz, 2H), 5.08 (tt, *J* = 6.8, 4.2 Hz, 1H), 4.45 – 4.33 (m, 1H), 4.26 – 4.13 (m, 2H), 3.93 (dd, *J* = 11.5, 4.3 Hz, 1H), 2.49 (s, 3H), 2.42 (t, *J* = 7.0 Hz, 2H), 2.17 (t, *J* = 7.3 Hz, 2H), 1.92 (p, *J* = 7.2 Hz, 2H). **^{13}C NMR:** (101 MHz, $CDCl_3$) δ 177.76, 172.54, 145.84, 132.58, 130.24, 127.93, 67.11, 57.23, 54.93, 32.93, 30.29, 21.78, 19.57.

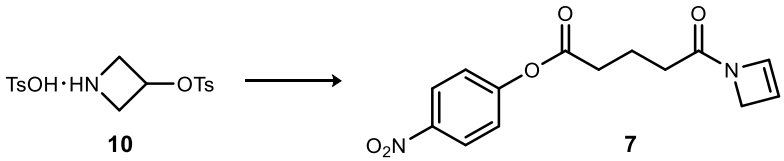

10 **7**

***p*-Nitrophenol Glutaric Acylazetine 7:** Compound **10** (8.9 mmol, 3.04 g, 1 eq) was co-evaporated with dioxane, redissolved in dry DMF (44.5 mL), and put under argon atmosphere. Next, a 1 M solution of potassium *tert*-butoxide in THF (18.7 mL, 2.1 eq) was added to the reaction mixture and left stirring for 1 hour. Subsequently the reaction mixture was charged with bis(para-nitrophenol)carbonate (9.8 mmol, 2.95 g, 1.1 eq) and left stirring for another 3 hours. The reaction mixture was diluted with EtOAc and washed twice with 10% aqueous sodium bicarbonate, twice with water and once with Brine. The combined organic layer were dried with magnesium sulfate, filtered and concentrated in *vacuo*. The crude product was purified with column chromatography (50% » 100% EtOAc in pentane), yielding compound **7** as a yellow crystalline substance (6.1 mmol, 1.78 g, 69%). **^{1}H NMR:** (400 MHz, $CDCl_3$) δ 8.26 (d, *J* = 9.2 Hz, 2H), 7.31 (d, *J* = 9.1 Hz, 2H), 6.91 (s, 0.5H), 6.71 (s, 0.5H), 5.75 (d, *J* = 5.3 Hz, 1H), 4.61 (s, 1H), 4.48 (s, 1H), 2.97 (t, *J* = 6.6 Hz, 2H), 2.75 (t, *J* = 6.5 Hz, 1H), 2.66 (t, *J* = 6.5 Hz, 1H). **^{13}C NMR:** (101 MHz, $CDCl_3$) δ 170.76, 165.26, 164.88, 155.48, 145.32, 137.43, 136.64, 125.22, 122.55, 114.19, 113.93, 77.16, 58.67, 56.91, 29.13, 29.03, 26.74, 25.76.

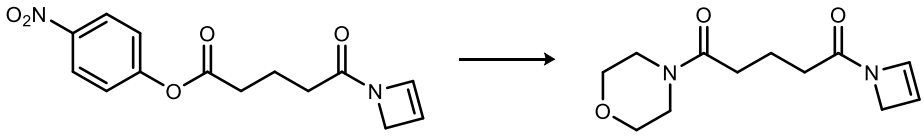

7 **14**

Morpholine Glutaric Acylazetine 14: Morpholine (0.099 ml, 1.137 mmol) was added to a solution of 4-nitrophenyl 5-(azet-1(2H)-yl)-5-oxopentanoate **7** (0.11 g, 0.379 mmol) in DCM (1 mL). After 1 hour, the reaction mixture was directly purified by column chromatography (DCM » DCM:Acetone:EtOH 80:20:1 » 50:45:5) to give **14** (88 mg, 0.369 mmol, 97%). **^{1}H NMR:** (400 MHz, $CDCl_3$) δ = 8.27 (d, *J*=9.1, 2H), 7.29 (d, *J*=9.1, 2H), 6.80 (dd, *J*=100.2, 1.7, 1H), 5.73 (d, *J*=6.9, 1H), 4.51 (d, *J*=35.3, 2H), 2.74 (t, *J*=7.2, 2H), 2.46 (t, *J*=7.1, 1H), 2.37 (t, *J*=7.1, 1H), 2.13 (p, *J*=7.2, 2H). **^{13}C NMR:** (101 MHz, $CDCl_3$) δ = 170.72, 155.28, 145.20, 137.40, 136.68, 125.13, 122.37, 113.71, 113.41, 58.53, 56.56, 33.23, 30.60, 29.56, 19.96, 19.78. HRMS $[M+H]^+$ m/z calc. for $[C_{14}H_{14}N_2O_5]$ = 291.09755, found 291.09744. **HRMS:** Calculated for $C_{12}H_{18}N_2O_3$ 239.13902 $[M+H]^+$; found 239.13900.

Synthesis of Model Compounds

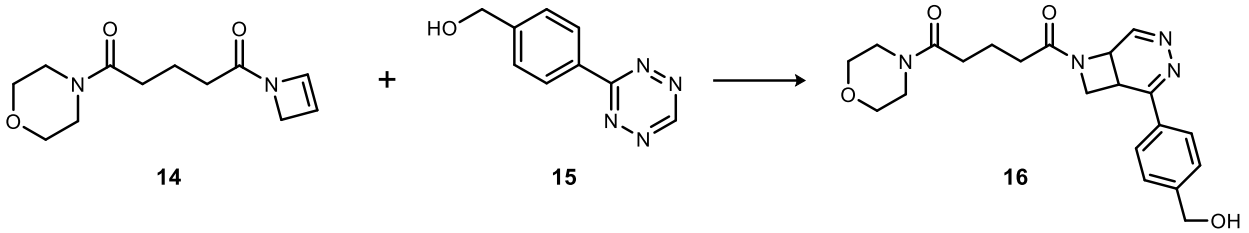

IEDDA Adduct 16: Tetrazine **14** was added to a solution of acylazetidine **15** in a H_2O:THF mixture (1:1, 1 mL). The reaction was stirred for 0.5 hour, diluted with water and washed with EtOAc. The water layer was separated and reduced in volume and co-evaporated with dioxane. The residue was redissolved in DMSO (1 mL). Diethyl ether (10 mL) was added and the mixture was sonicated for 0.5 hour. The ether was decanted and the remaining off-yellow powder was dried in *vacuo* to give adduct **16**.

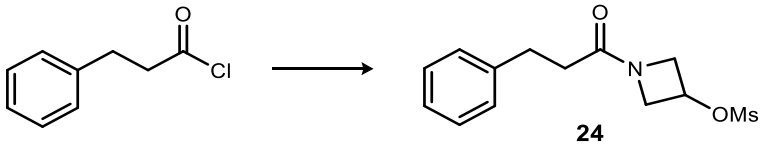

Model Acylazetidine 24: 3-Phenylpropionyl chloride (2.228 ml, 15.00 mmol) was added to a cooled solution (-78 °C) of azetidin-3-yl methanesulfonate hydrochloride (2.81 g, 15 mmol) and TEA (4,60 ml, 33,0 mmol) in DCM (60 mL), under argon atmosphere. The reaction mixture was stirred for 30 minutes, before being quenched with water. The aqueous layer was extracted twice with DCM (30 mL). The organic layer was isolated and dried over magnesium sulfate, filtered and concentrated in *vacuo*. The residual oil was purified by flash column chromatography (70% » 100% EtOAc in pentane), yielding **24** (3.04 g, 10.73 mmol, 72%) as a white crystalline substance. **^{1}H NMR** (400 MHz, $CDCl_3$) δ 7.30 (dd, *J* = 8.1, 6.7 Hz, 2H), 7.24 – 7.16 (m, 3H), 5.12 (tt, *J* = 6.7, 4.1 Hz, 1H), 4.36 – 4.25 (m, 1H), 4.18 (ddd, *J* = 10.1, 6.6, 1.5 Hz, 1H), 4.11 – 3.97 (m, 2H), 3.03 (s, 3H), 2.93 (t, *J* = 7.6 Hz, 2H), 2.43 – 2.32 (m, 2H). **^{13}C NMR** (101 MHz, $CDCl_3$) δ = 172.36, 140.81, 128.60, 128.41, 126.42, 66.61, 57.17, 54.89, 38.35, 33.77, 31.04.

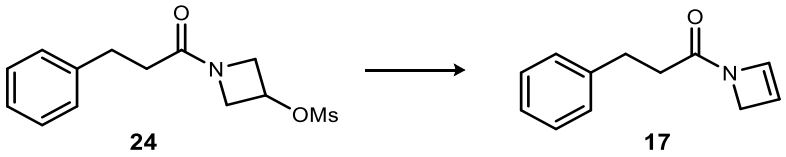

Model Acylazetine 17: Potassium tert-butoxide (1,459 g, 13.00 mmol) was added to a solution of **24** (2.83 g, 10 mmol) in *t*BuOH (30 mL), under argon atmosphere. The reaction mixture was stirred for 4h at 50 °C. The reaction mixture was poured into a diluted ammonium chloride solution and extracted with DCM. The organic layers were dried over magnesium sulfate, filtered and concentrated in *vacuo*. Purification by silica gel column chromatography (40% » 50% EtOAc in pentane) yielded **17** (1.09 g, 5.84 mmol, 58%) as a colorless oil that solidified upon standing. **^{1}H NMR** (400 MHz, $CDCl_3$) δ 7.80 (dd, *J* = 7.1, 1.7 Hz, 2H), 7.62 (s, 1H), 7.53 (t, *J* = 6.0 Hz, 1H), 7.45 – 7.38 (m, 1H), 7.38 – 7.23 (m, 7H), 7.14 – 7.01 (m, 6H), 4.27 (d, *J* = 5.9 Hz, 2H), 2.88 (t, *J* = 7.6 Hz, 2H), 2.51 (t, *J* = 7.7 Hz, 2H). **^{13}C NMR** (101 MHz, $CDCl_3$) δ 172.92, 159.03, 157.98,

140.49, 137.75, 135.72, 129.90, 129.07, 128.85, 128.72, 128.41, 128.27, 128.07, 126.92, 126.03, 122.63, 39.77, 37.48, 31.28.

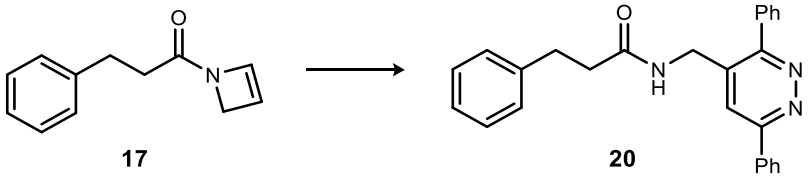

17 20

IEDDA Adduct 20: 3,6-diphenyl-1,2,4,5-tetrazine (62.6 mg, 0.267 mmol) was added to a solution of 1-(azet-1(2H)-yl)-3-phenylpropan-1-one (50 mg, 0.267 mmol) in H_2O:THF (1:4, 0.5 mL). The reaction mixture was stirred overnight. TLC (20% EtOAc in DCM) showed conversion into a single product. The solution was concentrated in *vacuo* and purified by column chromatography, yielding adduct **20** as a pale yellow oil. **^{1}H NMR** (400 MHz, $CDCl_3$) δ 7.80 (d, *J* = 7.1, 1.7 Hz, 2H), 7.62 (s, 1H), 7.53 (t, *J* = 6.0 Hz, 1H), 7.45 – 7.38 (m, 1H), 7.38 – 7.23 (m, 7H), 7.14 – 7.01 (m, 5H), 4.27 (d, *J* = 5.9 Hz, 2H), 2.88 (t, *J* = 7.6 Hz, 2H), 2.51 (t, *J* = 7.7 Hz, 2H). ^{13}C NMR (101 MHz, $CDCl_3$) δ 172.92, 159.03, 157.98, 140.49, 137.75, 135.72, 129.90, 129.07, 128.85, 128.72, 128.41, 128.27, 128.07, 126.92, 126.03, 122.63, 39.77, 37.48, 31.28.

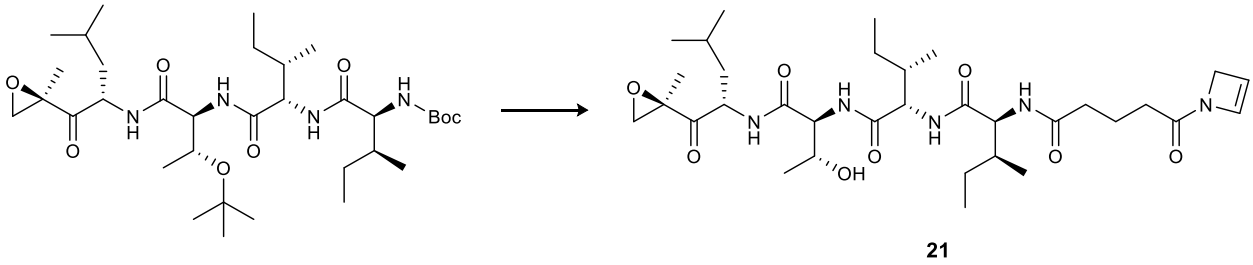

21

Acylazetine Epoxomicin 21: Epoxomicin-Thr(tBu)-Boc (0.05 g, 0.076 mmol) was dissolved in 0.5 ml TFA and stirred for 15 minutes. The reaction mixture was diluted with toluene and concentrated *in vacuo*. The residue was co-evaporated with toluene and redissolved in DMF (0.5 mL). DIPEA (0.053 ml, 0.305 mmol) was added, followed by perfluorophenyl 5-(azet-1(2H)-yl)-5-oxopentanoate (**6**) (0.026 g, 0.076 mmol). The reaction progress was followed by TLC-MS analysis. Upon completion, the reaction mixture was purified by HPLC to give **21** (15 mg, 0.023 mmol, 30%). **^{1}H NMR** (600 MHz, DMSO-d6) δ = 7.96 – 7.74 (m, 4H), 6.95 (d, *J*=20.1, 1H), 5.81 (d, *J*=48.3, 1H), 4.84 – 4.71 (m, 1H), 4.54 (d, *J*=4.9, 1H), 4.42 – 4.35 (m, 1H), 4.31 (s, 1H), 4.27 – 4.15 (m, 3H), 3.87 (h, *J*=5.7, 1H), 3.18 (d, *J*=5.3, 1H), 3.00 (d, *J*=5.3, 1H), 2.27 – 2.08 (m, 3H), 1.81 – 1.58 (m, 3H), 1.39 (s, 3H), 1.36 – 1.24 (m, 2H), 1.12 – 1.02 (m, 2H), 0.99 (d, *J*=6.3, 3H), 0.89 (d, *J*=6.7, 3H), 0.85 – 0.73 (m, 15H). **^{13}C NMR** (151 MHz, DMSO-d6) δ = 208.00, 171.63, 171.17, 170.85, 170.06, 138.49, 137.20, 113.98, 112.74, 66.43, 58.79, 58.36, 57.86, 56.86, 56.03, 51.55, 49.23, 43.30, 38.69, 36.44, 36.17, 34.69, 34.28, 32.55, 30.67, 29.53, 24.27, 23.16, 21.10, 21.05, 20.97, 19.70, 15.32, 15.19, 10.90, 10.84.

Kinetics Experiments

Determination of the pseudo-first order reaction rate constant

A 1.2 mM stock solution of tetrazine **15** in 12% DMSO:Water (v:v) and a 12 mM stock solution of acylazetine **14** in 12% DMSO:Water were prepared. 1 mL of the 1.2 mM tetrazine **15** stock solution was brought into a quarts cuvette (10 mm width, 2 mL volume), which was placed in the measurement chamber of a Cary 300 UV-Vis spectrophotometer (Agilant Technologies). Then, 1 mL of the 12 mM acylazetine **14** stock solution was added to the cuvette and the measurement was immediately started. Upon addition of the second solution, the concentration became 0.6 mM for **15** and 6 mM for **14**. The absorption decay was followed at 517 nm, measuring at 13 second intervals over 30 minutes. The experiments were conducted at uncontrolled room temperature (±20 ˚C).

The reaction rate was derived from four data sets using every measurement interval up to 600 seconds (absorption range from 100% to >10%). This gave 4 data points per value of time (x). This array was subjected to the LINEST function (Microsoft Excel 2013) to determine the slope and the standard deviation. The slope represents the pseudo first-order rate constant.

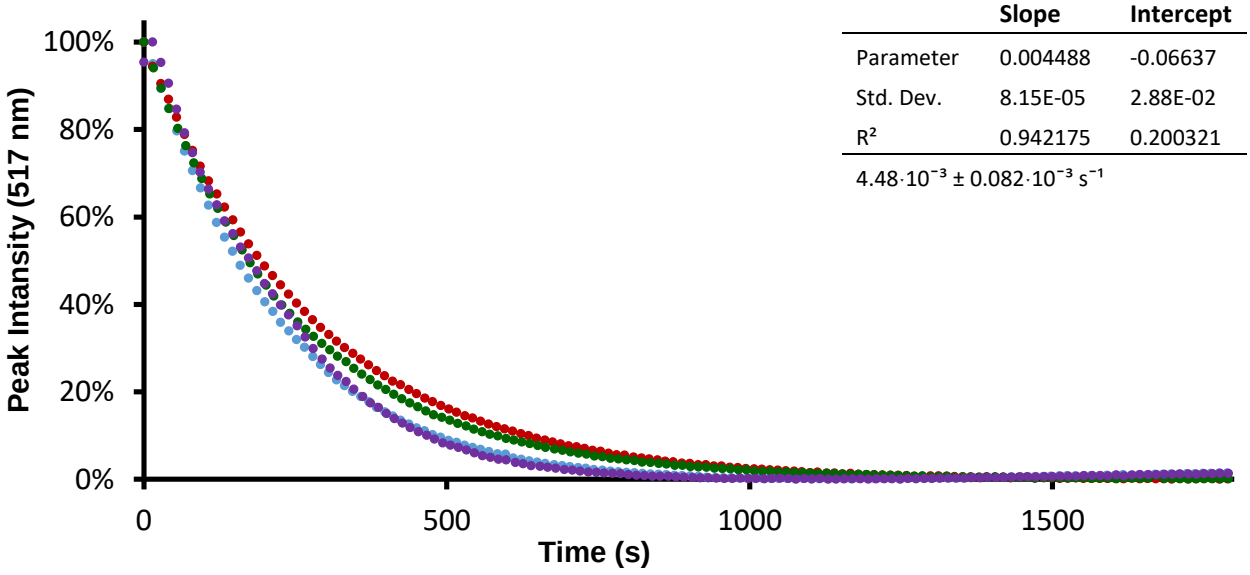

	Slope	Intercept
Parameter	0.004488	-0.06637
Std. Dev.	8.15E-05	2.88E-02
R^2	0.942175	0.200321

$4.48 \cdot 10^{-3} \pm 0.082 \cdot 10^{-3}\ s^{-1}$

Determination of the second order rate constant

The second order rate was derived from the observed pseudo-first order reaction rates at three different (excess) concentrations of **14**. These experiments were conducted at uncontrolled room temperature (approximately 20 ˚C). The slope of this plot represents the second order rate constant.

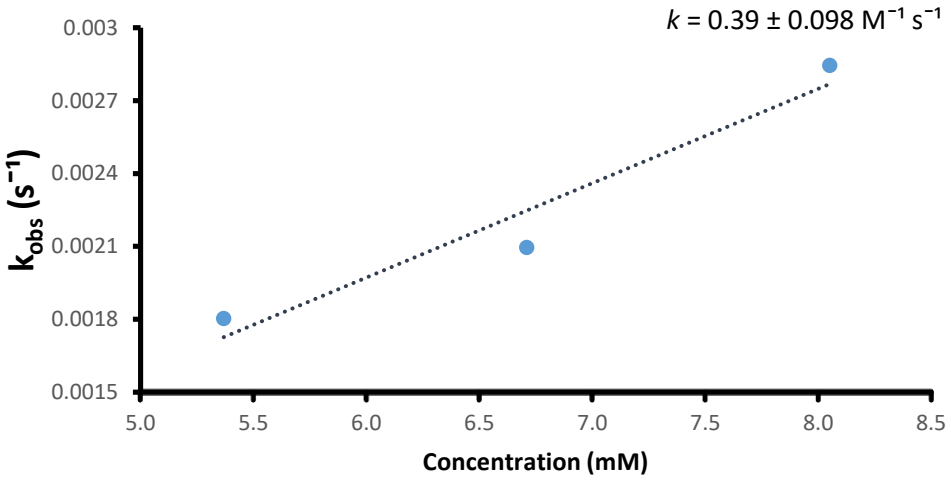

Biological Essays

Preparation of cell extracts

Human Embryonic Kidney (HEK) cell extracts were prepared from cultured HEK-293T cells by harvesting, washing with PBS (2x) and cell lysis in digitonin lysis buffer (50 mM Tris pH 7.5, 250 mM sucrose, 5 mM $MgCl_2$, 1 mM DTT, 2 mM ATP, 0.025% digitonin) for 30 min on ice followed by sonication on ice for 3x 10 s. After centrifugation of the cells at 16,100 g for 15 min at 4 °C, the supernatants were collected and the protein concentration was determined by Bradford assay.

Competition assay versus MV151

HEK cell lysates (20 µg total protein per experiment) in lysis buffer (9 µL) were exposed to the indicated concentrations of **21** (1 µL 10x solution in DMSO) for 1 hr at 37 °C, after which the lysates were incubated with 1 µM MV151 (1.1 µL 10 µM in DMSO) for 1 hr at 37 °C. The reaction mixtures were then boiled at 100 °C for 5 minutes with 4 µL 4x Laemmli's sample buffer containing 2-mercaptoethanol and resolved on 12.5% SDS-PAGE. In-gel visualization of the fluorescent labeling was performed in the wet gel slabs directly using a Typhoon Variable Mode Imager (Amersham Biosciences) with Cy3/TAMRA settings (excitation wavelength 532 nm, emission wavelength 580 nm). As a loading control gels were stained with Coomassie Brilliant Blue. As a protein standard the PageRuler Plus Prestained Protein Ladder (Thermo Scientific) was used.

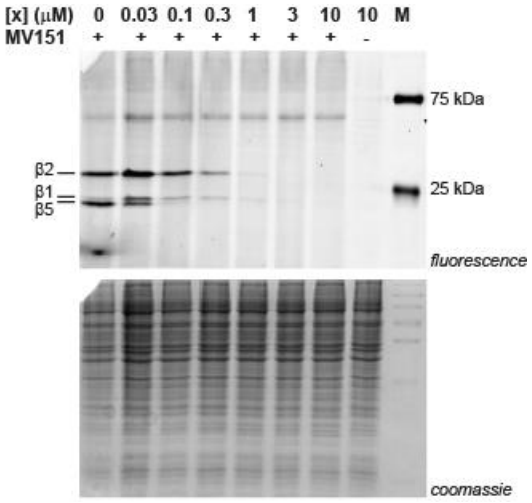

Figure E1. Competition experiment in HEK cell extracts. Cell extract were first exposed to 0 - 10 µM of azetidine-functionalized ABP **21** for 1 hr and then to fluorescent proteasome ABP MV151 for 1 hr. 12.5% SDS-PAGE with fluorescent readout followed by coomassie brilliant blue staining. Proteasome β-subunits are designated on the basis of reported labeling by MV151. 'M': protein marker.

Tetrazine ligation in cell extracts

HEK cell lysates (20 µg total protein per experiment) in lysis buffer (19 µL) were exposed to 5 µM of **12** or **11** (1 µL 100 µM in DMSO) for 1 hr at 37 °C. As a control, lysates were incubated with **11** in the presence of 100 µM epoxomicin (1 µL 2 mM in DMSO) or labeled with 1 µM MV151 (1 µL 20 µM in DMSO) for 1 hr at 37 °C. The cell extracts were then exposed to the indicated concentrations of **13** (1.1 µL 20x solution in DMSO) for the indicated time at 37 °C. After quenching by chloroform/methanol precipitation,[24] the proteins were taken up in 10 µL Laemmli's sample buffer containing 2-mercaptoethanol, boiled at 100 °C for 5 minutes and resolved on 12.5% SDS-PAGE. In-gel visualization of the fluorescent labeling was performed in the wet gel slabs directly using a Typhoon Variable Mode Imager (Amersham Biosciences) with Cy3/TAMRA settings (excitation wavelength 532 nm, emission wavelength 580 nm). As a loading control gels were stained with Coomassie Brilliant Blue. As a protein standard the PageRuler Plus Prestained Protein Ladder (Thermo Scientific) was used.

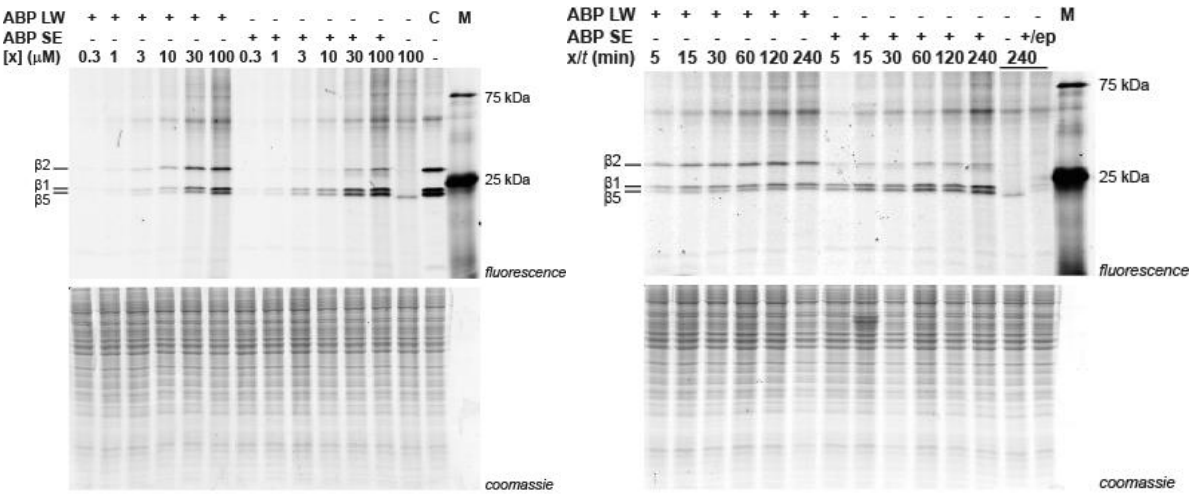

Figure E3: Full depiction of data presented in Figure 4.

Test of cross-reactivity in cell extracts

HEK cell lysates (20 µg total protein per experiment) in lysis buffer (19 µL) were exposed to 5 µM of **21** (1 µL 100 µM in DMSO) for 1 hr at 37 °C. The cell extracts were then exposed to 100 µM biotin-phosphine, 100 µM biotin-dibenzocyclooctyn, 50 µM azido-Bodipy, 50 µM Bodipy-alkyne or 50 µM tetrazine-Bodipy (each 1 µL 20x in DMSO) for 1 hr at 37 °C. After quenching by chloroform/methanol precipitation,[16] the proteins were taken up in 10 µL Laemmli's sample buffer containing 2-mercaptoethanol, boiled at 100 °C for 5 minutes and resolved on 12.5% SDS-PAGE. In-gel visualization of the fluorescent labeling was performed in the wet gel slabs directly using a Typhoon Variable Mode Imager (Amersham Biosciences) with Cy2/Blue Fam settings (excitation wavelength 488 nm, emission wavelength 520 nm). Next, the proteins were transferred onto a PVDF membrane for detection of biotinylated proteins. The membrane was blocked with 1% BSA in TBS-t(+) (0.1% Tween 20) for 1 hr at room temperature, hybridized with Streptavidin-HRP for 45 min at room temperature (1:10,000 in blocking buffer) (Molecular Probes, Life Technologies), washed with TBS-t(+) and TBS and then visualized using an ECL+ Western Blotting detection kit (Amersham Biosciences). As a loading control the membrane was stained with Coomassie Brilliant Blue.

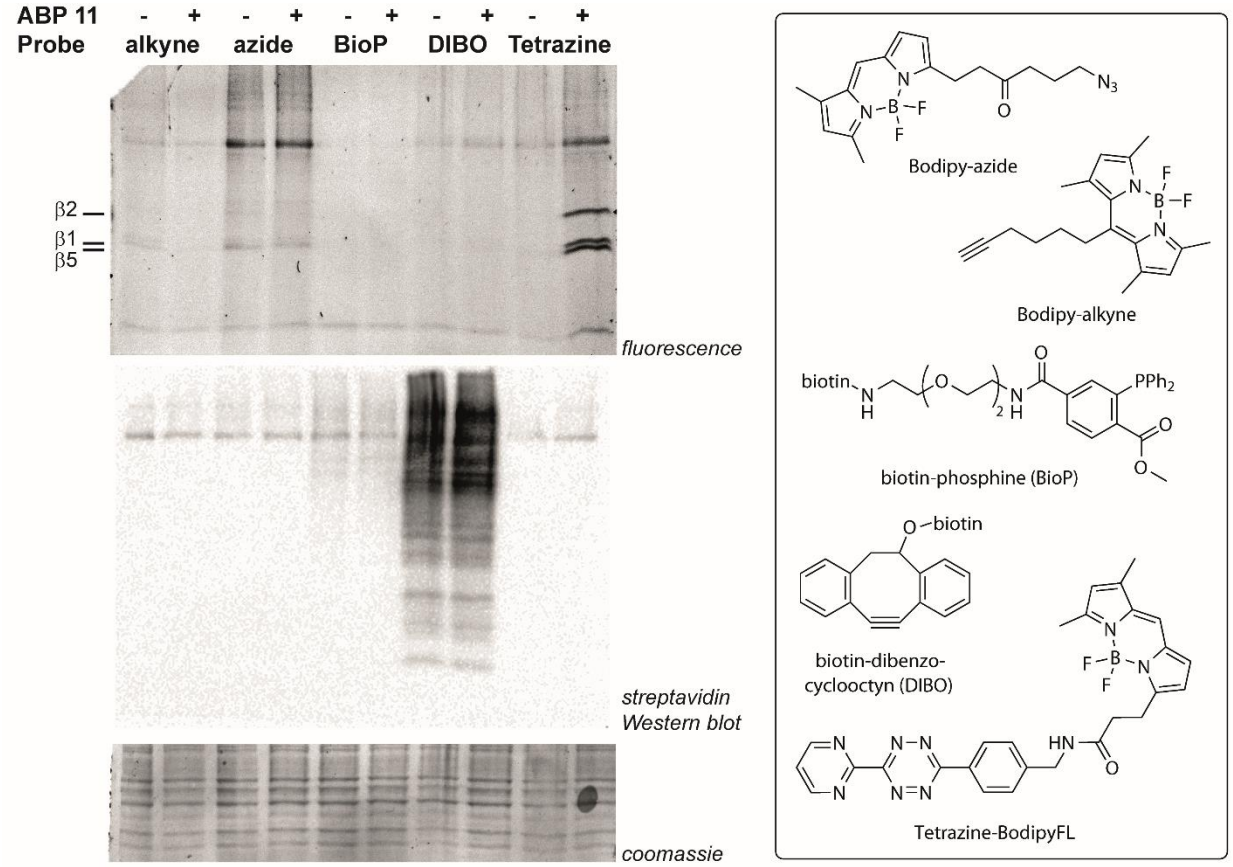

Figure E4. Test of cross-reactivity in HEK cell extracts. Cell extract were first exposed to 5 µM of azetidine-functionalized ABP **21** for 1 hr and then to Bodipy-azide (50 µM), Bodipy-alkyne (50 µM), tetrazine-BodipyFl (50 µM), biotin-phosphine ('BioP', 100 µM) or biotin-dibenzocyclooctyne ('DIBO', 100 µM) for 1 hr. 12.5% SDS-PAGE with fluorescent readout for detection of Bodipy-labeled proteins followed by streptavidin Western blotting to detect biotinylated proteins. Coomassie brilliant blue staining is shown as a loading control. 'M': protein marker.

References

1. D. M. Patterson, L. A. Nazarova, J. A. Prescher, **2014**.
2. L. I. Willems, W. A. Van Der Linden, N. Li, K. Y. Li, N. Liu, S. Hoogendoorn, G. A. Van Der Marel, B. I. Florea, H. S. Overkleeft, *Acc. Chem. Res.* **2011**, *44*, 718–729.
3. E. Saxon, C. R. Bertozzi, *Science (80-.).* **2000**, *287*, 2007–2010.
4. F. Himo, T. Lovell, R. Hilgraf, V. V. Rostovtsev, L. Noodleman, K. B. Sharpless, V. V. Fokin, *J. Am. Chem. Soc.* **2005**, *127*, 210–216.
5. N. J. Agard, J. A. Prescher, C. R. Bertozzi, *J. Am. Chem. Soc.* **2004**, *126*, 15046–15047.
6. M. L. Blackman, M. Royzen, J. M. Fox, *J. Am. Chem. Soc.* **2008**, *130*, 13518–13519.
7. N. K. Devaraj, R. Weissleder, S. A. Hilderbrand, *Bioconjug. Chem.* **2008**, *19*, 2297–2299.
8. F. Liu, R. S. Paton, S. Kim, Y. Liang, K. N. Houk, *J. Am. Chem. Soc.* **2013**, *135*, 15642–15649.
9. J. Yang, J. Šečkute, C. M. Cole, N. K. Devaraj, *Angew. Chemie - Int. Ed.* **2012**, *51*, 7476–7479.
10. F. Thalhammer, U. Wallfahrer, J. Sauer, *Tetrahedron Lett.* **1990**, *31*, 6851–6854.
11. D. De Smaele, Y. Dejaegher, G. Duvey, N. De Kimpe, *Tetrahedron Lett.* **2001**, *42*, 2373–2375.
12. M. E. Jung, Y. M. Choi, *J. Org. Chem.* **1991**, *56*, 6729–6730.
13. V. V. R. M. Krishna Reddy, D. Udaykiran, U. S. Chintamani, E. Mahesh Reddy, C. Kameswararao, G. Madhusudhan, *Org. Process Res. Dev.* **2011**, *15*, 462–466.
14. J. Yang, M. R. Karver, W. Li, S. Sahu, N. K. Devaraj, *Angew. Chemie - Int. Ed.* **2012**, *51*, 5222–5225.
15. M. Verdoes, L. I. Willems, W. A. van der Linden, B. A. Duivenvoorden, G. A. van der Marel, B. I. Florea, A. F. Kisselev, H. S. Overkleeft, *Org. Biomol. Chem.* **2010**, *8*, 2719.
16. M. Verdoes, B. I. Florea, V. Menendez-Benito, C. J. Maynard, M. D. Witte, W. A. van der Linden, A. M. C. H. van den Nieuwendijk, T. Hofmann, C. R. Berkers, F. W. B. van Leeuwen, et al., *Chem. Biol.* **2006**, *13*, 1217–1226.
17. M. Hanada, K. Sugawara, K. Kaneta, S. Toda, Y. Nishiyama, K. Tomita, H. Yamamoto, M. Konishi, T. Oki, *Epoxomicin, a New Antitumor Agent of Microbial Origin.*, **1992**.
18. L. Meng, R. Mohan, B. H. B. Kwok, M. Elofsson, N. Sin, C. M. Crews, *Proc. Natl. Acad. Sci.* **1999**, *96*, 10403–10408.
19. N. Sin, K. B. Kim, M. Elofsson, L. Meng, H. Auth, B. H. B. Kwok, C. M. Crews, *Bioorg. Med. Chem. Lett.* **1999**, *9*, 2283–2288.
20. M. Verdoes, U. Hillaert, B. I. Florea, M. Sae-Heng, M. D. P. Risseeuw, D. V. Filippov, G. A. van der Marel, H. S. Overkleeft, *Bioorganic Med. Chem. Lett.* **2007**, *17*, 6169–6171.
21. L. I. Willems, N. Li, B. I. Florea, M. Ruben, G. A. Van Der Marel, H. S. Overkleeft, *Angew. Chemie - Int. Ed.* **2012**, *51*, 4431–4434.
22. M. Verdoes, B. I. Florea, U. Hillaert, L. I. Willems, W. A. van der Linden, M. Sae-Heng, D. V. Filippov, A. F. Kisselev, G. A. van der Marel, H. S. Overkleeft, *ChemBioChem* **2008**, *9*, 1735–1738.
23. X. Ning, J. Guo, M. A. Wolfert, G. J. Boons, *Angew. Chemie - Int. Ed.* **2008**, *47*, 2253–2255.
24. D. Wessel, U. I. Flugge, *Anal. Biochem.* **1984**, *138*, 141–143.

6 Reaction Rates of Various Acylenamines in the Inverse-Electron-Demand Diels–Alder Reaction

Introduction

The inverse-electron-demand Diels-Alder (IEDDA) reaction between (cyclic) alkenes and tetrazines has been well-studied for several decades.[1–8] Scientific interest spiked in 2008, due to the breakthrough of tetrazine ligation in the field of bioorthogonal chemistry.[9,10] Bioorthogonal ligation handles require an intricate balance between several physical properties. Preferably the handle should be sterically small in size and be stabile under physiological and preparative conditions, while maintaining high reactivity towards tetrazines. An additional beneficial property is the moderate- to high hydrophilicity, to assist the water solubility of the functionalized chemical probe. By now, a strong positive correlation had been established between the ring-strain within cyclic alkenes and enhanced reactivity towards tetrazines.[5] Although surprising, considering the nature of the reaction, significantly less effort has been directed towards studying the effects of alkene electron density on reactivity. Chapter 5 describes a new compact ligation handle featuring an *N*-acylazetine as the reactive partner, which was designed to utilize both ring-strain and electron donating properties to enhance reactivity towards tetrazines.[8] A reactive *N*-acylazetine tag was synthesized and successfully applied in an activity-based protein profiling experiment. These advancements warranted further investigation into the structure-reactivity relationship of the *N*-alkene structure. This chapter describes the synthesis of various *N*-vinyl derivatives (Figure 1, **3**-**7**) and the empirical assessment of their stability and reactivity towards tetrazines. By comparing the reaction-rate constants with those of model *N*-acylazetines **1** and **2**, fundamental insight could be gained in the contribution of both ring-strain and electron donating effects on the tetrazinophilicity. Ultimately this knowledge may lead to improved handles for the tetrazine ligation strategy.

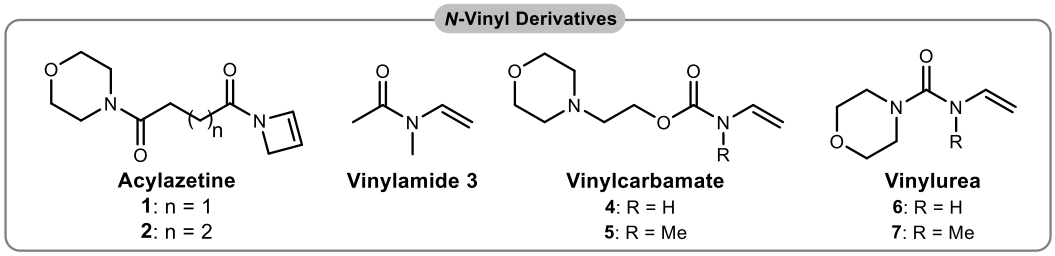

Figure 1: The *N*-acylazetine and five model *N*-vinyl derivatives.

As entries for the reaction-rate comparative study the *N*-vinylamide (**3**), *N*-vinylcarbamates (**4** and **5**) and *N*-vinylurea (**6** and **7**) were considered. As a result of the tautomerization equilibrium between the amine and imine form, these *N*-vinyl groups are simultaneously electrophilic at the α-carbon and nucleophilic at β-carbon.[11] This ambivalent nature makes them susceptible to hydrolysis, or polymerization in either acid catalyzed or radical mediated processes.[12,13] Alkylation at the nitrogen of the *N*-vinyl derivatives stabilizes the groups by preventing tautomerization. In addition, an analysis of the *N*-acylazetine core reveals that a disconnection between the *N*-CH_2 and the *N*-vinyl-β-CH_1 leads to the *N*-methyl-*N*-vinylamide (**3**) structure. With these considerations in mind, one can view methylation at the vinyl nitrogen of the earlier suggested *N*-vinyl derivatives as a logical modification that more thoroughly isolates the effects of the ring-strain during the comparative IEDDA reaction-rate study, while at the same time stabilizing the *N*-vinyl group. Morpholine based nucleophiles were chosen in the preparation of the *N*-vinylcarbamate and -urea analogue to ensure the required water solubility for the kinetic experiments.

Results and Discussion

Commercially available *N*-methyl-*N*-vinylamide (**3**) was considered a convenient model substrate to study the influence of ring-strain and was directly used in IEDDA kinetic experiments. Literature provides several methods for the preparation of *N*-vinylcarbamates.[14–18] The most prevalent strategy makes use of the Curtius rearrangement of acryl azide (**9**), *in situ* generated from acryloyl chloride (**8**) and sodium azide (Scheme 1). Through heating the acryl azide rearranges to vinyl isocyanate (**10**), which can react with an alcohol of choice to provide an *N*-vinylcarbamate. A small amount of base and radical scavenger, such as hydroquinone or phenothiazine, is added to suppress dimerization and radical polymerization. Following this strategy, a solution of acryl azide in toluene was prepared and slowly added to a reaction mixture containing 2-morpholinoethanol, pyridine and hydroquinone in toluene at 100 ˚C, providing *N*-vinylcarbamate **4** in 29% isolated yield. The vinyl nitrogen was methylated with sodium hydride and methyl iodide in THF at 0 ˚C, to give *N*-methyl-*N*-vinylcarbamate **5**.

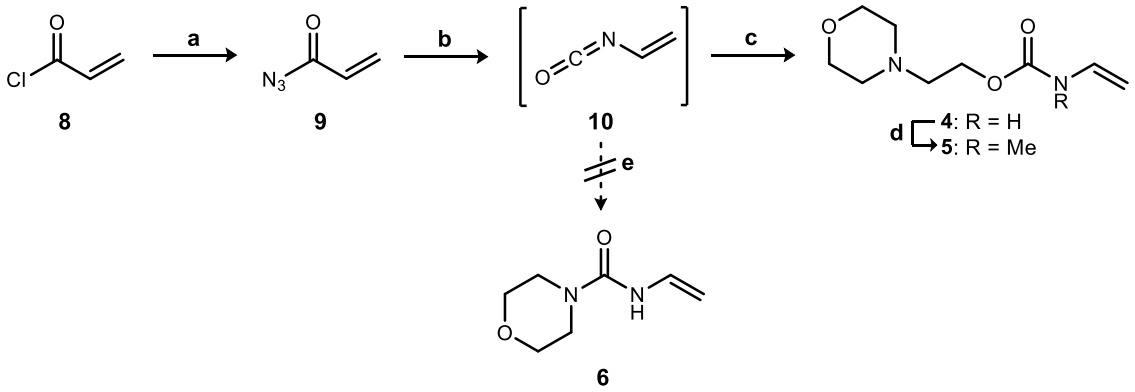

Scheme 1: Overview of research conducted for the synthesize *N*-vinyl derivatives **5** and **6** via Curtius rearrangement. Reagents and Conditions: [**a**] NaN_3, H_2O/Toluene (1:1), 6h. [**b**] Pyridine, hydroquinone, 100 ˚C, 1.5h. [**c**] 2-morpholinoethanol, toluene, 1h. [**d**] i: NaH, THF, MeI, 0 ˚C, 1.5h, 75%. [**e**] Morpholine, toluene, 1h.

In this transformation, substituting 2-morpholinoethanol for morpholine should theoretically result in *N*-vinylurea **6**. However, considering the discussed ambivalent reactivity and the lack of literature reports supporting the *N*-vinylurea structure, this class of compounds is likely too unstable to be isolated under preparative conditions. Indeed, no product could be isolated when morpholine was reacted with *in situ* generated vinyl isocyanate (**10**). Alternatively, carboxylic acids can be converted into isocyanates using the milder Lossen rearrangement (Scheme 2).[19] Using this method, acrylic acid (**11**) was converted into acryl hydroxamide (**12**) via a carbonyldiimidazole-assisted (CDI) condensation. *In situ* activation of the hydroxamide **12** with CDI generated dioxazalone intermediate **13**, which was expected to decarboxylate into vinyl isocyanate upon heating to 80 ˚C in acetonitrile. Again, attempts to capture the vinyl isocyanate with morpholine were unsuccessful. In a final attempt to synthesize a vinyl urea derivative, efforts were made to directly prepare the more stable *N*-methylated derivative **7** (Figure 1). Derived from the optimized synthesis for the *N*-acylazetines (Chapter 5), it was considered that the *N*-vinyl urea could be accessed through tosylate elimination. In a one-pot procedure, phosgene was unsymmetrically functionalized with morpholine and *N*-methylethanolamine, to provide urea **15**. However, tosylation of the primary alcohol lead to degradation into various side-products. With these final results, the synthesis of the urea derivatives (**6** and **7**, Figure 1) was abandoned.

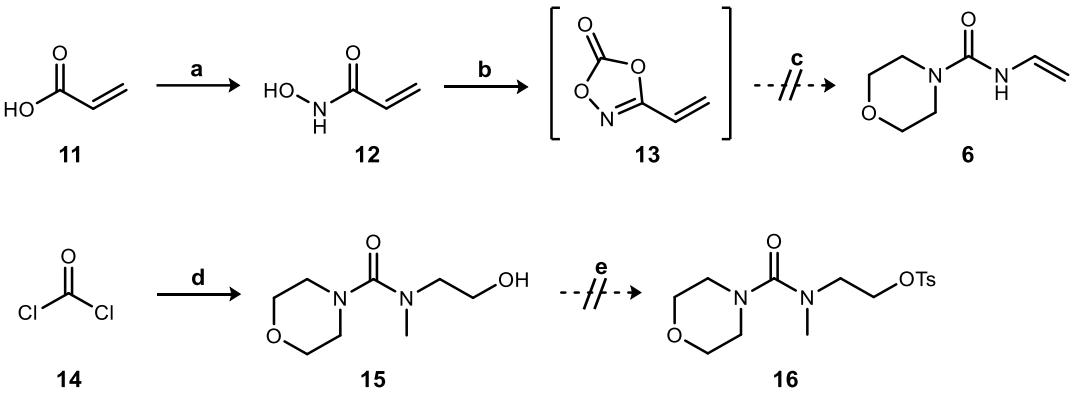

Scheme 2: Alternative methods explored for the synthesis of *N*-vinylurea **6**. Reagents and Conditions: [**a**] i: CDI, MeCN, 1.5h. ii: $NH_2OH{\cdot}HCl$, 2h, used crude. [**b**] CDI, 0.5h. [**c**] Morpholine, 60 ˚C, 1h. [**d**] Morpholine, Et_3N, DCM, 0 ˚C » Phosgene in toluene, 1h. 51% [**e**] TsCl, Et_3N, DCM, 0 ˚C, 16h.

Considering the discussed reactivity of *N*-vinyl compounds, the influence of potential degradation of these substrates during both the kinetic experiments and biorthogonal tagging reactions had to be excluded. The aqueous stability of *N*-acylazetine **2** and *N*-vinylcarbamates **4** and **5** was evaluated by dissolving the respective compounds in deuterated water and monitoring the solution over a 13 hour period at 37 ˚C through ^{1}H-NMR spectroscopy. After the full duration, secondary *N*-vinylcarbamate **4** showed 4% hydrolysis of the vinyl group, as determined by integration of the formyl hydrogen (δ = 9.74) resulting from the formed acetaldehyde. Fortunately, this rate of decomposition proved to be insignificant within the thirty minute timeframe required for the kinetic experiments (Table 1). *N*-acylazetine **2** and *N*-vinylcarbamate **5** proved to be stable during the experiment. In addition, the *N*-acylazetine group stability was evaluated in the presence of 100 mM of ethanethiol and 2-aminoethanol, to mimic the physiological conditions used during *in vitro* ABPP experiments. Again, no decomposition occurred.

Reaction Kinetics

With the *N*-acylazetines **1**, **2** and *N*-vinyl derivatives **3**, **4**, **5** in hand, the stage was set for determining the rate of their reaction with tetrazine **17** (Chapter 5). For comparative purposes the same conditions were used as reported by Devaraj *et al* in their work featuring the 1-methylcyclopropene ligation handle.[20] The pseudo-first-order and second-order reaction-rates were assessed by reacting a ten-fold excess of the respective dienophile with tetrazine **17** in 12% aqueous DMSO. The rate of tetrazine consumption was measured by monitoring the characteristic tetrazine absorption at 517 nm. Each experiment was conducted thrice at both room temperature (RT = 20 ˚C) and cell temperature (CT = 37 ˚C). The results are summarized in Table 1.

Table 1: Reaction-rates for addition of various dienophiles to tetrazine **17**. The first-order reaction rates were calculated from three data sets each using all measurement intervals up until $t_{1/2}$. The errors ranges are the standard deviations derived from the generated first-order rate data. Half-life values are calculated from first-order rate constant: $t_{1/2} = \ln(2) / k$.

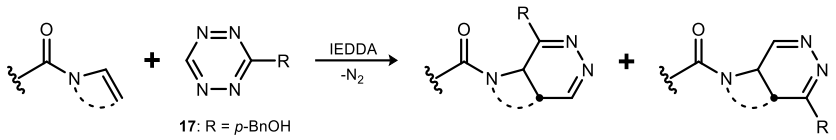

#	Dienophile	T (˚C)	1st Order (s^{-1})	2nd Order ($M^{-1}\cdot s^{-1}$)	Half-life (s)
1	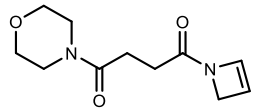	20	$4.10 \cdot 10^{-3} \pm 3.71 \cdot 10^{-4}$	$6.88 \cdot 10^{-1} \pm 6.23 \cdot 10^{-2}$	169
		37	$7.11 \cdot 10^{-3} \pm 8.95 \cdot 10^{-5}$	$1.21 \pm 1.42 \cdot 10^{-2}$	97
2	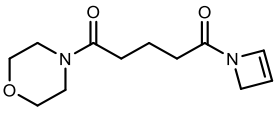	20	$4.40 \cdot 10^{-3} \pm 1.57 \cdot 10^{-4}$	$7.50 \cdot 10^{-1} \pm 2.62 \cdot 10^{-2}$	157
		37	$7.78 \cdot 10^{-3} \pm 4.25 \cdot 10^{-5}$	$1.32 \pm 7.40 \cdot 10^{-3}$	89
3	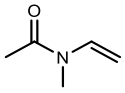	20	$3.12 \cdot 10^{-4} \pm 2.16 \cdot 10^{-6}$	$5.27 \cdot 10^{-2} \pm 3.67 \cdot 10^{-4}$	2223
		37	$5.05 \cdot 10^{-4} \pm 1.68 \cdot 10^{-6}$	$8.54 \cdot 10^{-2} \pm 2.88 \cdot 10^{-4}$	1372
4	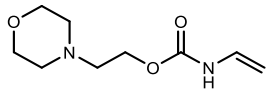	20	$1.27 \cdot 10^{-3} \pm 2.04 \cdot 10^{-5}$	$2.16 \cdot 10^{-1} \pm 3.48 \cdot 10^{-3}$	544
		37	$1.97 \cdot 10^{-3} \pm 9.34 \cdot 10^{-5}$	$3.34 \cdot 10^{-1} \pm 1.59 \cdot 10^{-2}$	351
5	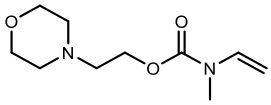	20	$7.53 \cdot 10^{-4} \pm 8.54 \cdot 10^{-6}$	$1.27 \cdot 10^{-1} \pm 1.44 \cdot 10^{-3}$	920
		37	$1.63 \cdot 10^{-3} \pm 4.65 \cdot 10^{-5}$	$2.76 \cdot 10^{-1} \pm 7.90 \cdot 10^{-3}$	424

Chapter 5 describes the synthesis and reaction kinetics at RT of model *N*-acylazetine **2**. To further establish the *N*-acylazetine reaction-rate data, the experiments were repeated and supplemented with the four-carbon variant **1** and include CT rates. The data shows that shortening the spacer length by one carbon results in minor decrease in reaction-rate, which can be explained by the increased proximity of the electron withdrawing carbonyl group relative to the azetine moiety. When comparing the reaction rates for *N*-acylazetine **2** and *N*-vinylamide **3**, the influence of ring-strain can be assessed. Evidently, ring strain

contributes significantly to the reaction rate, as the acyclic *N*-vinylamine results (both at RT and CT) in a 15-fold increase in half-life time. A similar comparison between **3** and **5** reflects the increase in electron density by progressing from an *N*-vinylamide to an *N*-vinylcarbamate. Here the results show that an approximate 2.8-fold decrease in half-life time, considerably less impactful than the effects induced by ring-strain. Methylation at the nitrogen of **5** into secondary *N*-vinylamide **4** only induces a minor (1.5-fold) increase in half-life time.

Conclusion

This chapter describes an investigation into the contribution of ring-strain and electron donating effects upon the IEDDA reactivity of acylenamines towards tetrazines. To this end, efforts were made to prepare *N*-vinyl derivatives **4**-**7** to allow a comparison with the *N*-acylazetine **1** and **2**. *N*-vinylcarbamate **4** and **5** could accessed through the Curtius rearrangement of acryl azide. The synthesis of *N*-vinylureas **6** and **7** was unsuccessful via a similar approach. Alternative attempts, involving the Lossen rearrangement and elimination of tosylate, were also unfruitful. The IEDDA rate constants were determined for *N*-acylazetine **1** and **2** and *N*-vinyl compounds **3**-**5** at 20 ˚C and 37 ˚C. Comparison between the reaction rates of *N*-acylazetine **2** and *N*-vinylamide **3** shows a 15-fold higher reaction rate for the four-membered ring. The influence of the differences in electron donation between a *N*-vinylamide and a *N*-vinylcarbamate (**5**) was significantly less, resulting in a 2.8-fold increase in reaction rate for the latter.

Experimental Section

General: All solvents and reagents were obtained commercially and used as received. Reactions were executed at ambient temperatures unless stated otherwise. Reactions were monitored by TLC-analysis using Merck aluminum DC Silicagel 60 F_{254} with detection by spraying with various sprays; an aqueous solution of cerium molybdate ($(NH_4)_6Mo_7O_{24}{\cdot}4H_2O$ 25 g/L) or an aqueous solution of potassium permanganate (5 g $KMnO_4$, 25 g K_2CO_3 per L). Column chromatography was performed on Fluka silicagel (0.04 – 0.063 mm). ^1H and ^{13}C-APT spectra were recorded on a Bruker AV-400 (400 MHz), Bruker DMX-600 (600 MHz) or Bruker BioSpin (850 MHz). All present ^{13}C-APT spectra are proton decoupled. The high resolution mass spectrometry were recorded by direct injection (2 µL of a 2µM solution in water/acetonitrile; 50/50; v/v and 0.1% formic acid) on a mass spectrometer (Thermo Finnigan LTQ Orbitrap) equipped with an electrospray ion source in positive mode (source voltage 3.5 kV, sheath gas flow 10, capillary temperature 250 ˚C) with resolution R = 600000 at m/z 400 (mass range m/z = 120-400).

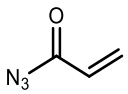

9

Acryloyl Azide (9): Acryloyl chloride (10 mmol, 0.81 mL, 1 eq) in toluene (1.3 mL) was added to an ice-cooled solution of NaN_3 (683 mg, 10.5 mmol, 1.05 eq) in water (2.5 mL). The ice-bath was removed and the two-layered reaction mixture was stirring vigorously for 4 hours. Toluene was added (1.3 mL) and the mixture was poured into a separation funnel and washed twice with saturated aqueous sodium hydrogen carbonate, twice with water and once with brine. The organic layer was dried over magnesium sulfate, filtered and the solution was stored overnight at 4 ˚C. The product was used in solution without further purification.

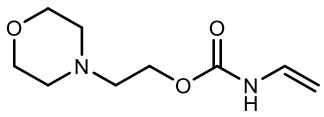

4

2-Morpholinoethyl vinylcarbamate (4): A solution of hydroquinone (55 mg, 0.5 mmol, 0.05 eq), pyridine (36 µL, 0.5 mmol, 0.5 eq), *N*-ethoxymorpholine (20 mmol, 2.4 mL, 2 eq) in toluene (2 mL) was put under argon atmosphere and heated to 100 ˚C. The prepared solution of acryloyl azide in toluene was added dropwise over one hour. After complete addition, the reaction mixture was stirred for an additional 30 minutes at 100 ˚C, before being allowed to cool to RT. The mixture was filtered and concentrated *in vacuo*. The crude product was purified by column chromatography (0% » 5% EtOH/DCM), yielding vinylcarbamate **4** as a yellow oil. (2.85 mmol, 570 mg, 29% over two steps). **^{1}H NMR:** (400 MHz, $CDCl_3$) δ 7.19 (s, 1H), 6.62 (dt, *J* = 15.8, 10.0 Hz, 1H), 4.41 (d, *J* = 15.8 Hz, 1H), 4.21 (d, *J* = 8.9 Hz, 1H), 4.20 – 4.13 (m, 2H), 3.71 – 3.61 (m, 4H), 2.60 – 2.52 (m, 2H), 2.44 (s, 4H). **^{13}C NMR:** (101 MHz, $CDCl_3$) δ 153.68, 129.99, 93.23, 66.69, 61.80, 57.33, 53.68. **HRMS:** Calculated for $C_6H_{16}N_2O_3$ 201.12392 $[M+H]^+$; found 201.12337.

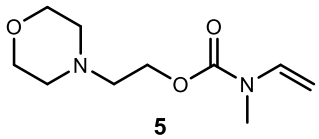

5

2-Morpholinoethyl methyl(vinyl)carbamate (5): Sodium hydride (60% in mineral oil, 2.4 mmol, 96 mg, 1 eq) was added potion-wise to a solution of vinylcarbamate **4** (2.4 mmol, 480 mg, 1 eq) in dry THF (8 mL), under argon atmosphere. The reaction mixture was sonicated until hydrogen evolution ceased. The reaction mixture was cooled to 0 ˚C and methyl iodide (2.52 mmol, 0.16 mL, 1.05 eq) was added. The reaction mixture was stirred for 1.5 hours, quenched with $Et_3N{\cdot}HCl$ and concentrated *in vacuo*. The crude product was purified by column chromatography (2% » 5% EtOH in DCM), yielding *N*-methyl-vinylcarbamate **5** as a yellow liquid. (1.81 mmol, 387 mg, 75%). **^{1}H NMR:** (400 MHz, $CDCl_3$) δ 7.24 – 7.01 (m, 1H), 4.37 – 4.15 (m, 4H), 3.76 – 3.59 (m, 4H), 3.01 (s, 2H), 2.65 (t, *J* = 5.8 Hz, 2H), 2.54 – 2.38 (m, 4H). **^{13}C NMR:** (101 MHz, $CDCl_3$) δ 134.20, 133.51, 91.95, 66.86, 63.42, 57.25, 53.80, 30.23. **HRMS:** Calculated for $C_7H_{18}N_2O_3$ 215.13957 $[M+H]^+$; found 215.13911.

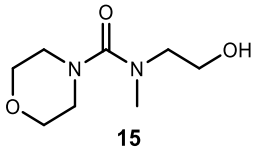

15

***N*-(2-hydroxyethyl)-*N*-methylmorpholine-4-carboxamide (15):** A solution of morpholine (5 mmol, 0.43 mL, 1 eq) and Et_3N (10 mmol, 1.4 mL, 2 eq) in dry DCM (37.6 mL) was prepared under argon atmosphere. Phosgene (1.9M solution in toluene, 2.9 mL, 1.1 eq) was added dropwise over 1 hour. The reaction mixture was allowed to warm to RT and stirred for additional 15 minutes. The reaction was quenched by the addition of MeOH and concentrated *in vacuo*. The residue was redissolved in MeCN (25 mL) and 2-(methylamino)ethanol (5.5 mmol, 0.44 mL, 1.1 eq), DIPEA (5 mmol, 0.87 mL, 1 eq) and DMAP (5.5 mmol, 672 mg, 1.1 eq) were added. The reaction mixture was heated to 45 ˚C and left stirring for 2 hours. The reaction mixture was concentrated *in* vacuo and the crude product was purified by column chromatography (49% Acetone in DCM + 1% MeOH » 46% Acetone in DCM + 4% MeOH), yielding compound **15** as a yellow oil (2.55 mmol, 480 mg, 51%). **^{1}H NMR:** (300 MHz, $CDCl_3$) δ 4.42 (s, 1H), 3.77 – 3.71 (m, 2H), 3.69 – 3.63 (m, 4H), 3.37 – 3.30 (m, 2H), 3.28 – 3.20 (m, 4H), 2.89 (s, 3H). **^{13}C NMR:** (75 MHz, $CDCl_3$) δ 165.66, 66.68, 60.26, 52.09, 49.83, 47.26, 37.03.

Kinetic Data Plots

A 0.6 mM stock solution of tetrazine **17** in 12% DMSO:H_2O (v:v) was prepared and 1mL was transfered into a quarts cuvette (10 mm width, 3 mL volume) equipped with a small magnetic stirrer. The cuvette was placed in the measurement chamber of a Cary 300 UV-Vis spectrophotometer (Agilent Technologies). A 12 mM solution of the corresponding probe (**1**-**5**) was prepared in 12% DMSO:H_2O (v:v), of which 1 mL was transfered to the cuvette. The measurement was immediately started upon closing the chamber. The absorption decay was followed at 517 nm. The experiments were conducted at climate controlled room

temperature (20 ˚C) and at cell temperature (37 ˚C). For experiments conducted at cell temperature, the probe solutions were pre-heated in a stove, while the tetrazine solution was warmed by a Cary Temperature Controller (Agilent Technologies).

The reaction rate was derived from three data sets using every measurement interval from the start until the second of the three runs reached 50% of the starting absorption. The datasets following from the experiments were subjected to the LINEST function (Microsoft Excel 2013) to determine the slope and the standard deviation for both pseudo first- and second order rate constant. The slope represents respectively the pseudo first-order rate constant and second order.

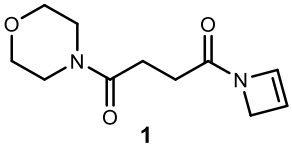

1

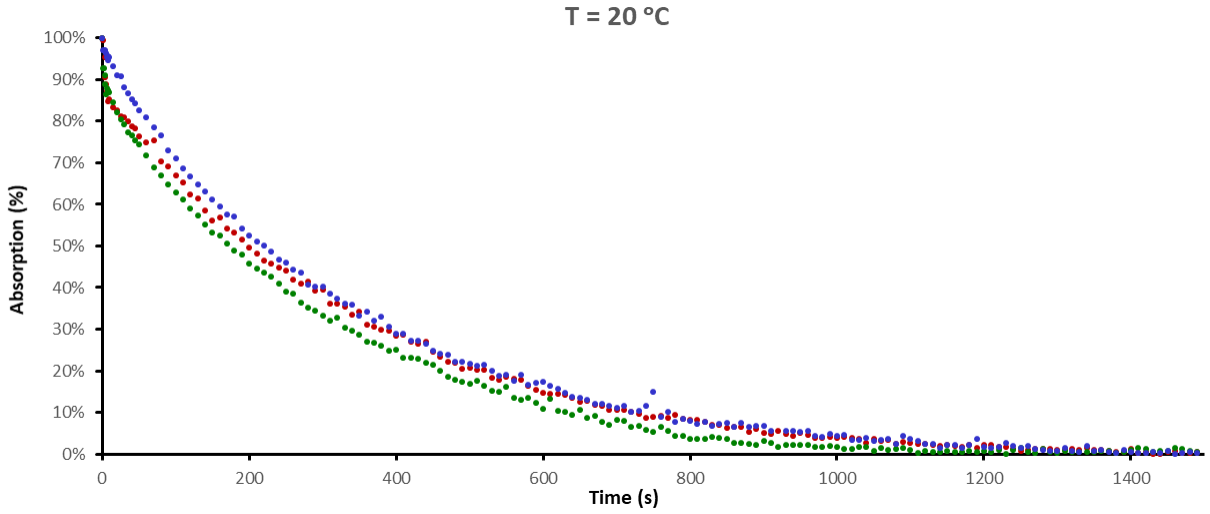

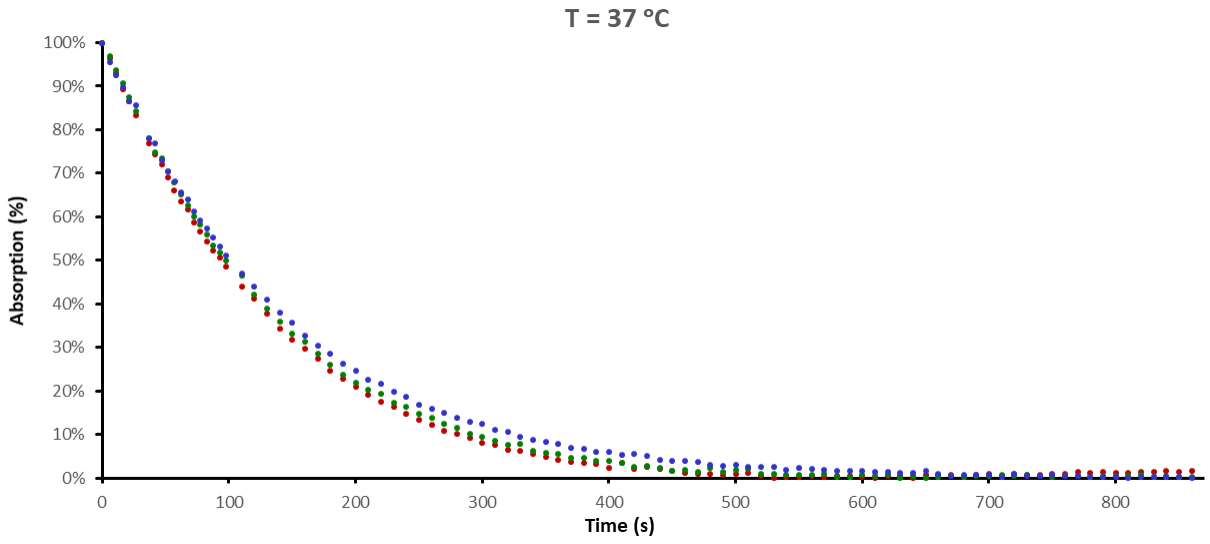

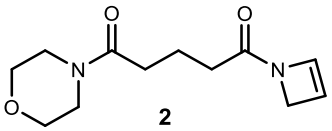
O
O
N
N
O

2

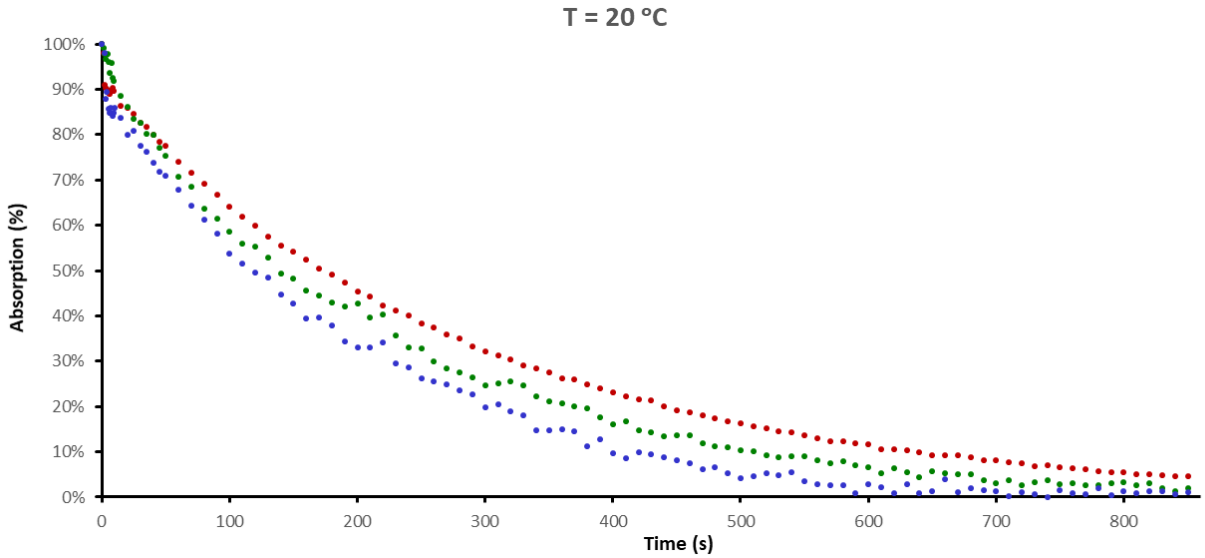
T = 20 °C
Absorption (%)
100%
90%
80%
70%
60%
50%
40%
30%
20%
10%
0%
0
100
200
300
400
500
600
700
800
Time (s)

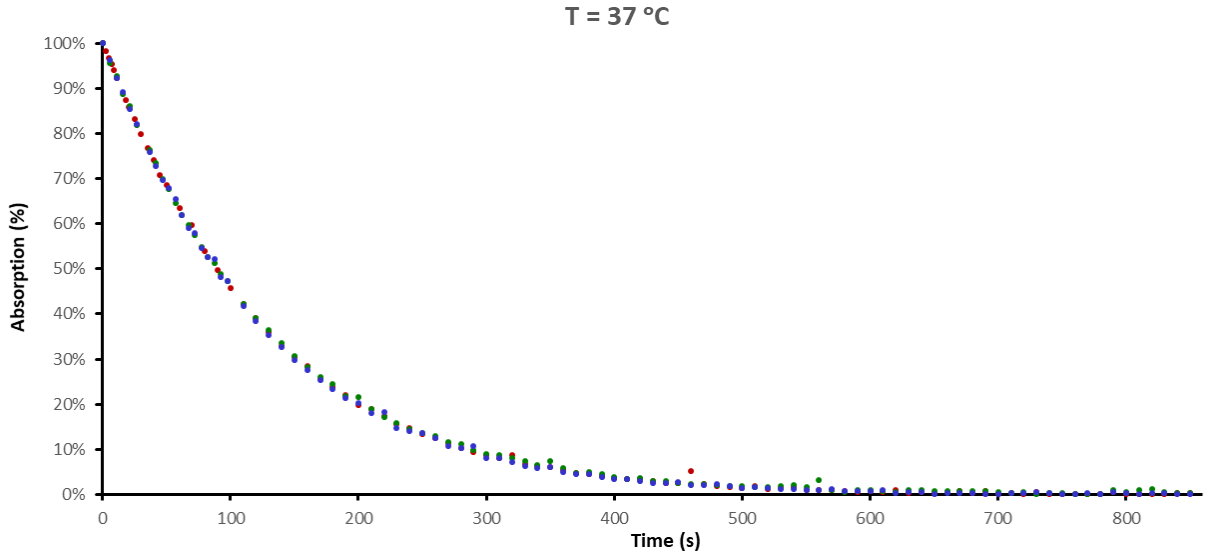
T = 37 °C
Absorption (%)
100%
90%
80%
70%
60%
50%
40%
30%
20%
10%
0%
0
100
200
300
400
500
600
700
800
Time (s)

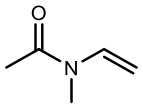

3

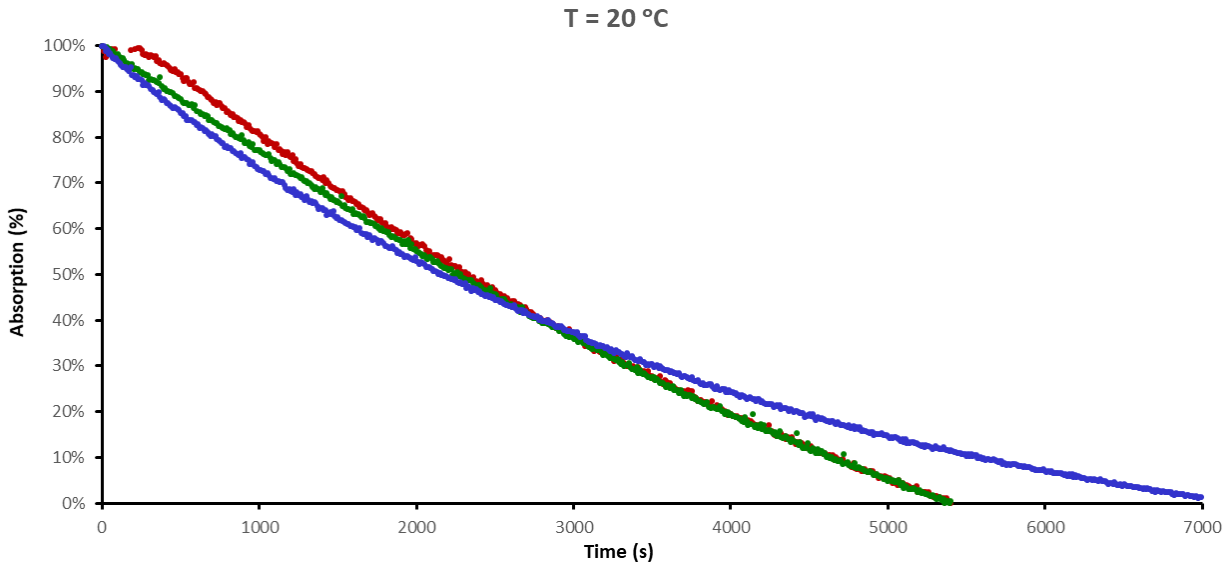
T = 20 °C
100%
90%
80%
70%
60%
50%
40%
30%
20%
10%
0%
Absorption (%)
0
1000
2000
3000
4000
5000
6000
7000
Time (s)

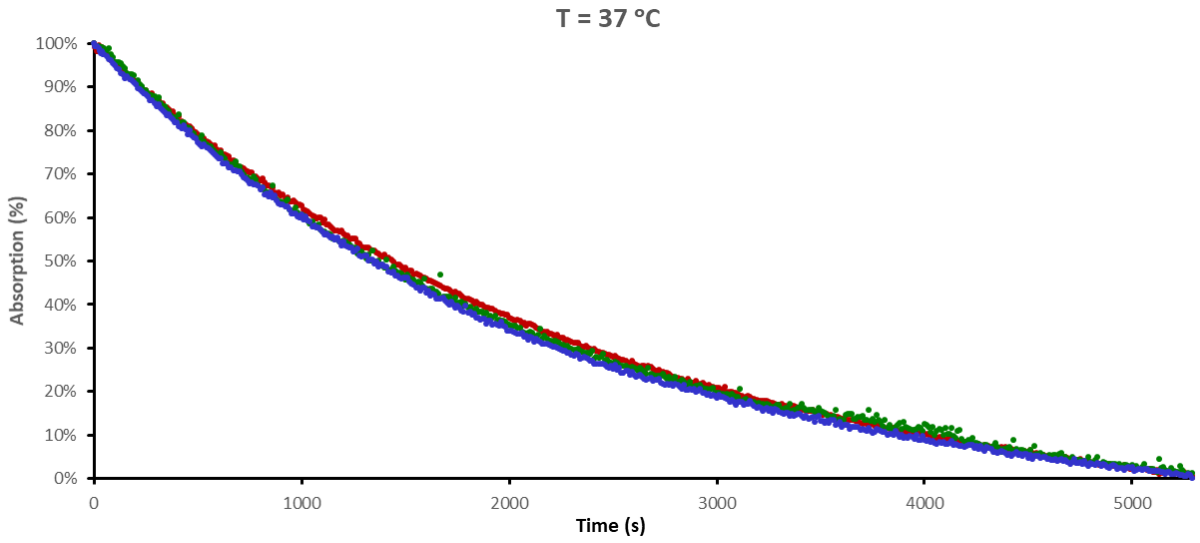
T = 37 °C
100%
90%
80%
70%
60%
50%
40%
30%
20%
10%
0%
Absorption (%)
0
1000
2000
3000
4000
5000
Time (s)

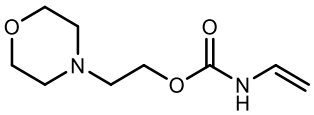

4

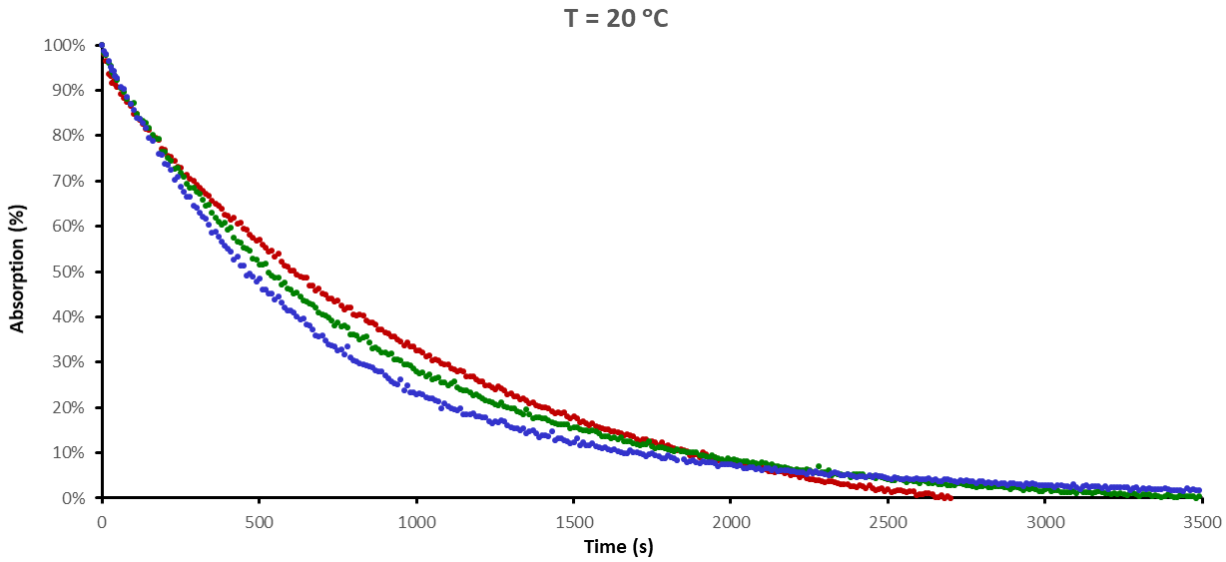
T = 20 °C
100%
90%
80%
70%
60%
50%
40%
30%
20%
10%
0%
Absorption (%)
0
500
1000
1500
2000
2500
3000
3500
Time (s)

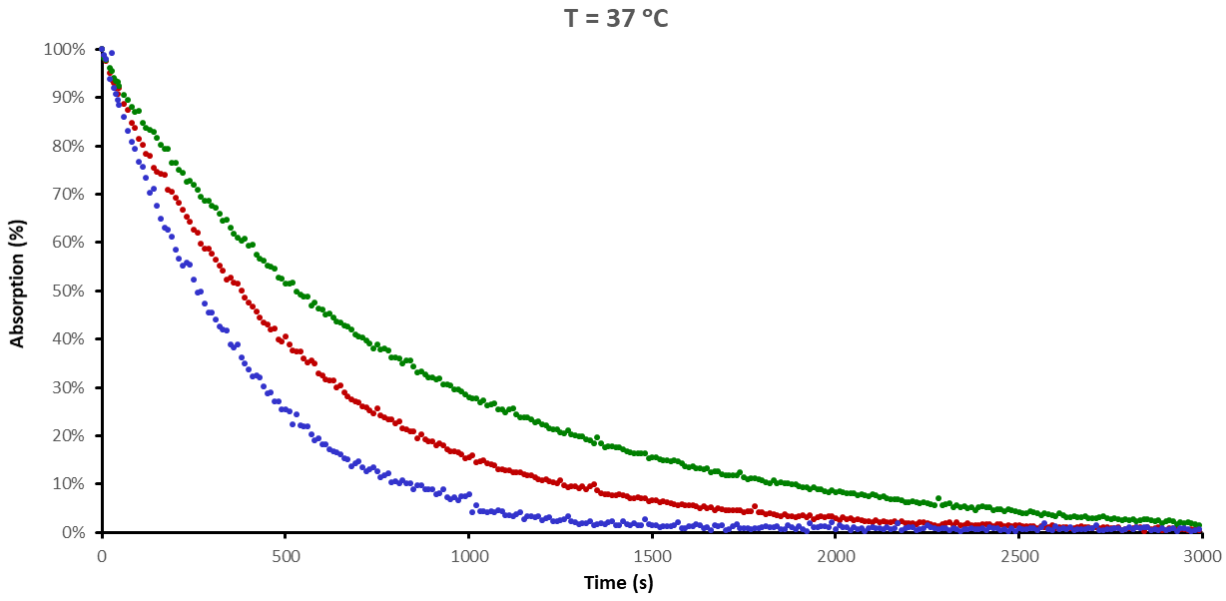
T = 37 °C
100%
90%
80%
70%
60%
50%
40%
30%
20%
10%
0%
Absorption (%)
0
500
1000
1500
2000
2500
3000
Time (s)

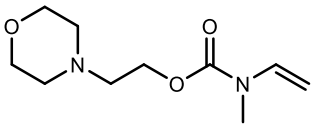

5

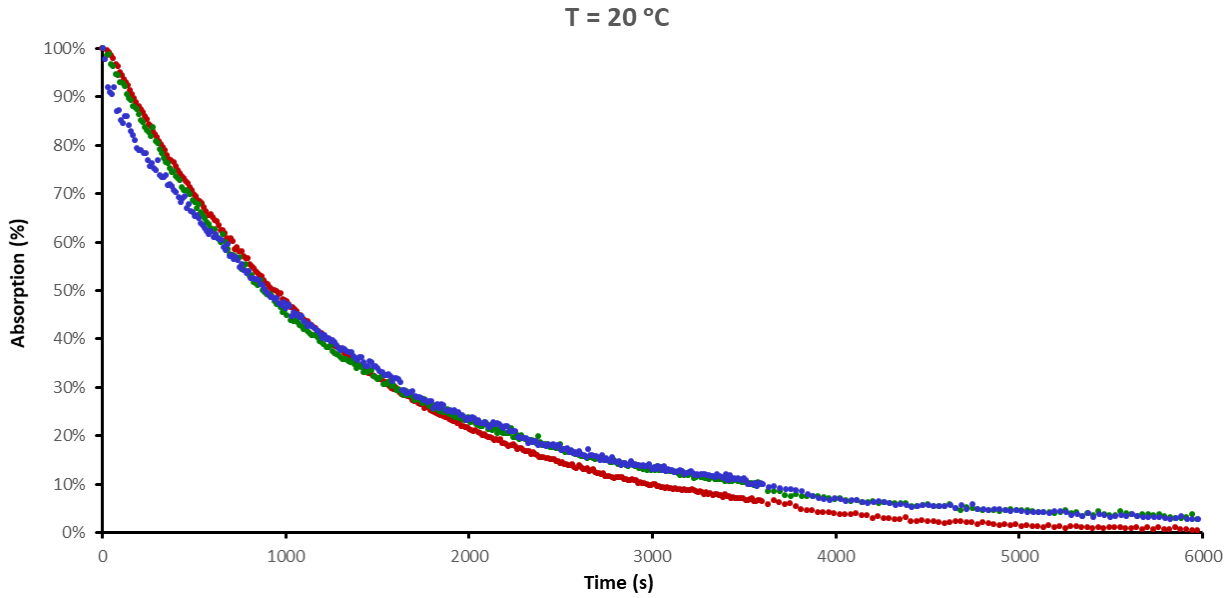
T = 20 °C
Absorption (%)
100%
90%
80%
70%
60%
50%
40%
30%
20%
10%
0%
0
1000
2000
3000
4000
5000
6000
Time (s)

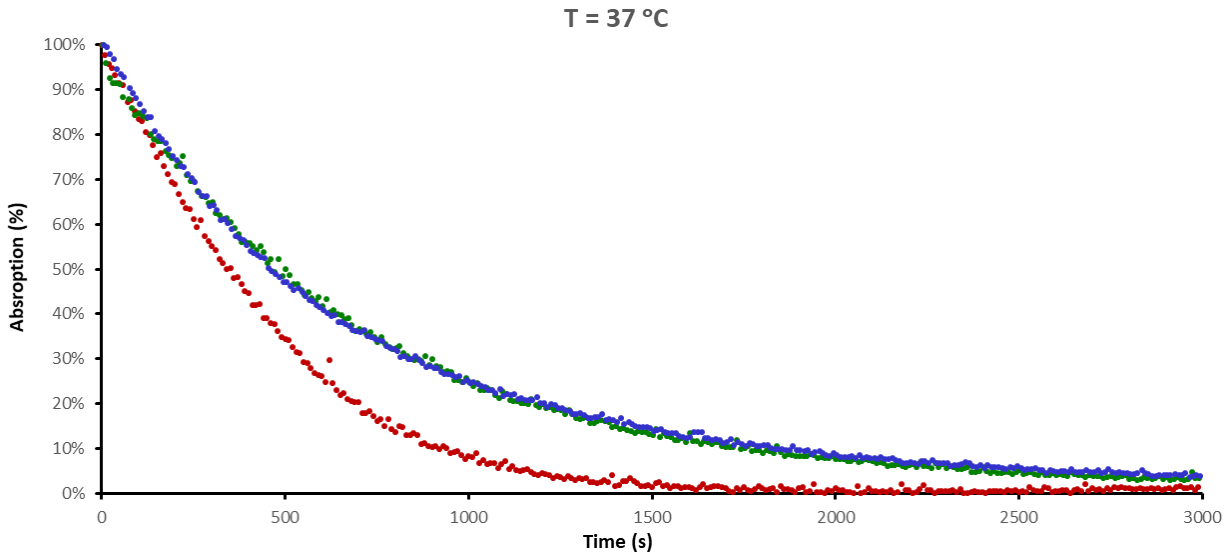
T = 37 °C
Absorption (%)
100%
90%
80%
70%
60%
50%
40%
30%
20%
10%
0%
0
500
1000
1500
2000
2500
3000
Time (s)

References

1. J. Sauer, D. K. Heldmann, J. Hetzenegger, J. Krauthan, H. Sichert, J. Schuster, *European J. Org. Chem.* **1998**, *1998*, 2885–2896.
2. J. S. H. Schuster, H. Sichert, **1983**, *24*, 0–3.
3. A. C. Knall, M. Hollauf, C. Slugovc, *Tetrahedron Lett.* **2014**, *55*, 4763–4766.
4. D. R. Soenen, J. M. Zimpleman, D. L. Boger, *J. Org. Chem.* **2003**, *68*, 3593–3598.
5. F. Thalhammer, U. Wallfahrer, J. Sauer, *Tetrahedron Lett.* **1990**, *31*, 6851–6854.
6. L. Törk, G. Jiménez-Osés, C. Doubleday, F. Liu, K. N. Houk, *J. Am. Chem. Soc.* **2015**, *137*, 4749–4758.
7. W. Chen, D. Wang, C. Dai, D. Hamelberg, B. Wang, *Chem. Commun.* **2012**, *48*, 1736–1738.
8. S. B. Engelsma, L. I. Willems, C. E. van Paaschen, S. I. van Kasteren, G. A. van der Marel, H. S. Overkleeft, D. V Filippov, *Org. Lett.* **2014**, *16*, 2744–2747.
9. M. L. Blackman, M. Royzen, J. M. Fox, *J. Am. Chem. Soc.* **2008**, *130*, 13518–13519.
10. N. K. Devaraj, R. Weissleder, S. A. Hilderbrand, *Bioconjug. Chem.* **2008**, *19*, 2297–2299.
11. D. J. Amende, K. M. DeVries, P. J. Clifford, S. J. Brenek, *Org. Process Res. Dev.* **1998**, *2*, 382–392.
12. D. J. Dawson, R. D. Gless, R. E. Wingard, *J. Am. Chem. Soc.* **1976**, *98*, 5996–6000.
13. R. W. Stackman, R. H. SummervllleT, *Ind. Eng. Chem. Prod. Res. Dev.* **1985**, *24*, 242–246.
14. M. SATO, *J. Org. Chem.* **1961**, *26*, 770–779.
15. A. Ciiakey, **1961**, *2290*, 2597–2599.
16. G. M. Wieber, L. S. Hegedus, B. Åkermark, E. T. Michalson, *J. Org. Chem.* **1989**, *54*, 4649–4653.
17. R. A. Batey Yuri Bolshan, *Angew. Chem. Int. Ed.* **2008**, *47*, 2109–2112.
18. P. García-Reynaga, A. K. Carrillo, M. S. Vannieuwenhze, *Org. Lett.* **2012**, *14*, 1030–1033.
19. P. Dubé, N. F. Fine Nathel, M. Vetelino, M. Couturier, C. L. Aboussafy, S. Pichette, M. L. Jorgensen, M. Hardink, *Org. Lett.* **2009**, *11*, 5622–5625.
20. J. Yang, J. Šečkute, C. M. Cole, N. K. Devaraj, *Angew. Chemie - Int. Ed.* **2012**, *51*, 7476–7479.

7 Summary and Future Prospects

Phosphate esters are ubiquitous functionalities in a wide variety of fundamental biochemical processes, from interlinking the nucleotides in our DNA, to protein regulation and cellular respiration. Therefore, it is not surprising that all four major biomolecules are directly, or indirectly, subjected to various types of phosphorylation reactions. A specific example of a post-translation modification that involves phosphate esters is adenosine diphosphate ribosylation (ADP-ribosylation). This post-translation modification (PTM) is regulated by ADP-ribose transferases that utilize NAD^+ as a glycosyl donor and transfer one (mono) or more (poly) ADP-ribose residues onto a nucleophilic heteroatom of an acceptor biomolecule. In humans, both mono(ADP)ribosylation and poly(ADP)ribosylation are modifications primarily introduced by enzymes of the PARP family. Particularly the PARylation processes of PARP-1, PARP-2 and PARP-3 have become subject of scientific interest due to their roles in DNA damage repair, inflammation, telomere maintenance and regulation of apoptosis. During PARylation, ADP-ribose oligomer grows on a nucleophilic amino acid residue, either in the auto-modification domain of PARP itself or that of another target protein, to form linear or branched chains of poly-ADP-ribose, consisting of up to 200 monomeric units. The produced dendritic ADPR-polymer triggers a conformational change that is essential to the respective biological event, such as the recruitment of DNA repair enzymes. Synthetic organic chemistry has already provided access to structurally well-defined ADP-ribosylated oligopeptides and poly-ADPr fragments, and thereby helped advance our understanding of this important PTM. However, these native constructs contain labile functionalities, such as the pyrophosphate moiety and glycosidic bond, which can constrain both synthesis and biological application due to their susceptible to hydrolytic or enzymatic degradation. An organic chemical approach to address such limitations is to introduce chemical modifications that stabilize specific labile bonds, while retaining similar overall physical and chemical properties. The research described in this Thesis focuses on the development of new molecular tools aimed to facilitate the study of the adenosine diphosphate ribosylation PTM, with an emphasis on stabilizing the aforementioned labile functionalities. In this context new reagents and methodology have been developed for the synthesis of stabilized pyrophosphorylated bioisosteres.

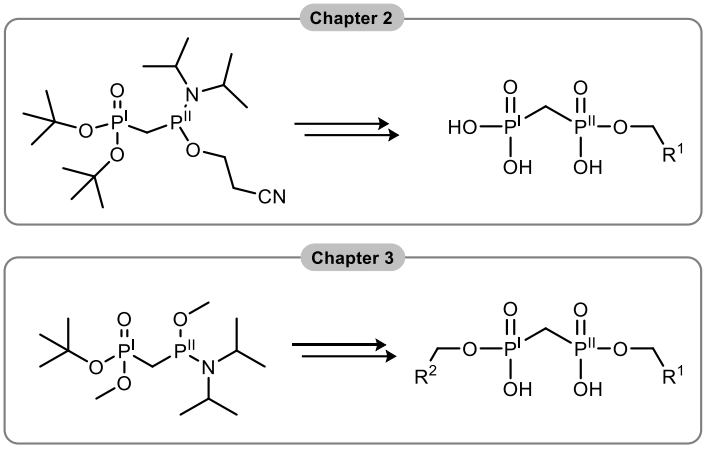

Figure 1: The two primary reagents designed to introduce methylene bisphosphonates in biomolecules described in Chapter 2 and 3.

Chapter 2 discusses a new class of orthogonally protected phosphanylmethylphosphonate reagents that have been developed for the controlled synthesis of methylene bisphosphonate monoesters. Methylene bisphosphonates are stabilized analogues of pyrophosphates in which the oxygen atom, conjoining the two phosphates in the original pyrophosphate, is replaced by a methylene to provide resistance to cleavage. After refinement of reactions conditions, the phosphanylmethylphosphonate reagents became readily accessible through a one-pot procedure by reacting a lithiated methylphosphonate diester with a chlorophosphoramidite. Condensation of the presented reagents with an alcohol of choice through azole-mediated phosphoramidite chemistry, followed by *in situ* oxidation, efficiently provides orthogonally protected methylene bisphosphonate tetraesters. Global deprotection of the acquired tetraester yields the respective terminal methylene bisphosphonate. Using these reagents, several methylene bisphosphonate analogues of biologically relevant nucleoside di- and triphosphates where synthesized. In addition, the method has proven to be compatible with solid-phase chemistry.

The research described in **Chapter 3** expands on that of Chapter 2, by adopting the concept to the synthesis of unsymmetrical methylene bisphosphonates. This uses a second generation of the reagent, which is protected with two methyl groups and a single *tert*-butyl protective group at the P^V. After installment of the first alcohol, using the phosphoramidite coupling-oxidation sequence, the terminal *tert*-butyl in the methylene bisphosphate tetraester is selectively cleaved. This allows for introduction of a second alcohol, through PyNTP-mediated condensation, yielding the protected methylene bisphosphate with two different alkyl substituents at its termini. Subsequent global deprotection via a two-step-one-pot procedure provides the respective unsymmetrical methylene bisphosphate. The power of this methodology was demonstrated in the synthesis of the methylene bisphosphonate analogues of ADPR and flavin adenine dinucleotide (FAD).

The lithiation conditions used during the assembly of the phosphanylmethylphosphonate reagent prevent the direct installment of base labile protecting groups at the phosphonate end of the molecule. This restriction in orthogonality limits the scope to acid stable substrates, as exemplified by the degradation of the methylene bisphosphonate analogues of farnesyl pyrophosphate and isopentenyl pyrophosphate during *tert*-butyl cleavage (Chapter 2; Scheme 6). A strategy to circumvent this limitation

can be envisioned in the implementation of 2-hydroxyethyl methyl sulfide as a "masked" base-labile protecting group. In order to synthesize prenoids the phosphonate could be fitted with two 2-hydroxyethyl methyl sulfide moieties (**1**), then lithiated and reacted with bis(diisopropylamino) chlorophosphoramidite to provide **2**, which in turn would be converted to reagent **3** (Scheme 1). During the phosphanyl coupling-oxidation sequence, an additional oxidation step would be added to fully oxidize the thioether. This could be achieved selectively by treatment with hydrogen peroxide in the presence of cyanuric chloride.[1] The resulting sulfonyl (**4**) is now susceptible to base mediated β-elimination, similarly to the cyanoethyl.

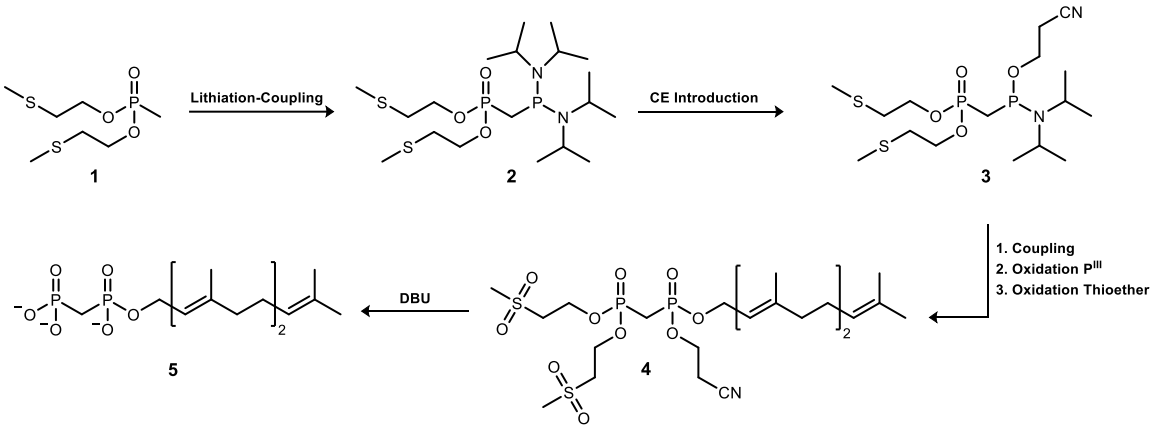

Scheme 1: Proposed variant of the phosphanylmethylphosphonate reagent, which makes use of a "masked" base-labile protecting group 2-hydroxyethyl methyl sulfide. The group becomes base cleavable after oxidation to the corresponding sulfone.

Chapter 4 describes the synthesis of a stabilized analogue of a mono-ADP-ribosylated *N*-terminal peptide of histon H2B, which is a relevant fragment involved in the ADP-ribosylation process triggered by single-strand DNA damage. The Glu-2, corresponding to the native H2B conjugate, is a well-studied site of ADP-ribosylation. Previous attempts at synthesizing the native conjugate were unsuccessful due to the propensity of the anomeric glutamyl ester to migrate. The migration can be circumvented by instalment of glutamine as a glutamate bioisostere, effectively substituting the more stable amide bond for the ester. However, this form of stabilization does not fully exclude epimerization or (acidic) hydrolysis. The intrinsic lability of the glycosidic bond primarily stems from the oxocarbenium resonance enabled by the adjacent ring-oxygen. Therefore, a *carba*-riboside was incorporated as a stabilized replacement of the naturally occurring riboside. A new synthesis towards the α-*carba*-ribosylamine was developed. D-Ribose was converted into a protected 5-iodoriboside and subjected to a tandem fragmentation-vinylation reaction. The diallylic product was ring-closed and oxidized, providing cyclopentenone precursor **6**. Ensuing photochemical addition of methanol, to install the C^5-*CH_2OH*, efficiently produced the *carba*-ribonolactone core structure. The ketone was converted into a methoxyimine and stereoselectively reduced to obtain the pseudo-anomeric α-configured amine (**7**). Coupling of the amine with a glutamic acid derivative, followed by deprotection and phosphorylation of the C^5-*OH* afforded final *carba*-ribosylated glutamine building block **8**. Incorporation of the building block into the H2B conjugate fragment was achieved through solid-phase peptide synthesis. On-resin phosphorylation of the *carba*-ribosyl phosphate was used to construct the ADP-pyrophosphate. Successive global deprotection and

release from resin provided the target mono-ADP-*carba*-ribosylated H2B conjugate **9** in multi-milligram amounts.

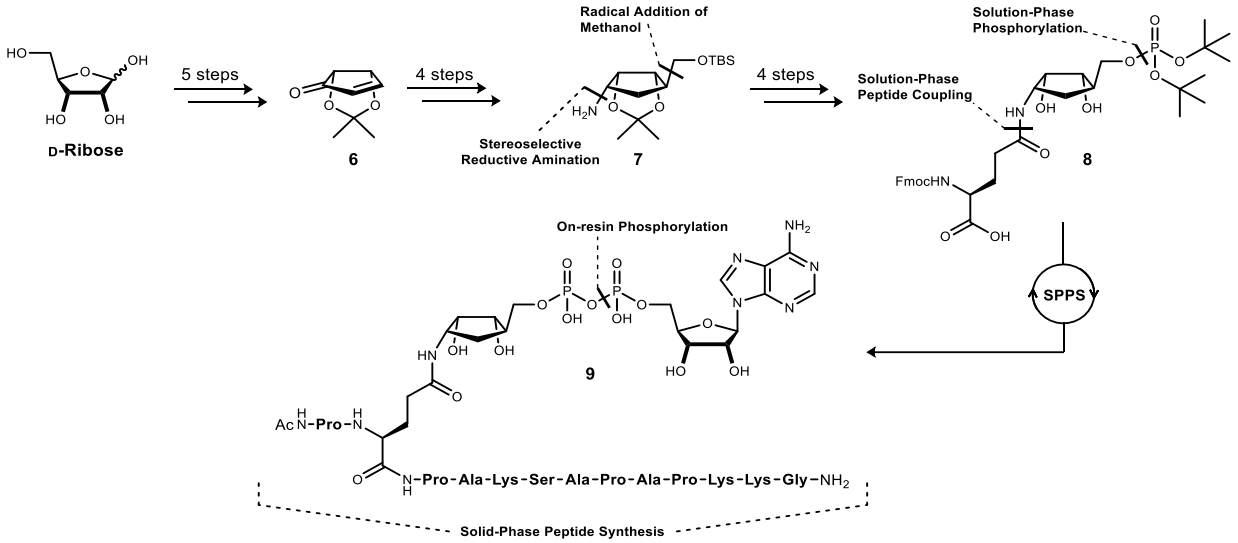

Scheme 2: Summarized synthesis of the mono-ADP-*carba*-ribosylated H2B conjugate described in Chapter 4.

Given the established usefulness of synthetic MARylated oligopeptides as tools for studying the ADP-ribosylation PTM[2], it is not unreasonable to think that improving accessibility to such constructs would benefit the field of biochemistry. In this context shelf-stable pre-ADP-ribosylated amino acids, that are compatible with standard solid phase peptide chemistry, could be envisioned as powerful tools to provide convenient access to a wide variety of MARylated oligopeptides. However, both the anomeric linkage and pyrophosphate bridge presented in native construct would pose incompatibility with SPPS. Chapter 4 presents a solution for the former, while the chemistry described in Chapter 2 and 3 could be adopted to incorporate a methylene bisphosphonate to address the latter. This would require an iteration of the phosphanylmethylphosphonate reagent fitted with protecting groups that are orthogonal with Fmoc-based SPPS (Figure 2). The use of two *p*-methoxybenzyl groups in combination with the masked base-labile protecting group strategy described above is expected to present the desired orthogonality. The resulting reagent **10** is then first to be coupled to an adenosine protected with acid-cleavable groups (**11**). This order of installment would be mandatory due to incompatibility of base-labile MSE group with the integrity of the Fmoc-protection. After basic removal of the MSE, the protected me-ADP can be condensed with the appropriate *carba*-ribosylated asparagine or glutamine (**12**), which itself is easily accessible from **7** (Scheme 2). Final selective removal of the allyl, by $Pd(PPh_3)_4$, would yield the respective pre-ADP-ribosylated amino acid (**13**). Building blocks of this design are expected to be compatible with the standard Fmoc-based SPPS. After incorporation into an oligopeptide of choice, the Boc, PMBs and isopropylidene acetals can be removed by treatment with TFA, with concomitant release from the solid support.

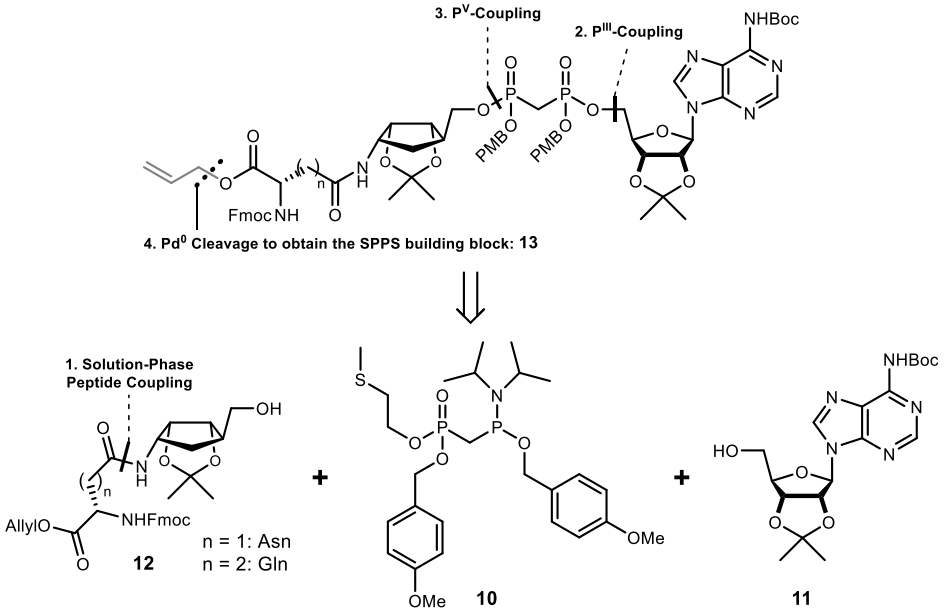

Figure 2: Retrosynthetic analysis of the proposed pre-ADP-ribosylated building block designed for SPPS.

In the same context of facilitating PARylation related research, Kistemaker *et al* developed a synthetic route for the synthesis of structurally well-defined native ADP-ribose oligomers.[3] The methodology employs a pre-phosphorylated disaccharide building block to construct the PAR-polymer via on-resin phosphorylation reactions, similar to that described for compound **9**. An interesting point of continuation would be to combine this disaccharide approach with the methylene bisphosphonate chemistry described in Chapter 2 and Chapter 3. The envisioned building block **14** (Figure 3) could be polymerized onto a resin bound peptide via block synthesis, to result in a methylene bisphosphonate enriched PARylated peptide. First, the disaccharide would have to be functionalized with a methylene bisphosphonate, which is proposed to be done via the phosphanylmethylphosphonate-based methodology. Difficulty arises from finding the correct orthogonality, since the glycosidic bond in 2'-*O*-ribosyladenosine is incompatible with strong acidic conditions. A benzyl at the P^V-position and two masked MSE groups are envisaged as suitable protecting groups for the phosphanylmethylphosphonate reagent (similar to **10** in Figure 2). After installment of the reagent onto the adenosine 5'-*OH*, the benzyl would be cleaved reductively. While adhering to the published route, the 5'-*OH* of the 2'-*O*-ribosyl residue would at this stage be protected with a TIPS-group, which is to be exchanged for a DMT. It is however uncertain if the DMT-group can selectively be installed on the 5'-*OH* in the presence of the methylene phosphoric acid triester. Although it is considered unlikely that the P^V-*OH* would form a stabile bond with the DMT-moiety at all, the difference in stability between a P^V*O-DMT* bond and a 5'-*O-DMT* is expected to be significant, and thus distinguishable. Alternatively, the reagent could be fitted with an allyl instead of the benzyl, which could be removed selectively over the DMT by applying a palladium catalyst. PAR assembly at the C^5-*OH* of an immobilized *carba*-ribosylated peptide is envisioned to be possible by repetitive coupling cycles with building block **14**; each cycle would consist of P^v-coupling, capping and DMT deprotection (Figure 3). In this instance phosphortriester-based chemistry has to be used for the solid-phase phosphorylative

elongations, over the more established phosphoramidite approach.[4] Nevertheless, the viability of the phosphortriester approach has thoroughly been demonstrated by the solid-phase synthesis of DNA.[5,6]

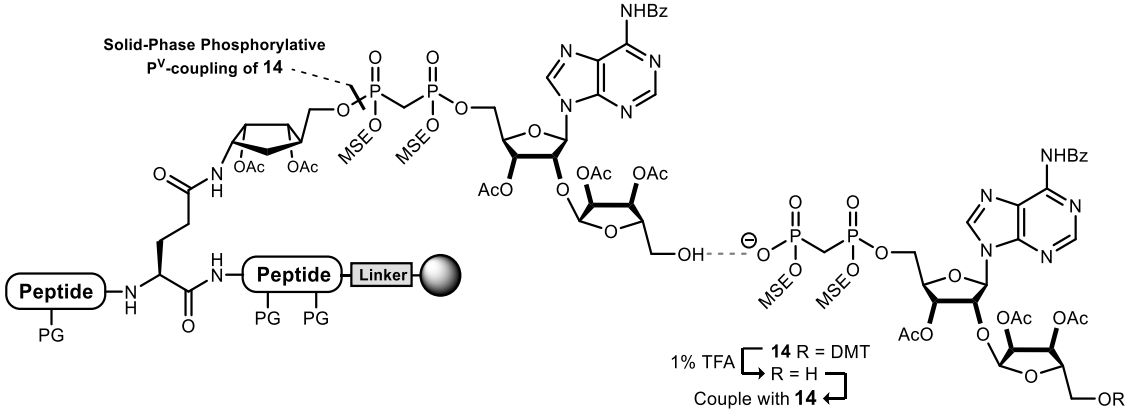

Figure 3: Proposed solid-phase synthesis of a methylene bisphosphonate enriched PARylated peptide. Building block **14** is coupled to the terminal hydroxyl, following DMT deprotection to provide the hydroxyl for the succeeding cycle.

Chapter 5 and Chapter 6 describe the development of new biorthogonal reagents. Bioorthogonal reactions are defined as selective reactions between two artificial moieties that are inert to the diverse spectrum of functional groups that reside in a biological system. These have significantly advanced the field of molecular biology providing tools to study biochemistry in living cells or even complete organisms, enabling the conjugation of functional moieties to proteins or the *in vivo* assembly of molecular tags used for imaging. In the same way, bioorthogonal chemistry has also proven to be a key component in the molecular toolbox used to unravel ADP-ribosylation processes. Various NAD^+ analogues functionalized with a bioorthogonal handles have been developed and employed in the mapping of ADP-ribosylation activity. The inverse-electron-demand Diels–Alder (IEDDA) reaction is the most recent addition to bioorthogonal reactions. It involves a Diels–Alder reaction between an electron deficient tetrazine (diene) and strained alkene or alkyne. The main advantage of the IEDDA reaction is that it exhibits the fastest reaction kinetics among bioorthogonal reactions, while the main disadvantages are that both the tetrazine and most reactive dienophiles are relative lipophilic and sterically encumbered. These properties may have a negative effect on both water solubility and the biological response of the functionalized molecules. The contemporary IEDDA dienophiles – norbornene, *trans*-cylcooctene and cyclopropene – use ring strain to acquire the desired reactivity towards tetrazines.

Chapter 5 describes a new compact bioorthogonal ligation handle suitable for IEDDA ligation strategy, based on the *N*-acylazetine core. This moiety was envisioned as the smallest viable structure that could utilize ring-strain in conjunction with the electron-donating properties to increase the dienophilicity. The initial five-step synthesis started by reacting benzhydrylamine with epichlorohydrin, to afford the protected azetidine core. Mesylation of the alcohol, followed by benzhydryl cleavage, yielded 3-mesylazetidine hydrochloride. Application of the former in the ring-opening of glutaric anhydride provided a linker that is sutable to attach the *N*-acylazetine to a biomolecule via an amide bond. In a one-pot procedure, the mesyl-moiety was eliminated by KO*t*Bu, to install the double bond, and the carboxylate was converted into either the pentafluorophenol or *p*-nitrophenol activated ester (PNP). The PNP-tag was

used to create a model compound to determine the reaction kinetics with tetrazine. The *N*-acylazetine showed a second-order rate constant of 0.39 ± 0.1 s^{-1} M^{-1}; a value comparable to that of the methylcyclopropene mini-tag. Secondly, the handle was used to functionalize epoxomicin (a broad-spectrum proteasome inhibitor), which in turn was used to successfully label the proteasome through tetrazine ligation. Because the practicality of a ligation handle is highly dependent on its synthetic accessibility, efforts were redirected at optimizing the synthesis. However, several key steps in the original synthesis proved to be constraining to the overall efficiency and scalability. Therefore it was opted to develop a new synthetic route, in which 3-hydroxyazetidine was first *N*-Boc-protected and then tosylated. The tosyl group was selected for it is UV-detectable, has a lower polarity and a better leaving-group capacity. After deprotection of the nitrogen, the resulting azetidine was used to ring-open succinic and glutaric anhydride, yielding the respective four- and five-carbon spacers. Elimination proceeded smoothly at room temperature due to the improved solubility of the tosylated hydroxyazetidine. The thus obtained *N*-acylazetine carboxylate intermediates were converted *in situ* into the corresponding PNP-esters by addition of bis(*p*-nitrophenyl)-carbonate. With this the *N*-azetine tags have become accessible through an efficient four-step synthesis.

Chapter 6 is an extension of the work described in Chapter 5. The research described here delves further into the reaction kinetics, separating the effects of electron induction and ring-strain on the reactivity of the *N*-acylenamines to tetrazines. To this end efforts were made to prepare model *N*-acylazetines, *N*-vinylcarbamates, *N*-vinylureas and a *N*-vinylamide. The *N*-acylazetines were obtained by reacting the four- and five-carbon spacer PNP-esters with morpholine. The *N*-vinylcarbamates were accessed through the Curtius rearrangement of acryl azide. The various attempted synthesis of *N*-vinylureas were unsuccessful due to their instability. Through a comparative study between *N*-acylazetines, *N*-vinylcarbamates and an *N*-vinylamide it was shown that ring-strain has a more significant effect on the rate of the IEDDA cycloaddition of *N*-acylenamines to tetrazines than electron donation.

References

1. K. Bahrami, M. M. Khodaei, S. Sohrabnezhad, *Tetrahedron Lett.* **2011**, *52*, 6420–6423.
2. H. A. V. Kistemaker, A. P. Nardozza, H. S. Overkleeft, G. A. van der Marel, A. G. Ladurner, D. V. Filippov, *Angew. Chemie - Int. Ed.* **2016**, *55*, 10634–10638.
3. H. A. V. Kistemaker, L. N. Lameijer, N. J. Meeuwenoord, H. S. Overkleeft, G. A. Van Der Marel, D. V. Filippov, *Angew. Chemie - Int. Ed.* **2015**, *54*, 4915–4918.
4. N. Oka, M. Shimizu, K. Saigo, T. Wada, *Tetrahedron* **2006**, *62*, 3667–3673.
5. J. E. Marugg, M. Tromp, P. Jhurani, C. F. Hoyng, G. A. Van Der Marel, J. H. Van Boom, *Tetrahedron* **1984**, *40*, 73–78.
6. V. A. Efimov, A. A. Buryakova, S. V Reverdatto, O. G. Chakhmakhcheva, O. YuA, *Nucleic Acids Res.* **1983**, *11*, 8369–8387.

List of Publications

[1] **Reaction Rates of Various *N*-Acylenamines in the Inverse-Electron-Demand Diels-Alder Reaction.** Sander B. Engelsma, Thomas C. van den Ende, Hermen S. Overkleeft, Gijsbert A. van der Marel*, Dmitri V. Filippov*. European Journal of Organic Chemistry, published 8 March 2018, Volume 20-21, pp. 2587-2591 (2018). DOI: https://doi.org/10.1002/ejoc.201800094

[2] **Combined Phosphoramidite-Phosphodiester Reagents for the Synthesis of Methylene Bisphosphonates.** Sander B. Engelsma, Nico J. Meeuwenoord, Hermen S. Overkleeft, Gijsbert A. van der Marel,* and Dmitri V. Filippov*. Hot Paper in Angewandte Chemie, published 7 February 2017, Volume 56, Issue 11, pp. 2955-2959 (2017). DOI: https://doi.org/10.1002/anie.201611878

[3] **Acylazetine as a Dienophile in Bioorthogonal Inverse-Electron-Demand Diels-Alder Ligation.** Sander B. Engelsma, Lianne I. Willems, Claudia E. van Paaschen, Sander I. van Kasteren, Gijsbert A. van der Marel, Herman S. Overkleeft*, and Dmitri V. Filippov*. Organic Letters, published May 5 2014, Volume 16, Number 10, pp. 2744-2747 (2014). DOI: https://doi.org/10.1021/ol501049c

[4] **Synthesis of L-altro-1-deoxynojirimycin, D-allo-1-deoxynojirimycin and D-galacto-1-deoxynojirimycin from a single chiral cyanohydrin.** Adrianus M. C. H. van den Nieuwendijk, Mark Ruben, Sander B. Engelsma, Martijn D. P. Risseeuw, Richard J. B. H. N. van den Berg, Rolf G. Boot, Johannes M. Aerts, Johannes Brussee, Gijs A. van der Marel and Herman S. Overkleeft. Organic Letters, Volume 12, pp. 3957-3959 (2010). DOI: https://doi.org/10.1021/ol101556k

[5] **Synthesis and Binding Capacity of a *Carba*-Ribose Incorporated Mono-ADP-Ribosylated H2B Histone Peptide.** Manuscript is in preparation.

Nederlandse Samenvatting

Fosfaatesters zijn functionele groepen die aanwezig zijn in tal van biologisch actieve moleculen die op hun beurt deelnemen aan een breed scala van fundamentele processen in organismen en in de daarbij behorende cellen. Het meest bekend zijn de fosfaatdiesters in DNA en RNA die de bouwstenen van nucleïnezuren of de nucleosiden onderling verbinden. Daarnaast komen verschillende klassen van fosfaatesters voor in moleculen die behoren bij de overige hoofdgroepen van biomoleculen, de eiwitten, koolhydraten en vetten. Fosforyleringen zijn reacties waarbij een fosfaatgroep op een specifieke positie in een biomolecuul wordt geïntroduceerd. Fosforylering van eiwitten in cellen bijvoorbeeld is een post-translationele modificatie (PTM), waarbij het gefosforyleerde eiwit door deze reactie functioneel of juist inactief wordt. Een belangrijke PTM, waar op het ogenblik veel onderzoek naar wordt verricht is adenosine difosfaat ribosylering (ADP-ribosylering). Gedurende dit cellulaire proces wordt met behulp van nicotinamide adenine dinucleotide (NAD^+) één of meerdere adenosine difosfaat ribose eenheden enzymatisch covalent gebonden aan de nucleofiele zijketen van een specifieke aminozuur in een doeleiwit. In mensen worden zowel mono- als poly-ADP-ribosylering (PARylerings) hoofdzakelijk gekatalyseerd door enzymen behorend tot de PARP-familie. Vooral vanwege hun betrokkenheid bij DNA-schadeherstel, ontstekingsreacties, genoom onderhoud en het reguleren van geprogrammeerde celdood is uitgebreid onderzoek gedaan naar PARP-1, PARP-2 en PARP-3 enzymen. Een PARylerings proces voorziet een doeleiwit van een polymeer die een lengte tot 200 ADP-ribose eenheden kan hebben. Het ADPR-polymeer brengt vervolgens de fysiologische verandering teweeg die benodigd is voor het betreffende biologische proces, bijvoorbeeld het rekruteren van een DNA-reparatie enzym. Een belangrijk onderzoeksdoel is het vergroten van het inzicht in mono- en poly-ADP-ribosylering processen. Eén van de benaderingen is de organische synthese van goed gedefinieerde ADP-geribosyleerde oligopeptiden en de toepassing daarvan om de hierboven genoemde cellulaire processen op moleculair niveau te bestuderen. Echter een eigenschap van natuurlijk voorkomende mono- en poly-ADP geribosyleerde eiwitten en fragmenten daarvan is dat deze chemisch instabiel zijn, waardoor zowel de synthese als de biologische toepasbaarheid worden beperkt. Een organisch chemische aanpak van dit probleem is het stabiliseren van de labiele chemische bindingen zonder dat biologische eigenschappen van het oorspronkelijke molecuul sterk worden aangetast. Het onderzoek beschreven in dit proefschrift richt zich op het ontwikkelen van gestabiliseerde ADP-geribosyleerde fragmenten, om het biochemische onderzoek naar ADP-ribosylering te faciliteren. In deze context zijn onder andere nieuwe reagentia ontwikkeld voor het synthetiseren van gestabiliseerde pyrofosfaatesters.

In **Hoofdstuk 1** worden een aantal biochemische aspecten van het PARP gekatalyseerde ADP-ribosyleringsproces toegelicht. Om het ADP-ribosyleringsproces op moleculair niveau te bestuderen zijn synthetische fragmenten van natuurlijk voorkomende ADP-geribosyleerde eiwitten niet altijd geschikt. De oorzaak hiervan is de instabiliteit van de volgende structuurelementen in deze moleculen; de pyrofosfaatbrug, de glycosidische band tussen de adenosine en de riboside, en de binding die het anomere centrum van ribose met de zijketen van het aminozuur verbindt. Dit inleidend hoofdstuk geeft een overzicht van verschillende gestabiliseerde analoga die hebben bijgedragen aan het ophelderen van het ADP-ribosyleringsproces. Ook wordt de synthese en modus operandi van een aantal gestabiliseerde analoga behandeld. Vervolgens worden methyleenbisfosfonaten geïntroduceerd als gestabiliseerde analoga voor pyrofosfaten. In methyleenbisfosfonaten is het zuurstofatoom, dat de twee fosfor atomen

in pyrofosfaten verbindt, vervangen door een methyleengroep waardoor breukresistentie wordt verkregen. Een aantal gebruikelijke synthese strategieën en hun beperkingen worden besproken. Met deze uiteenzetting wordt duidelijk gemaakt waarom het ontwikkelen van nieuwe chemische methoden voor de synthese van gestabiliseerde ADPr-gerelateerde fragmenten wenselijk is. Tot slot wordt het belang van de bio-orthogonale chemie, die voor veel biologische vraagstukken breed wordt toegepast toegelicht voor het ADP-ribosyleringsonderzoek. Bio-orthogonale reacties maken het mogelijk om artificiële moleculen binnen het complexe milieu van levende cellen selectief met elkaar te verbinden. De meeste recente ontwikkeling is de IEDDA-reactie die de grootste reactiesnelheidsconstante heeft. Hierbij reageert een alkeen onder ringspanning met een tetrazine, waarbij de twee covalent verbonden worden. Meestal zijn de hiervoor geschikte alkenen omvangrijk. Deze eigenschap is nadelig voor de wateroplosbaarheid en biologische beschikbaarheid van het gefunctionaliseerde molecuul. Hieruit kan worden opgemaakt dat het ontwikkelen van kleine, polaire alkenen waardevol kunnen zijn.

Hoofdstuk 2 beschrijft orthogonaal beschermde fosfanylmethylfosfonaten als reagentia voor de gecontroleerde synthese van methylbisfosfonaat monoesters. Na optimalisatie van de reactiecondities zijn de fosfanylmethylfosfonaat reagentia toegankelijk geworden via een één-kolf procedure; reactie van een gelithieerd methylfosfonaatdiester met een chlorofosforamidiet. Onder invloed van een azole kan het zo gevormde reagens gekoppeld worden aan een alcohol naar keuze, waarna het product direct geoxideerd wordt om zo de volledig beschermde methylfosfonaattetraester op efficiënte wijze te verkrijgen. Ontscherming van de fosfonaat-groepen leidt tot de gewenste eindstandige methylbisfosfonaat monoester. De praktische toepasbaarheid van de reagentia werd gedemonstreerd door de synthese van de methylbisfosfonaat analoga van verscheidene biologisch relevante di- en trifosfaten. Bovendien bleek de methodologie ook geschikt voor vaste-drager synthese.

Het onderzoek beschreven in **Hoofdstuk 3** bouwt voort op datgene wat beschreven wordt in hoofdstuk 2. Hier wordt een tweede generatie van het reagens gebruikt om complexere niet-symmetrische methylfosfonaatdiesters te synthetiseren. Het ontwikkelde reagens maakt gebruik van een aangepast patroon van beschermgroepen, bestaand uit twee methyl groepen en een *tert*-butyl groep aan de P^V. Na koppeling aan een eerste alcohol, door middel van de in hoofdstuk 2 beschreven koppeling-oxidatie sequentie, wordt de eindstandige *tert*-butylgroep selectief afgesplitst. Hierna kan een tweede alcohol worden geïnstalleerd via een PyNTP-gedreven condensatiereactie. Afsplitsing van alle beschermgroepen leidt tot de respectievelijke niet-symmetrische methylfosfonaatdiester. De potentie van deze methodologie werd gedemonstreerd door de synthese van methylbisfosfonaat analoga van ADPR en flavine adenine dinucleotide.

In **Hoofdstuk 4** wordt de synthese van een gestabiliseerd mono-ADP-geribosyleerd H2B oligopeptide beschreven. Het H2B eiwit is betrokken in het ADP-ribosyleringsproces dat optreedt als gevolg van DNA-schade. Eerdere pogingen om het natuurlijk voorkomende conjugaat te synthetiseren zijn niet geslaagd, doordat de anomere binding tussen de ribose en het aminozuur migreerde, hydrolyseerde of anomeriseerde. Deze nevenreacties zijn een gevolg van de labiliteit van anomere esters. Door de ringzuurstof in de ribose te vervangen door een methyleengroep wordt een aanzienlijk stabieler molecuul verkregen. Een dergelijk analoog wordt ook wel een *carba*-riboside genoemd. Een nieuwe syntheseroute naar de α-*carba*-ribosylamine werd ontwikkeld. D-Ribose werd omgezet naar een beschermde 5-iodo-riboside en vervolgens onderworpen aan een fragmentatie-vinyladditie sequentie. Het diallylische product werd ring-gesloten en geoxideerd tot een cyclopentenon bouwsteen. Onder fotochemische condities werd methanol geaddeerd op de dubbele band, om zo op elegante wijze *carba*-ribonolacton, een voorloper van *carba*-riboside te verkrijgen. Het keton werd geconverteerd naar het methoxyimine

en stereoselectief gereduceerd. Het verkregen α-amine werd gekoppeld aan een beschermd glutaminezuur derivaat. Na ontscherming werd op de 5-*OH* een di-*tert*-butyl fosfaattriester geïnstalleerd, waarmee de *carba*-geribosyleerde glutaminezuur bouwsteen werd verkregen. Deze werd ingebouwd in het H2B conjugaat via vaste drager peptide synthese. De pyrofosfaat werd vervolgens geconstrueerd door fosforylering van het geïmmobiliseerde *carba*-ribosylfosfaat met een beschermd adenosine fosforamidiet. Globale ontscherming, met gelijktijdige afsplitsing van de vaste drager, gaf het gewenste mono-ADP-*carba*-geribosylated H2B conjugaat in milligram hoeveelheden.

Hoofdstuk 5 beschrijft de ontwikkeling van een nieuwe compacte ligatiegroep ter verbetering van de bio-orthogonale IEDDA ligatiestrategie. De *N*-acylazetine ligatiegroep kan worden beschouwd als de kleinst mogelijke structuur die in staat is om ringspanning te combineren met elektronen donerende eigenschappen, om zo de reactiviteit naar tetrazines te verhogen. Ook werd onderzoek verricht om deze ligatiegroep zo efficiënt mogelijk op een doelmolecuul aan te brengen. De *N*-acylazetinegroep werd daarom voorzien van een verbindingsmolecuul van vier of vijf koolstofatomen lang, die eindstandig een geactiveerde para-nitrofenyl ester bevat; een zogenaamde ligatiehandle. Hiermee kan het geheel eenvoudig aan aminegroepen van een doelmolecuul gekoppeld worden. Na optimalisatie werd de ligatiehandle toegankelijk via een vier-stapsynthese. Het onderzoek naar de reactiekinetiek tussen de *N*-acylazetine groep en tetrazine leverde een tweede-orde shelheidsconstante van $0.39 \pm 0.1\ s^{-1}\ M^{-1}$ op wat gelijkwaardig is aan de vergelijkbare cyclopropeen ligatiehandles. De ligatiehandle werd vervolgens gebruikt om epoximicin, een bekende proteasoomremmer, te voorzien van de *N*-acylazetinegroep. De resulterende moleculaire sonde was in staat het proteasoom te labelen in een twee-staps labelingsexperiment. Hiermee werd de toepasbaarheid van de *N*-acylazetinegroep als bio-orthogonale handle bewezen.

Het werk besproken in **Hoofdstuk 6** bouwt voort op dat uit hoofdstuk 5. De invloed van de structuur op de kinetiek van de reactie tussen de *N*-acylaminekern en tetrazines werd onderzocht. Hiervoor werd een aantal model *N*-acylazetines, *N*-vinylcarbamaten, *N*-vinylurea's en een *N*-vinylamide gesynthetiseerd. Door de tweede-orde reactiesnelhedsconstanten van deze verbindingen met een tetrazine te bepalen en onderling te vergelijken, kon er worden opgemaakt dat ringspanning significanter bijdraagt aan reactiesnelheidsconstante van deze reacties dan elektronendonatie. Het afsluitende **Hoofdstuk 7** geeft een samenvatting van de behaalde onderzoeksresultaten en doet op grond daarvan aanbevelingen voor toekomstig onderzoek.

Curriculum Vitae

Sander Bob Engelsma was born on the 2nd of November 1986 in Amsterdam, the Netherlands. After completing his secondary HAVO education at the Openbare Schoolgemeenschap Bijlmer in 2004, he started studying chemistry at the University of Applied Science in Leiden. In the final year, he conducted his internship in the bio-organic synthesis group of prof. dr. G. A. van der Marel and prof. dr. H. S. Overkleeft, where he worked on the synthesis of 1-deoxynojirimicin analogues as glycosidase inhibitors. After receiving his HLO bachelor degree in organic chemistry in 2009, he started the master Chemical Research – Design & Synthesis at Leiden University. As part of this study a research internship was carried out at the bio-organic synthesis group. This research, under supervision of prof. dr. H. S. Overkleeft, resulted in the master thesis 'Molecular Tools for the Two-Step Activity-Based Profiling of Glycosidases' and with that he finalized his master's studies and obtained Master degree in March 2012.

In Januari 2012 he started his PhD studies at Leiden University in the bio-organic synthesis group, under the supervision of prof. dr. G. A. van der Marel (promotor) and the daily guidance of dr. D. V. Filippov (co-promotor). Parts of the work described herein were orally presented at the Dutch Peptide Symposium (May 2015) and CHAINS (December 2015). Poster presentations were given at Cambridge (July 2015) and several national conferences.

In March 2017 the author started working as a Process R&D Chemist at Sonneborn B.V. in Amsterdam.